2002

Behavior and Design of FRP-Reinforced Longitudinal Glulam Deck Bridges

Melanie Marie Bragdon
University of Maine - Main

BEHAVIOR AND DESIGN OF FRP-REINFORCED LONGITUDINAL GLULAM DECK BRIDGES

By

Melanie Marie Bragdon

B.S. University of Maine, 1995

A THESIS

Submitted in Partial Fulfillment of the

Requirements for the Degree of

Master of Science

(in Civil Engineering)

The Graduate School

The University of Maine

December, 2002

Advisory Committee:

Habib J. Dagher, Professor of Civil Engineering, Advisor

William G. Davids, Assistant Professor of Civil Engineering

Roberto Lopez-Anido, Assistant Professor of Civil Engineering

BEHAVIOR AND DESIGN OF FRP-REINFORCED LONGITUDINAL GLULAM DECK BRIDGES

By

Melanie Marie Bragdon

Thesis Advisor: Dr. Habib J. Dagher

An Abstract of the Thesis Presented
in Partial Fulfillment of the Requirements for the
Degree of Master of Science
(in Civil Engineering)
December, 2002

In 1977, the Weyerhaeuser Company developed a system for short-span timber bridges. The girder-free system consisted of longitudinal, vertically-laminated glulam panels joined by below-deck Transverse Stiffener Beams (TSB). This project addresses two potential areas of improvement in the construction and design of these bridges: a reinforced deck panel and an improved method for TSB design.

This project has two objectives: (1) To evaluate the behavior and advantages of longitudinal glulam deck panels reinforced with Fiber-Reinforced Polymers (FRP) and (2) To evaluate existing AASHTO empirical TSB design criteria.

The tension-reinforced deck panels can alleviate reliance on high grade wood laminations and allow longer spans and lighter decks. The new panels have the middle two-thirds of the tension side reinforced with longitudinal E-glass FRP. The research

addressed the selection of the FRP material system, the manufacturing process used for applying the reinforcement to the panels, the structural and economic benefits of FRP-glulam panels, and the durability of the FRP.

The approach included design, laboratory manufacture, and construction of a municipal pier in Milbridge, Maine. Wet-impregnated unidirectional E-glass fabrics were used to reinforce the 16-ft. wide, 167-ft. long, 7-span vehicular pier. A cross-section reinforcement ratio of one percent was used, increasing panel stiffness by six percent. The pier showed the FRP-glulam deck as cost competitive with a prestressed concrete deck. The pier was load tested and performed as predicted under full design live load. The FRP has performed well after two years of harsh marine exposure.

To evaluate AASHTO designs of the TSB, a parametric study was performed using a finite element model developed for this study. The model was validated against full-scale laboratory tests conducted at The University of Maine and Iowa State University. The finite element model incorporated orthotropic plate elements for deck panels, offset beam elements for TSB, nonlinear models for deck-to-TSB connections, elements to allow pretensioning of the connections, and elements to model bearing between the deck and TSB.

The parametric study focused on shear and bending response of the TSB and the relative movement between adjacent panels. Over 140 analyses were conducted on 43 southern pine bridges designed according to current AASHTO criteria, using 50 load cases. Results showed that the empirical AASHTO design criteria for the TSB may be unconservative. In the most critical cases under AASHTO HS20 loading, TSB designed according to AASHTO criteria may experience maximums of either 68% more shear

stress than allowable or 61% more bending stress than allowable. In addition, relative panel deflection may exceed the 0.1-inch asphalt serviceability criteria by 79%.

Based on the parametric study performed on curb-free bridges, the following design criteria are recommended to replace the current AASHTO TSB design criteria. "In lieu of a more accurate analysis, the transverse stiffener beam shall be designed for the following bending moment and shear values: Shear = 0.45*wheel load and Bending Moment = (3.5 inches) *wheel load, as the wheel load represents the maximum wheel load for HS & H vehicles and 1.75*maximum wheel load for alternate military loading."

ACKNOWLEDGEMENTS

The author would like to thank Dr. Habib Dagher for his guidance and assistance throughout this research process. She would also like to thank Dr. Bill Davids and Dr. Roberto Lopez-Anido for their comments and advice. Those who have contributed to the work and ideas that have culminated in this thesis are far too numerous to list here, however, the author freely acknowledges her indebtedness to the technical assistance of professionals at the Maine Department of Transportation, the untiring labor of undergraduates that worked on the project, the unfailing assistance of the laboratory technicians, lab managers, and administrative assistants, the invaluable encouragement and advice of fellow graduate students, the support of family, and the grace of God.

The research was funded by the Maine Department of Transportation and the Federal Highway Administration through the Innovative Bridge Research and Construction Program.

TABLE OF CONTENTS

LIST OF TABLES

LIST OF FIGURES

Chapter 1

INTRODUCTION

1.1 General

This chapter provides an overview of this thesis, starting with the needs and objectives of the study. Following this, background information is given on reinforced longitudinal glued-laminated (glulam) deck bridges.

1.2 Need for Research in Longitudinal Glulam Deck Bridges

Longitudinal glulam deck bridges consist of vertically-laminated glulam panels spanning from support to support and joined below the deck by Transverse Stiffener Beams (TSB). No girders are necessary for the bridge.

Although longitudinal glulam deck bridges have been designed and built since the late 1970s, the below-deck TSB design is empirical, and its behavior is not well understood. Published work on this bridge system has consistently called on further research into TSB behavior (Sanders *et al.* 1985; Funke 1986; Ritter 1990; Hajdu 1994). Additionally, with the large number of short-span bridges that are in need of replacement (Bhide 2001), economically-feasible options should be fully investigated. Longitudinal deck bridges are often a viable superstructure replacement solution for short-span bridges when the abutments are in good condition or for short-span bridges with low-profile requirements. It has been also shown (Dagher *et al.* 1998b) that reinforcing glulam beams with a Fiber-Reinforced Polymer (FRP) can add strength and stiffness to the beam

while keeping the system economically competitive. To build on this work, research is needed on the benefits of reinforcing glulam panels with FRP.

1.3 Objective and Workplan

This study's objectives are two-fold: (1) to understand the behavior and benefits of FRP-reinforced, vertically-laminated glulam deck bridges and (2) to develop a design approach for the TSB.

The workplan under the first objective included (1) developing a methodology of reinforcing glulam panels with an FRP using a Phenol Resorcinol Formaldehyde (PRF) matrix, (2) evaluating the environmental durability of these FRP-glulam panels in a marine environment, and (3) evaluating the benefits of longitudinal FRP-glulam panel bridges, as compared to conventional materials including economics, durability, and ease of construction.

The workplan under the second objective included (1) developing a Finite Element Model (FEM) that accurately predicts the behavior of these bridges, (2) validating the model through laboratory testing at The University of Maine (UMaine) and through published test results, (3) determining adequacy of current TSB design methodology of the American Association of State Highway and Transportation Officials (AASHTO) (AASHTO 1996) through analysis of "worst-case" scenarios for these bridges systems, (4) developing improved design criteria for the below-deck TSB, and (5) making any necessary recommendations for changes to AASHTO design methodology for TSB. Results are expected to facilitate increased use of both FRP-reinforced and conventional longitudinal glulam deck bridges.

1.4 Overview of FRP-Reinforcing of Glulam

FRP can be used to reinforce glulam beams in a manner similar to the way that steel reinforces concrete. FRP can be used to replace high-quality tension laminations that may be difficult or expensive to source. With sufficient tensile strength, the more ductile compressive failure of the wood can control failure modes. Without reinforcement, a horizontally-laminated beam will experience a brittle failure. Although vertically-laminated panels typically have more ductile behavior, they too can benefit from FRP-reinforcing.

FRP-reinforcing consists of adhering FRP to the glulam panel in such a way as to ensure that the wood and the FRP act as a composite section. This is typically done through an adhesive between a preconsolidated FRP and the glulam or by using the matrix of the FRP as the adhesive to the wood substrate. The latter method was used for this study, as described in Chapter 3. When reinforcing panels, the amount of reinforcing is measured by the ratio of the cross-sectional area of FRP to the cross-sectional area of wood. The panels in this study have a 1% reinforcement ratio. FRP was applied to the middle two-thirds of the tension-side (bottom) of the panels (Figure 1.1). A summary of published benefits of FRP-glulam and environmental durability of FRP-glulam can be found in Chapter 2.

1.5 Overview of Longitudinal Glulam Deck Bridges

1.5.1 Description of System

Longitudinal glulam deck bridges were initially developed by the Weyerhaeuser Company in 1977 (Funke 1986). These stringer-less bridges consist of glulam panels that

are placed parallel to the direction of traffic. Below the panels, a stiffener beam is placed transverse to traffic across the entire width of the bridge at longitudinal spacing of eight to ten feet (Figure 1.2). The TSB are the only means for distribution of load between the panels; no other means – dowels or other connectors – are provided.

The glulam deck panels are typically 48-inches wide but may vary from 42-54 inches wide. They are economical for bridges with spans of 16-35 feet designed for AASHTO HS20-44 live loading. The panels are vertically-laminated glulam loaded parallel to the wide faces of the laminations with panel thickness typically varying from approximately 5 to 14.25 inches. Panels with thickness of 12 inches or more are made of multiple-piece laminations that either must be edge-glued (Figure 1.3) or allowable horizontal shear strength is reduced approximately 50 percent (AASHTO 1996, Table 13.5.3B).

The TSB is usually a horizontally-laminated glulam beam, but other materials can be used, such as FRP, steel, and aluminum. Dimensions of the TSB are typically in the range of four to seven inches, but no design guidance on dimensions, area, or an aspect ratio (width/depth) currently exists. The only current specification for the TSB is a minimum stiffness factor (Modulus Of Elasticity (MOE or E) multiplied by the beam's moment of Inertia (I): EI = MOE*I) of 80,000 kip-in^2 (AASHTO 1996). This stiffness factor would make it appear that the optimum TSB would be oriented for strong-axis bending, with the depth greater than the width (an aspect ratio less than 1.0).

The TSB is connected to the panels through connection hardware. The connection systems most commonly used are shown in Figure 1.4. Timber through-bolts and aluminum brackets are the most common connectors used (Funke 1986). However,

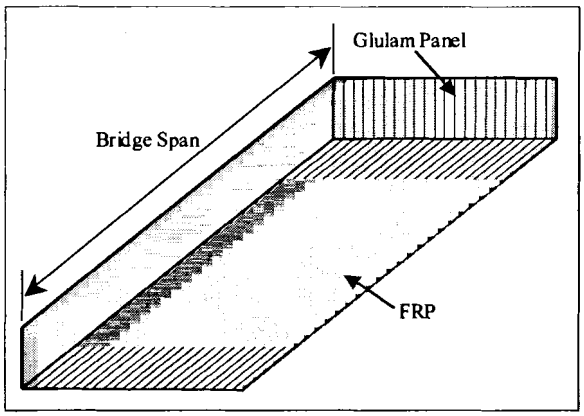

Figure 1.1 Partial FRP-reinforcing of glulam panel

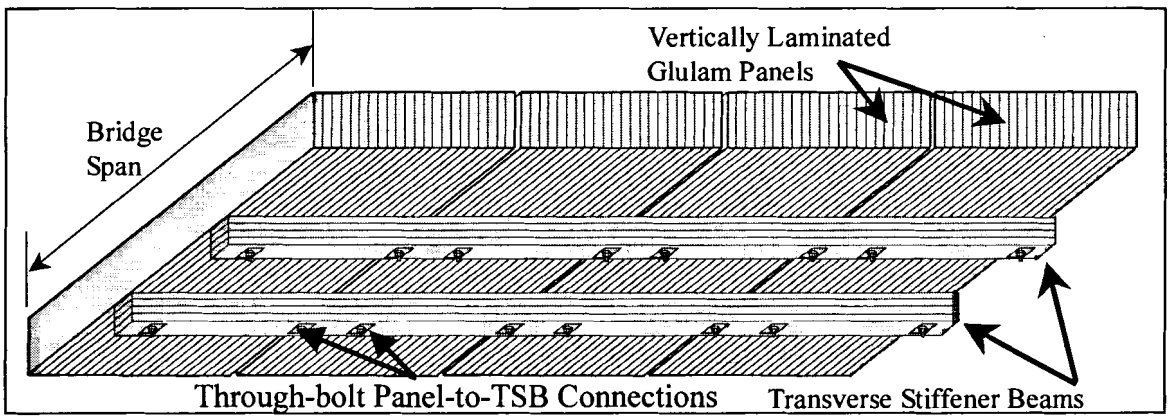

Figure 1.2 Typical longitudinal glulam deck bridge superstructure

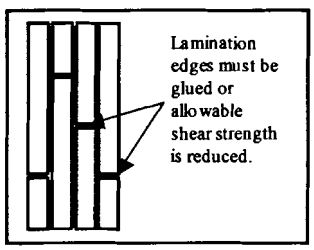

Figure 1.3 Edge-gluing for panels of thickness greater than 12 in.

these connections may induce stresses in the system through restriction of movement during the inevitable hygrothermal cycling of the glulam components. As the wood's moisture content changes, shrinkage and expansion in the radial and tangential-to-grain directions can be comparatively considerable, but dimensional change in the longitudinal-to-grain direction is essentially negligible. As shown in Figure 1.5, as moisture content increases, the panels undergo radial and tangential expansion in the bridge's transverse direction, but the TSB has greater dimensional stability and does not. The connection hardware, if through-bolts or aluminum brackets are used, can restrict this relative movement, damaging the connection or the wood around it. Glulam treated with oil-borne preservatives has more dimensional stability, and this differential expansion is not as likely to become critical with them; however, in glulam with water-borne preservatives and bridges that may experience extreme moisture content variability, consideration should be given to the possibility of differential relative expansion causing additional stress and bending in the connection. A seated-beam (steel-plate) connection (Figure 1.4b) alleviates this condition by allowing relative movement between the panels and the TSB.

1.5.2 Design of System

Current design criteria and methods were developed after extensive testing and modeling had been performed at Iowa State University (ISU), as reported in Chapter 2. The AASHTO Standard Specification design methodology (AASHTO 1996) for longitudinal decks is described below and compared with design recommendations by Ritter (1990) and the American Institute for Timber Construction (AITC) (1994). A

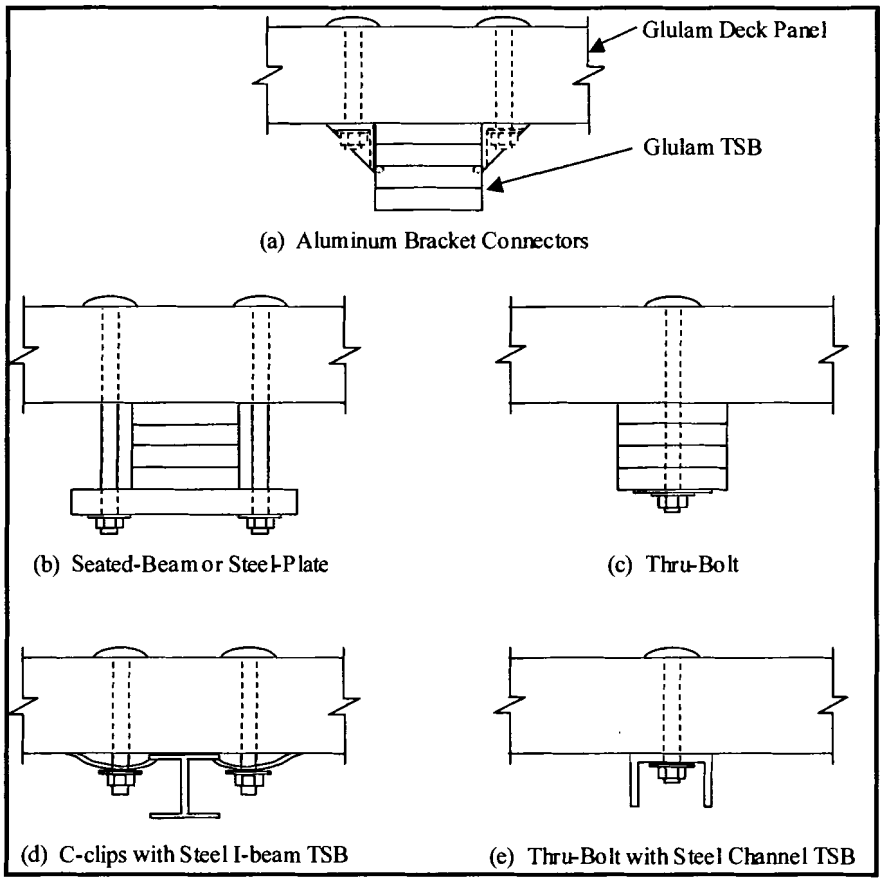

Figure 1.4 Types of common panel-to-TSB connections (Ritter 1990)

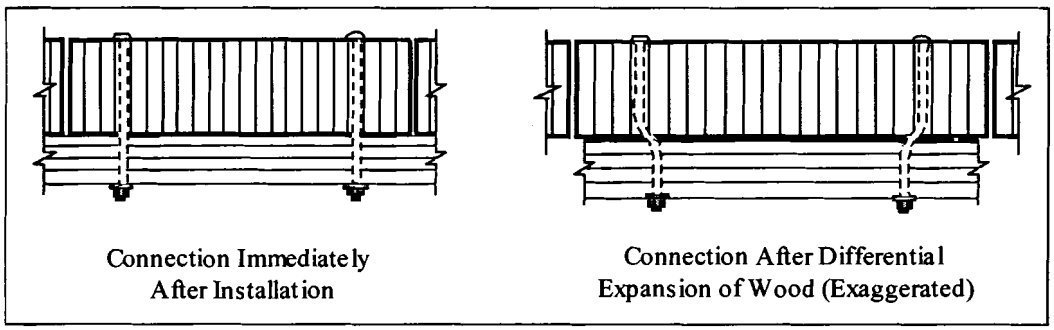

Figure 1.5 Thru-bolt connection with moisture-induced expansion of the glulam

MathCad (2000) worksheet that follows the AASHTO design requirement was developed for use in this thesis and is presented in Appendix A as an example of the current design methodology.

The primary design component of the longitudinal glulam deck bridge superstructure is the deck panel. As with any bridge, the bridge span, width, number of lanes, and AASHTO design live load is initially determined. Wood species is typically predetermined, as well. Ritter recommends using a douglas fir glulam of Combination Symbol 2 or a Southern Pine glulam of Combination Symbol 47 (SP47) for an economical design. The SP47 layup material properties are used in the parametric study reported in Chapter 6. The panel is assumed to act as a simply-supported beam carrying its dead load and a fraction of the live load from a single wheel line of the design vehicle. The bending wheel load fraction (WLF) is a function of the number of lanes, panel width, and bridge span (see Appendix A for formula). In current AASHTO, a different WLF, based on panel width, is used for bearing and shear close to the reactions. As opposed to AASHTO and due to publication prior to the AASHTO WFL change, Ritter's Timber Bridge Manual does not use a separate WLF for shear and bearing (Ritter 1990). The panel is assumed to be loaded under wet-use conditions. AASHTO specifications do not give an allowable live load deflection but recommend L/500. Ritter uses L/360 as an allowable based on the ISU studies that showed that, with this allowable, Relative Panel Displacement (RPD) would not significantly exceed 0.10 inches. (In Funke's experiments at ISU, maximum measured RPD was 0.26 in. The design (using a WLF of 0.772) predicted a L/330 deflection (1986)). Keeping RPD below 0.1 inches should

prevent cracking of the asphalt wearing surfaces at longitudinal panel joints (Ritter 1990). AITC uses an L/300 allowable for live load deflection.

Once the deck panels have been designed, a stiffener beam is selected. The stiffener must have a stiffness factor (EI) greater than or equal to 80,000 kip-in^2. Ritter recommends a maximum stiffness factor of twice the AASHTO minimum value, but AASHTO and AITC do not set or recommend a maximum.

The only other requirement with regard to the TSB is maximum spacing. AASHTO requires a TSB at midspan and maximum TSB spacing of 10 feet. It also states "stiffener spacing required will depend upon the spacing needed in order to prevent differential panel movement" (AASHTO 1996, Section 3.25.3.4) but does not give any guidance on correlations between TSB spacing and differential panel movement. Ritter concurs with AITC's recommendation of maximum TSB spacing of 8 feet. AITC does not require a TSB at midspan.

1.6 Overview of Thesis

This thesis is divided into seven chapters and five appendices. Chapter 2 is a review of literature relevant to this study. Chapter 3 describes the municipal pier built in Milbridge, Maine, a seven-span, longitudinal FRP-glulam deck bridge built using the technology developed in this study, and the results of the field load-testing and monitoring accomplished to evaluate performance of the pier. Chapter 3 also gives in-depth description of the FRP and the reinforcing methodology used in this study. Chapter 4 describes the experimental laboratory testing done at UMaine with a full-scale longitudinal FRP-glulam deck bridge and reports the results. Chapter 5 describes the

finite element model developed in this study for longitudinal deck bridges and its validation by experimental testing. Chapter 6 reports the results of the parametric study performed using the finite element model described in Chapter 5 to evaluate stress in the TSB. Chapter 7 gives the conclusions and recommendations of this study. Appendix A contains the Mathcad (Mathcad 2000) worksheet for longitudinal glulam deck bridge design for the Milbridge Pier. Appendix B contains results of the Milbridge Pier load test. Appendix C contains results of the laboratory tests performed at UMaine. Appendix D presents charts and graphs of the FEM validation by experimental results. Appendix E contains charts and tables relating to the parametric study accomplished in this thesis and its results.

Chapter 2

LITERATURE REVIEW

2.1 Introduction

This chapter is a review of literature relevant to this study. The objectives of this chapter are (1) to provide an overview of FRP-glulam research as it pertains to this study, (2) to provide detailed summaries of research done on longitudinal glulam deck bridges and their components, and (3) to summarize conclusions and recommendations from previous studies of these bridge systems.

2.2 FRP-Glulam

FRP-reinforced glulam can have significant advantages over unreinforced glulam. It has been shown that FRP-glulam can be cost-competitive with conventional materials (Dagher *et al.* 2001). The mechanical advantages have also been repeatedly shown through laboratory testing, demonstration projects, and analytical studies (Dagher *et al.* 1996, Dagher *et al.* 1998a), but the environmental durability of FRP is still an area of concern.

2.2.1 Mechanical Properties

FRP-glulam beams and panels have been shown to have gains in both bending strength and stiffness over conventional glulam. Previous studies at The University of Maine have demonstrated that GFRP tension reinforcement ratios of 2-3% can increase

the allowable bending strength of glulam beams by over 100% and stiffness by 10-15% (Dagher *et al.* 1998b).

Research on FRP-glulam sandwich panels (Figure 2.1) at UMaine has shown that reinforcement of panels can improve failure modes, bending strength, and stiffness (Xu 2001). The E-glass reinforced panels had more ductile failure modes than unreinforced panels. FRP reinforcement on top and bottom of a glulam panel with a 2.1% reinforcement ratio (top and bottom reinforcing included) increased the composite panel's ultimate load capacity by 47%. The reinforced glulam panels carried a load at deflection service limit 24% greater than unreinforced panels. Even with these benefits, the tensile reinforcement is under-utilized with extreme fiber strain in the composite panel at failure only 30% of the ultimate tensile strain of the FRP (Xu 2001).

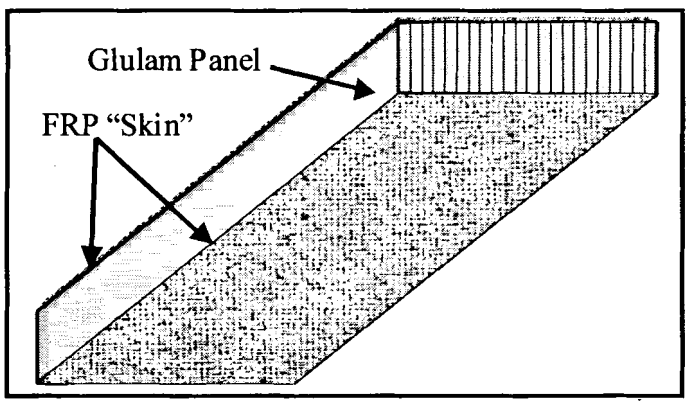

Figure 2.1 FRP-glulam sandwich panel configuration

2.2.2 Environmental Durability of FRPs

FRP performance is a function of the matrix (resin) type, fiber type, fiber orientation and lay-up, fillers, additives, manufacturing processes, microstructure, architecture, geometry, and many other factors. The number of factors that can affect performance makes quantitative analysis of the effect of each very difficult. To add to

the difficulty, the synergistic effects are not negligible. Durability of any structural member in civil infrastructure application is of utmost concern, and there are many environmental attacks on such members. (CERF 2001). Aqueous or high moisture environments can cause substantial damage to glass fibers. UV can cause separation of polymer chains. Degradation is also affected by thermal environment, stress level, cyclic loading, and duration of load.

Degradation is typically determined by observing changes in Young's modulus of elasticity, tensile strength, interlaminar shear strength, and interlaminar bond strength (Waldron *et al.* 2001). Although other material properties could be used, research has focused on tensile strength and modulus for degradation analysis.

2.2.2.1 Moisture/Aqueous Environmental Degradation

It has long been known that moisture can diffuse in organic polymeric matrices. This additional moisture can cause both reversible and irreversible changes in thermophysical, mechanical, and chemical characteristics of the polymer and thus the FRP. Moisture adsorption is affected by resin type and curing methodology, laminate composition and geometry, laminate thickness, quality of laminate, curing conditions, resin-fiber interface, and manufacturing processes. Even if there were not interaction between moisture degradation, stress conditions, and other degradation, the parametric studies that would quantify degradation to various FRP would be daunting (Busel 2000).

In the matrix, polymer resins can be plasticized by the presence of moisture. Moisture can also cause hydrolysis. Often moisture travels along the fiber-matrix interface damaging the bond and increasing the volume of fiber exposed to the moisture. In an FRP, moisture can deteriorate both the matrix and the fiber (CERF 2001). The

fibers are even more susceptible than the matrix to moisture-induced degradation. E-glass is the most susceptible to moisture and alkalinity degradation. Hydrogen ions replace sodium ions on the glass surface through ion exchange. The glass surface at the fiber-matrix interface wants to shrink but is restricted. This causes tension on the glass surface and eventually tensile failure of the surface (Agarwal and Broutman 1990).

The presence of an aqueous environment degrades the FRP's modulus, strength, ultimate strain, and toughness. E-glass FRP (GFRP) has shown a 10% loss of modulus over ten to fifteen years in aqueous environments. FRP moisture contents below 1% have a negligible effect on strength of unidirectional and quasi-isotropic laminates. FRP with moisture contents above 1% show decreases in strength as moisture content increases. In quasi-isotropic and unidirectional laminates moisture content has very little effect on Young's modulus. However, both strength and modulus of 90-degree laminates experience significant decreases of modulus due to the matrix domination of the properties (CERF 2001).

Fiber protection from moisture is the most crucial aspect to prevent FRP degradation in high moisture environments. A low-permeability resin can provide this protection. In addition to the resin, a gel coat or resin rich layer should be provided as a barrier layer (Agarwal and Broutman 1990). Sizings can also help prevent moisture movement in the FRP, but the resin must be fully cured prior to exposure. Achievement of full cure for resins is particularly critical for ambient-cure systems (CERF 2001).

2.2.2.2 UV Radiation Degradation

UV radiation exposure typically does not occur during service life for most FRP in structural bridge applications. The critical times of protecting an FRP from UV seem

to be during storage. The primary concern is that the UV degradation of the matrix allows passage of moisture and chemicals to the fibers. This results in accelerated damage from stress, moisture, salt water, etc. (Busel 2000.). Most UV degradation occurs at the surface of the FRP. This surface effect causes stress concentrations that will start fracture of fiber and/matrix at significantly lower stresses (CERF 2001). In one reported experiment, GFRP experienced an 8% loss after 500 hours of accelerated UV exposure, and no further reduction was observed with continued exposure (Waldron *et al.* 2001.). CERF recommends that due to moisture degradation of FRP that design allowable strength should be significantly less than the guaranteed design strength, recommending the designer use 25% of guaranteed strength for GFRP (CERF 2001).

2.2.3 Environmental Durability of Phenol Resorcinol Formaldehyde (PRF) Wet-Lay-up FRP

A wet-lay-up PRF FRP similar to the FRP used in this study showed a reduction in ultimate tensile strength of approximately 35% after exposure to heat aging, freeze-thaw cycling, artificial weathering, calcium carbonate, and water (Battles 2000). Saltwater exposure caused a dramatic 80% reduction of ultimate tensile strength. The modulus of elasticity (MOE) and interlaminar shear strength (ILSS) did not degrade as much as the ultimate tensile strength, most exposed specimens retaining above 85% of unexposed values of MOE and ILSS. Saltwater, water, and calcium carbonate caused MOE reduction of 19%, 18%, and 20%, respectively (Battles 2000). Heat aging, retaining 92% of ILSS, and UV degradation, retaining 96% of ILSS, were the only exposures to pass the ILSS retention requirement. It was also found that a protective coating of polyurethane would reduce the exposure impact (Battles 2000). However, the

benefit of the protective coating was not explicitly defined through experimental results in the report.

2.3 Longitudinal Glulam Deck Bridges

Longitudinal glulam deck bridge research has primarily been conducted by Weyerhaeuser and Iowa State University (ISU). Weyerhaeuser's testing was reported in the late 1970s and early 1980s in a series of proprietary publications. Only a few of these reports were able to be obtained for this study. Weyerhaeuser's research focused on connection behavior, testing of full-scale bridges, and analysis of the system. ISU's research has focused on load distribution behavior of the system with regard to bending moment and shear in the panels. They have also developed several numerical/Finite Element (FE) models and conducted extensive laboratory testing.

2.3.1 Experimental Testing of Longitudinal Glulam Deck Bridges

Research on longitudinal glulam deck bridges involving experimental testing can be divided into two general areas: testing of the entire system and testing of components of the system. Much research has been done on testing of the entire system, but Weyerhaeuser also researched the panel-to-TSB connection behavior.

Although Iowa State University has been the primary research institution for longitudinal glulam deck bridges, Weyerhaeuser performed the first experiments on the systems as it developed the technology. Then, sponsored by AITC, ISU performed over 116 tests on a full-scale longitudinal bridge deck in their laboratory. The primary

purpose of this testing and a parametric study done using FE models was to develop improved transverse load distribution criteria for the deck panels (Funke 1986).

2.3.1.1 Weyerhaeuser's Experiments

2.3.1.1.1 Bridge Tests

As reported by Funke (1986), Hale tested a 72-foot long, 3-span continuous longitudinal glulam deck bridge consisting of two panels under static loading. In 1979, he tested a 24-foot long, single span bridge constructed of four 48-inch wide panels. In the single span bridge tests, Hale varied stiffener beam size, spacing and material as well as connection hardware. Hale found that seated-beam, through-bolt, and C-clip connections limited relative panel displacements better than aluminum bracket connections, but did not address stiffener beam behavior.

2.3.1.1.2 Connection Tests

Hale performed another series tests to determine the load-slip curves of panel-to-TSB connectors. He tested the load-deflection behavior of timber bolts of $^1/_2$", $^5/_8$", $^3/_4$", and $^7/_8$" diameters in bearing on douglas fir glulam. The bolts had bearing areas of 1.77, 3.76, 5.41, 7.37, and 16 in^2 respectively. The slip measured was the deflection between the head of the timber bolt and the surrounding wood, taking only the bearing of the wood under the bolt head into consideration. He also tested seated-beam/steel-plate, aluminum bracket, and C-clip connections. The seated-beam connection used a glulam stiffener and a ¾" x 4" steel plate with two $^5/_8$"-diameter timber bolts. The aluminum bracket connections used a glulam stiffener and two standard aluminum brackets with two $^5/_8$"-diameter timber bolts. The glulam stiffener was constructed of douglas fir and was either 5.125-inches wide by 9-inches deep or 6.75-inches wide by 9-inches deep.

Hale did not indicate that the stiffener size affected the load-deflection curves of the tests. The C-clip connection used a steel beam and two ½" or $^5/_8$"-diameter timber bolts. Hale did not find a significant difference between the bolt diameters tested with the C-clip connection. The glulam representing the deck panel was an 8.75-inch thick douglas fir glulam. The connection tests measured the vertical deformation of the entire connection system. Figure 2.2 shows the components of the measured vertical deformation (Hale 1978). Hale found that the seated-beam provided the stiffest connection and the aluminum brackets the least stiff. The load-deflection curves determined by Hale are found in Figure 2.3. Hale also found that aluminum bracket connections tend to split the stiffeners when overloaded (Hale 1978).

2.3.1.2 Laboratory Tests Performed at Iowa State University (ISU)

ISU performed extensive testing and research, their work is the basis for most of what is published on longitudinal glulam deck bridges. Their work is presented in more detail than would typically be found in a literature review because of its influence on the FE model developed in this study, its use in that model's validation, and its agreement with the findings of the parametric study reported in this thesis. In the analysis of the testing, ISU used the then-current publications of wood allowable stresses. In reviewing the literature here, the older allowable stress values have been kept for consistency, regardless of current allowable wood stresses.

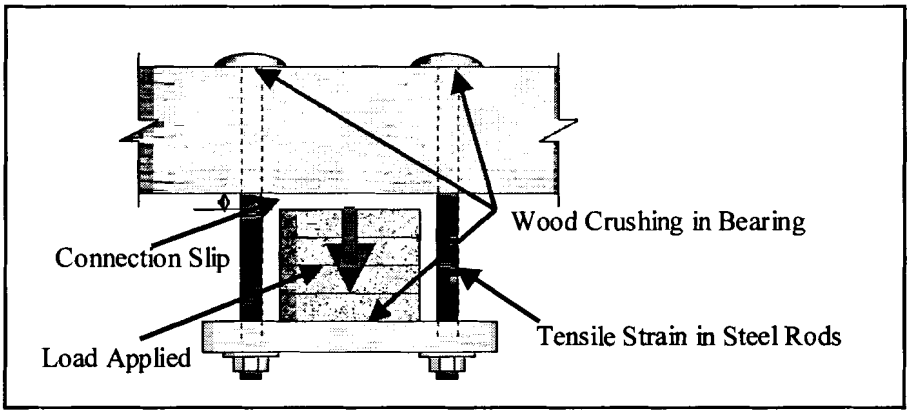

Figure 2.2 Slip measured in load-slip experiments of connection types

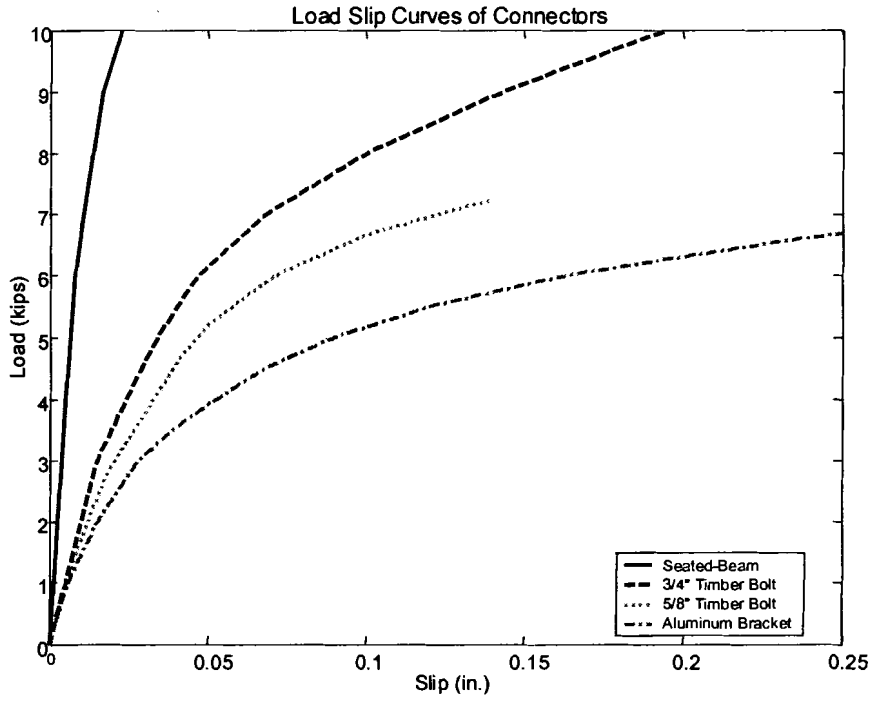

Figure 2.3 Experimental load-slip curves of connectors (Hale 1978, Funke 1986)

2.3.1.2.1 Description of Experiments

ISU ran 116 experiments to establish and validate the design criteria for longitudinal glulam deck bridges. The testing at ISU used three bridge widths, one to three stiffeners, two different connection systems, and various load cases. Three tests of the 116 will be discussed in detail because of the failure of the TSB that occurred during the tests. This failure supports the concern of the TSB being overstressed in some bridge configurations and loadings. So that they can be easily referenced later in this thesis, the tests will be designated by the ISU author and his reference system for the test. These three tests are Funke#6 and Funke#31, in both of which the TSB failed by splitting at a connection before the bridge was loaded to design, and Funke#78, in which the TSB experienced the highest measured bending strain (Funke 1986).

For all the testing performed by Funke, a 26-foot span test bridge was constructed from four to six panels, creating bridge widths of 16 to 24 feet. The douglas fir panels were 27-feet long, 48-inches wide, and 10.75-inches thick. The stiffener beams were also douglas fir and were 4.5-inches deep by 6.75-inches wide by 24-feet long. The two different connectors used during testing were ¾-inch diameter timber through-bolts and aluminum brackets. Consistent with standard procedure, each panel had two connections per stiffener beam. (Connections for longitudinal glulam deck bridges are typically spaced at stiffener beam locations six inches from panel edges.) Through-bolts connections need a slightly oversized hole in the TSB, and the aluminum bracket connections require a groove (1 in. x 1 in. x 7 in.) cut into each side of the TSB. The testing used AASHTO HS20-44 loading with one or two trucks on the bridge and with each truck having the possibility of one or two axles on the bridge. Further details on the

load cases tested are given in Chapter 5 to show validation of the finite element model developed in this study (Funke 1986). Figure 2.4 shows the bridge and loading configuration for the ISU tests discussed in detail in this thesis.

Instrumentation for the ISU tests included electrical-resistance strain gages (strain gages), mechanical displacement gages, and Direct Current Linear Variable Differential Transformers (DCDT). Thirty-six strain gages were on bonded to the panels with five gages bonded six-inches from midspan on each panel and one at one end of each panel. One TSB had 30 strain gages bonded on its bottom side to measure bending strain. Displacements were measured on each panel near midspan, one inch from each edge (Funke 1986).

2.3.1.2.2 Findings

Consistent with its primary goal, ISU's testing in which Funke was involved led to recommendations and eventual changes in AASHTO's design criteria for the panels of longitudinal glulam deck bridges; however, its other findings are of more interest in this study. TSB failures that occurred with aluminum bracket connections showed weaknesses in the system. Edge loading directly above the TSB was found to be the critical loading for the TSB in this system of 48-inch wide panels. The study also showed that connection type does influence relative panel movement (Funke 1986).

ISU found that the stiffener beam may experience splitting or crushing near the connections when aluminum brackets are used. It was believed that the connections were overstressed and that some eccentricity in the connections exacerbated the issue, rotating the connector and causing high stress concentrations. One stress concentration was significant tension perpendicular-to-grain in the TSB. Wood is very weak in this tension

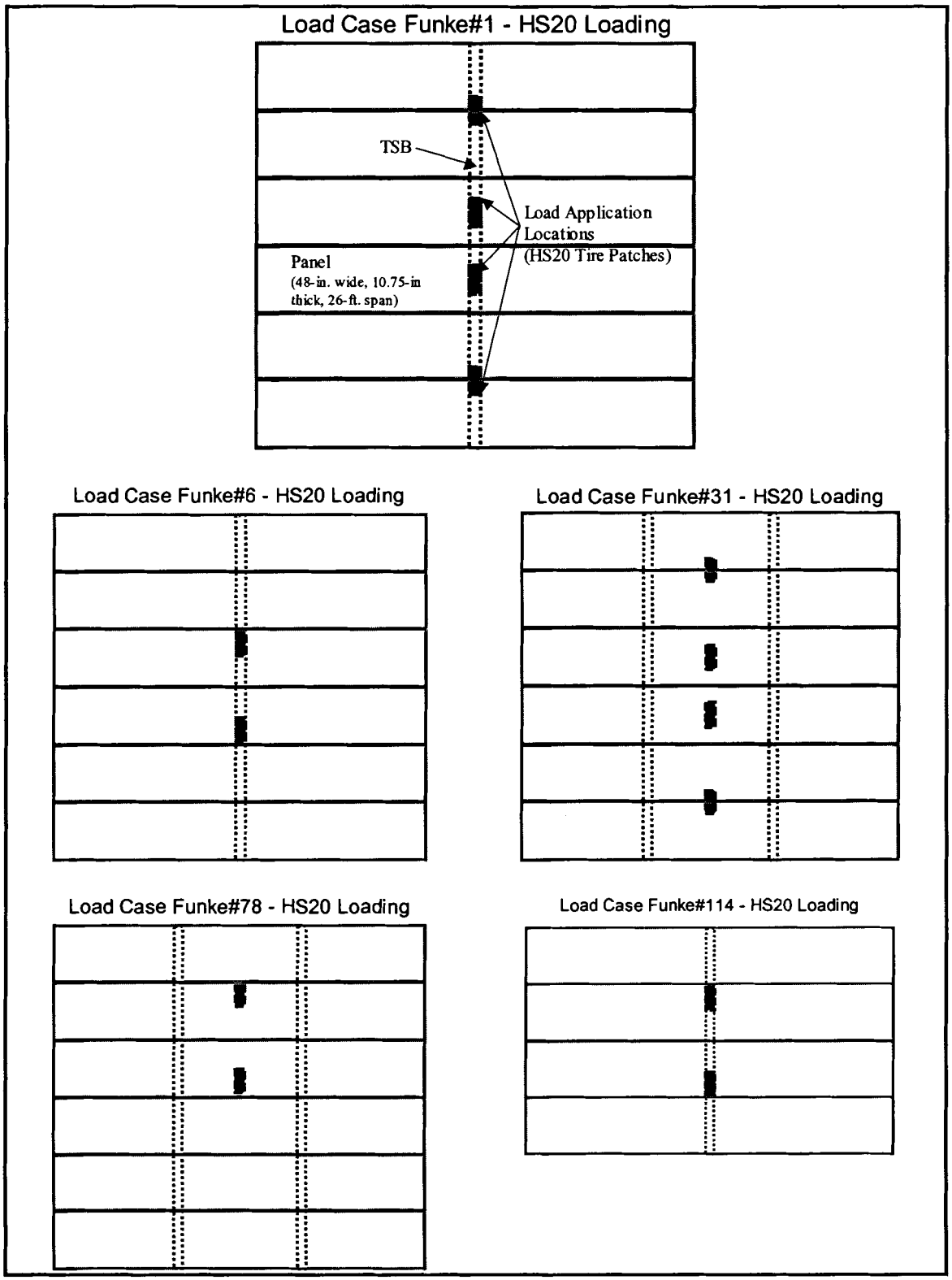

Figure 2.4 Bridge configurations and load cases tested by ISU

and the wood failed, splitting locally at the connector. Under the bearing edge of the aluminum connector the wood failed as well, being crushed. The strains measured in the TSB during one of these tests (Funke#6) where the stiffener failed showed bending stresses 40% greater than allowable (Wood Handbook 1974).

The first test where TSB splitting failure occurred was Funke#6. Loading in the test placed a single axle of one truck centrically on a 6-panel bridge (Figure 2.4). This placed both wheels at panel edges directly above the single stiffener, thus placing the TSB under its critical loading. The loading had not reached its full AASHTO HS20-44 loading of 16 kips per wheel when the failure occurred. Failure occurred when the loading was between 12 and 16 kips per wheel. ISU calculated that the failed connections carried approximately 4.2 kips (+/- 0.6 kips) and 2.2 kips (+/- 0.3 kips) of tensile force at TSB failure. Allowable bearing forces over the 6.4 in^2 of bearing area of connector on the panel would have been 2.30-4.93 kips (compression perpendicular to grain at proportional limit for interior north douglas fir was 360 to 770 psi) (Wood Handbook 1974). Thus the crushing failure may be explained by the published bearing values. Published maximum tensile strength perpendicular-to-grain for interior north douglas fir were 340 – 390 psi (Wood Handbook 1974). TSB perpendicular-to-grain tensile stresses exceeded these maximums, causing splitting failures (Funke 1986).

A similar TSB failure occurred in Funke#31 (Figure 2.4 for loading configuration). There were two transverse stiffeners connected to the panels through aluminum brackets for this test. Failure occurred in both TSB at the same locations as in Test #6. Load at failure was 13.5 – 14.0 kips per wheel. Forces in the failed connections of the instrumented TSB were 2.38 kips and 1.49 kips, comparing well to the allowable

bearing forces. Using a finite element model, forces in the failed connections of the un-instrumented TSB were calculated to be 30% greater than those in the other TSB (Funke 1986).

With more than a single stiffener used, critical (that which caused maximum TSB bending stress) loading for the TSB occurred when only a single truck was on the bridge with a wheel placed on a panel edge. In a test with the through-bolt connections (Funke#78), high strain was measured a six-panel, two-TSB bridge with a single axle of a HS20-44 truck loading the bridge. See Figure 2.4 for loading configuration. The same loading configuration and connectors, but with three TSB, resulted in a maximum measured strain of only 2.4% less, an insignificant reduction. ISU determined that the stiffeners may have experienced a maximum bending stress of twice the allowable (Funke 1986).

ISU found that relative panel movement is highly dependent on connection type/stiffness. As compared to aluminum bracket connections, through-bolts connections greatly reduce relative panel movement (Funke 1986). This reduction in relative movement between adjacent panels is important to limit or eliminate cracking in the wearing surface applied to the bridge. Relative panel movement should be limited to 0.10 inches for asphalt wearing surfaces (Ritter 1990).

2.3.2 Analysis of Longitudinal Glulam Deck Bridges

It has been shown that longitudinal glulam deck bridges can be modeled using the finite element method (Sanders *et al.* 1985; Funke 1986; Hajdu 1994; Kurain 2001). Evans at Weyerhaeuser (Funke 1986) and Sanders *et al.*, Funke, Hajdu, and Kurain at

ISU have all successfully modeled these bridges analytically. The validated models were then used for parametric studies to further analyze and study the specific aspect of interest under study.

As reported by Sanders *et al.*, Evans found only a slight sensitivity of stiffener beam size on transverse load distribution behavior (1985). Funke reports that Evans recommended analysis of stiffener beam stresses using his analytical stiffness-method-based model (Funke 1986) rather than selecting an empirically-designed TSB.

Funke's model used thin plate elements for the panel, beam elements for the TSB, and beam elements with only axial stiffness for the panel-to-TSB connections. The connections were located at their actual location even though the mesh was 48-in. by 52-in. Funke based his convergence on midspan deflections. A rigid beam was included in the panels at midspan to all the connection to be accurately located loaded with only vertical loads. The connections assumed linear tension behavior of 80 kip/in and 150 kips/in for aluminum bracket and ¾-in. through-bolts respectively. The initial analysis of a bridge was run with connections modeled with the tensile behavior. Then, any connection that was in compression had its properties changed to model the bearing between the panel and the TSB as a very stiff connection. Loading was based on tributary area (Funke 1986).

Sanders' and Funke's objectives were to develop the load distribution factor for bending and to verify the adequacy of the design methodology of the longitudinal glulam deck panels. They accomplished this through parametric studies using their validated finite element models. Sanders *et al.* found that connector stiffness had a significant effect on load distribution; the stiffer connectors caused greater distribution of load to

adjacent panels. Since a survey of the literature showed minimal load distribution sensitivity of stiffener beam size, they used a single TSB size (5 inches by 7 inches) for the analytical study. They also investigated the effect of panel width on distribution behavior. They found a slight sensitivity to panel width (Sanders *et al.* 1985). They also varied bridge span, deck thickness, and stiffener beam spacing. Single and multiple span bridges were analyzed all using HS20-44 live loading. They found that reduced stiffener spacing while not significantly affecting load distribution, did reduce relative panel movement. TSB flexural stiffness did not significantly affect load distribution (Funke 1986). Funke did not perform a parametric study with his analytical model.

Hajdu's finite element model consisted of thin plate elements for the panels, beam elements for the TSB, and beam elements with only axial stiffness for the connections. Hajdu's model converged with a mesh size of 48-in. by 52-in. Connections were located at panel edges minimizing the high stress regions of the TSB. Loads were placed at nodes using the contributory area method (Hajdu 1994).

Hajdu's finite element model was part of a study whose purpose was to determine bridge dynamic characteristics and behavior of the bridge-vehicle system, as well as shear distribution criteria. One conclusion pertinent to this thesis is that relative panel deflection in dynamic testing is within 5% of relative panel deflection from static tests (Hajdu 1994). This is important because it can therefore be concluded that the longitudinal cracks often found in the wearing surfaces of longitudinal glulam bridges may be explained by the calculated relative panel displacements determined by static loading.

Kurain's finite element model included bridge curbs increasing the stiffness of the outer panels and increasing observed TSB bending stresses. His model converged with a finer mesh (12-in. by 18-in.) than the others since he considered TSB bending as well as midspan deflections for convergence. Although Kurain's model includes the important aspect of curbs, their effect is magnified because of the rigid connections he used for the curb-to-panel and panel-to-TSB connections. Both types of connections had very high axial and flexural stiffness. He used an energy-equivalent loading methodology (Kurain 2001).

Kurain developed a model using ANSYS, creating a pre and postprocessor for the program to simplify its use. Kurain included curbs in his finite element model and connected the panels to the stiffeners with rigid links as connections. Kurain found that the panel longitudinal modulus of elasticity (MOE) and the curb size significantly affected bridge response. Kurain recommended that since MOE will vary within a species and over time, a unspecified range of MOE should be considered in the analysis rather than using a single value (Kurain 2001).

2.4 Summary

2.4.1 FRP-Glulam Research

FRP can significantly improve performance of glulam beams and panels, however the FRP must be durable in order to safely capitalize on those benefits. After the project reported in this thesis had already begun, it was found that, without some protection, the PRF wet-layup FRP used in this study may not show sufficient environmental durability in laboratory testing (Battles 2000, Iqbal 2000, Wood 2000). Battles showed that

degradation decreased when a polyurethane coating, such as was used in the study reported in this thesis, was used to protect the FRP (Battles 2000). The vinyl ester/E-glass FRP used to reinforce transverse deck panels in Xu's work (2001) is an alternative to the PRF wet-lay-up FRP used in the study reported in this thesis.

2.4.2 Longitudinal Glulam Deck Bridges Research

Although load distribution has been extensively researched, the panel-to-TSB connection and TSB behavior is not well understood. However, some insight to their behavior and interaction with the panels can be gleaned in relevant findings from the literature review. It was repeatedly found that aluminum bracket connections could split stiffeners when overstressed (Hale 1978; Funke 1986). If this splitting failure were to happen in the field it is not likely that it would be immediately noticed. It has been recommended that aluminum brackets no longer be used for panel-to-TSB connections, since when aluminum brackets are used, a connection force as low as 1.49 kips may cause failure in a 4.5 inch by 6.75 inch TSB (Funke 1986). On bridges with 48-inch wide panels, critical loading for the TSB occurs when a wheel is placed as close to the panel edge as possible (Funke 1986). The TSB can be overstressed in bending when connected to the deck with aluminum brackets and critically loaded (Funke 1986). The published literature did not report any research or concerns of the TSB being overstressed in shear. Previous research has repeatedly highlighted the need for further research into the behavior of the TSB. The bending overstress has been reported, but the extent of possible overstress, the consideration of overstress for TSB shear, and the design

recommendations necessary to prevent the overstress have not been researched. This thesis is an attempt to address the research need.

A summary of relevant parameters as determined from previous experimental and analytical studies of longitudinal glulam deck bridges can be found in Table 2.1. Often the parameter range was not given in the literature; in these situations the Table lists "Not specified" in the "Range Considered" column. Since most of the previous research has focused on load distribution among panels, the sensitivity to that parameter is listed. If the Load Distribution Sensitivity is "Significant," the parameter significantly affects load distribution. If it is listed as "Not significant," the load distribution does not substantially change as the parameter varies.

The analytical models of longitudinal glulam deck bridges have not looked in detail at the TSB. None have modeled the connections nonlinearly, which is more accurate than the linear approximation. All previous models have used relatively coarse meshes, and not modeled bearing separately or at locations other than where the connection elements are located. When the curbs were modeled, they were connected with rigid links making the deck and curb composite. These issues indicate a need for an improved finite element model.

Table 2.1 Parameters that affect longitudinal glulam deck bridge response as reported in the literature review (Hale 1978; Sanders *et al.* 1985; Funke 1986; Hajdu 1994; Kurain 2001)

Parameter	Range Considered	Load Distribution Sensitivity[1, 2]	Other Significant Sensitivities[2]	Researcher
Live loading	Static & dynamic HS20-44	Significant	Not signif. to relative panel displacement (RPD)	Kurain
Bridge span	9 – 33 feet	I-I	None reported	Sanders
Bridge width/ # of panels	16 – 40 feet	Consistent range of trans. distrib.	None reported	Sanders
Curb size	Not specified	Significant	None reported	Kurain
Panel width	42 – 54 inches	Slightly signif.	None reported	Sanders
Panel thickness	6.75 – 12.25 inches	Significant	None reported	Sanders
Panel longit. MOE	Not specified	Significant	None reported	Kurain
TSB size	Not specified	Slightly signif.	None reported	Evans
TSB spacing	Not specified 6.5 – 13 feet	Not significant Slightly signif.	RPD – I-I RPD – I-I	Sanders Funke
TSB flexural stiffness	"Practical range"	Not significant	None reported	Sanders
Connection type/ stiffness	Aluminum bolt, seated beam, through-bolt, C-clip	I-I (conn. stiffness)	RPD – D-I	Hale, Sanders, Funke
Connection bearing area & Through-bolt diameter	1.77 – 16 in^2 1/2 – 7/8 inch	Not explicitly tested	Conn. stiffness – I-I	Hale
Bolt diameter used with C-clip connection	1/2 & 5/8 in.	Not explicitly tested	Not significant to conn. stiff.	Hale

1. Typically, if there is an increase in load distribution due to an increase of the parameter, maximum midspan panel deflection will correspondingly decrease.
2. I-I: Factor (load distribution, relative panel movement, etc.) significantly increases as the parameter increases within the range. D-I: Factor significantly decreases as the parameter increases within the range.

If a response is significant, the bridge response is affected by the parameter.

Chapter 3

MILBRIDGE MUNICIPAL PIER

3.1 Introduction

This chapter discusses the Milbridge Municipal Pier that was built as a demonstration project using the technology developed in this study. The chapter is divided into the description of the pier, its design, and components, the methodology used for reinforcing the glulam panels, the construction of the pier, the wearing surface system used on the pier, the load testing of the pier, the pier performance and durability, the cost of the pier superstructure, and conclusions and recommendations.

3.2 General Description

The Milbridge Municipal Pier is situated on coastal Maine's Narraguagas River and serves the community in its commercial fishing and recreational boating and fishing activities. The L-shaped, 167-ft. long, 16-ft. wide pier has seven spans of approximately 21.5 feet each (Figure 3.1). Designed for AASHTO HS20-44 loading, each simple span consists of four vertically-laminated glulam panels reinforced using wet-impregnated FRP technology. The pier is unique in that the FRP-reinforcing is specified only in the most crucial location. The FRP reinforces the middle two-thirds of the panel on the tension side. The wearing surface system used on the pier also makes the project unique.

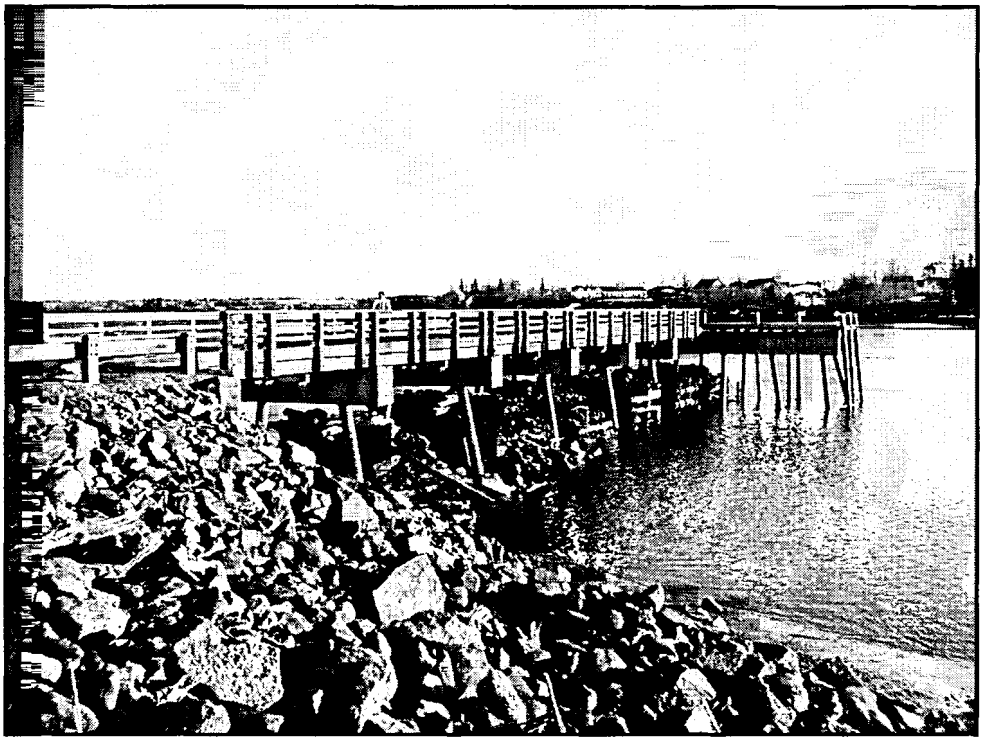

Figure 3.1 Milbridge Municipal Pier after reconstruction

The Milbridge Municipal Pier had long been in need of repairs and prior to UMaine's involvement, the town had obtained bids for reconstructing the pier with a prestressed concrete deck. That bid proved too costly, and the town turned to The University for help. The location was excellent for a demonstration project. Highly visible, it offered a chance to examine the issues that would be faced during multiple panel reinforcement, during construction, and during long-term exposure to a marine environment. The town of Milbridge has maintenance and capital-improvement responsibility of the pier. Funding for the reconstruction of the pier was from the Federal Highway Administration through Innovative Bridge Research and Construction Program (IBRC), the MDOT, the Maine Department of Economic and Community Development, and the Town of Milbridge, Maine.

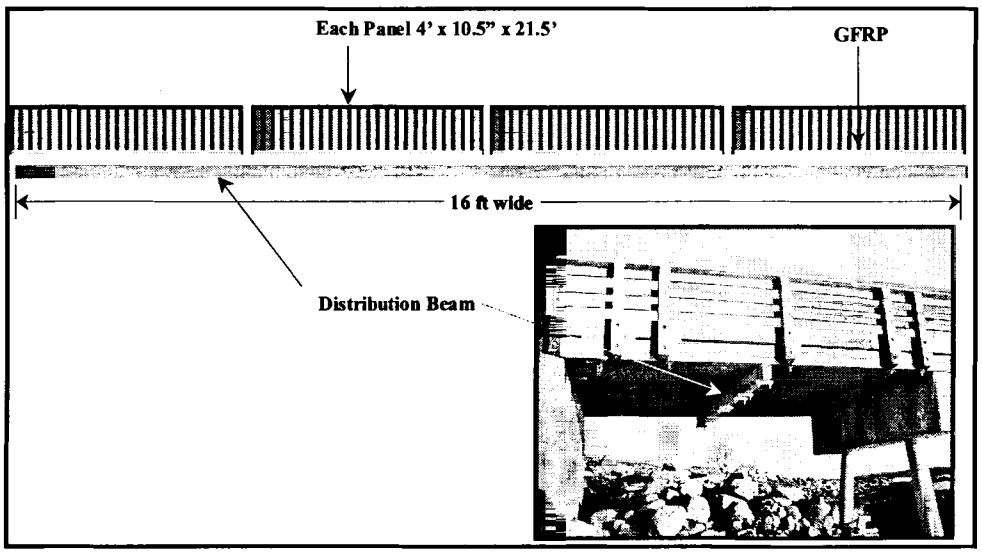

Figure 3.2 Section of span of the Milbridge Pier

3.3 Milbridge Municipal Pier Superstructure Design

The Milbridge Pier superstructure was designed as a longitudinal glulam deck bridge according to *AASHTO Standard Specifications* (AASHTO 1996). Live loading was specified to be HS20-44, as required by the MDOT. Woodard & Curran, Inc. of Bangor, Maine, designed the pier substructure and The University of Maine designed the superstructure. The MDOT was the Engineer of Record on the project. The MathCad worksheet developed for the superstructure design, design specifications, and drawings for the Milbridge Pier are given in Appendix A. The pier was designed with consideration both for structural strength and for durability.

3.3.1 Durability Design

The harsh marine environment can cause significant deterioration in a very short time if preventative measures are not taken. The metal components must be corrosion resistant, and wood components, if not naturally durable, must be treated with

preservative to retard biological deterioration. Chromated Copper Arsenate (CCA) preservative was used for the panel and TSB laminations prior to lamination. The literature review and the research that was ongoing at the time of panel fabrication indicated a need to coat the FRP with a polyurethane coating for environmental protection. More discussion of each aspect of the durability is provided in this section and its subsections. The pier will be monitored for a period of five years from completion with particular emphasis on FRP degradation and the FRP-wood bond integrity. To further retard biological deterioration of the wood an impermeable membrane covers the pier deck.

3.3.1.1 Wood Durability

3.3.1.1.1 Preservative

CCA preservative was used for all timber. CCA is a waterborne preservative that has been used since the 1940's. CCA, coal-tar creosote (creosote), and pentachlorophenol (penta) are the common preservatives for southern pine timber bridges. Oil-borne preservatives such as creosote or penta are preferred over waterbornes. Oil-borne preservatives help seal the wood, reducing the moisture transport through the wood and thus shrinkage and swelling cracking damage. However, use of creosote or penta was not possible in this project due to restrictions placed on marine structures in Maine. The marine environment coupled with the fact that it is not uncommon to have water splashing on the bottom of the deck, restricted preservative choice to CCA. However, as can be seen from Figure 3.3, the use of a waterborne preservative resulted in checking from the shrinkage and swelling stresses when the deck had to go through the winter unprotected.

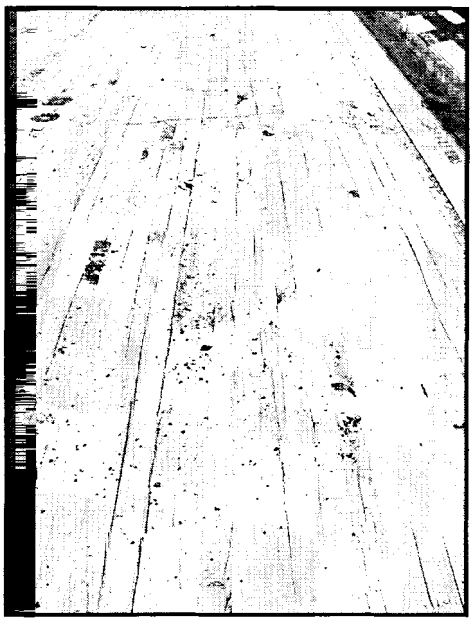

Figure 3.3 Cracks in pier deck after 6 months of exposure

MDOT typically specifies CCA preservative retention levels of 2.5 pounds per cubic foot (pcf) for wood in marine environments. However due to the preservative's potential toxicity to humans, wood with such a high CCA retention level should not be highly contact-accessible. Therefore the railings have a 0.4 pcf retention and the curbs have 1.0 pcf CCA retention. For the Milbridge Pier, all glulam laminations were treated to 0.4 pcf retention prior to panel fabrication. Preservative treatment of laminations before gluing provides more and better preservative coverage, however, it limits the retention level. The glulam manufacturer was reluctant to use 0.6 pcf CCA retention prior to treatment because of potential for poor adhesion between the wood laminations.

Preservative treatment affects both the glulam manufacturing and FRP-application. With CCA preservative, the individual laminations must be treated and returned to 16-19% moisture content prior to gluing. Because of extractives, southern pine can be difficult to glue even without any preservative to complicate issues, and CCA increases poor adhesion difficulty. Sentinel Structures, the fabricator for the panels used

in the Milbridge Pier, would not glue laminations with CCA-retention levels higher than 0.4 pcf. The treated wood also increased difficulty of bonding the impermeable membrane and wearing surface to the pier deck.

3.3.1.1.2 Impermeable Membrane and Wearing Surface

An impermeable membrane was needed to minimize moisture transport in the wood structural members and a wearing surface was needed to protect the glulam deck from damage and the impermeable membrane from perforation.

Due to the unique possible use and environment of a working pier, the wearing surface needed for a marine pier has to meet a more stringent set of criteria than the wearing surface needed for a bridge. The pier criteria include suitability for vehicular traffic, skid resistance, water impermeability, petroleum-product spill resistance, flexibility, impact resistance, and adhesion to the substrate. Since the pier is a working pier the wearing surface needed to be suitable for vehicular traffic and provide skid resistance for both vehicles and pedestrians. Durability of the superstructure requires provision of an impermeable membrane on the deck surface. A working pier is often used for transfer of petroleum products between containers, thus requiring a system that is durable under the petroleum-product spills. Asphalt and petroleum-based membranes failed to meet this criteria; and although many polymer membranes do satisfy the petroleum-spill resistance criteria, the system needed both flexibility and impact resistance as well. The flexibility was necessary over the panel-to-panel joints where relative panel displacements could cause cracking of an overly stiff system and thus allow water passage to the timber deck below. Flexibility is also necessary for the membrane to remain impermeable through the wood's hygrothermal cycling. Working

piers often have heavy objects with sharp corners dropped on them, which would damage the deck and possibly penetrate glulam preservative treatment. Of course, the system needed to adhere to the substrate, CCA-treated southern pine. Additionally, it was found that the panel thickness varied considerably (Figure 3.4), and that for aesthetic reasons as well as safety, the wearing surface system should be self-leveling and fill any gaps from checking or knots in the industrial grade glulam.

After thorough testing of a several systems, the CIM 1000 membrane from CIM Industries, Inc. of Menomonee Falls, Wisconsin, combined with the Transpo T-45 epoxy overlay from Transpo Industries, Inc. of Berwick, Pennsylvania, was chosen for the Milbridge Pier wearing surface system. The impermeable CIM 1000 membrane adhered to the CCA-treated southern pine glulam deck and provided flexibility and petroleum-product spill resistance. It also could have provided a surface suitable for skid resistance and vehicle traffic. Although it had some self-leveling and gap-filling characteristics, the membrane was not thick enough to provide a smooth surface. The CIM 1000 layer alone did not provide adequate impact resistance. The T-45 epoxy overlay gave the necessary impact resistance and leveling. It also bonded to the aggregate seeded in the CIM 1000 membrane, uniting the two systems. The T-45 provides a better and longer-lasting wearing surface for vehicle traffic, has petroleum-product spill durability, and is impermeable when intact. The T-45 system alone was not adequate since it is very stiff and cracks under stresses from hygrothermal cycling (Figure 3.5) and relative panel displacement. The T-45 system alone does not adequately bond to CCA-treated SP. Thus, the combined systems were the wearing surface system chosen.

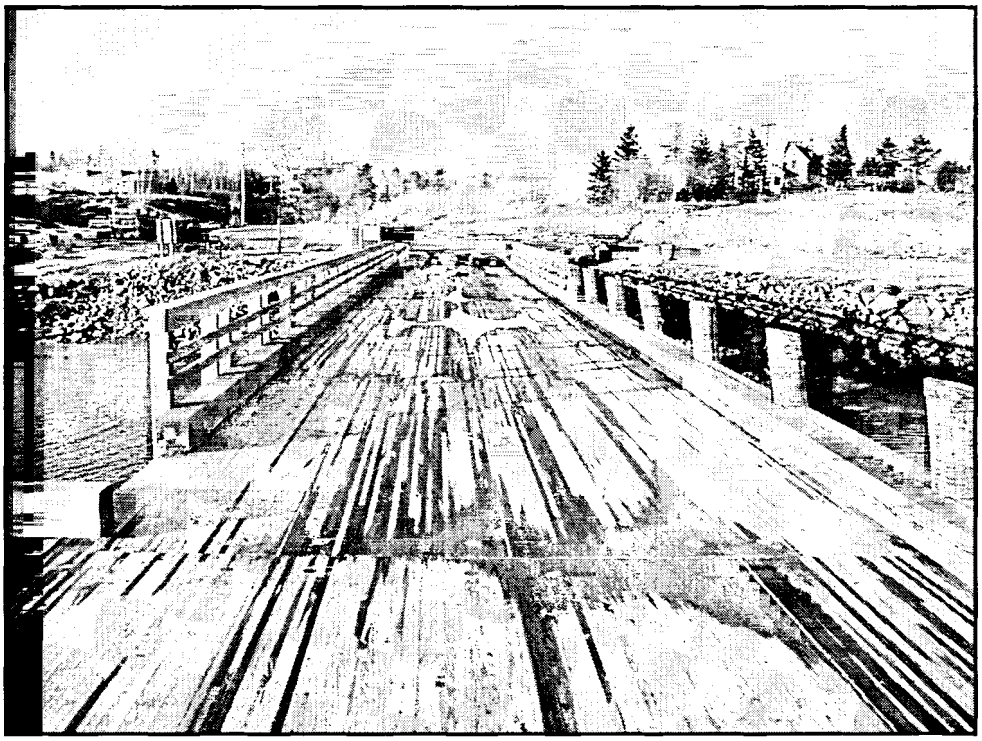

Figure 3.4 Variation in panel thickness shown by water pooling on pier deck

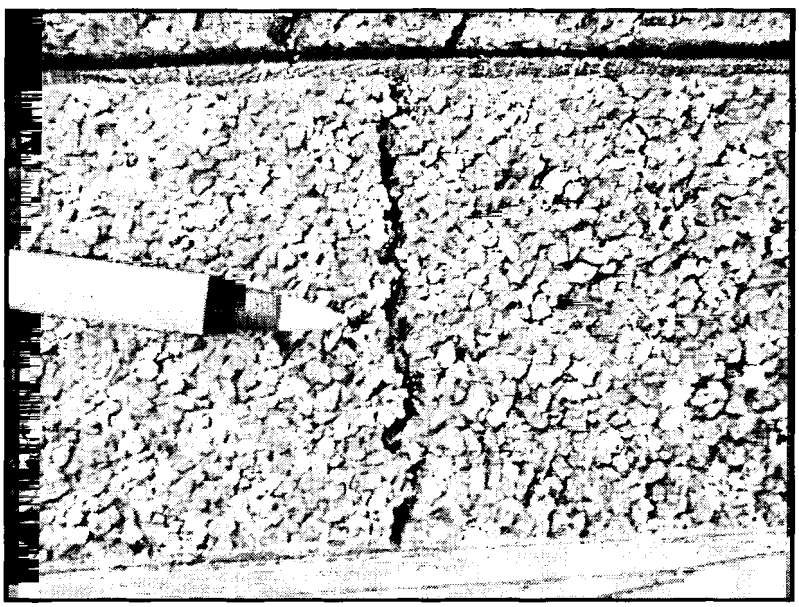

Figure 3.5 Cracks in T-45 from hygrothermal cycling

As part of another UMaine study, Novotoney performed a more extensive testing of wearing surfaces, increasing the number of materials tested and the battery of tests. Out of the systems he tested, the CIM 1000/T-45 system was the only one to meet all criteria (Novotoney 2001).

3.3.1.2 Hardware and FRP Durablitity

The connection hardware was hot-dipped galvanized in accordance with ASTM A153 (ASTM 2000a) for corrosion resistance. The FRP was coated with a polyurethane coating for environmental protection as recommended by previous research (Battles 2000).

3.3.2 Structural Design

Due to the experimental nature of the project and the lack of data on long-term performance of the FRP, the structure was designed without relying on the strength of the FRP. Since deflection controlled the design, however, it was decided to use the FRP for deflection design. No allowable limit is specified in the AASHTO design (AASHTO 1996).

The superstructure was designed according to the AASHTO specifications. The southern pine panels specified were all 10.5-inches thick and varied in length according to the span. One percent FRP reinforcing for the middle two-thirds of the tension-side of the panel was specified to meet a L/500 deflection service limit. The stiffeners were also made of southern yellow pine glulam and specified to be 6.75-inches deep by 4.5-inches wide. The beam's stiffness factor of 196000 kip-in^2 was over twice the AASHTO-

required minimum stiffness factor of 80000 kip-in^2. Glulam fabrication specifications are given in Table 3.1.

3.3.3 Material Specifications

3.3.3.1 Glulam Panels and Beams

The laminations for the panels and stiffener beams were specified as southern yellow pine (*Pinus* spp.) glulam. The southern yellow pine species group was selected partly due to the preservative used and partly due to time constraints. Four-foot wide panels were used since the pier was to be a single lane. The design properties of the vertically-laminated glulam panels are given in Table 3.1. Simple spans simplified design, reinforcement, and construction.

3.3.3.2 FRP Specifications

The FRP used is a Phenol Resorcinol Formaldehyde (PRF) adhesive, reinforced with unidirectional E-glass, fabricated by wet lay-up, consolidated by mechanical pressure, and cured at ambient temperature. The PRF was a two-part resin (Resorsabond® 4242 Resin and Resorsabond® 4554 Hardener) manufactured by Georgia-Pacific Resins, Inc. of Decatur, Georgia, with a 45-minute pot life. PRFs are well known for their ability to achieve good bonds to wood for glulam with exterior applications. It is a low-cost resin system for FRP, as well, and had already been structurally tested for reinforcing beams (Foster 1998). Another benefit of PRF FRP is the familiarity that glulam manufacturers already have with the resin, allowing easier and faster implementation of FRP-glulam into the engineered wood industry. The unidirectional E-glass fabric (VEW260v2003) was 26 oz/yd^2 and produced by Brunswick Technologies,

Inc. (now St. Gobain) of Brunswick, Maine, in 47-inch wide rolls. The viscosity of the PRF required wet impregnating the E-glass fabrics prior to wet layup. The actual FRP fabrication and glulam reinforcing processes are described later in this chapter.

3.3.3.3 Panel-to-TSB Connections

Seated-beam connections with 5/8-inch-diameter threaded rods were chosen to allow for differential movement between the panels and stiffeners due to hygrothermal cycling. The ASTM B7 threaded rods had 3-inch diameter, ¼-inch thick washers bearing on the glulam panels. For the bottom of the rod, connecting them to the 2-inch by 2-inch by 3/16-in thick, 10-inch long steel tube that the stiffener was seated on, standard galvanized washers and nuts were used (Figure 3.6).

3.3.3.4 Panel-to-Pile Cap Connection

The pile cap and deck panels are connected by 1-inch diameter galvanized A325 threaded rods. A neoprene pad is placed between the panel and the pile cap to prevent direct contact of the wood and concrete that can allow moisture transport into the wood and cause deterioration.

3.4 Panel Fabrication and Reinforcement

The panels were fabricated by Sentinel Structures of Peshtico, Wisconsin. They were then shipped to the AEWC Structures Laboratory for reinforcing.

Table 3.1 Specifications for Milbridge Pier glulam

Glulam Panel Properties Glue laminated timber shall be manufactured from species and grades of lumber which will produce design values equal to or exceeding the following when loaded parallel to the wide faces of the laminations: Bending (F_b) = 2000 psi Shear parallel to grain (F_v) = 90 psi Modulus of elasticity (E) = 1,700,000 psi Compression perpendicular to grain ($F_{c\perp}$) = 560 psi
Glulam Spreader Beam Properties Glue laminated timber shall be manufactured from species and grades of lumber which will produce design values equal to or exceeding the following when loaded perpendicular to the wide faces of the laminations: Bending (F_b) = 2400 psi Shear Parallel to grain (F_v) = 90 psi Modulus of elasticity (E) = 1,700,000 psi Compression perpendicular to grain ($F_{c\perp}$) = 560 psi

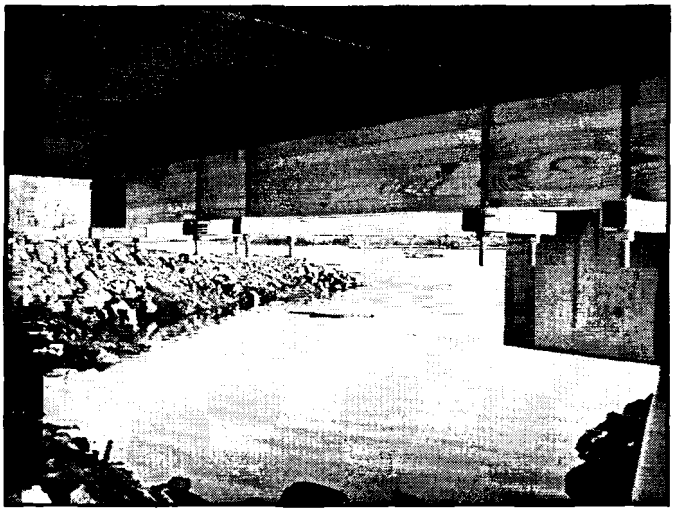

Figure 3.6 Seated-beam panel-to-TSB connection

3.4.1 FRP Application

A total 37 panels were reinforced with the FRP designed at UMaine. Thirty-three of the panels were used in the Milbridge Pier and four in the testing reported in Chapter 4. The FRP is three layers of a unidirectional E-glass fabric wet-impregnated with a PRF resin. During wet-impregnation, the fabric was impregnated with Georgia-Pacific Resorsabond PRF resin (Figure 3.7), and then placed the resin-impregnated fabric (wet-preg) onto the inverted glulam panel (Figure 3.8). Three layers of wet-preg were placed on each. After the final layer of wet-preg was placed, 35 pounds per square inch (psi) of mechanical pressure was applied through steel channels, threaded rod, calibrated torque wrenches, and another panel for uniform pressure distribution (Figure 3.9). The pressure was maintained for a minimum of eight hours, and the FRP cured under ambient conditions. The entire width of each panel and the central two-thirds of its length were reinforced (Figure 3.10). The cured FRP is 1/10-inch thick, giving a 1% reinforcement ratio by cross-sectional area to the panel. After the panels were removed from the clamps, the polyurethane protective coating was applied to the FRP.

One panel for the final span of the Milbridge Pier was six feet wide. This required adaptation of the mechanical clamping system (Figure 3.11). Four plies of wet preg were used to reinforce this panel. Given the difficulties that were faced and the fact that the 72-inch panel width is greater than the 42-54 inch range in the specifications, the extra wide panel and the three regular panels adjacent to it should probably have been 54-inch wide panels instead.

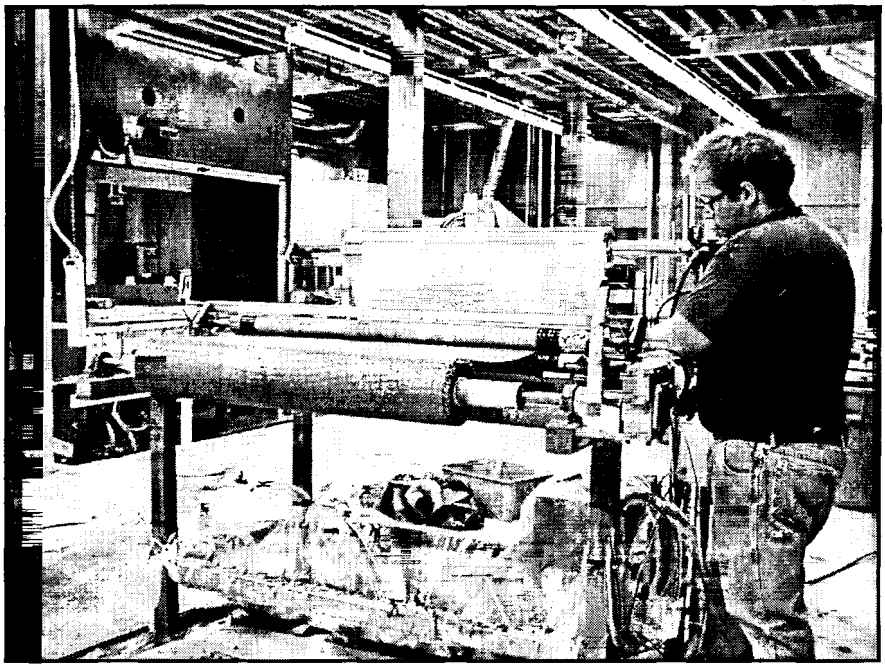

Figure 3.7 E-glass fabric impregnated with resin

Figure 3.8 Placing the a layer of wet-impregnated glass onto glulam panel for Milbridge Pier

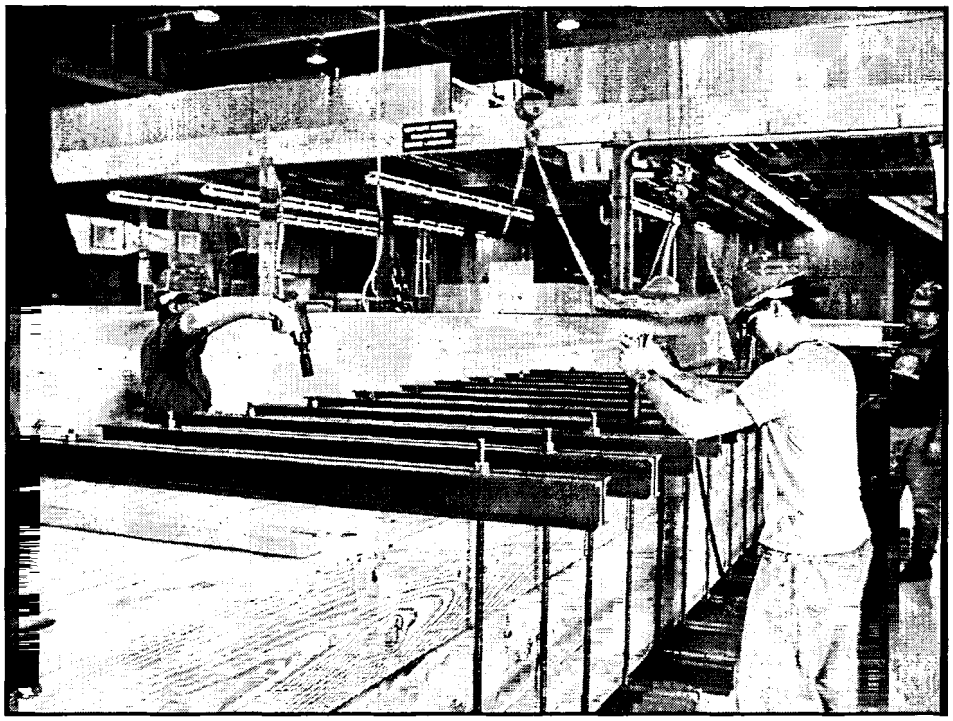

Figure 3.9 Reinforced panels are clamped for FRP consolidation and ambient cure

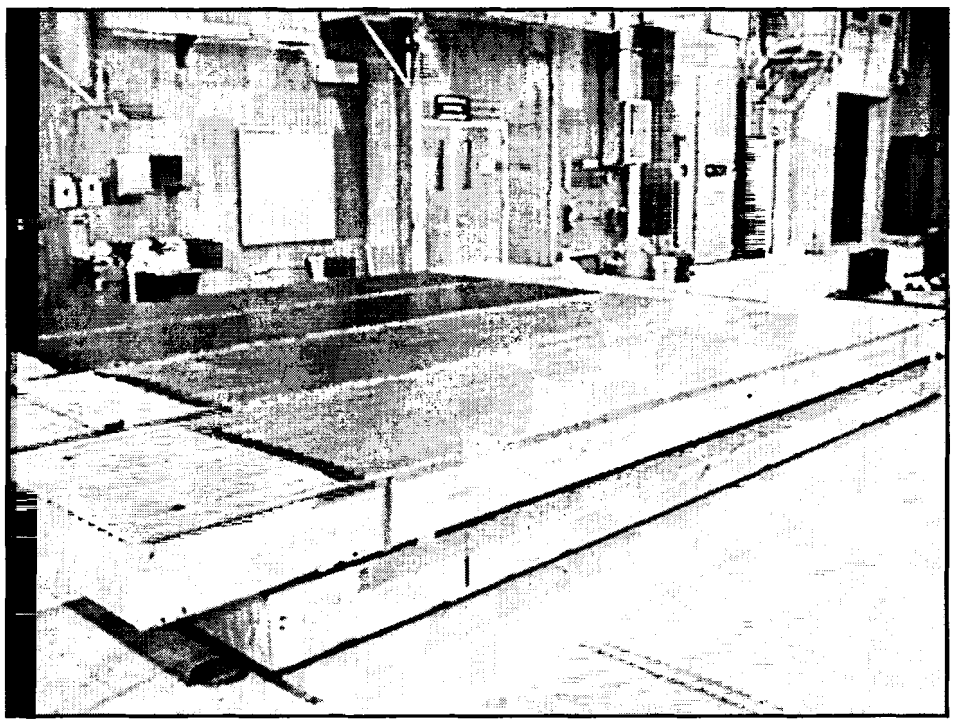

Figure 3.10 Cured FRP reinforcing the bottom/tensile side of the panels (panels are upside-down)

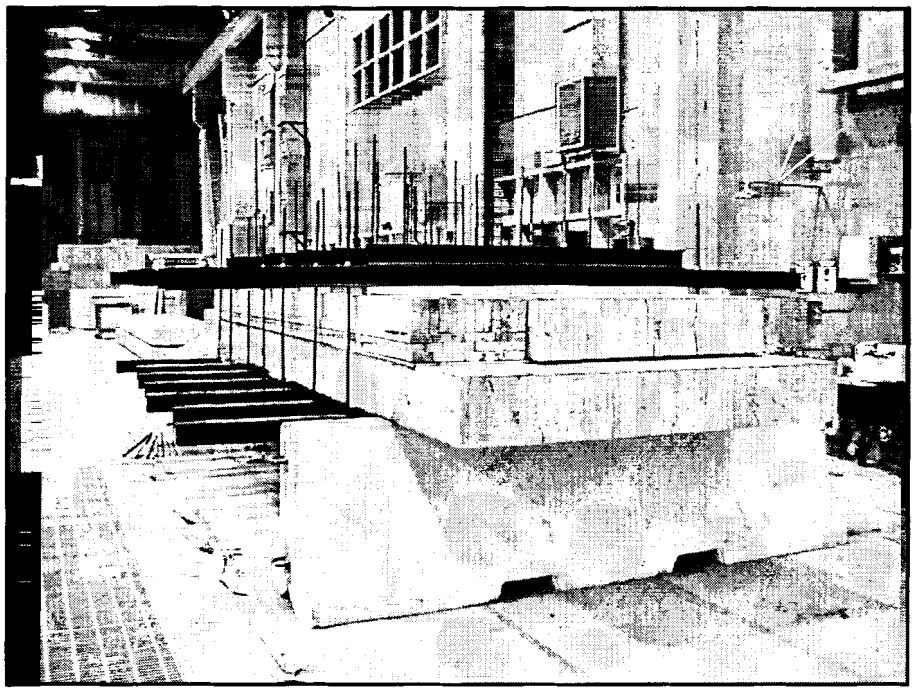

Figure 3.11 Clamping methodology modified for reinforcing the 72-inch wide panel

3.4.2 Comments on FRP System Used

To conclude this section, the advantages and disadvantage of the FRP system chosen for this study need to be noted. It has already been reported in Chapter 2 that this FRP performs well with regard to structural strength but performs poorly with regard to environmental durability if not protected. The FRP on the Milbridge Pier has not shown deterioration in the two years since construction. PRF is a low-cost resin system, making PRF-FRP-glulam a cost-competitive option for bridge construction. Additionally, the PRF resin is already familiar to glulam manufacturers increasing the ease of implementation of FRP-reinforced glulam into an existing facility. The resin's pot life is sufficient for a reasonable fabrication. One major disadvantage, which increases the rate of deterioration due to environmental forces and which weakens the FRP structurally, is

the shrinkage that occurs due to condensation reaction during curing. The glulam restricts the shrinkage, and, in a panel with a relatively thin FRP, longitudinal cracks are formed throughout the FRP (Figure 3.12). A chopped-strand-mat layer in the FRP may prevent the majority of cracking, but stresses would be developed and some damage may still occur with possible bowing of the panel. Fillers in the resin may prevent this shrinkage by absorbing the hydrolyzed water, but the filler may increase resin viscosity, forcing an alternative fabrication methodology. Overall, this FRP is not recommended for further exterior structural use until the environmental durability and shrinkage issues have been fully addressed.

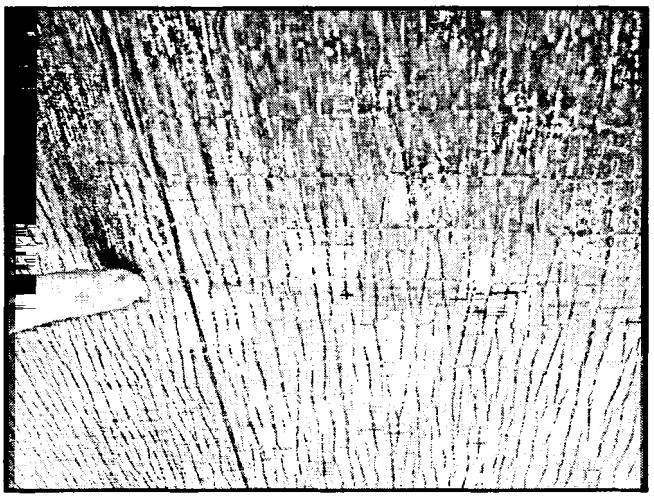

Figure 3.12 Longitudinal cracks in FRP from shrinkage

3.5 Construction

The Milbridge Municipal Pier was reconstructed in the fall of 2000 (September to December). Construction stopped during the winter and the impermeable membrane and wearing surface were placed in the summer of 2001. Construction was done by Prock Marine of Rockland, Maine. Construction went quickly and smoothly with few problems and showed that the FRP-glulam panels are a reasonable alternative to conventional

construction materials. A 2x6 (nominal), CCA-treated, No. 2 and better, southern pine board was placed on top of the stiffener as a spacer between the panels and stiffener. This board was needed due to insufficient thread length on the rods connecting the panels to the TSB. Due to the coldness and wetness of the fall weather, the wearing surface could not be placed until summer and the deck weathered the winter unprotected. The pier was not open to vehicular traffic until the wearing surface had been placed.

3.5.1 Substructure of Pier

The deck is supported on reinforced cast-in-place concrete pile caps. Each pile cap has two epoxy-coated steel pipe piles filled with concrete. Every other pier was anchored to the bedrock to resist lateral loading from boat impacts and ice loadings. On the final span, the two end piles on the piers shown in Figure 3.13 are the only anchored piles, giving the structure ten anchored piles. The second pier from shore to moved two to three inches toward shore upon removal of the concrete formwork. The probable reason for the movement was that the second pier was probably not anchored correctly and caused bending in the pile. The deck panels were not able to fit into place until the pile cap was forced back into place. The deck panels of the second and third spans were put into axial compression and tension, respectively.

Some pile caps experienced damage due to improper construction (Figure 3.13). The damage at location #1 and #2 (Figures 3.14, 3.15, and 3.16) may have been due to the improper anchoring as well. The damage at locations # 3 and #4 (Figures 3.17 and 3.18) may have been partially due to the hygrothermal cycling of the wood.

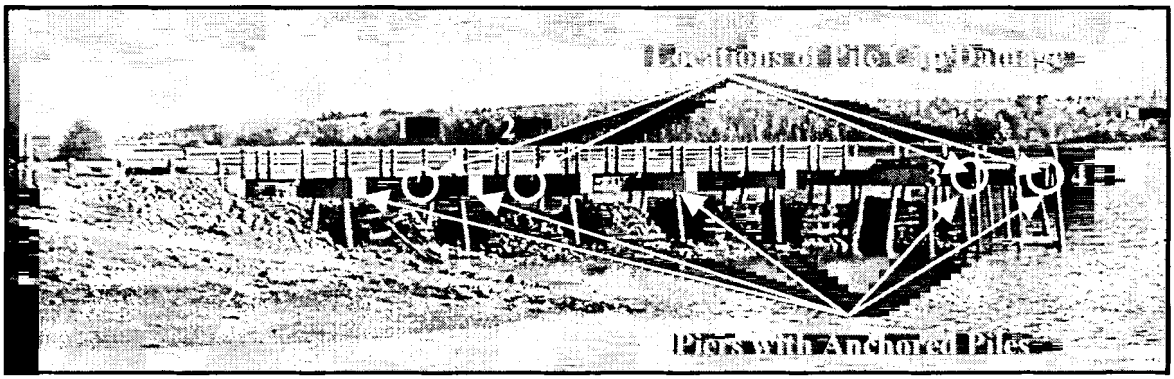

Figure 3.13 Location of piles anchored to bedrock and pile cap damage

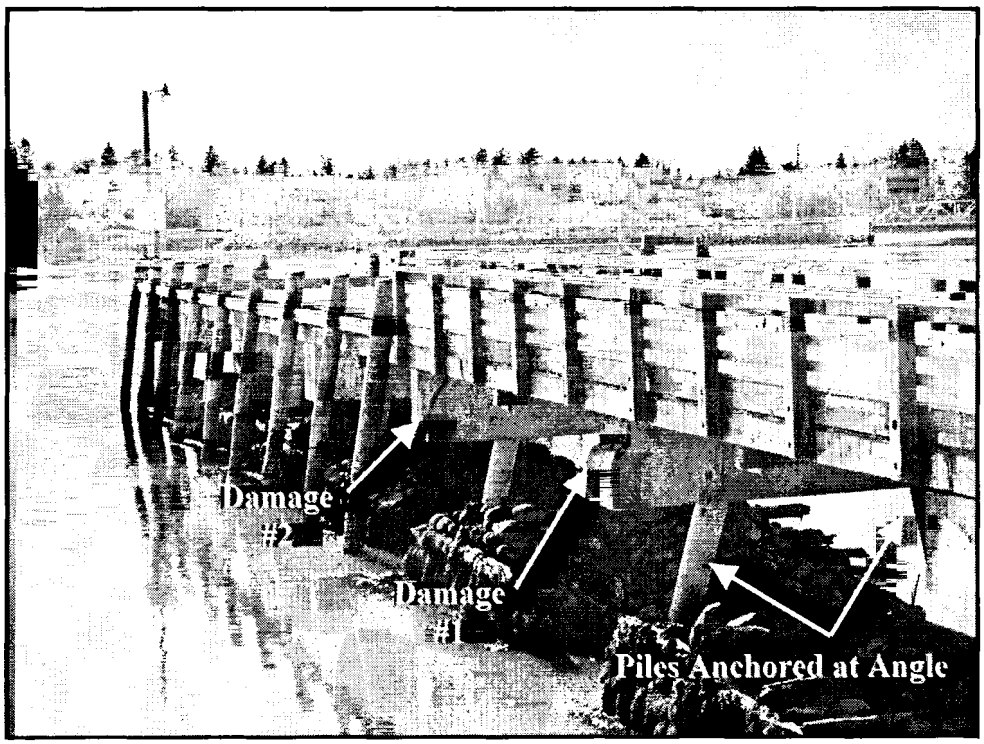

Figure 3.14 Pile cap damage due to improper anchoring of pile

Figure 3.15 Close-up of pile cap damage at location #1

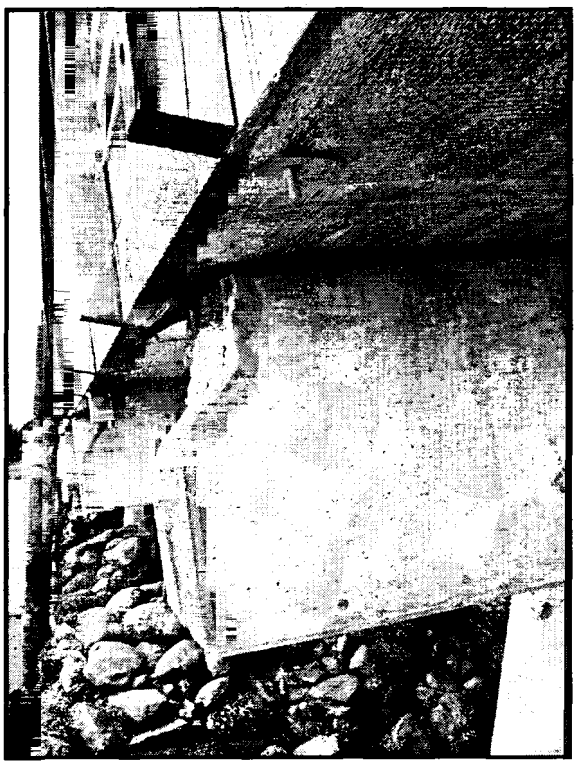

Figure 3.16 Pile cap damage at locations #1 and #2

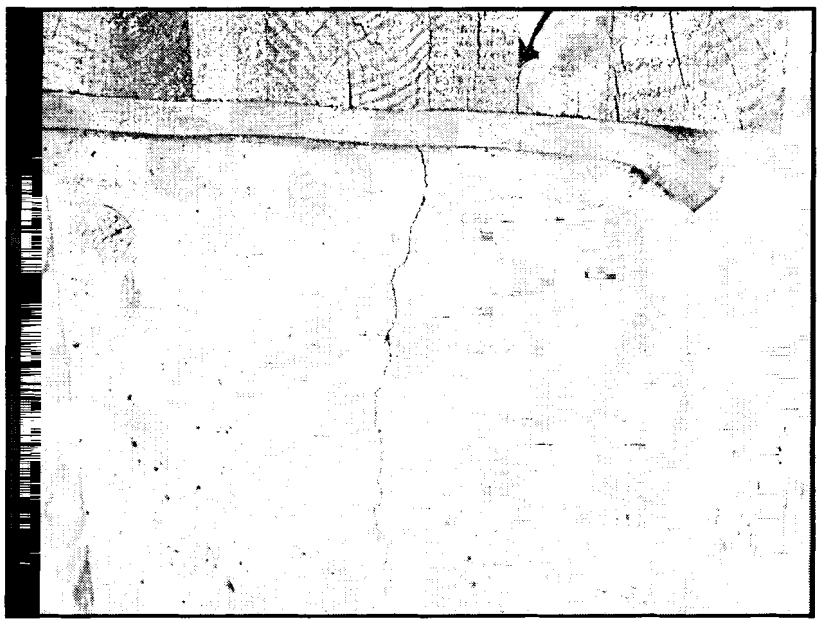

Figure 3.17 Close-up of pile cap damage at location #3

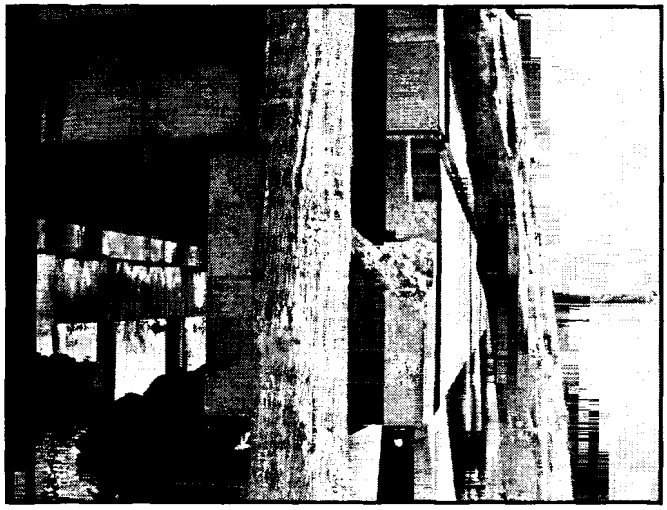

Figure 3.18 Pile cap damage at location #4

3.5.2 Superstructure Construction

One main advantage of the FRP-glulam deck design is its lightweight nature that can reduce construction costs. At approximately 3000 lbs. each, the FRP-glulam deck panels weigh only one-third as much as an equivalent prestressed concrete deck panel and were easily lifted into place for quick construction. Since the pier was completely reconstructed and a high-capacity barge crane was on sight, the cost savings of using a smaller crane were not realized.

The panels were lifted into place by the crane on the barge (Figure 3.19). Prock Marine did not report any difficulties with the panels and indicated a willingness to use them again. The panels on the last span were a tight fit, due to swelling that occurred while the panels were on site before placement. Due to weather conditions, the tops of the last panels were saturated with rain before placement.

During construction, some of the connections were over-tightened so that the wood was crushed (Figure 3.20). Finger-tight connections were specified, but differential thickness of the panels may have required tighter connections. Some of the connections

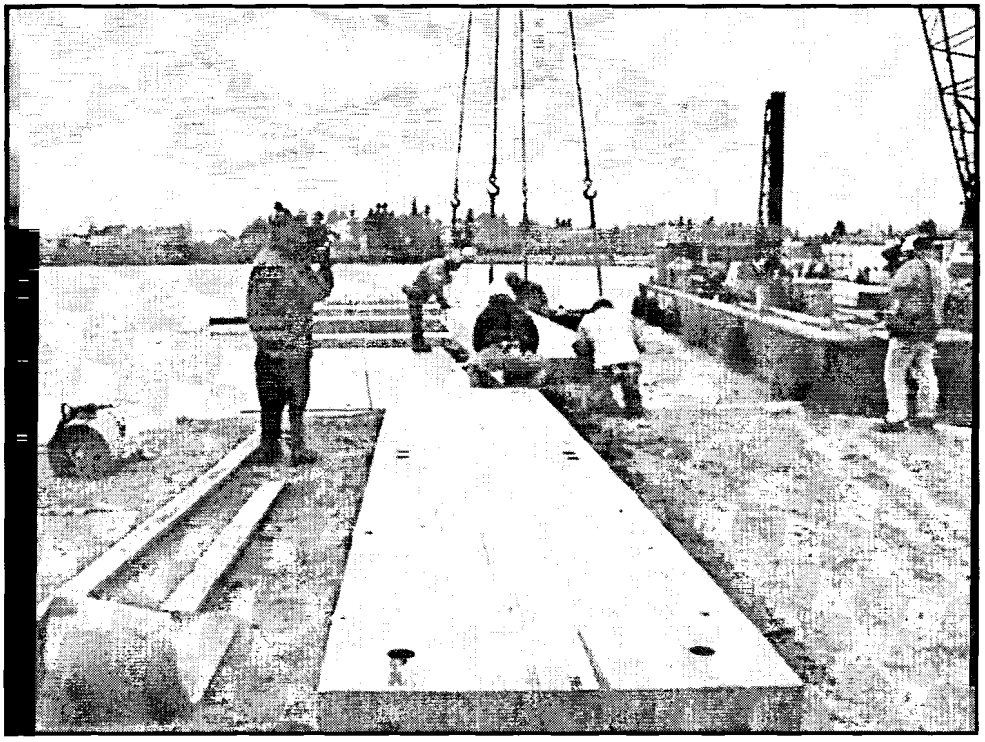

Figure 3.19 Panels moved into place by barge crane and aligned to the threaded rod anchored in the pile cap

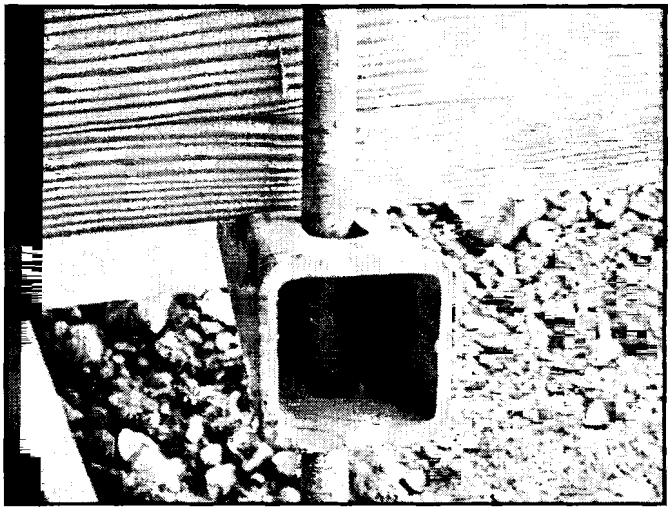

Figure 3.20 Some connections were tightened to point of crushing the TSB

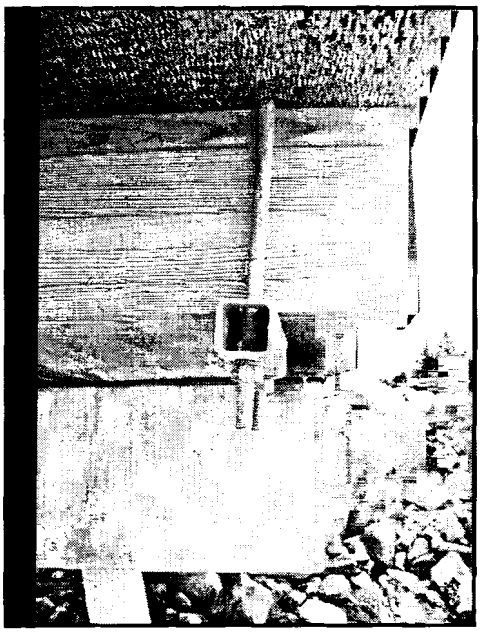

Figure 3.21 Some eccentricity and bending in the connection

were angled as well, due to the hole in the panel being drilled at an angle or poor construction practices. Epoxy (Transpo T-45 neat resin) was used to fill the countersunk holes for the panel-to-pile cap and panel-to-TSB connections.

3.5.3 Wearing Surface System Application

The cold and wet weather at the completion of the rest of reconstruction of the pier prevented immediate placement of the membrane and wearing surface. For placement of the membrane and wearing surface, the deck must have moisture content of 19% or less, and the deck and air temperatures have to be greater than 50 °F. Once these conditions were met, the entire wearing surface system was applied in four layers using the broom and seed method during the late spring once the wood deck had dried out and the weather was favorable. The CIM1000 membrane was applied in two coats: the first approximately 60 mils thick with no aggregate and the second approximately 30 mils thick and seeded with basalt Indag™ #8 aggregate provided by Transpo Industries. To apply the CIM1000 membrane or the T-45 overlay, the two product components, the resin and the catalyst/hardener, are thoroughly mixed. The product is then poured onto the deck and spread with a squeegee to a uniform thickness. The CIM1000 membrane cured in about an hour on the day of placement. A second, thinner layer of the CIM1000 was placed. Before the second coat of CIM1000 cured, the aggregate was seeded (gently and uniformly dispersed into the membrane by throwing) into the membrane. In a similar manner, the T-45 epoxy overlay was also applied in two coats, both seeded with basalt Indag™ #8 aggregate. The entire system, on a level surface, is about 3/8-inch thick. Figure 3.22 is a cross-section drawing showing the complete system. Figures 3.23 and

3.24 show the application of the system. The wearing surface system had to be placed under the curbs separately since the membrane and epoxy overlay were too viscous to flow under the curbs.

There are many other possibilities for a wearing surface system that were not tested or that were not considered for this pier. There are many polymer systems marketed as wearing surfaces and waterproofing membranes. A different wood species group and/or a different preservative could change the criteria, as well. Asphalt with an impermeable membrane would be a economical alternative on structures that do not have the petroleum-product spill durability criterion. Timber or plastic-lumber planking could provide an acceptable wearing surface if an impermeable membrane was provided for the glulam deck. Although the system chosen met all criteria and has performed well; given the cost of this wearing surface system, future piers should consider other possibilities.

3.5.4 Cost

One of the key outcomes of this project is the economic comparison between the innovative FRP-glulam and prestressed concrete panels. Since the town obtained bids for both systems, a direct cost comparison can be made. Adjusted for inflation and for the differences in the construction market, the concrete deck alternative would have cost $35.64 per square foot delivered to the site. The actual cost for the FRP-glulam deck delivered to the construction site was $36.37 per square foot without the wearing surface. A breakdown of costs is provided in Table 3.2. The 20% market factor applied to the 1998 prestressed concrete bid equivalizes the prestressed concrete bid and the

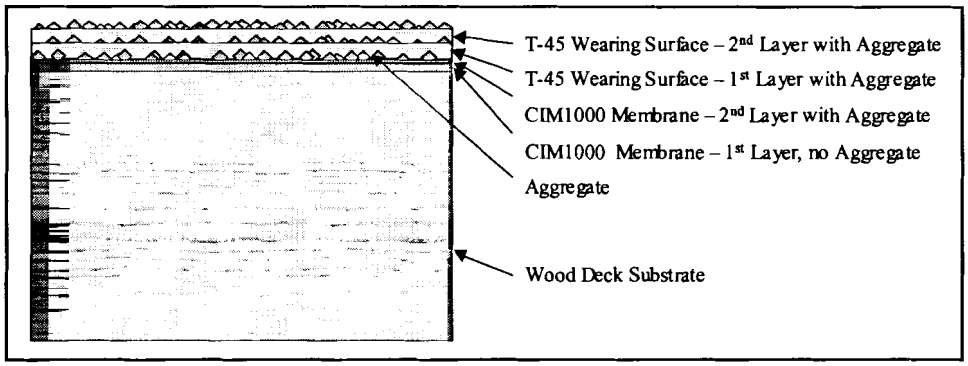

Figure 3.22 Membrane and wearing surface system used on the Pier (not to scale)

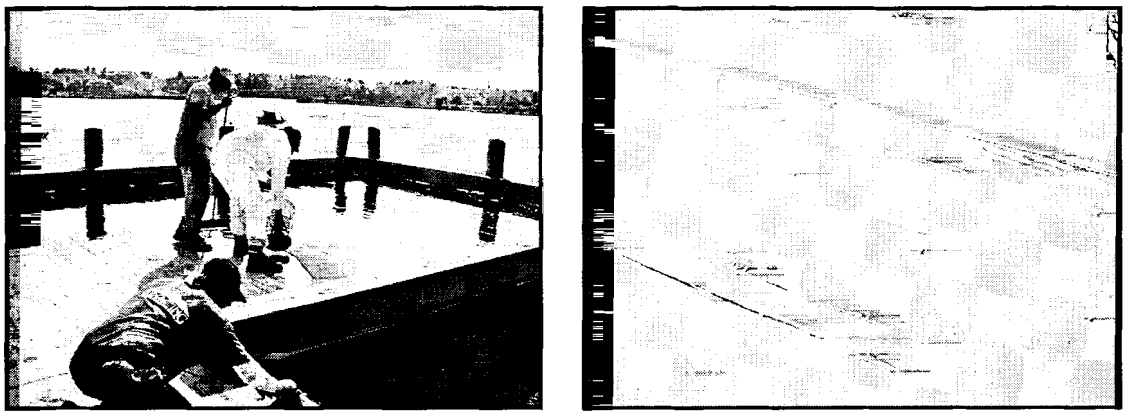

Figure 3.23 First coat of CIM 1000 application and appearance after curing

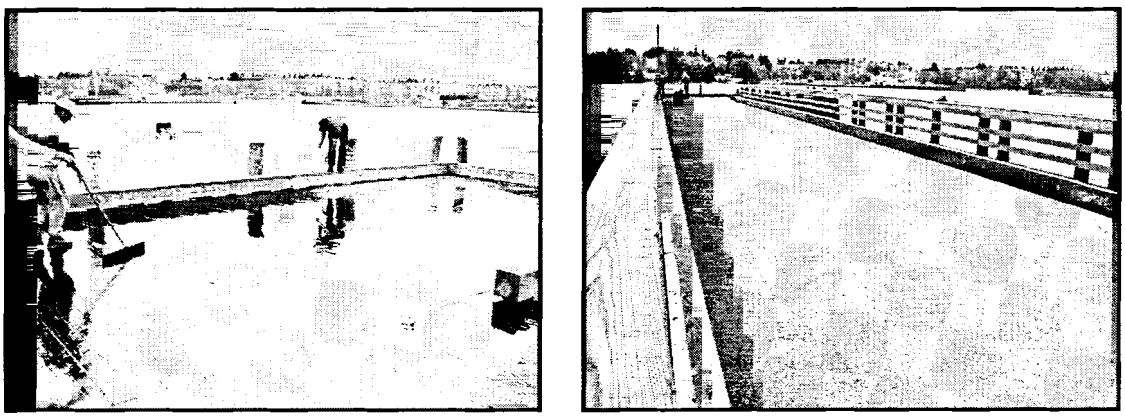

Figure 3.24 Second coat of CIM 1000 application and appearance after curing

actual FRP-glulam deck costs over the differences in the construction markets and typical contractor bids as given by Paul Pottle of the MDOT (Pottle 2000). Ignoring the aesthetic benefits of the wooden pier, with only a 2% difference in cost, the two systems are very competitive. Additional savings could also be realized if it had been possible to capitalize on many of the potential benefits of the innovative system. These benefits not accounted for include construction savings from the light-weight panels, material cost savings from utilizing the strength of the FRP in design, material cost savings from panels manufactured from under-utilized Maine species, and shipping savings from having the glulam manufactured and FRP applied at a single location.

Table 3.2 FRP-reinforced glulam deck pier table of costs

FRP-Glulam Deck Costs		
Glulam Deck Panels & Stiffeners		$87,800
Stiffener Beam Hardware		$2,130
Reinforcement (FRP)		$4,750
E-glass	$2,120	
Resin	$1,245	
Protective Coating	$670	
Supplies	$715	
Cuprinol		$145
Material Cost of FRP-Glulam Deck		**$94,825**

It should be noted as well that the exorbitant cost of the wearing surface system is not as much of a factor if an alternative is chosen or if the system is used in a bridge. In a Maine highway bridge, all systems need a bituminous wearing course, making the systems essentially the same cost.

Table 3.3 Comparison of cost of prestressed concrete deck to FRP-glulam deck

FRP-Glulam Composite Deck		**Prestressed Concrete Deck**	
Material Cost	$94,825	1998 Bid	$80,000
Labor at AEWC 700 man-hours (est.)	$7,000	Inflation	4.80%
		Market Factor	20%
FRP-Glulam Deck	**$101,825**	**Fall 2000 Cost**	**$99,800**
Wearing Surface System	$31,425	No wearing surface required for pier.	
Total Superstructure Cost	**$133,250**		

The Milbridge Pier has performed very well in the two years since its construction. It was load tested four months after opening to vehicular traffic. The FRP and wearing surface has been visually inspected every four to six months.

3.5.5 Load Test

In order to verify the pier's performance, the first span of the pier was load tested on November 8, 2001. Seven load cases were used and deflection measurements were made at 24 locations.

Instrumentation for the load test consisted of displacement gages. The displacement gages were constructed of strings (high test fishing line) and rulers (Schaedler precision rules marked to 1/50 inch and mounted on mirrors). The rulers were mounted on the bottom of the panels at the locations where deflection was to be measured. The strings were secured as close to the supports as possible and run just in front of ruler. To read the displacement gage, the reader read the initial position of the string on the ruler and then reread the position after the ruler had deflected due to the loading. To ensure that the readings were accurate and not read at an angle, a small

amount of mirror was visible on the side of the ruler. If the gage had been read correctly (the reader's eye at the same level as the string), the reader would have only been able to see a single string in the mirror. Figure 3.25 shows a closeup of the displacement gage. Figure 3.26 shows how the gage works. The system measured displacement from the bottom of the panels rather than the neutral axis since the neutral axis was inaccessible and automatically adjusted for any support settlement. Displacements were measured at two locations per panel near midspan, at two locations per panel at quarter span, and at eight locations along the TSB (Figure 3.29).

The truck used for the test is shown in Figure 3.28. Its footprint with the gravity load from each set of tires is shown in Appendix B. The actual truck tire positions in the seven load cases are given in Figures 3.29 through 3.32. Load cases # 2 and 3 are reasonable mirrors of each other, as are Load Cases #4 and 5 and Load Cases #6 and 7. However, a small difference in tire position can result in a different loading. This can be seen when comparing Load Case #4 and 5 (Figure 3.31). In Load Case #4, each wheel line loads a single panel, but in Load Case #5, one wheel line of loading is carried by two panels. This loading change also occurred between Load Cases #6 and 7.

The load test results are presented in the following graphs and Appendix B. The deck did not behave symmetrically. There are several possible explanations for this. Some of the panels were bowed, and this would have made them stiffer (Figure 3.37). As can be seen in the MOE tests of the panels used in the laboratory tests reported in Chapter 4, there can be considerable variation in stiffness among the panels. The movement of the string for the displacement gages fourth from the left may have been restricted.

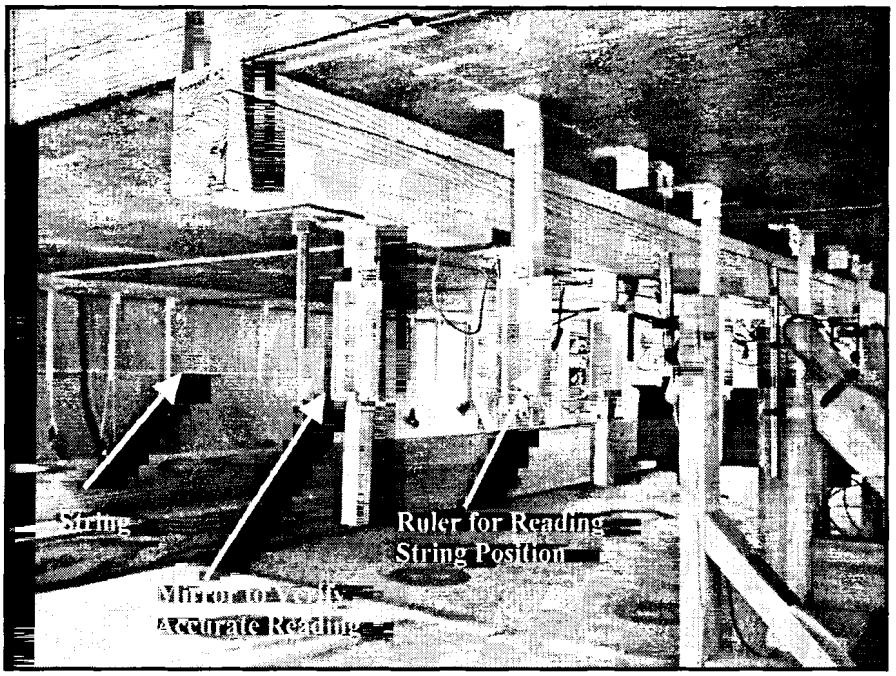

Figure 3.25 Deflection gages used during load test

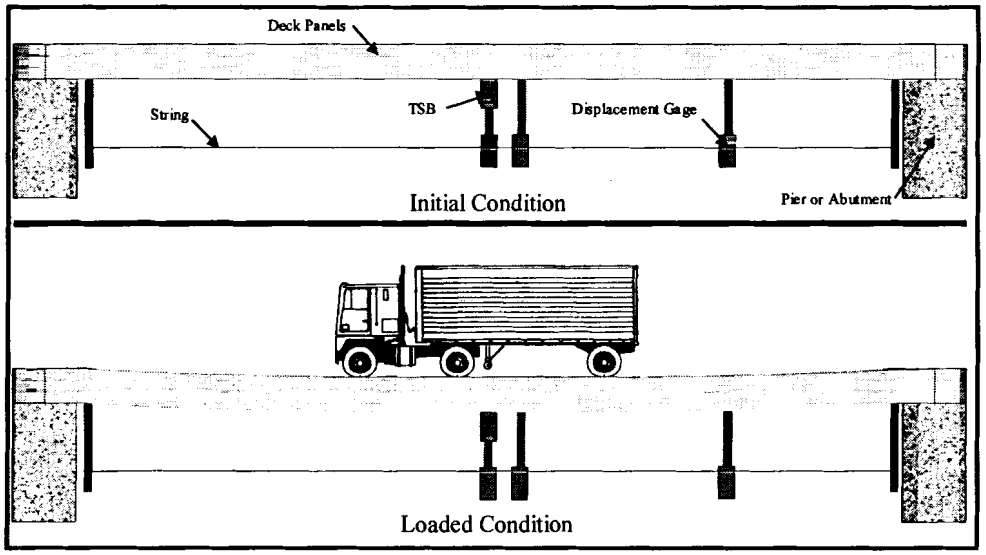

Figure 3.26 Illustration of displacement gages during load test

Figure 3.27 Instrumentation for deflection measurements for load test

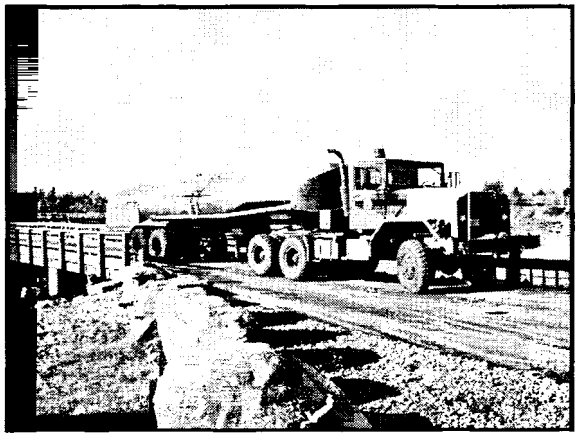

Figure 3.28 Truck used for load test

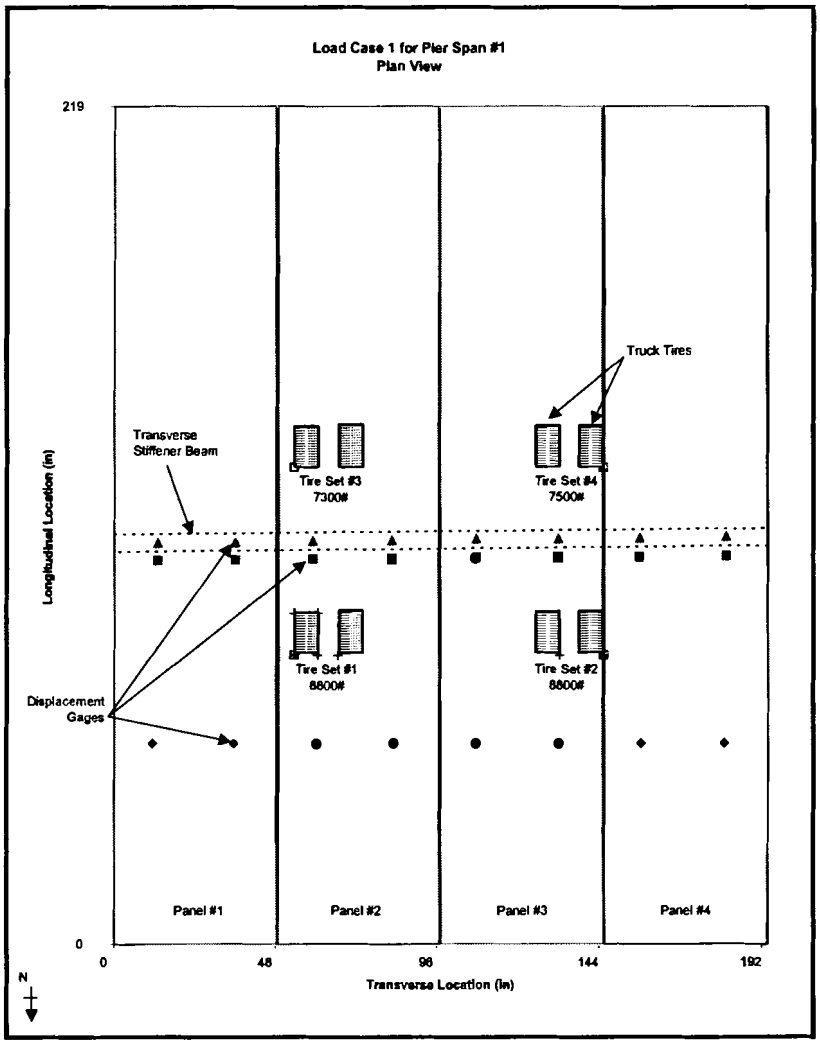

Figure 3.29 Load Case #1 for Milbridge Pier Load Test

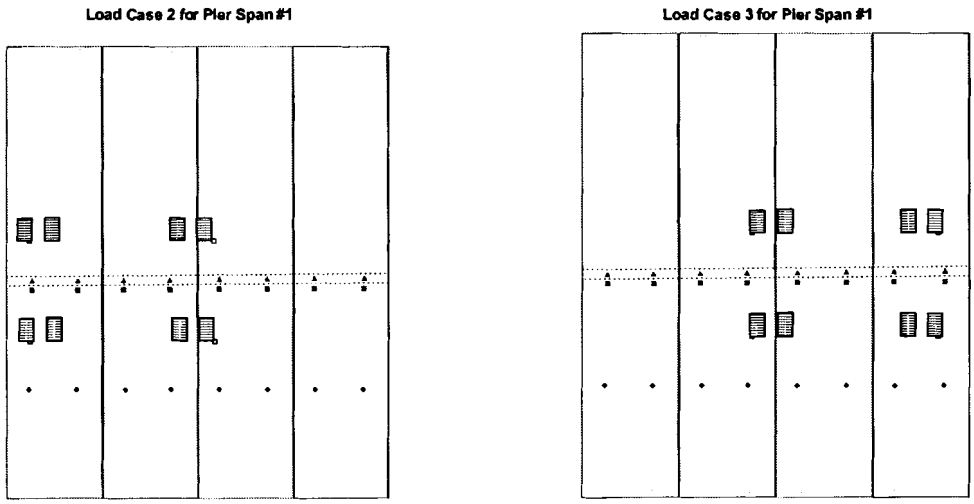

Figure 3.30 Load Cases #2 and #3 for load test

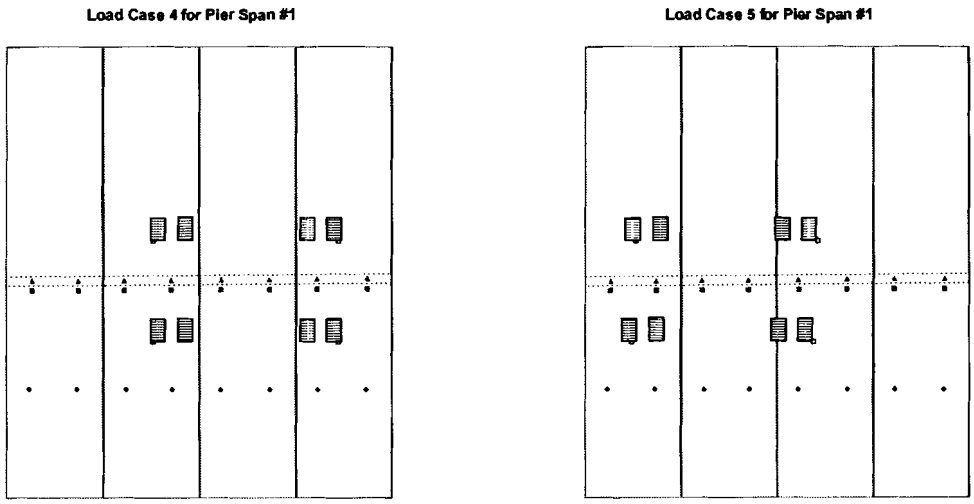

Figure 3.31 Load Cases #4 and #5 for load test

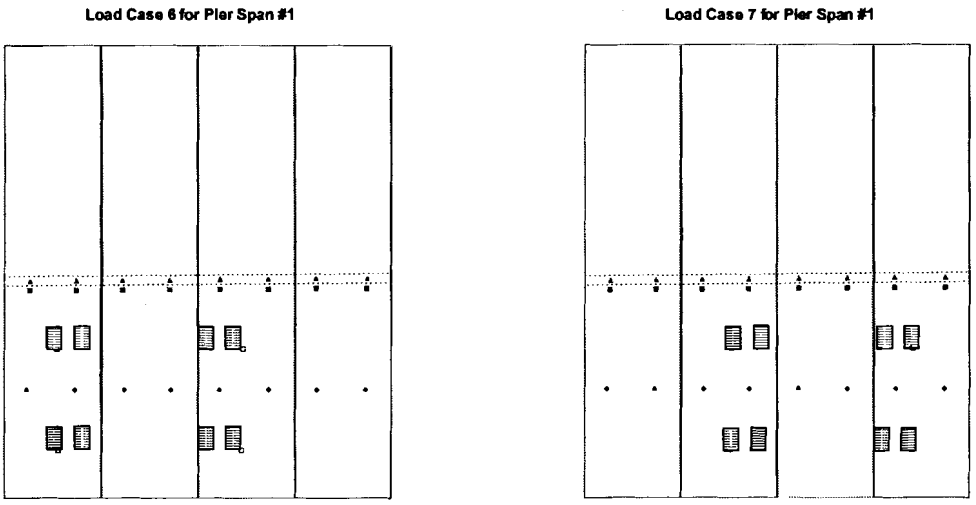

Figure 3.32 Load Cases #6 and #7 for load test

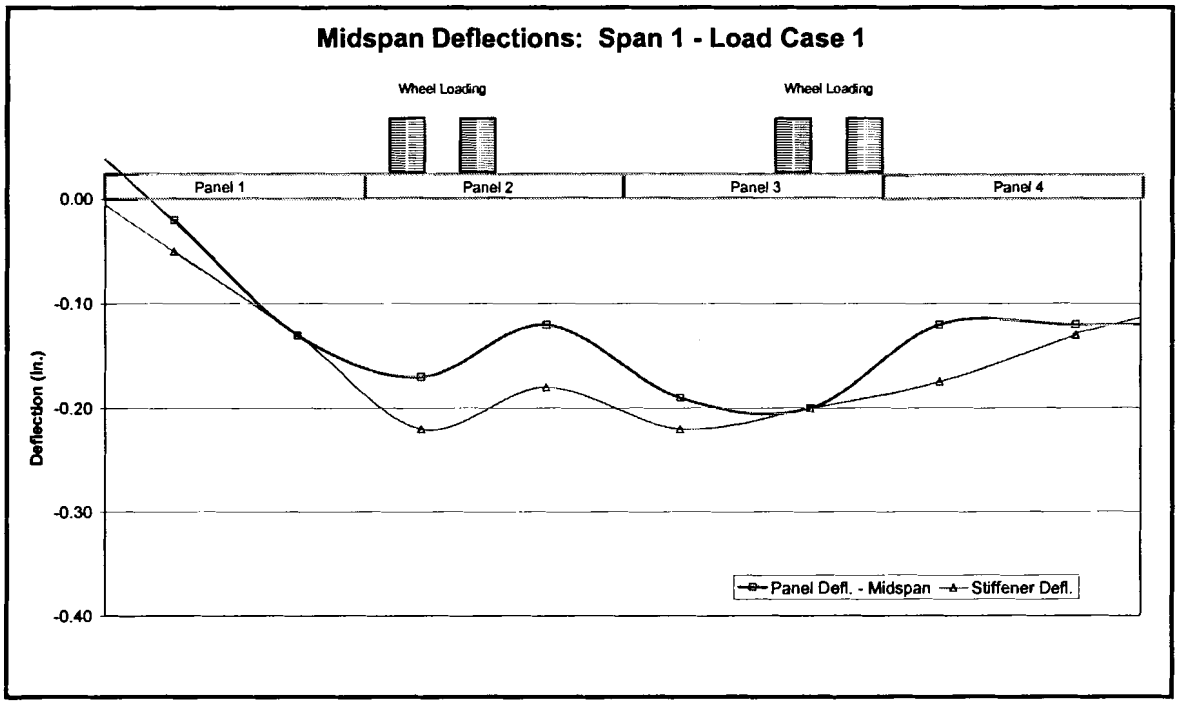

Figure 3.33 Midspan deflections during load test: Load Case 1

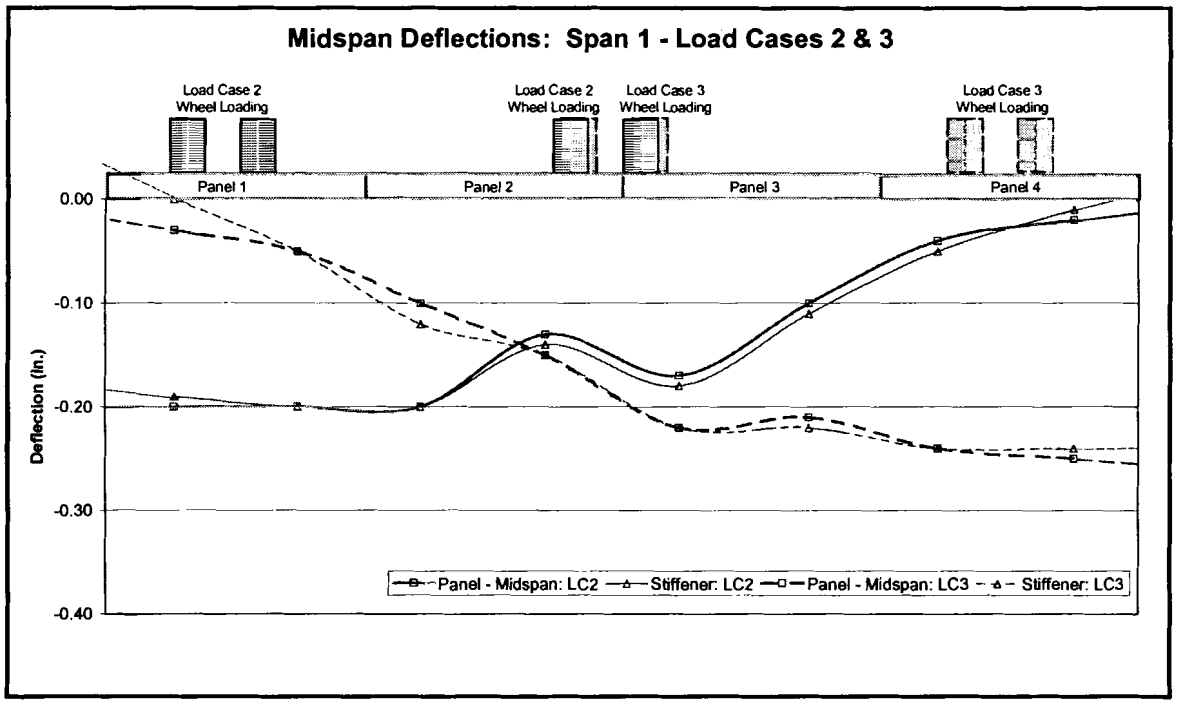

Figure 3.34 Midspan deflections for Load Cases #2 and 3 compared

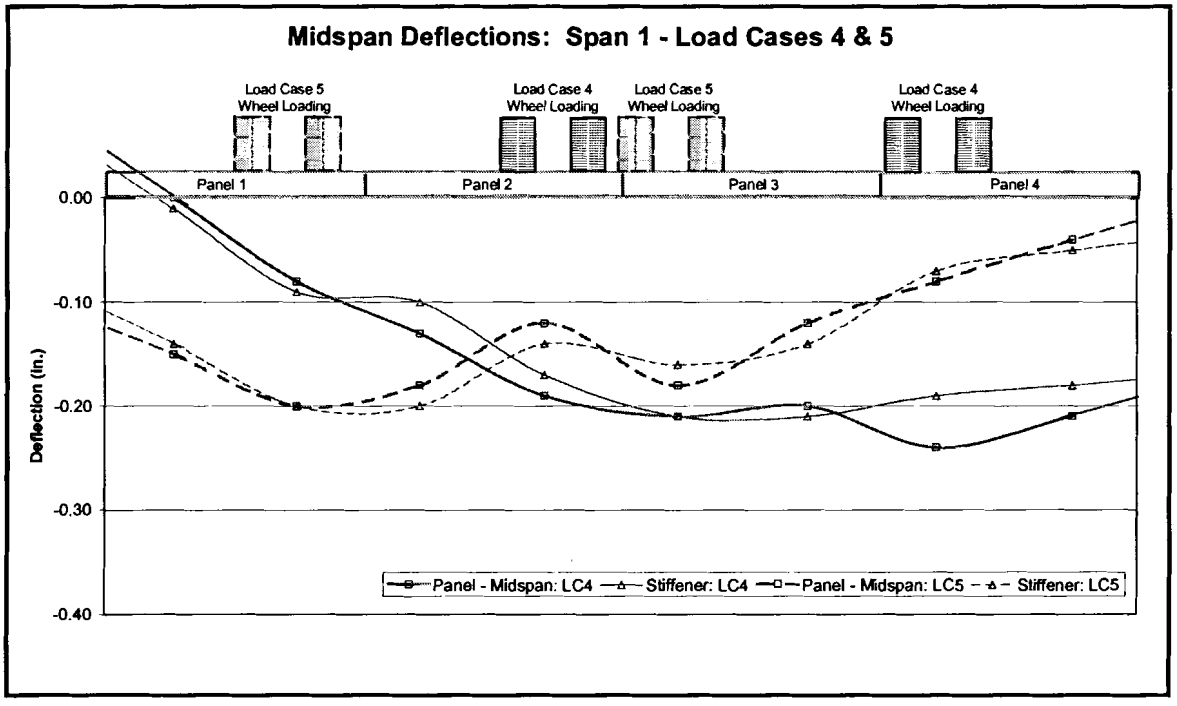

Figure 3.35 Midspan deflections for Load Cases #4 and 5 compared

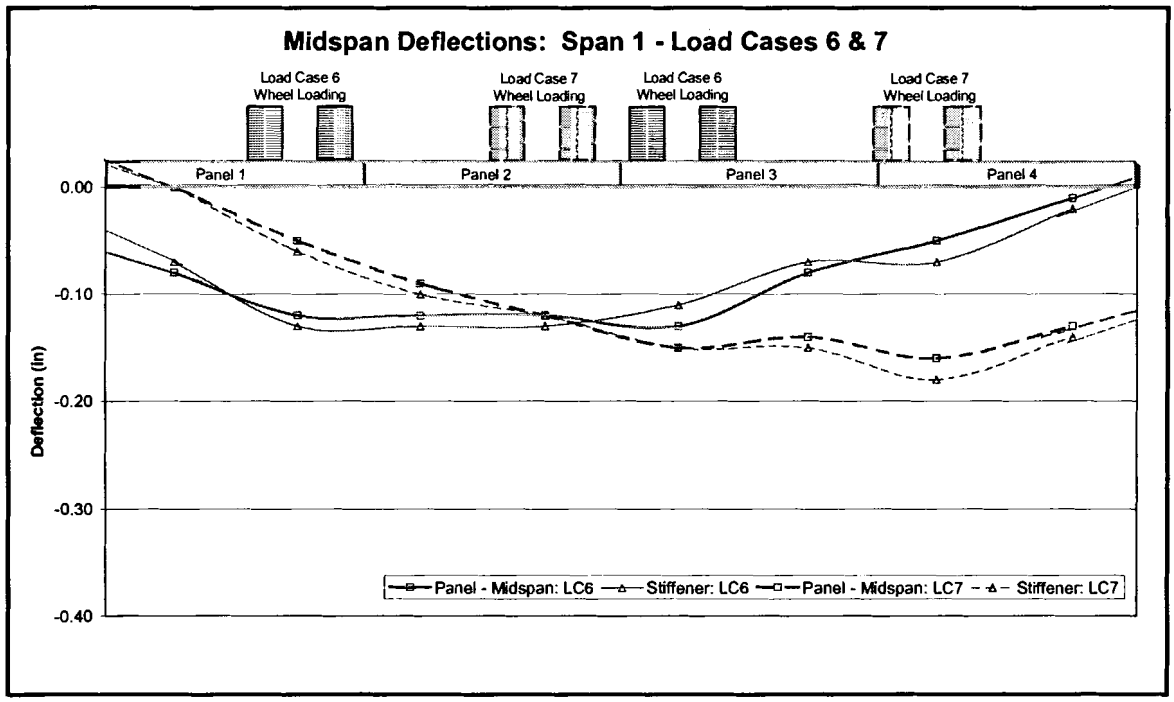

Figure 3.36 Midspan deflections for Load Cases #6 and 7 compared

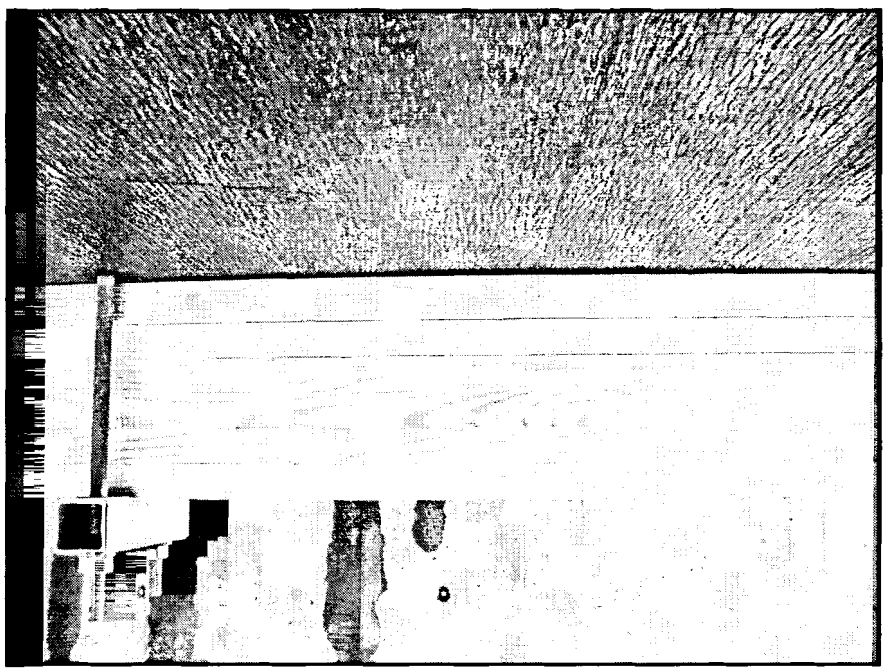

Figure 3.37 Bowed panels increased pier deck stiffness

However, typically, before to reading a gage the string was snapped so that the reading would be accurate. Although that reading was the most unusual, the other deflections measured on left side of the bridge are not symmetric with those measured on the right side. It is therefore believed that it was not a data collection error, but rather variability in panel properties and behavior and/or a connection that may have been over-tightened.

3.5.6 FRP Performance

The FRP has performed satisfactorily through its two years in the field. Some initial weathering and discoloring occurred during construction and the first winter's exposure (Figure 3.38). Further deterioration of the FRP itself has not been remarked. The additional discoloration that has been remarked appears to be the polyurethane coating deterioration, rather than the FRP itself. The protective polyurethane coating did not appear to have bonded well to the underlying FRP and has started to flake off (Figure 3.39). A copper napthanate preservative, Cuprinol No. 10 Green Preservative, was applied to all holes drilled in the panels after the FRP application and occasionally caused discoloration of the FRP and the polyurethane coating (Figure 3.40).

3.5.7 Wearing Surface System Performance

The wearing surface system has performed well since construction. The T-45 epoxy overlay has cracked in places as was expected (Figure 3.41). The CIM1000 membrane cannot be completely inspected, but it appears to have remained intact. No degeneration of either the T-45 or the CIM1000 has been seen, and the system appears to be meeting all other criteria.

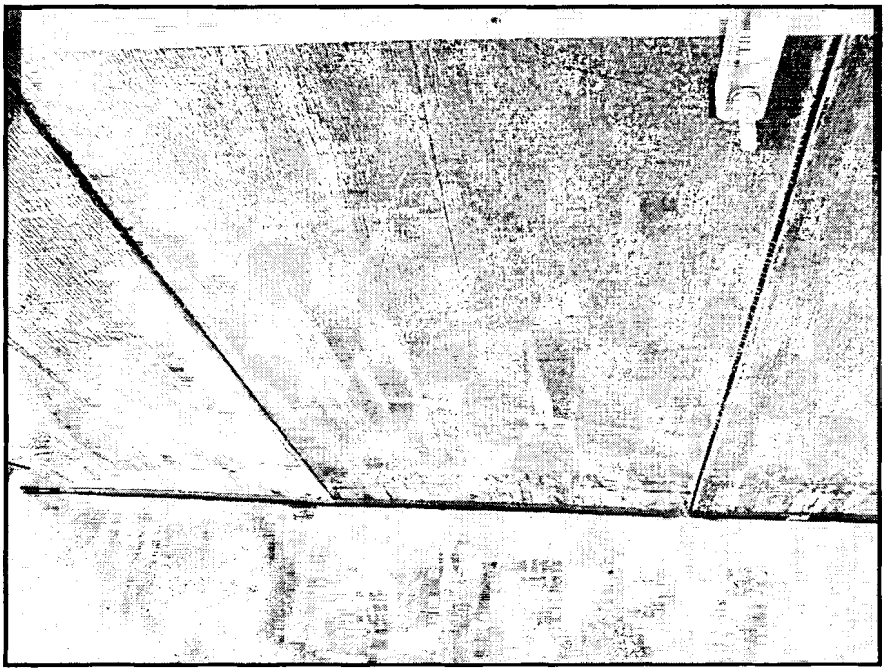

Figure 3.38 FRP on June 26, 2001, showing some spots of discoloration

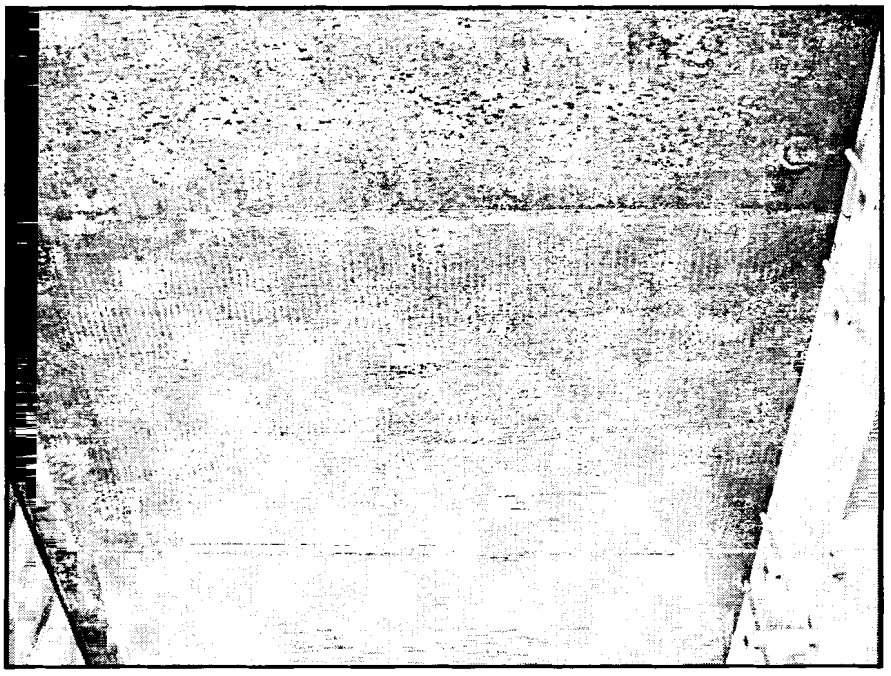

Figure 3.39 Polyurethane protective layer on a panel of the last span flaking off

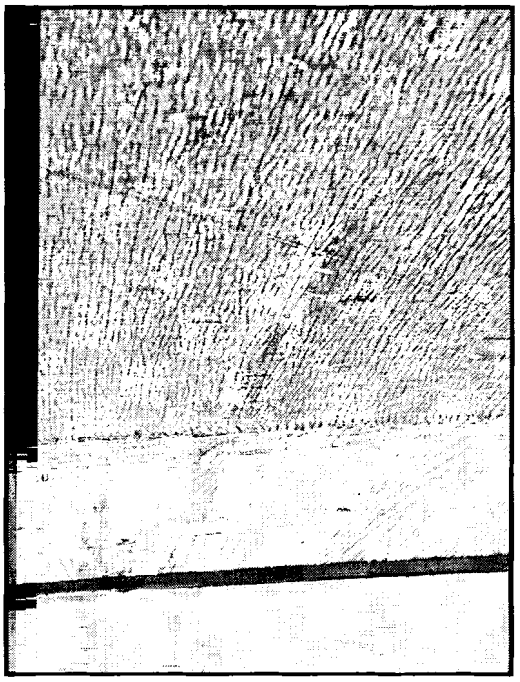

Figure 3.40 Discoloration of FRP and flaking of polyurethane layer from Cuprinol

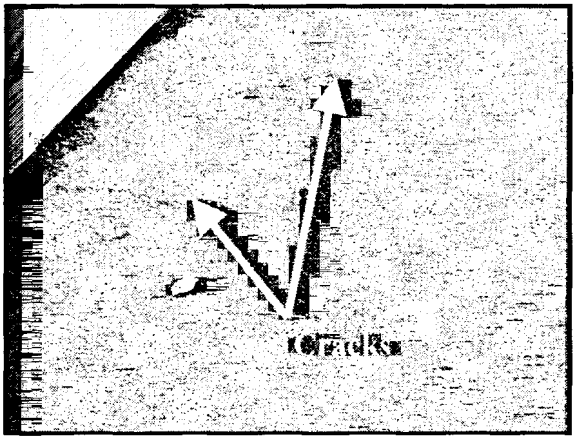

Figure 3.41 Cracks in T-45 wearing surface

3.6 Conclusions

The study has shown that FRP-reinforced glulam panels can be used in a longitudinal glulam deck bridge as an economically competitive alternative. Additional savings could be realized in other reconstruction situations and once large-scale production has begun, further lowering the cost of the system. The wearing surface system used is performing very well, but an alternative should be chosen for other situations due to the high cost. The pier has been load tested and inspected and is performing adequately.

Chapter 4

LABORATORY TESTING

4.1 Introduction

Laboratory testing was performed at The University of Maine upon a single 20-foot span, 16-foot wide bridge. The primary purpose of the testing was to provide data for refinement and validation of the finite element model that was developed in this study and that would be used for a parametric study. The secondary purpose of the testing was to perform a limited parametric study through the experiments themselves. The experiments used three stiffener beams, two connection systems, and three load cases in a full factorial (with a single exception). This chapter discusses the components of the tests, the instrumentation used, the load cases, the test results, and conclusions that can be drawn from the limited parametric study performed through the experiments.

4.2 System Components

The longitudinal FRP-glulam deck bridge consisted of four panels spanning 20 feet. The system is shown in Figure 4.1. The panels used in the testing are similar to those used on some of the spans of the Milbridge Pier. One of the TSB tested is similar to those used in Milbridge, and one of the connection systems, the seated beam, was used for the Milbridge Pier. The bridge had a single TSB at midspan. Jersey barriers were used to support the bridge. The bridge was loaded by a servo-hydraulic actuator located under the bridge in the structural testing floor of UMaine's AEWC.

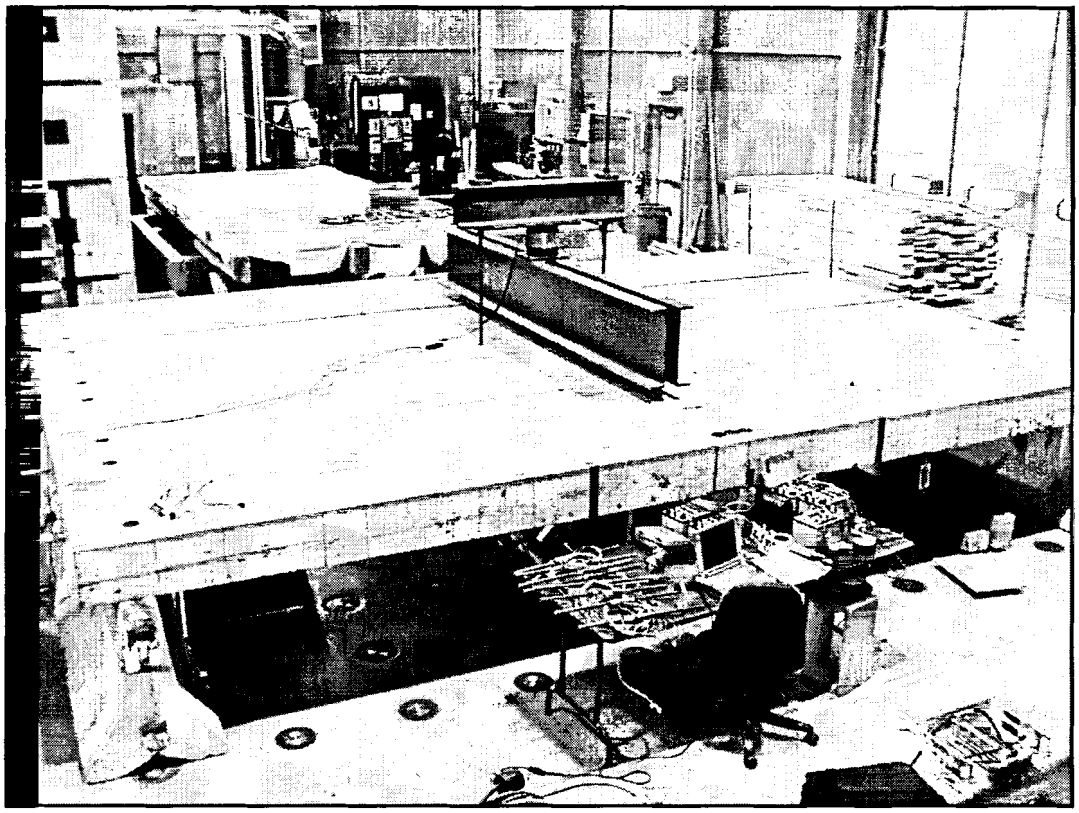

Figure 4.1 Bridge deck tested (Load Case 1)

4.2.1 Panels

The panels are vertically-laminated, FRP-reinforced, CCA-treated SP glulam. All panels were fabricated by Sentinel Structures, Inc. to the Milbridge Pier specifications. Each panel was approximately 10.3-inches thick, 47.3-inches wide, and 257.4-inches long. Dimensions varied by ±0.3 inches among panels and along a single panel. Preservative treatment and FPR reinforcement for the four panels tested were the same as the systems described for the Milbridge Pier in Chapter 3.

Tests were done before and after reinforcing to determine the apparent modulus of elasticity (MOE) of each panel and the increased stiffness due to the reinforcing. The 3-point bending tests were performed according to a modified ASTM D198 (ASTM 2000b) procedure. The test setup is shown in Figure 4.2. As can be seen from the results

reported in Table 4.1, the average increase in stiffness from 1% reinforcing was 6%. The un-reinforced MOE of panel A01 appears to be high, both compared to the other panels and compared to the panel's reinforced MOE, indicating an experimental error when the un-reinforced panel was tested. The cause of the experimental error is unknown as nothing unusual was observed during the tests. The table also indicates that panels with lower MOE receive a greater percent increase in stiffness due to the FRP.

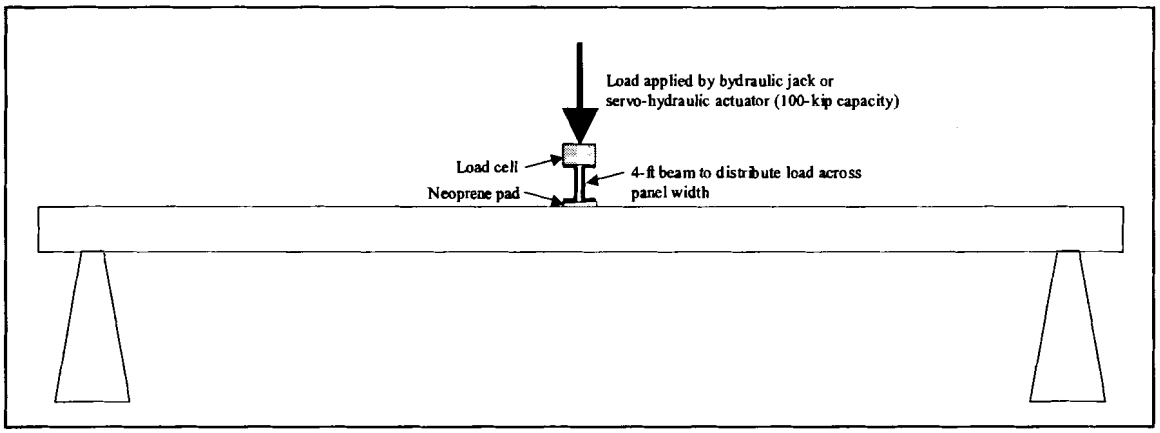

Figure 4.2 Test setup for apparent MOE of panels

Table 4.1 Panel apparent modulus of elasticity

Panel	Unreinforced Panel MOE	Reinforced Panel MOE	% Increase
Panel A1	1527	1650	8.02%
Panel A01	1720	1704	-0.92%
Panel A02	1663	1711	2.90%
Panel A3	1425	1530	7.40%
Average E Increase (without A01)			6.11%

The material properties of the FRP were tested in previous research at the AEWC Laboratory. The ultimate tensile strength of the unidirectional FRP is 61.2 ksi with a strain to failure of 1.14%. The FRP's longitudinal modulus of elasticity is 5.32 ksi. Its

interlaminar shear strength is 2.83 ksi. Without the shrinkage cracks in the FRP, the fiber volume fraction is approximately 64%; the resin volume fraction is approximately 27% (Battles 2000). The FRP used on the pier panels is 0.1-in. thick.

4.2.2 Stiffener Beams

Three different stiffener beams were used for the experimental tests. TSB #1 and #3 were fabricated in the AEWC laboratory from 0.4-pcf CCA-treated, No. 2 and better, SP 2x6 (nominal) boards from a local lumber supplier. TSB #2 was fabricated by Sentinel Structures to the specifications for the Milbridge Pier. Details of each TSB are given in Table 4.2. The range of stiffness factors of the TSB would indicate the sensitivity of the system to that parameter. Holes (7/8-inch diameter) were drilled through each TSB for the through bolt connections. Previous research that had indicated that TSB MOE did not significantly affect deflections and time constraints led to the decision to use published values for MOE.

Table 4.2 Transverse stiffener beams used in experimental tests

	TSB #1	TSB #2	TSB #3
Height (in.)	5.3	6.7	8.2
Width (in.)	3.6	4.5	5.1
A (in^2)	19	30	42
I (in^4)	46	112	236
MOE (ksi)	1600	1700	1600
EI ($kip\text{-}in^2$)	74000	191000	378000
EI/EI_{min}	0.9	2.4	4.7

4.2.3 Connection Systems

Two connection systems were used for the laboratory experiments. The seated-beam and the through-bolt connections are shown in Figure 4.3. The through-bolt connection was chosen due to its extensive use in longitudinal glulam deck bridges across the United States. The seated-beam connection was used in Milbridge and, since it does not restrict differential expansion movement between the panels and TSB, is a better connection for glulam with waterborne preservatives. The threaded rods used for the seated-beam connections were instrumented with electrical-resistance strain gages (strain gages), so the load transferred by the connection could be measured. In order to have a smooth surface for bonding the strain gage, the threads on the threaded rods were removed on the lathe prior to strain gage application. The instrumented rods then had a ½-inch diameter at the gage locations. Four rods were instrumented with six strain gages three ½-bridge circuits. The remaining twelve rods had two strain gages bonded to them, each in their own ¼-bridge circuit. The extensive handling of the rods and the delays between fabrication of the instrumented rods and the full-scale tests resulted in many strain gages being damaged. The gages could not replaced once wires had been connected since doing so was likely to damage the remaining gages on the rod. The multiple gages on the rods were averaged to cancel out bending effects and would then theoretically give the axial load carried by the rod.

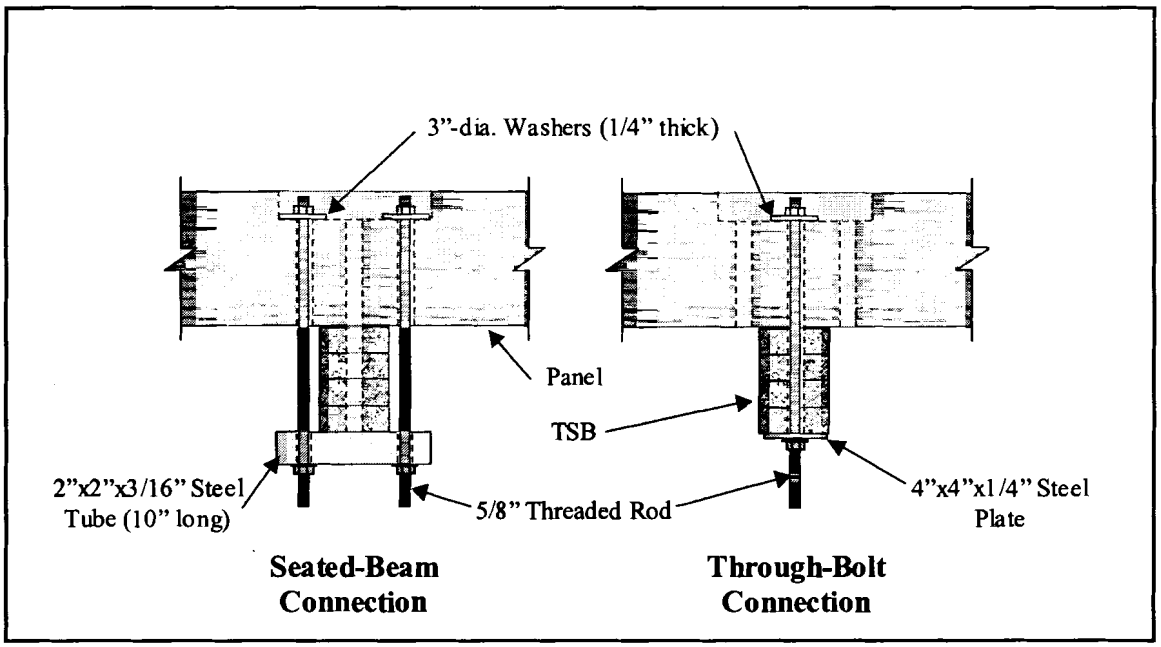

Figure 4.3 Connections tested

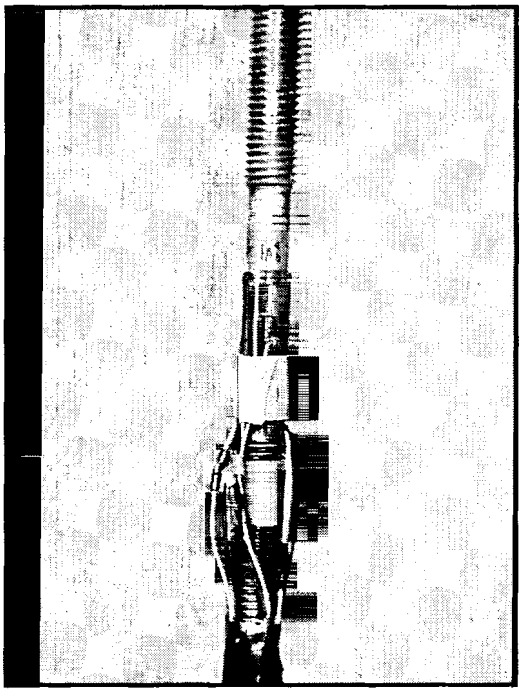

Figure 4.4 Threaded rod with six strain gages wired in three half bridge circuits

4.3 Instrumentation

Instrumentation of the laboratory test captured deflections at six locations, strains in the seated-beam connections, and the load applied to the bridge. Direct Current Linear Variable Differential Transformers (DCDT) were used to measure panel deflection across the width of the bridge The DCDT were calibrated before and after the experimental testing. Five had a ± 0.5-inch range over 15 volts, and one had a ± 3.0-inch range. DCDT readings were collected steadily (once every second typically) through computerized data acquisition. Load were measured using a 50-kip load cell and were collected on the same data acquisition system as the DCDT.

Strains in the seated-beam connections were measured through the strain gages bonded to the threaded rods. The strain from the gages on the threaded rods (Figure 4.4) was recorded at start of test, at 25% of test load, at 50% of test load, at 75% of test load, at test load, and after the load was removed. The strain was read with a MicroMeasurements P3500 strain indicator and several switch and balance units that allowed multiple strain gage circuits to be connected to a single strain indicator and be read in turn. In Load Case #1, strain readings were not obtained from one of the connections (Panel A3 to TSB connection) because of damage to strain gage wiring. The problem was remedied, however, and did not recur for most of the testing of Load Cases #2 and 3.

4.4 Load Cases

Three load cases were tested in the laboratory. The first load case was symmetrically placed at center span, to observe the symmetry of bridge behavior. The

second load case loaded the edge of the bridge, placing a tire two inches from the outer panel edge, much closer than would be possible in a bridge in service since there would be curb at that location. Load Case #3 was designed to maximize differential deflection between panels. The load was applied by a 100-kip static load capacity servo-hydraulic actuator located in the concrete strong floor that supported the bridge. The actuator pulled down on a series of distribution beams and steel rods to apply load to the two tire patches on the panels (Figure 4.5). The load cases are sketched in Figures 4.6 and 4.7. Figure 4.8 shows the actual load application configuration in Load Case #1. Load Case #2 also used the load cell and the actuator in a similar location centric location. In Load Case #3, the actuator could not be centered between the tire patches. Thus, the load cell was placed directly above the tire patch that edge loaded the panel. The tire patch that edge loaded the panel was loaded up to the full 16 kips, but due to the eccentric loading, only 10/62 of that load was seen by the other tire patch. This eccentric loading was acceptable because the purpose of the load case was to maximize differential panel deflection, which was accomplished by fully loading a panel at its edge.

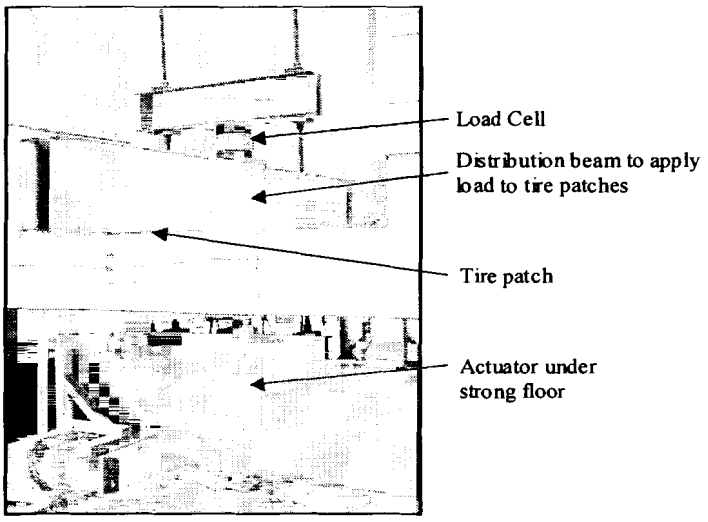

Figure 4.5 Method of load application for full-scale deck tests

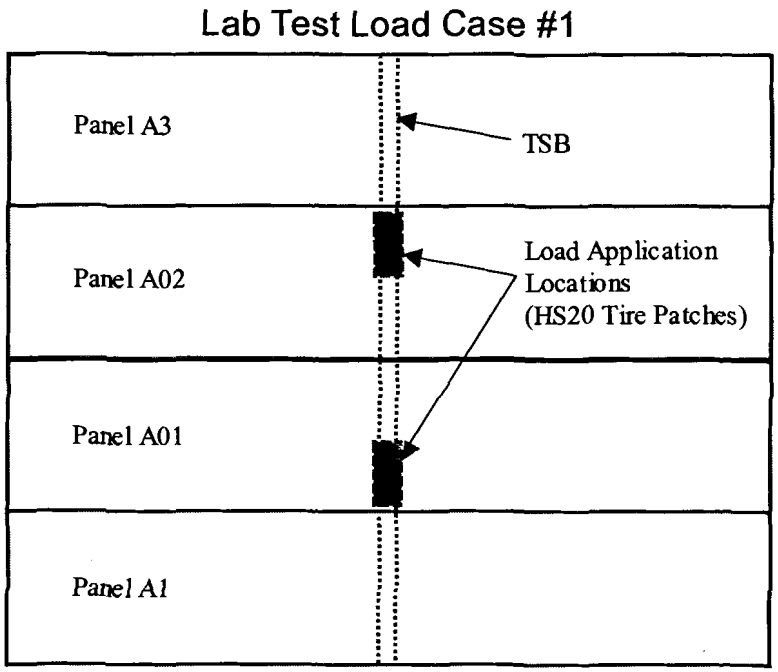

Figure 4.6 Load Case #1

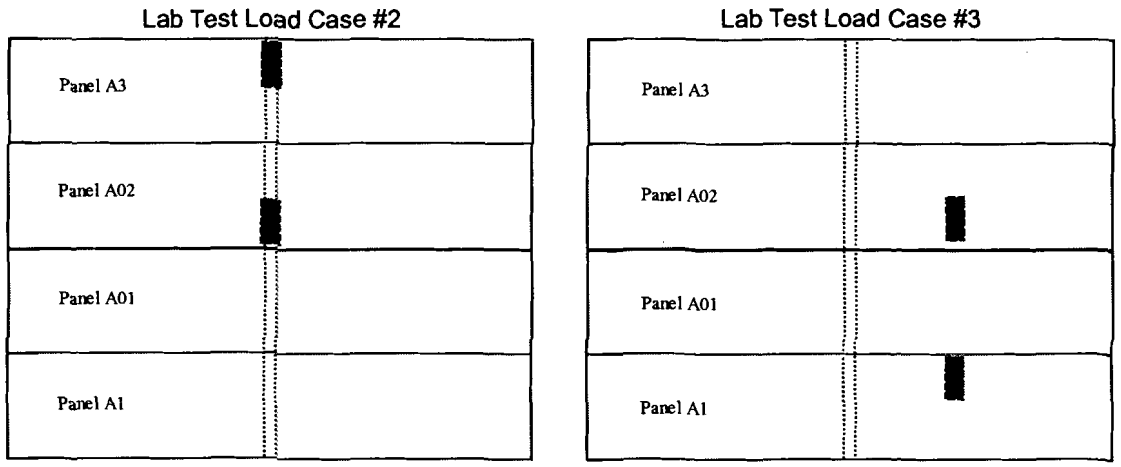

Figure 4.7 Load cases used in laboratory testing

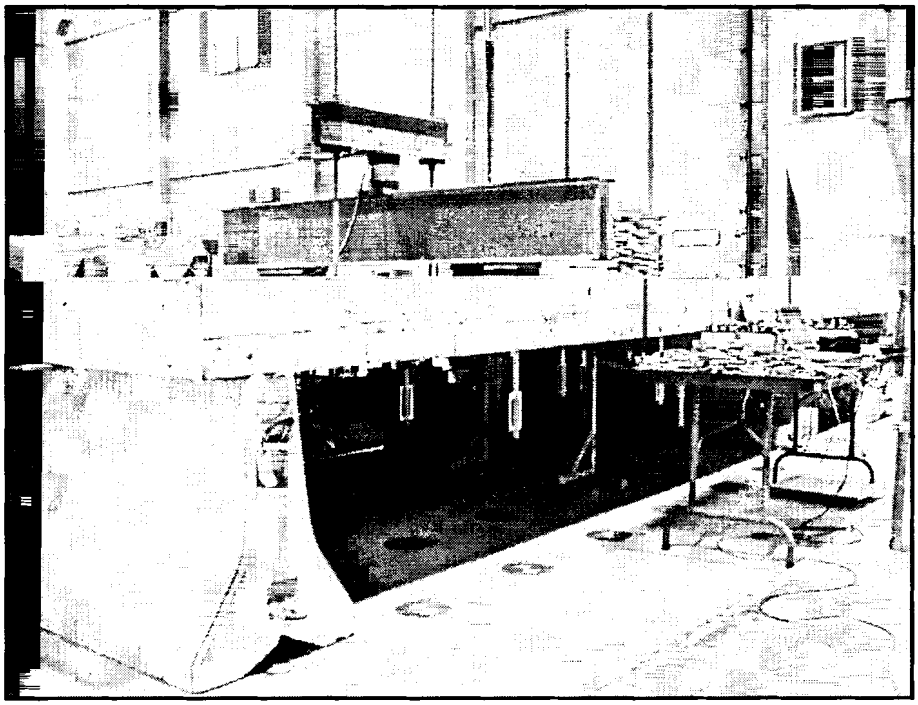

Figure 4.8 Picture of Load Case #1

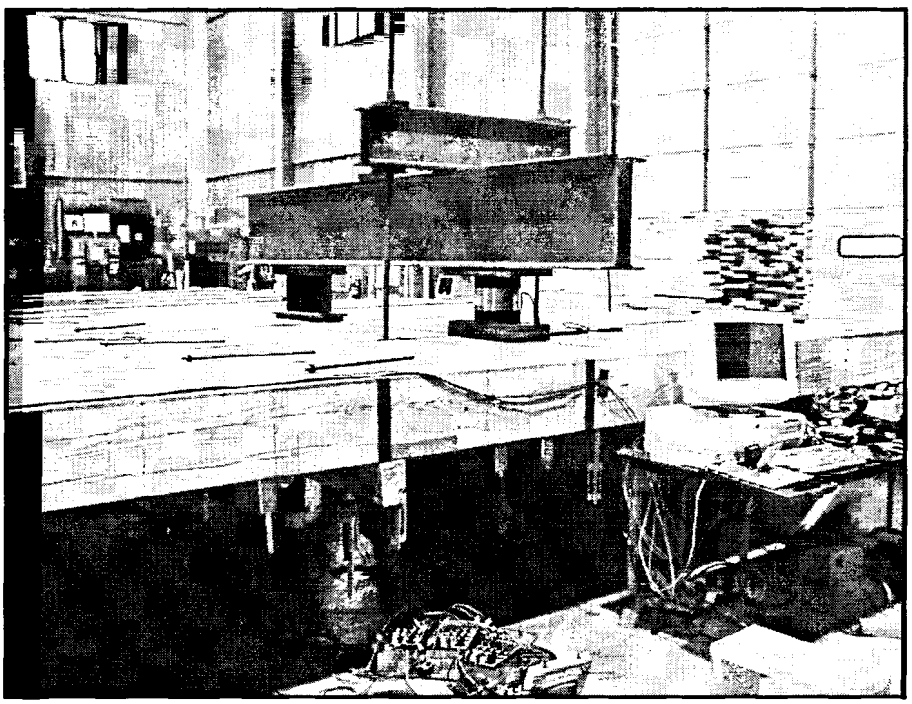

Figure 4.9 Picture of Load Case #3

4.5 Test Matrix

The laboratory testing at UMaine consisted 25 separate test setups. The testing used three stiffener beams, two connection systems, a single bridge configuration, and three load cases. In order to observe the effect of the loosening of connections between the deck and TSB, several tests were run with loose connections. Due to the variability of the TSB and panels it was difficult to obtain a uniform "looseness" for the connections. Table 4.3 gives a matrix of the parameters tested in this experiment. The "tight" connections referred to in this study were tightened by a hand wrench to maximum worker strength. Although a "finger-tight" torque would have given better, and, possibly, more uniform results, the non-uniformity of the panels and TSB, required an increased tightening in order that the panels and TSB maintain as much contact as possible. It was believed that this test matrix would be extensive enough to indicate some trends in system behavior. The test matrix was also designed to be broad enough to assist in finite element model validation and in compassing any recommendations that would be made as a result of the finite element model's parametric study with experimentally observed system behaviors.

4.6 Results

The observed deflections of the panels and strain in the seated beam connection systems are presented in this section. Further tables of data and results can be found in Appendix D.

Table 4.3 Matrix of experiments performed for UMaine's full-scale bridge test

Bridge Description	*Load Case #*	*TSB #*	*Connection System*	*State of Connection*	*Data Obtained*	
					Panel Deflections	*Threaded Rod Strains*
20-foot span, 16-foot width, four 48-in. wide, 10.5-in. thick panels	1	#1	Seated Beam	Tight	×	✓
			Through Bolt	Tight	✓	×
		#2	Seated Beam	Tight	✓	✓
				Loose	✓	✓
			Through Bolt	Tight	✓	×
		#3	Seated Beam	Tight	✓	✓
				Loose	✓	✓
			Through Bolt	Tight	✓	×
	2	#2	Seated Beam	Tight	✓	✓
			Through Bolt	Tight	✓	×
		#3	Seated Beam	Tight	✓	✓
			Through Bolt	Tight	✓	×
				Loose	✓	×
	3	#1	Seated Beam	Tight	✓	✓
				Loose	✓	✓
			Through Bolt	Tight	✓	×
				Loose	✓	×
		#2	Seated Beam	Tight	✓	✓
				Loose	✓	✓
			Through Bolt	Tight	✓	×
				Loose	✓	×
		#3	Seated Beam	Tight	✓	✓
				Loose	✓	✓
			Through Bolt	Tight	✓	×
				Loose	✓	×

Figure 4.10 shows that when the midspan panel deflections of the through bolt and seated beam connections for Load Case #1 are compared, the seated beam connection's higher stiffness causes more of the load to be distributed to adjacent panels. There is a 14% increase in maximum panel deflections comparing the through-bolt and seated-beam connections. However, the figure also shows that if the connection is loosened the stiffness of the connection is no longer as beneficial. Loosening of the connection will occur in service due to creep, hygrothermal movement of the wood, etc.

Load Case #2 loads two adjacent panels on the edge of the bridge, a situation that prevents much load distribution. Consequently, the stiffness of the connection system does not significantly affect the panel deflections (Figure 4.11). Again, in Load Case #3, where the load has been moved away from the TSB, the connection stiffness does not as significantly affect the panel deflections (Figure 4.12). There is an inconsequential three percent difference in panel deflections between the tight seated-beam and tight through-bolt connections of Load Case #3. When the stiffer TSB#3 is used on the test bridge, the connection system stiffness' effect on panel deflection is decreased (Figures 4.13, 4.14, and 4.15). (TSB #3 has twice the stiffness of TSB#2.) Typically, as the load has greater opportunity to be transferred to other panels through the TSB and as the TSB's stiffness increases panel deflections are more uniform. However, results may vary due to the tightness (prestress) of the connection.

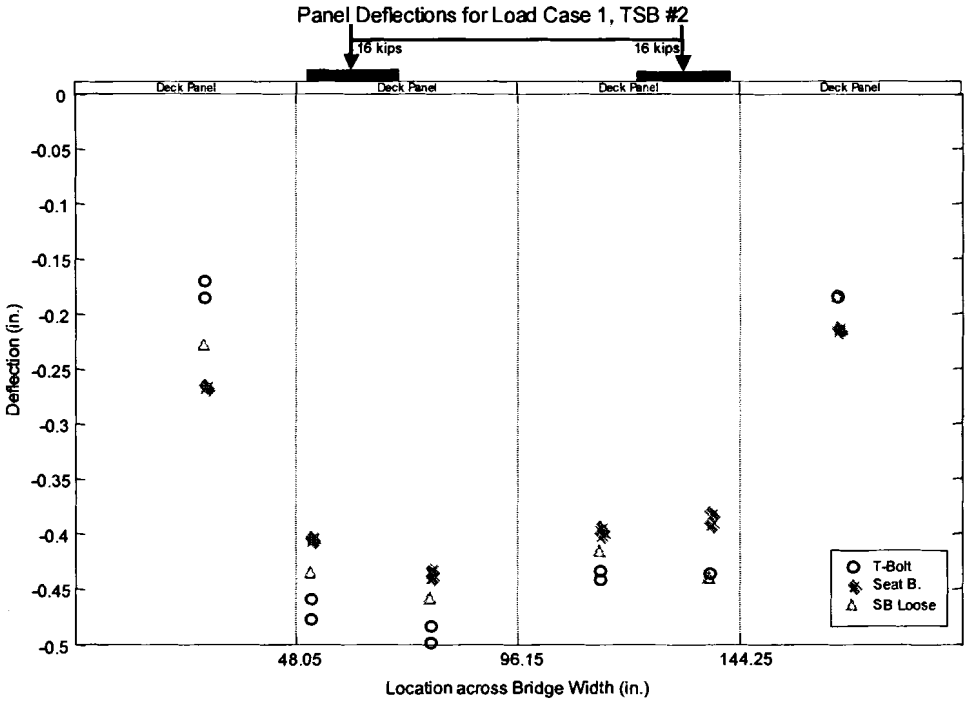

Figure 4.10 Midspan panel deflections for Load Case #1, TSB#2

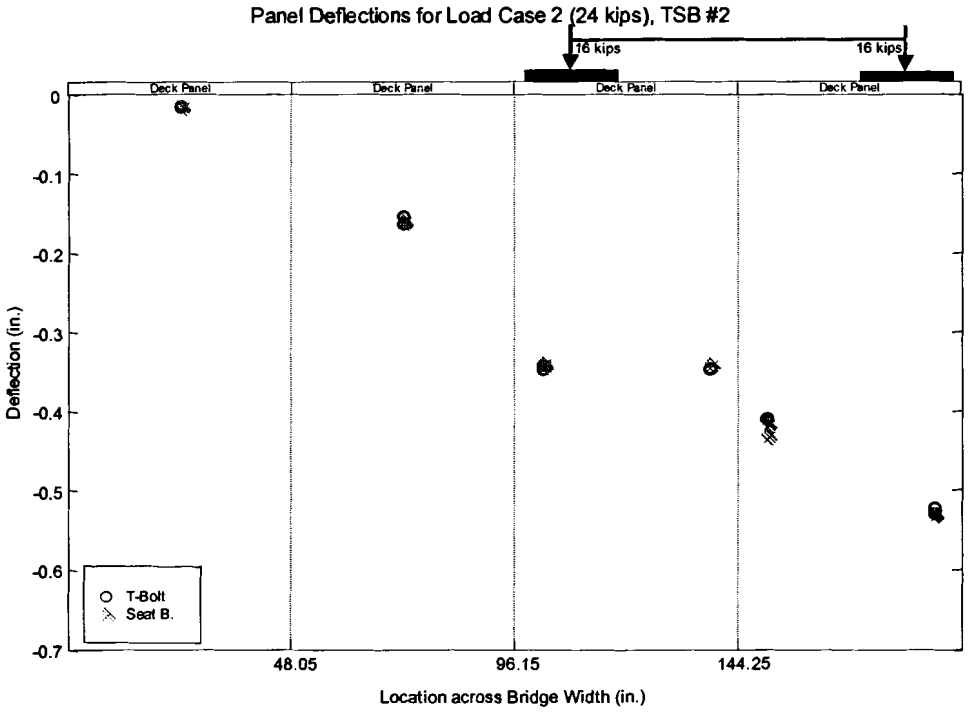

Figure 4.11 Midspan panel deflections for Load Case #2, TSB#2

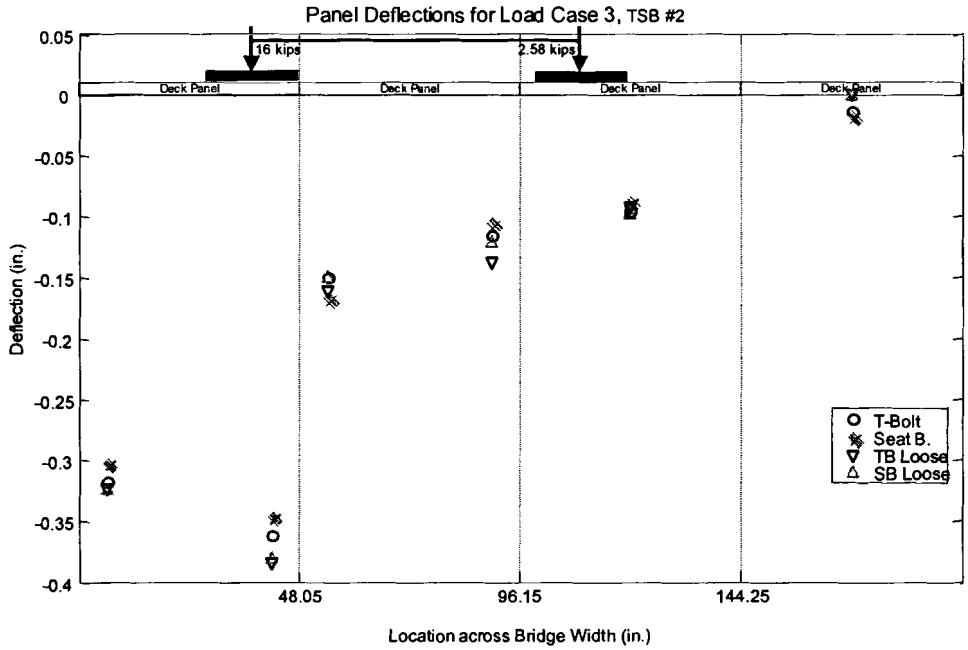

Figure 4.12 Midspan panel deflections for Load Case #3, TSB#2

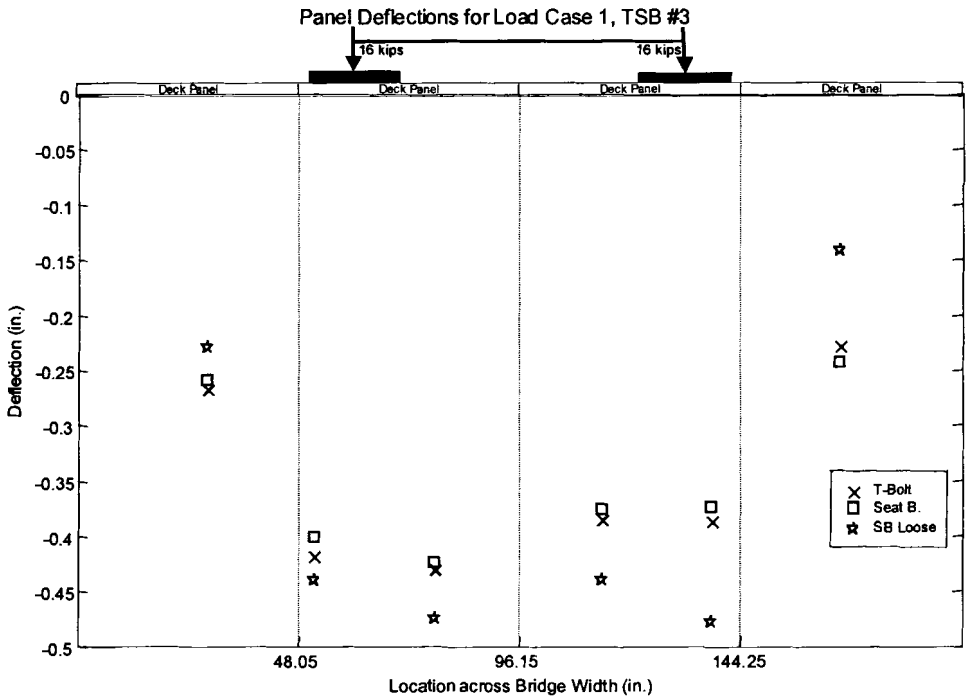

Figure 4.13 Midspan panel deflections for Load Case #1, TSB#3

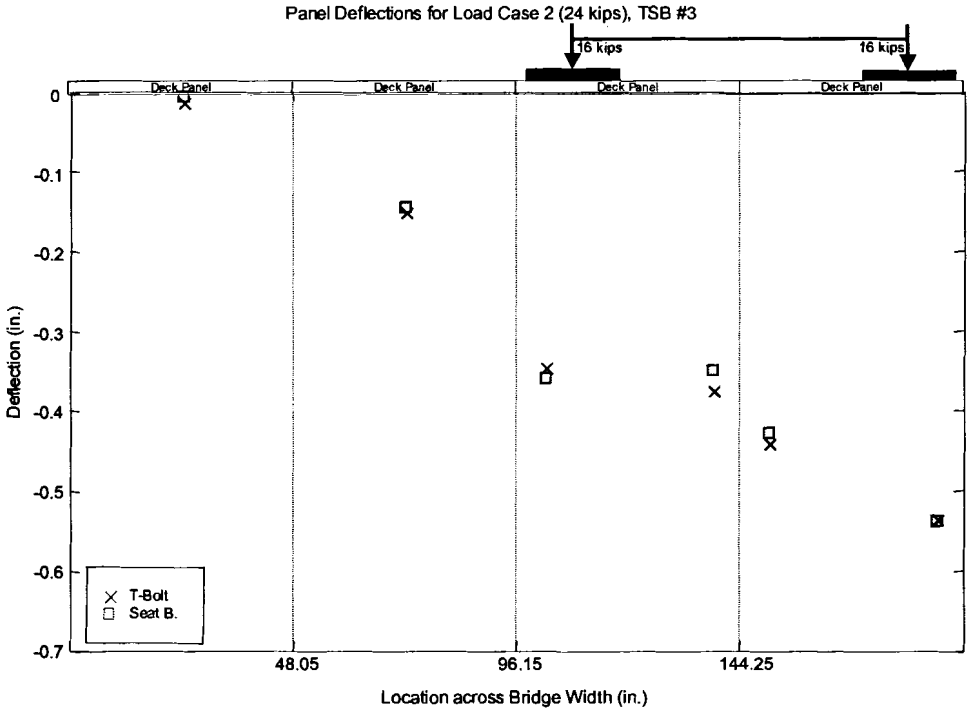

Figure 4.14 Midspan panel deflections for Load Case #2, TSB#3

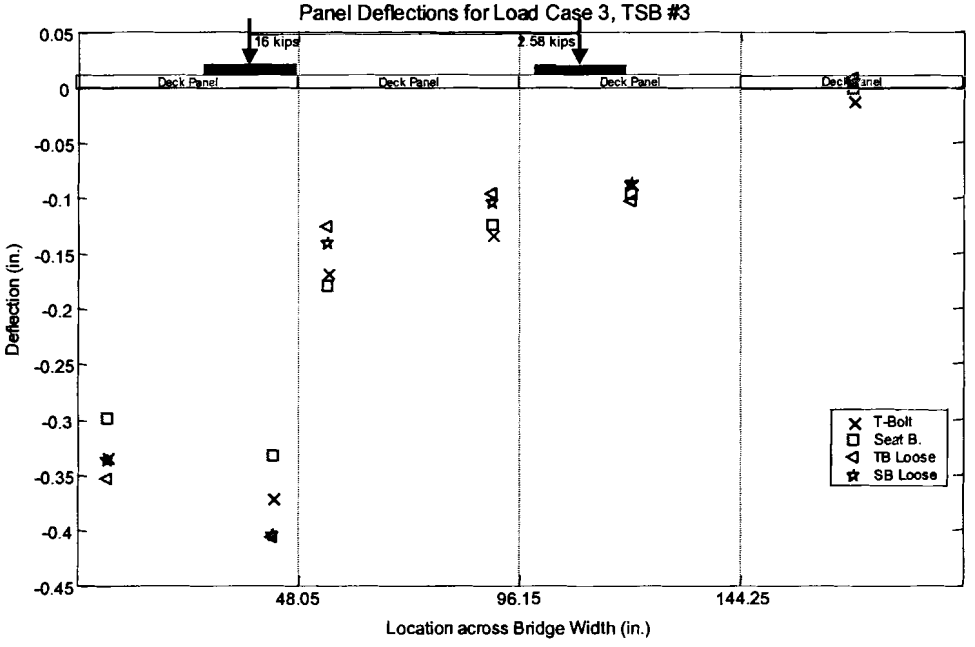

Figure 4.15 Midspan panel deflections for Load Case #3, TSB#3

Panel deflections appear to be dependent on connection prestress (initial tightening of the connection), as well as connection and TSB stiffness, according to the results from the experimental testing. The readings from the strain gages on the threaded rods are given in Appendix D. In the body of this thesis, comparisons will be made and trends explained. One of the difficulties of the rod strain is the bending and loss of strain gages that may have significantly affected the acquired data. These possibilities are further discussed in Chapter 5 when the experimental results are compared to the finite element analysis results obtained during the finite element model validation and refinement.

The strain in the seated-beam connections to all TSB during Load Case #1 can be seen in Figure 4.16. It is important to note in all strain diagrams from Load Case #1 that the strong appearance on an unsymmetric system response is due to the lack of data at the critical Panel A3 to TSB connection.. If that data are ignored, there is a reasonably symmetric response given the variability of the panel modulus of elasticity, the warp and geometric variability of the panels and TSB, the possibility of bending of connections, and the possibility of slight misalignment of the strain gages on the threaded rods. Figures 4.16 and 4.17 show that the stiffer TSB typically cause higher strain in the critical load distributing connections. In Load Case #3, the stiffer TSB gives very little strain in connections distant from loading, but the less stiff TSB allow greater bending and consequently have the connections away from the loading still may transfer high loads between the deck and the TSB.

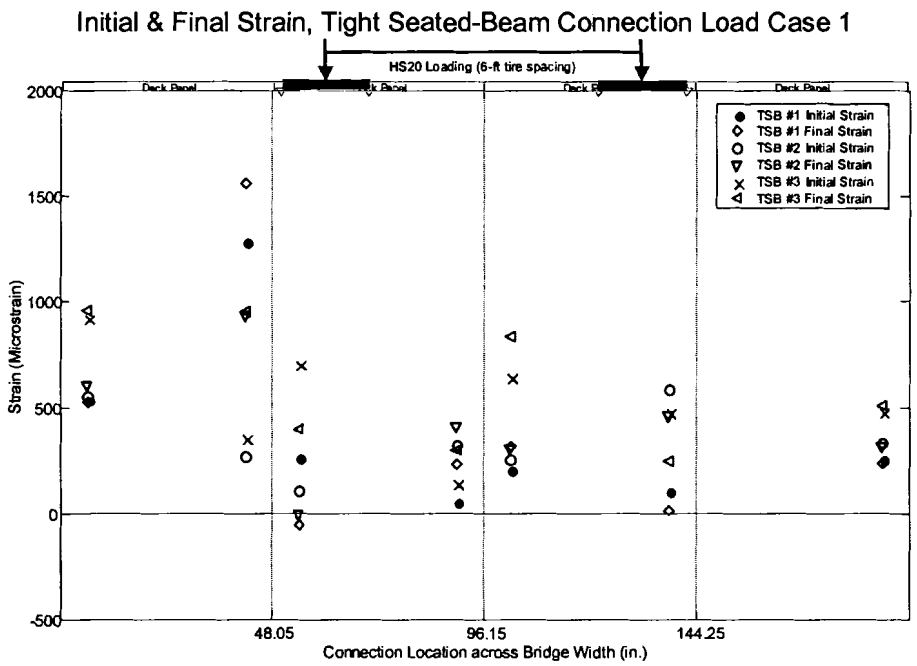

Figure 4.16 Initial and final strain in seated beam connections for all TSB tested in experimental Load Case #1

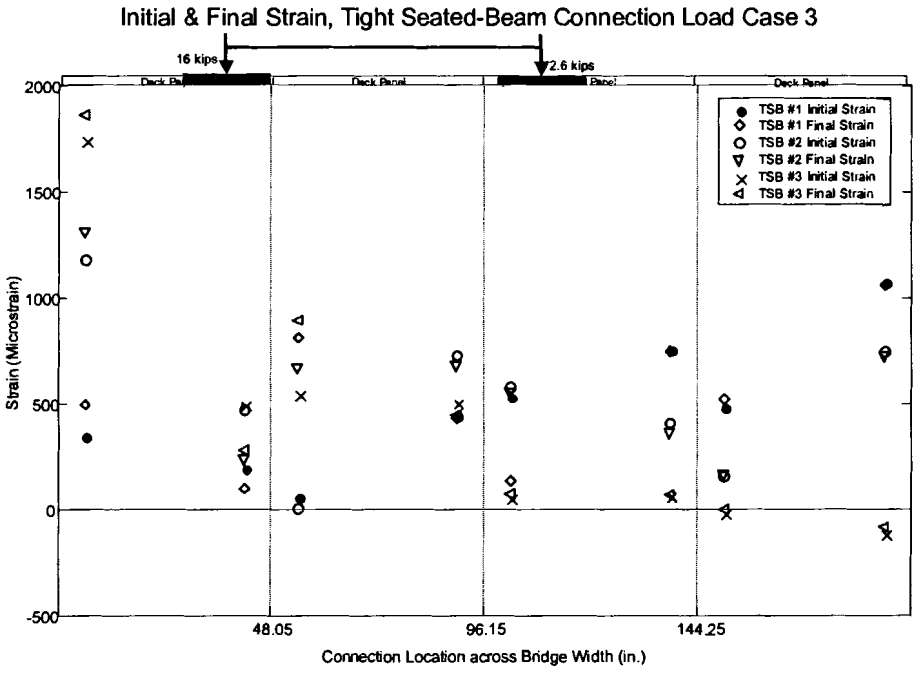

Figure 4.17 Initial and final strain in seated beam connections for all TSB tested in experimental Load Case #3

Figures 4.18, 4.19, 4.20, and 4.21 show the change in strain during the experimental testing. Absolute change in strain can simplify the behavior of the system, but extreme states of looseness or tightness in the connection can confuse trends. It can be clearly seen that the stiffness of the TSB does affect strain in the connection as does the initial tightness of the connection. The second connection from the left in the first panel experienced an exceptionally high prestrain when TSB #1 was tightened into place. (Figure 4.16) The change in strain figure (Figure 4.18) shows a change in strajn less than that which would be expected as a result of the overtightening of the connection. The change in strain diagrams show that the high stress areas are those between connection and panel edge (Figures 4.18 and 4.19). Although these areas were not noticeably damaged during testing, if the current AASHTO design criteria are insufficient these areas have high potential for failure in shear.

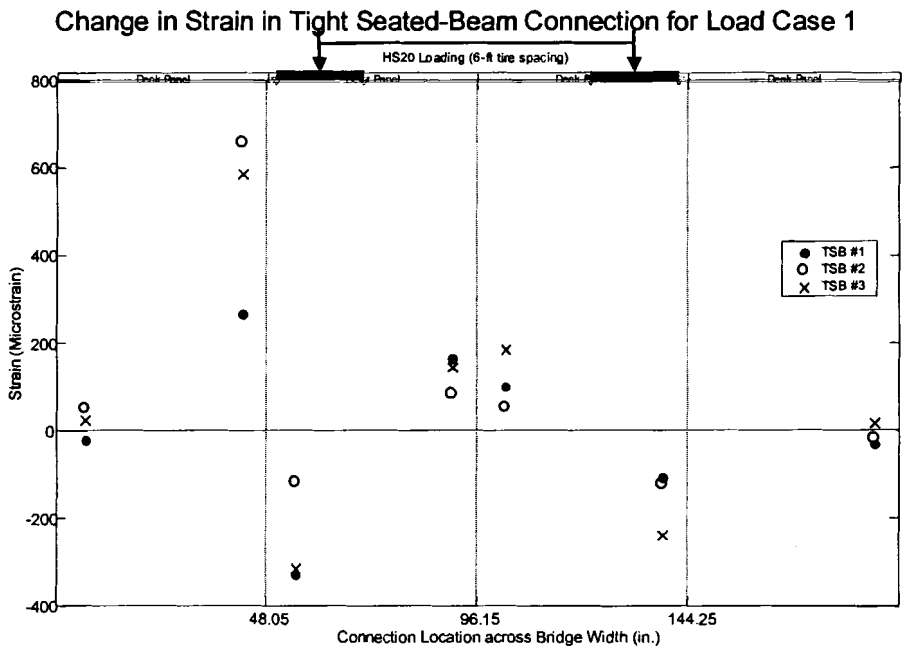

Figure 4.18 Change in strain in seated-beam connections for all TSB tested in experimental Load Case #1

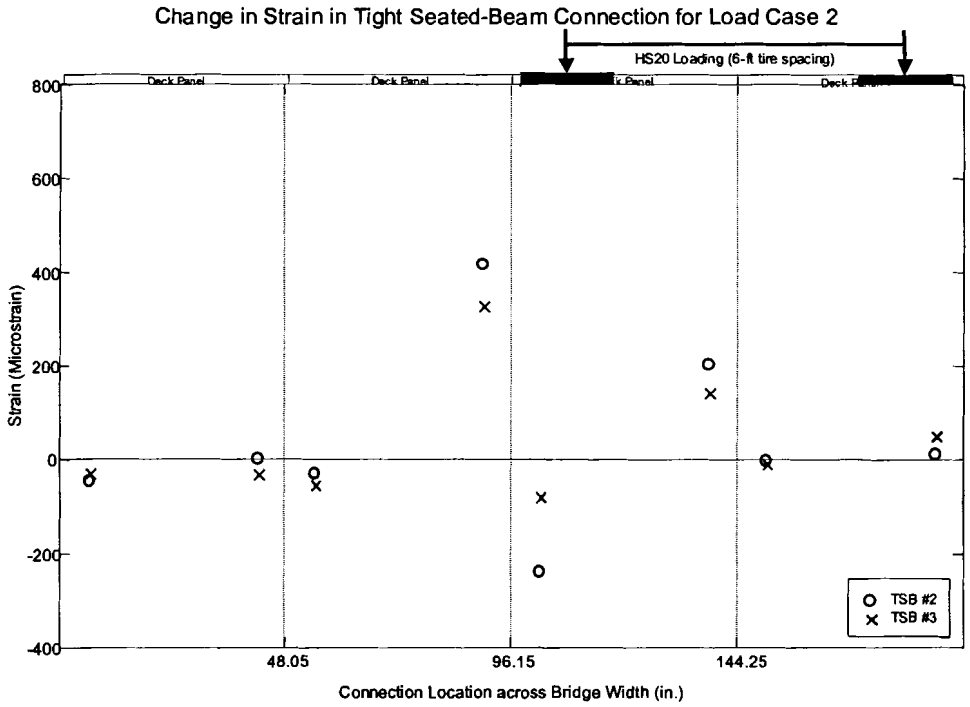

Figure 4.19 Change in strain in seated-beam connections for all TSB tested in experimental Load Case #2

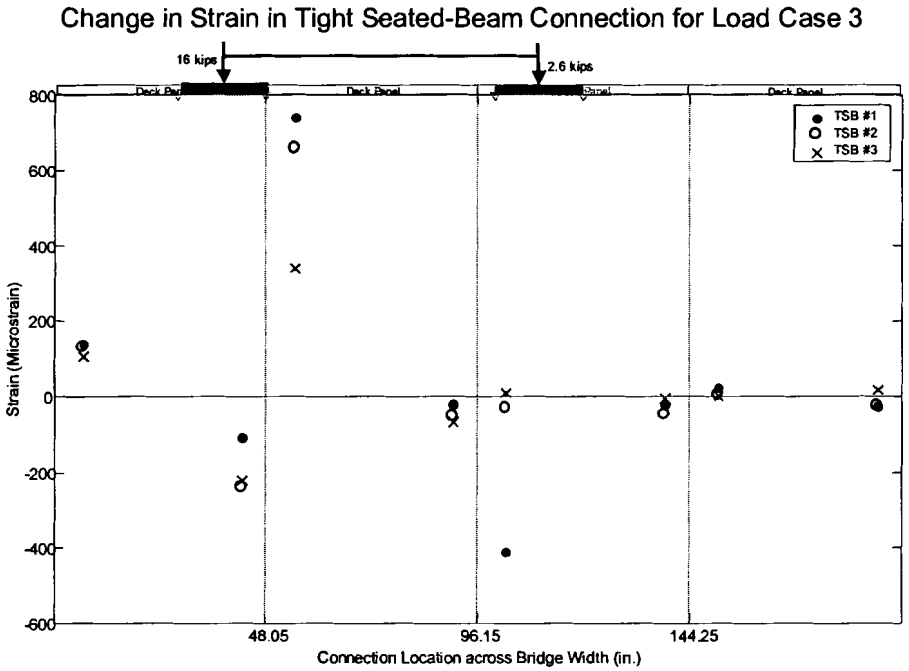

Figure 4.20 Change in strain in seated-beam connections for all TSB tested in experimental Load Case #3

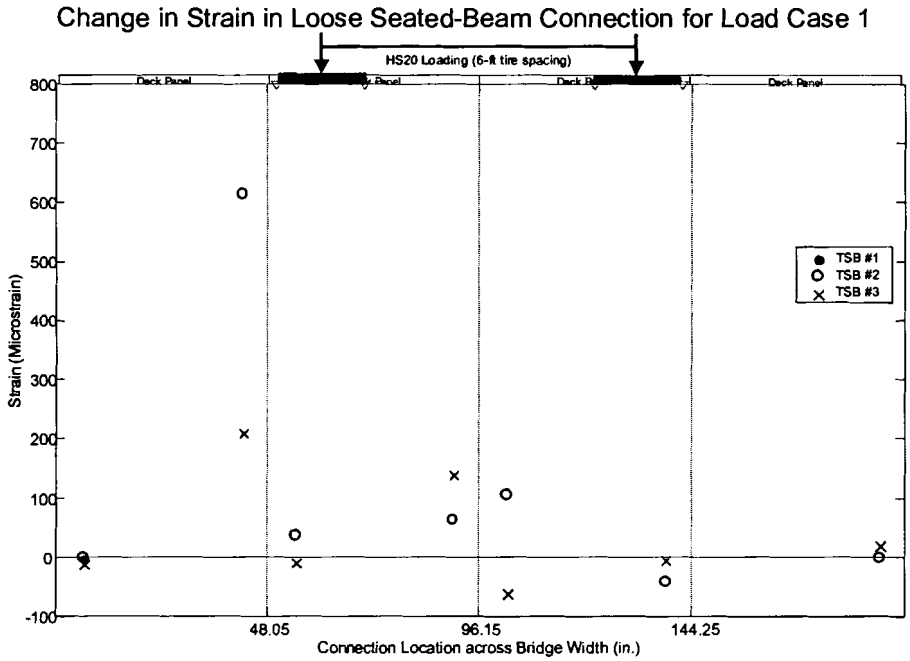

Figure 4.21 Change in strain in loose seated-beam connections for all TSB tested in experimental Load Case #3

Figure 4.21 graphs the change in the strain in the loose seated-beam connections under Load Case #1 loading. The stiffer TSB distributes more of the load to adjacent panels, increasing the strain in the connection.

4.7 Conclusions

From the laboratory testing that was done, several conclusions about longitudinal glulam deck bridges may be made. It can be concluded that the stiffness of the TSB can affect the panel deflections by stiffer TSB distributing more load to adjacent panels. Connection systems affect results as well. Stiffer connection systems should be used more often, because they distribute more of the load between panels. However, it must be realized that a loose connection behaves less stiff, and since connections are often loosened from their initial tightness during their service life, the potential of any

connection system performing with less stiffness should be considered in the engineering of these bridge systems. The test results appear reasonable considering the material being tested and the high potential variability in results due to differential initial tightness of the connection systems, bending of the threaded rod connections, and damage to the strain gages on the threaded rods.

Chapter 5

FINITE ELEMENT MODEL

5.1 Introduction

This chapter presents the Finite Element (FE) model developed in this study. The approach selected is first discussed, followed by details of the elements selected to represent the components of a longitudinal glulam deck bridge and of the boundary conditions, applied loading, and analysis used in the FE model. The deflection convergence study is presented, as well. The model is validated though correlation with experimental results from testing at The University of Maine (UMaine) and Iowa State University (ISU). The chapter concludes with results and recommendations with regard to the FE model.

5.2 Finite Element Model for Longitudinal Glulam Deck Bridges

This section describes the FE model selected for the study reported in this thesis. The approach taken and its rationale is first discussed and is followed by details of the modeling of components and loadings.

The FE model was developed using the ANSYS Finite Element Analysis (FEA) software, version 5.7 (ANSYS 2000a). The program was used due to its availability, versatility, good performance in FEA, and common use among practicing engineers. This program has also been used by others to model longitudinal glulam deck bridges (Kurain 2001, Hajdu 1994).

5.2.1 Modeling Approach

This section describes the selection of the model, the benefits of this FE model over previous models, and the limitations of the model in analysis of longitudinal glulam deck bridges.

The model was selected to capture the system behavior without overcomplicating the model or analysis. Although an option, the FE model selected does not use solid elements. The model does however model the bridge system in three-dimensional space. This allows the analysis to capture three-dimensional behavior. A sketch of a typical longitudinal glulam deck bridge is given in Figure 5.1. (The global coordinate system is shown on the bridge in the figure.) To model this bridge system, the FE model uses plate, beam, spar, and spring elements (Figure 5.1). Plate elements model the deck panels, beam elements model the TSB, and spar and spring elements model the connections and interface between the deck and the TSB. The elements are described in further detail later in this section.

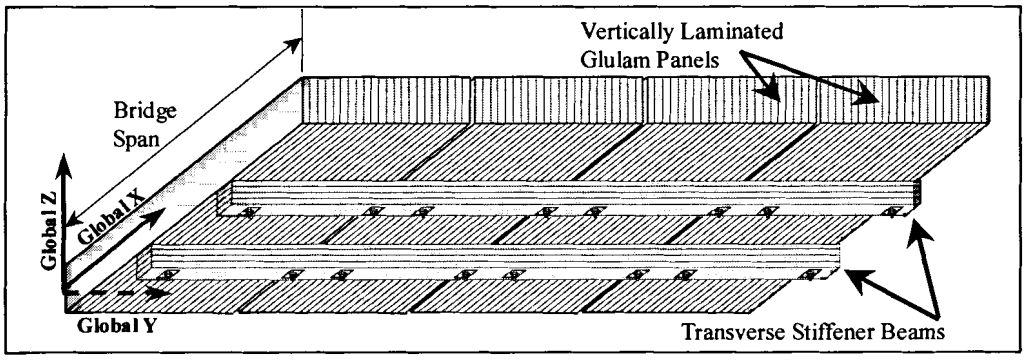

Figure 5.1 Typical longitudinal glulam deck bridge superstructure

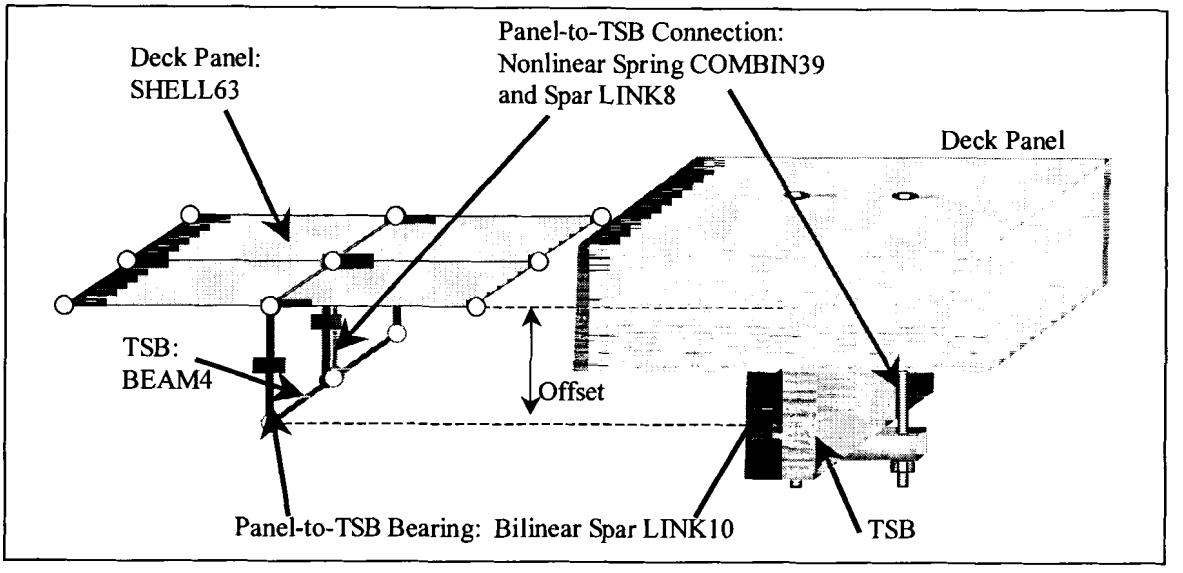

Figure 5.2 Finite element model used for longitudinal glulam deck bridge

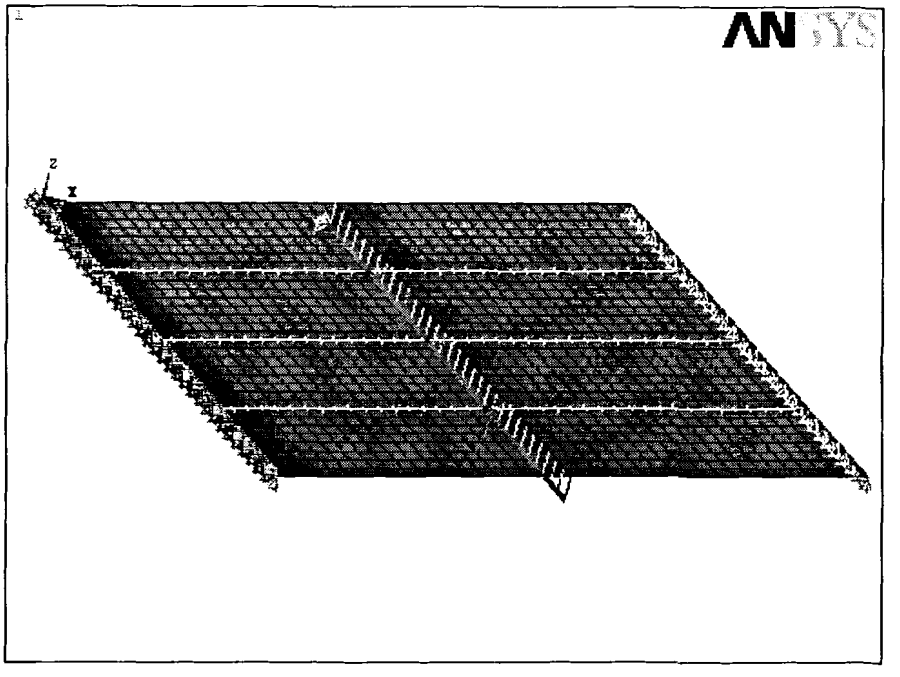

Figure 5.3 ANSYS schematic of finite element model used for longitudinal glulam deck bridge

Several important features were incorporated in model reported here that have not been in the in previous models investigated during the literature review. The model developed for this study models the nonlinear behavior of the connections and models the panel-TSB bearing interaction. It also places the connections six inches from the panel edge where they are located in the actual bridge. The mesh for the model developed in this study is much finer than that which has been used before. The smallest mesh used in ISU's work was 18-in. x 12-in. The model developed at UMaine uses a 6-in. by 6-in. mesh, allowing a better capture of panel and TSB behavior.

The model developed for this thesis had several limitations. Most limitations of the model used result from approximating a three-dimensional structure into a system of thin plates, beams, and springs. The limitations are listed below.

1. Since the model uses thin plates, the distribution of Z-stresses through the thickness of the panels is not accounted for. However, a solid model would require extensive additional computer resources for what is anticipated to be marginal gain.
2. Initial warp and twist in panels are not modeled either, since these could vary considerably in a bridge.
3. Shear stiffness and deformation in panels are not modeled.
4. Since the TSB is modeled using line elements, Z-stress through TSB depth is not modeled.
5. An actual bridge would have some fixity at the supports, rather than the free rotation the ideal pin connection models.

6. The model does not consider the transfer of horizontal shear between the deck panels and the TSB due to friction.

7. The model does not include curbs. Modeling the curbs was not included in this study due to time constraints, however they could be incorporated into the model. It is important to note that the added stiffness may significantly change the system behavior.

The impact of these limitations is evaluated at the end of this chapter through comparison with experimental results.

5.2.2 Deck Panels

The bridge deck panels were modeled using ANSYS' SHELL63 (Figures 5.1 and 5.4). SHELL63 is a four-noded, elastic, thin-shell element. Only bending stiffness is considered. Each node of the SHELL63 element has six degrees of freedom (three translational degrees of freedom in the nodal x, y, and z-directions and three rotational degrees of freedom about the nodal x, y, and z-axes). The panels were meshed into quadrilateral elements, with aspect ratios as close to one as possible. As a thin-shell model, no dissipation of stresses through the thickness of the panel are accounted for during analysis.

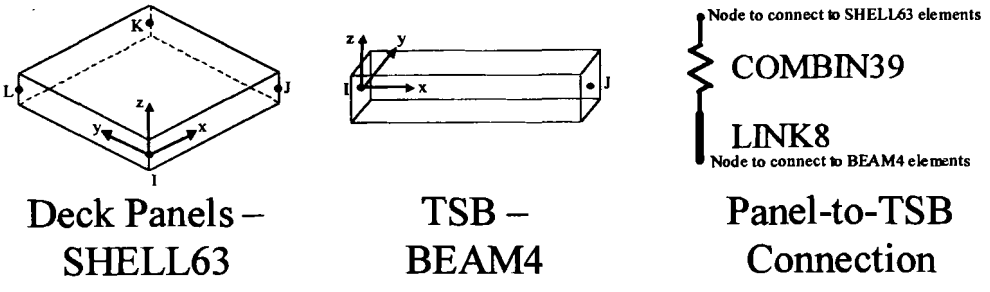

Figure 5.4 ANSYS' elements used to model the bridge superstructure

Material properties of the shell varied according to the wood species and, in the case of the UMaine laboratory experiments, the individual panel being represented. Orthotropic properties were used to approximate the actual behavior of the wood panels. Properties were obtained from a combination of laboratory testing and published values. The transverse MOE and shear modulus (G) were derived from the longitudinal MOE and typical correlations for the wood species being modeled (FPL 1999). The properties of loblolly, longleaf, shortleaf, and slash pine were averaged for the Southern Pine (SP) wood. Along the length of the panel (element x-direction), the material properties were assumed equivalent to the properties of the wood longitudinal-to-wood-grain. Since the panels are glulam, it is assumed that the radial and tangential wood grain is approximately randomly distributed through the width and thickness of the panel. Therefore, the material properties in the width and thickness directions (element y and z directions) are assumed equal and equivalent to the average of radial and tangential material properties. The actual material properties used in an FE analysis of a bridge are listed in the section that discusses that analysis. For bridges with FRP-glulam panels, the panels were modeled as a similar conventional glulam panel but with increased stiffness provided by the FRP. For the deck panel elements, the global coordinate system and the local coordinate system were coincident.

5.2.3 Transverse Stiffener Beams (TSB)

The below-deck transverse stiffener beam was modeled using ANSYS' elastic, prismatic beam element, BEAM4. It is uniaxial with six degrees of freedom at each end node (Figure 5.4). The element has tension, compression, bending, and torsion capacity.

Shear deflection was not considered. The material properties for the beam element were obtained the same as described for the panel elements. However, for the beam element the local and global coordinate systems are not coincidental. The actual material properties used for a TSB will be given in the section where the analysis is discussed.

5.2.4 Panel-to-TSB Connections

Although not always considered significant, the selection of the model used for connections is not inconsequential. The connections between the panels and the TSB were modeled using ANSYS' COMBIN39 and LINK8 elements (Figure 5.4). Used in series, the two elements arose from the desire to model the nonlinear behavior of the connection in tension and the possible need to pretension the connection. The connection must be limited to transmitting only tensile forces, since a compression force would not be transmitted through the connection, but rather through the bearing between the panel and the TSB.

The COMBIN39 element is a two-node, nonlinear, uniaxial spring element with three translational degrees of freedom at each node. A spring was selected since the connections between the panels and the TSB only transfer vertical loads by carrying axial loads. The physical connections do not provide significant bending stiffness to transfer bending moments or torsion to the stiffener beams. In the published literature, it was believed that the connector forces remained in the linear range, but for increased accuracy the entire load-deflection curve was used for this model. Since the element selected is nonlinear, the experimentally-measured behavior of the connections can be considered in the analysis. The experimentally-measured axial stiffness of the connection, the axial

load-deformation curve, is used for the element. The axial deformation is a function of the crushing of the wood at the top of the connection where the bolt head or washer bears on the panel, the crushing of the wood at the bottom of the connection where the connection bears on the bottom of the TSB, the elongation and bending of the metal of the connector itself, and any initial slack in the connection (Figure 5.5). Although in reality the connection has no capacity in compression, the element was given a very small compression stiffness to avoid convergence difficulties. For forces and deflections beyond the range of the input load-deflection curve, ANSYS maintains the last given slope of the element's load deflection curve.

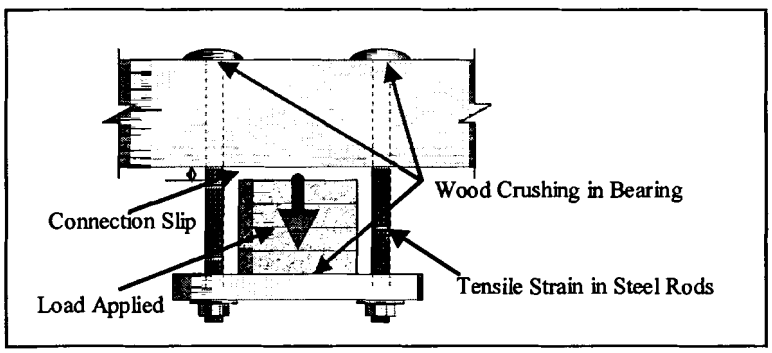

Figure 5.5 Sources of slip in load-deflection connector curves

As detailed in Chapter 2, previous models of longitudinal bridge deck systems have only considered the linear behavior of the connection (Sanders *et al.* 1985, Funke 1986, Hajdu 1994, Tomforde 1996, Witmer 1996, Lacross 1997, Kurain 2001); however, the axial force in the connector can exceed the connector's linear elastic range. It had been previously thought that load in all of the connections would remain under five kips (Funke 1986). The parametric study (reported in Chapter 6) shows that the load carried in the connection can, and often does exceed five kips. In the experiments performed at UMaine, in Load Case #1 maximum connection stress for TSB#1 (the least stiff) was

almost nine kips, and the maximum connection stress for TSB#2 & TSB#3 was over five kips. The nine kips seen in the lab was not matched in the parametric study, but this may be due to the fact that threaded rods used in the lab tests actually had a ½-in. diameter at the locations of the strain gage as well as due to the other factors detailed in Chapter 4.

LINK8 is a three-dimensional, two-noded, uniaxial tension/compression element with three translational degrees of freedom at each node that was used in solely to pretension the connections. Although LINK8 can carry compressive loads, in the model it is placed in series with COMBIN39 which cannot carry any compressive loads and thus controls the compressive connection behavior. The LINK8 element has no bending or torsional capacity. The element may be given an initial strain. In the models of the experiments performed at UMaine there was a known connector prestress for most connections. Prior to analysis under the HS20 loading, each connector was given (through a few iterations) an initial strain that, when the system was analyzed, would induce the measured connection prestress. LINK8 was kept as extremely stiff so that it would not contribute to the load-deflection behavior of the connection.

Pretensioning the connectors did not significantly affect the TSB shear and bending moment (Figure 5.6). Unless the pretension load in the connector was greater than the load that would be carried under the live load, the live load controlled the connection. Therefore, although the pretensioning assisted in validating the model, it does not appear necessary to consider it in other analyses.

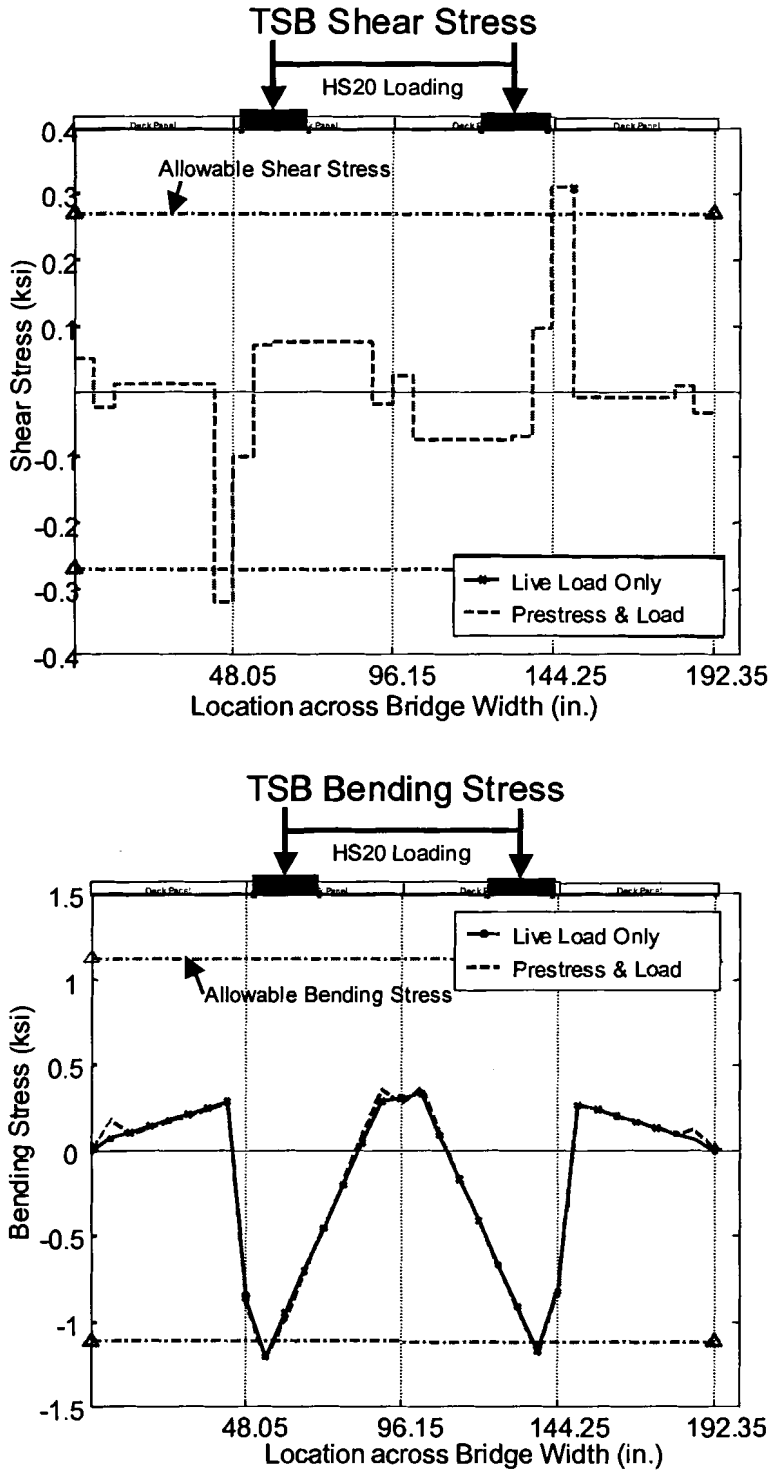

Figure 5.6 Comparison of shear and bending stress in TSB with and without prestressed connections

Connection and TSB behavior varies greatly with the connectors used. For most of the study reported in this thesis, Hale's research at Weyerhauser (Hale 1978) was used to model the behavior of the various connectors. Figure 5.7 shows the variability of connection behavior as determined by Hale. Hale's testing of the 5/8"-diameter bolt appears to only consider the bearing stiffness of the wood under the head of the timber bolt. In reality, the stiffness of the 5/8" through-bolt connection is a result of the stiffness of the wood under the head of the bolt in bearing, the stiffness of the timber bolt itself, and the stiffness of the wood under bearing of the plate or washer at the bottom of the bolt as well as any pretensioning of the connection. A FE Analysis (FEA) of the connection alone showed that the complete system is slightly less stiff than the bearing under the bolt head. The curve for the complete system was used for the FE analysis when running models to compare to UMaine experimental testing. Further discussion on the sensitivity of the model to the connection type and stiffness can be found in the parametric study reported in Chapter 6 and further discussion of Hale's test report may be found in Chapter 2. The curves show the behavior of a new connection. After the connection has been cycled through several loadings, some crushing of the wood, and thus permanent deformation, will occur. That deformation would be shown by a shift of the axial oad-deformation curve to the right.

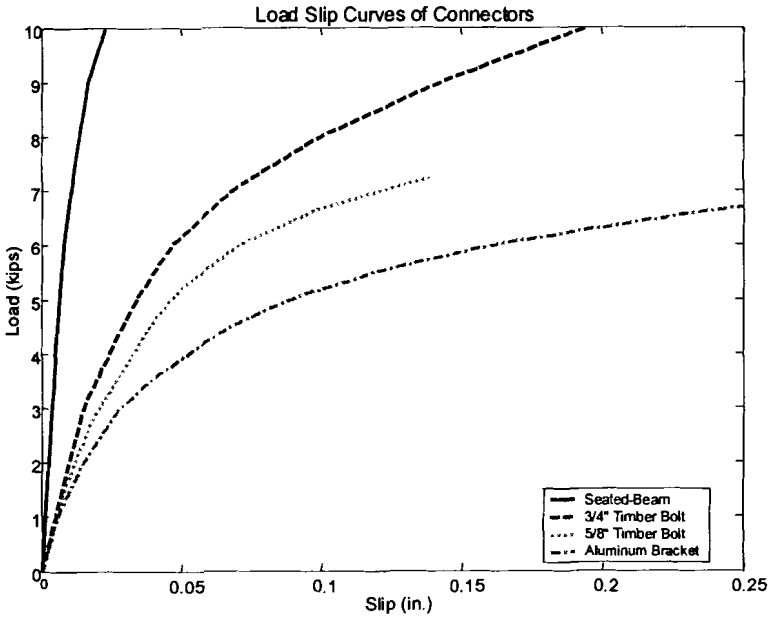

Figure 5.7 Load-deformation curves of connectors (Hale 1978, Funke 1986)

Some connector systems such as the seated-beam connection and aluminum brackets may be more accurately modeled using two elements on either side of the transverse stiffener beam. However, this was beyond the scope of this study, requiring experimental testing of connection systems to accurately capture the behavior.

The bearing stiffness of the wood controls the stiffness of bolted connections in these systems since the connection bolts are loaded parallel to their longitudinal axes. Since the wood bearing stiffness controls, connection stiffness may be increased or decreased by respectively increasing or decreasing the bearing area under the head of the bolt. As the connection is cycled through its lifetime loading, the axial load-deformation curves of Figure 5.7 to shift to the right, and thus transferring less load through the connection.

5.2.5 Panel-Transverse-Stiffener-Beam Bearing

LINK10 was used to model the bearing between the panel and the stiffener beam. Only compressive forces can be transmitted through the bearing of the panels on the stiffener, therefore the bilinear (minimal stiffness when in tension, calculated bearing stiffness when in compression) spar element was chosen, specifying its compression only option. To avoid instability, a small stiffness is allowed when the element is in tension. The element has three translational degrees of freedom at each node (). The element models the compression of the wood that causes vertical forces to be transmitted between the panel and stiffener beam. The assumed area of the wood that contributes to the force transfer is shown in Figure 5.8. This assumed cross-section area is multiplied by the mesh size in the transverse direction giving a volume of wood contributing to bearing force transfer. The panel and TSB stiffness that results in load transfer can be modeled as two springs in series. The stiffness of each is based on their modulus of elasticity perpendicular to grain, depth of wood assumed compressed (spring length), area of wood contributing to the compression. LINK10 is a single element that has stiffness equivalent to that of the two springs. LINK10 has a length equivalent to the distance from the neutral axis of the panels to the neutral axis of the stiffener beam. Its area is the width of the stiffener beam times the bearing element spacing. LINK10's modulus of elasticity is then adjusted so that its stiffness is equivalent to that of the panel and beam bearing in series.

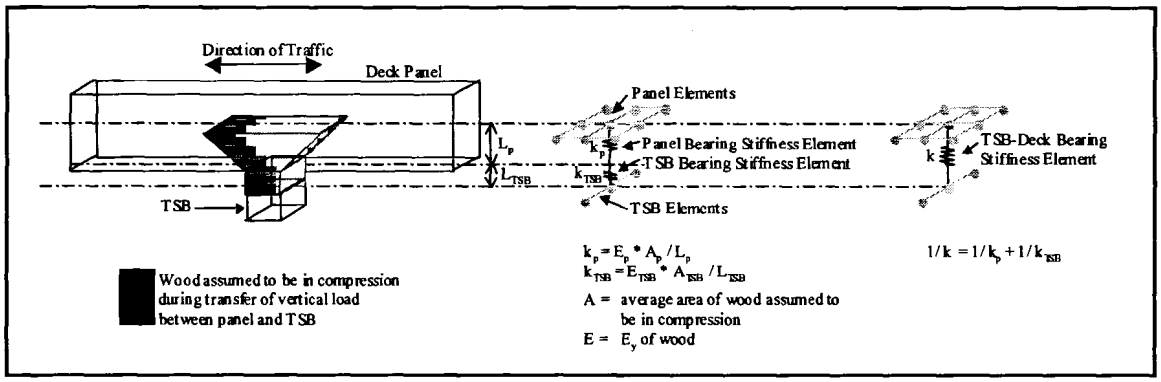

Figure 5.8 Derivation of panel-TSB bearing element stiffness

5.2.6 Boundary Conditions

The model is simply supported with global X, Y, and Z-translations fixed at the panel ends. For TSB stability, the global X and Y-translation and Y and Z-axes rotation are also fixed at one end of the TSB. Global X and Y-translation and rotation about the Z-axis are also fixed at the nodes joining the COMBIN39 and LINK8 connection elements.

5.2.7 Loading

To avoid stress concentrations that may result from modeling the AASHTO HS20 truck tires as point loads, the loading was modeled using two methods. The first used a simple distribution of the loads to nodes. The second used uniform surface loads on the elements. The different methods did not significantly affect the system response, except for transverse bending stress in the panels. The simple load distribution method distributed the AASHTO tire loading transversely by the tributary area method into point loads at the nodes (Figure 5.9). With this method, the loading was not distributed longitudinally. The element uniform surface loading distributed the AASHTO tire loading transversely and longitudinally into uniform loads for each element based on the

percent of tire the element has loading it (Figure 5.10). With the simple load distribution the loading truck axle was always coincident with the nodal locations, but with the uniform surface load, the tire load patches could be placed anywhere on the bridge deck.

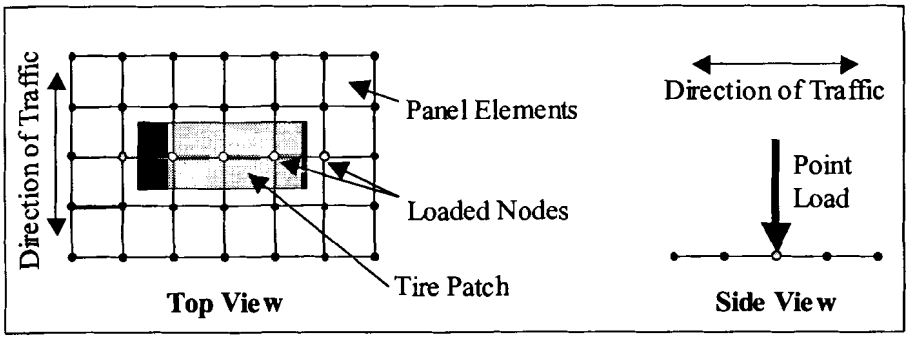

Figure 5.9 Simple load distribution scheme used for finite element model

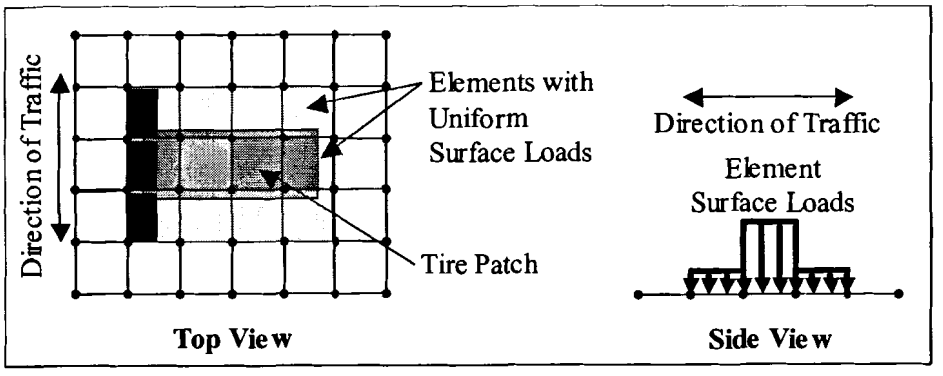

Figure 5.10 Uniform element surface load scheme used for finite element model

5.3 Convergence Study

Global deflections converge with a larger element size than the 6-inch mesh typically used in this study (Figure 5.11). However, TSB shear and bending moment converge at the 6" mesh (Figure 5.11). Additionally, it was felt that the connections should be placed at their exact locations and that the bearing elements should be reasonably close together in order to better capture the transverse stiffener behavior. The

convergence study used the UMaine experiment for the model geometry with TSB #2 and Load Case #1 (see Chapter 4 for UMaine experiment details).

5.4 FEM Validation

The finite element model described has been validated using the UMaine experimental test results (see Chapter 4 for details) and the Iowa State University (ISU) experimental test results (see Chapter 2 for details). The correlation considers deflection and strains from the panels, panel-to-TSB connections, and TSB.

5.4.1 Correlation with Experimental Results from The University of Maine

A complete description of the model geometry, material properties, loading, and testing for the UMaine experiments can be found in Chapter 4.

5.4.1.1 Panel Deflection

Most measured experimental deflections were within 0.05-inch of the deflections obtained predicted using the finite element model. Measured deflections from Panel A01 do not correlate as well as those for the other three panels. The panel had been warped significantly prior to the testing. This panel may have rocked (rigid body motion) during Load Case #1, causing the measured deflections to be different than the FEA. The setup for the direct current linearly variable differential transformers (DCDT) used to measure deflections was not ideal, and rocking or disturbance of a DCDT stand could have occurred as well. Although no support settlement was measured during the initial check prior to testing, continual monitoring of support settlement during testing was not possible, and some may have occurred. However, the deflections from the finite element

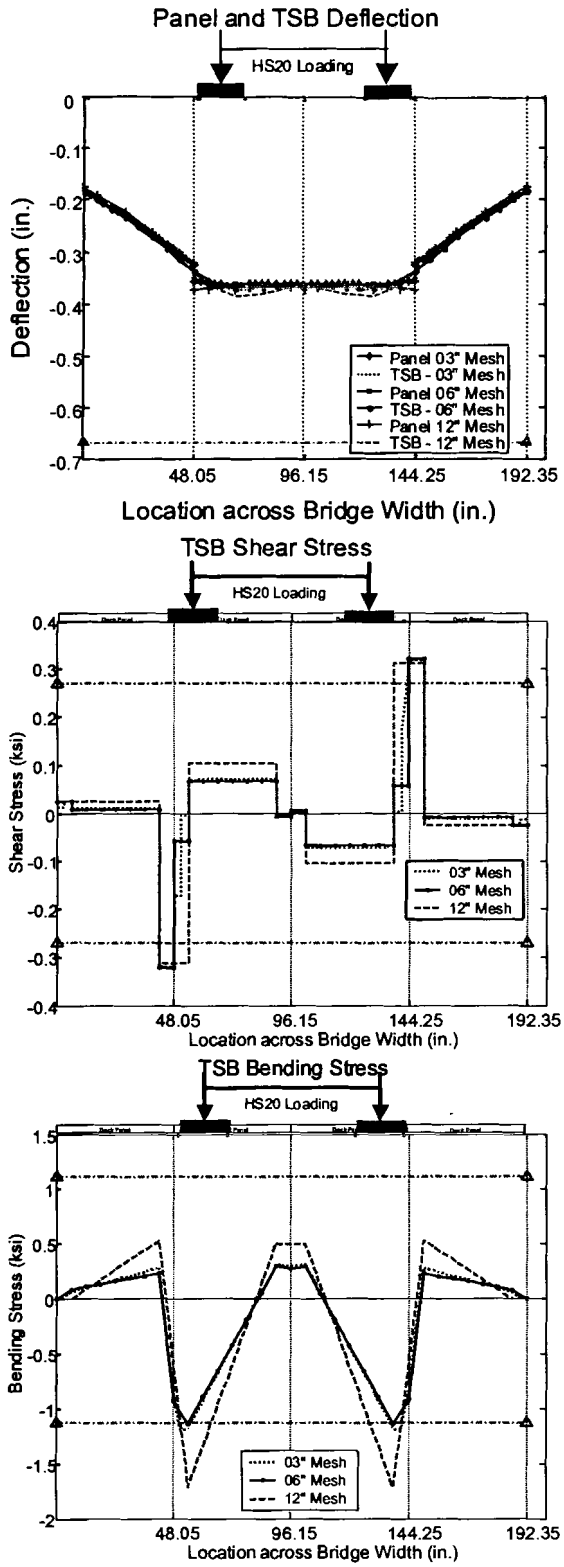

Figure 5.11 Convergence of deflections

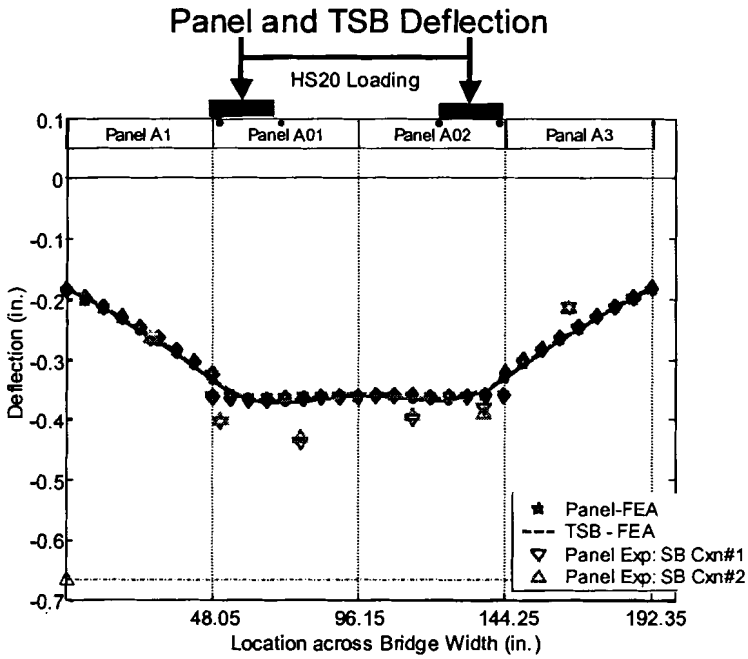

Figure 5.12 FEA-predicted midspan panel deflections vs. UMaine experimental results (Load Case #1, TSB #2, seated-beam connection)

analysis and the experiment were very close as can be seen in Figures 5.12, 5.13, and 5.14. These figures show the midspan panel deflections measured experimentally and the midspan panel and TSB deflections predicted by the FE model.

The deflections for panels A02 and A3 in Load Cases #2 and #3 do not correlate as well with the finite element model due to damage that occurred when the panels were overloaded during the first test configuration of Load Case #2 and some permanent damage may have occurred. Even with this damage, most measured deflections are within 0.05 in. of the deflections predicted from the finite element analysis. FEA correlations to other tests are shown in Appendix D.

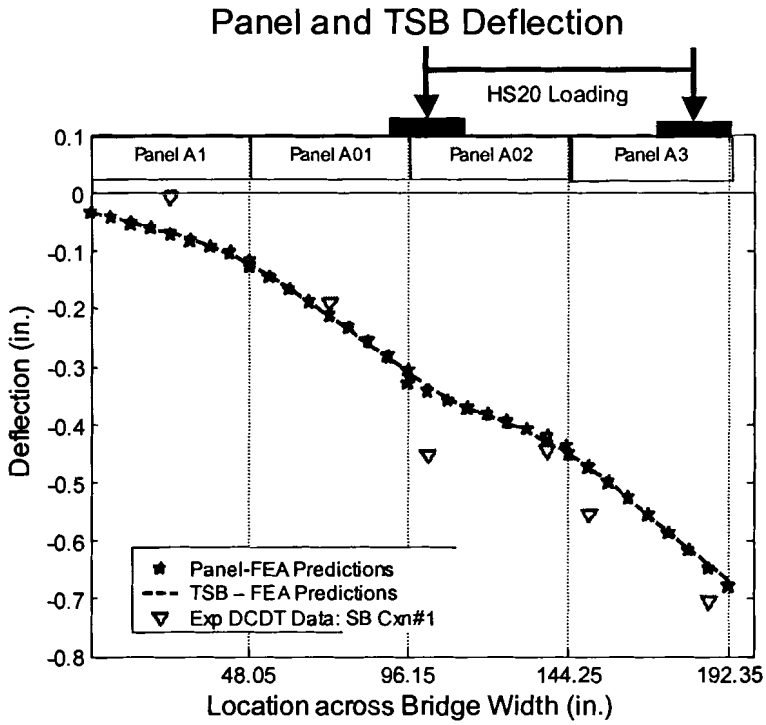

Figure 5.13 FEA-predicted midspan panel deflections vs. UMaine experimental results (Load Case #2, TSB #3, seated-beam connection)

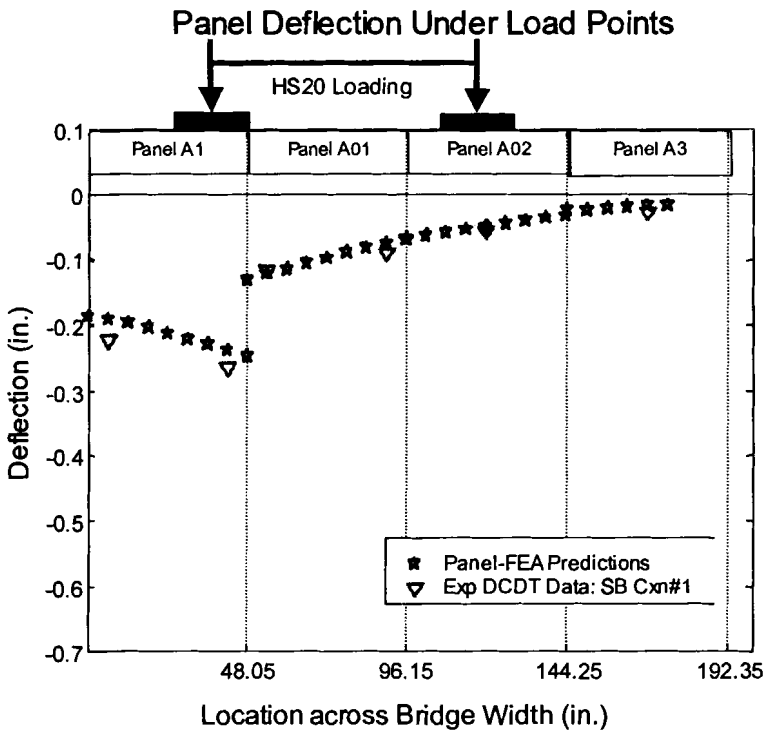

Figure 5.14 FEA-predicted panel deflections vs. UMaine experimental results (Load Case #3, TSB #1, seated-beam connection)

5.4.1.2 Axial Strain in Threaded Rods

The measured forces in the threaded rods used in the seated-beam connections did not correlate with the finite element analysis as well as the deflections. However, due to the delicate nature of the instrumentation, there were many more possibilities of error in these measurements. Initially all sixteen rods were instrumented with at least two strain gages on each; however, storage, transportation, and movement of the threaded rods destroyed several strain gages or their connections. Multiple strain gages on a rod could be averaged to minimize connection bending effects; however, if a strain gage on a rod was damaged there were no means of determining, and thus adjusting for, bending effects. Once a strain gage had been damaged, it was not possible to replace the gage due to time constraints and the potential damage that would be done to other gages on the same rod. The connections underwent much more bending than was anticipated due to the warping and dimensional variation of the panels. However, correlations are still reasonably accurate as can be see in Figures 5.15, 5.16, and 5.17. These figures show the measured strain in the connection converted to an axial force and the FEA predicted axial force. FEA correlations to other tests are shown in Appendix D.

5.4.2 Correlation of FE Model with Experimental Results from ISU

To further verify the finite element model developed in this study, the analysis predictions were compared with the experimental results measured at ISU (Funke 1986). This testing is more completely described in Chapter 2 and was done to validate the wheel load fraction predicted by ISU's finite element model. The AASHTO design methodology (1996) for longitudinal glulam deck bridges is based on this testing at ISU

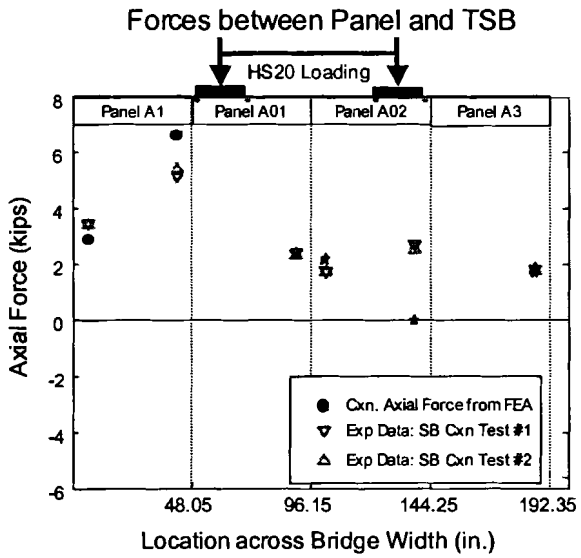

Figure 5.15 FEA predicted seated-beam connection forces vs. UMaine experimental results (Load Case #1, TSB #2)

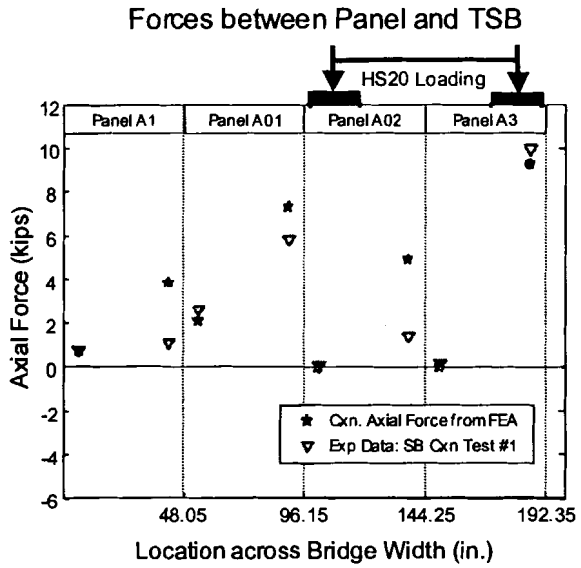

Figure 5.16 FEA predicted seated-beam connection forces vs. UMaine experimental results (Load Case #2, TSB #3)

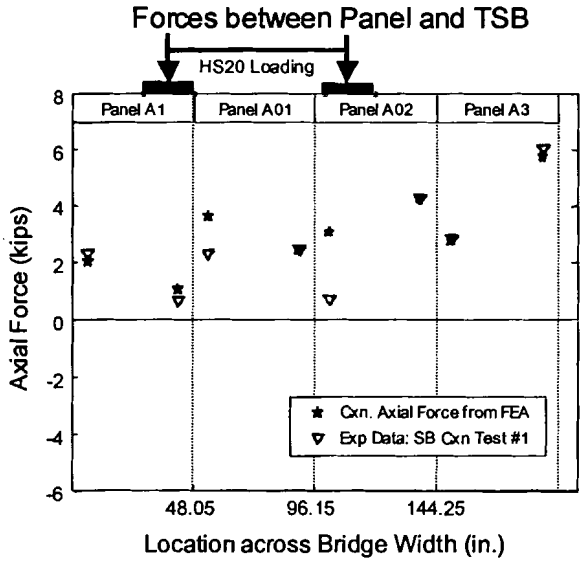

Figure 5.17 FEA predicted seated-beam connection forces vs. UMaine experimental results (Load Case #3, TSB #1)

(Sanders *et al.* 1985, Funke 1986, Ritter 1990), making this correlation crucial. The model developed gives results that correlate very well ISU's experimental results. Figure 5.18 compares well the measured midspan panel deflections to those predicted by the FE analysis. Figure 5.19 compares the measured midspan panel strains with FEA-predicted strains. Figure 5.20 compares the experimental and FEA-predicted TSB strains. FEA correlations to other tests are shown in Appendix D.

5.5 Conclusions

The longitudinal glulam deck bridge was modeled using the ANSYS finite element program. Orthotropic plate elements were used to model the panels, beam elements were used to model the TSB, TSB-to-deck-panel connections were modeled using nonlinear spring elements and link elements with pretensioning capability, and the bearing between the deck and the TSB was modeled with compression only spar elements.

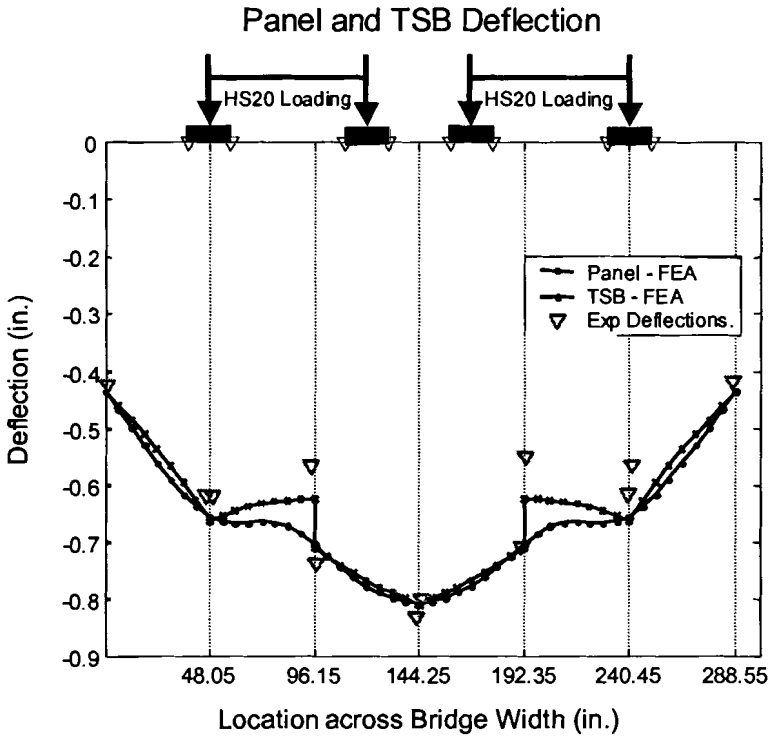

Figure 5.18 FEA-predicted midspan panel deflections vs. ISU experimental results (Funke#1)

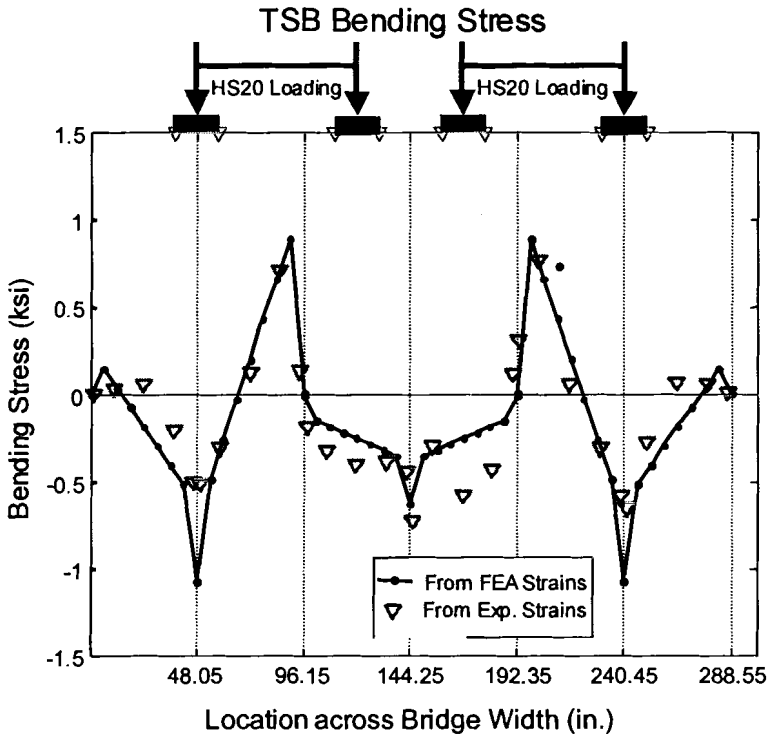

Figure 5.19 FEA-predicted TSB bending stress vs. ISU experimental results (Funke#1)

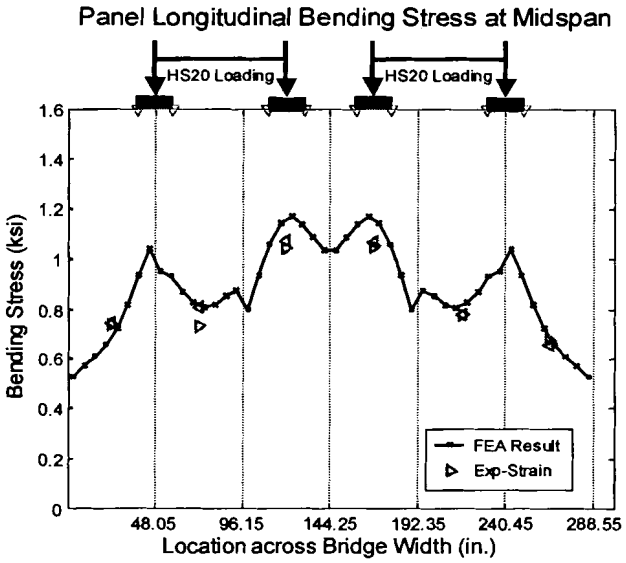

Figure 5.20 FEA-predicted midspan panel stress vs. ISU experimental results (Funke#1)

The model developed in this study gives predictions of a longitudinal glulam deck bridge behavior with reasonable accuracy. The model is valid for both non-reinforced and FRP-reinforced glulam deck panels. The model does not use solid elements and therefore does not capture stresses through the depth of the beam or the panel. The model does not include or account for the stiffening effects that curbs provide to a bridge. From experiments performed at UMaine and ISU, panel deflections and strains, connector forces, and TSB strains were correlated with the FE model. All UMaine and five ISU experimental tests were compared to the model with reasonably good correlations of the experimental data to the analytical predictions.

This model contributes to the previous analytical work on longitudinal glulam deck bridges in several aspects. The pretensioning capability and the nonlinear behavior of the connections had not been modeled in previously published literature. The bearing between the panels and the TSB based on the glulam stiffness also has not been modeled before in the published literature on these bridges.

Chapter 6

PARAMETRIC STUDY

6.1 Introduction

In order to investigate the behavior of longitudinal glulam deck bridges, in general, and the behavior of the Transverse Stiffener Beam (TSB), in particular, a parametric study was performed. The parametric study used the finite element model described in Chapter 5 of this thesis. The purpose of the parametric study was twofold: primarily, to determine the adequacy of current empirically-based AASHTO design criteria for longitudinal glulam deck bridges (AASHTO 1996), and, secondarily, to investigate any deficiencies found and propose recommendations to change AASHTO criteria. Preliminary FEA studies performed at UMaine showed potential inadequacy in the AASHTO 1996 TSB design criteria. These findings focused the parametric study on TSB behavior. Relative Displacement between Panels (RPD) was also investigated, since reflective cracking in the asphalt above panel joints running parallel to traffic has been reported to be a problem with these bridges. Prior to evaluating the adequacy of the AASHTO design criteria, the sensitivity of the TSB stresses and RPD to various design parameters was investigated. Once sensitivity and trends were understood, critical bridge configurations and loading were found. This chapter outlines the parametric study, presents results, identifies inadequacies in the AASHTO design criteria, and proposes simple "fixes" to the AASHTO design methodology for longitudinal glulam decks.

6.2 Overview

6.2.1 Scope

The parametric study started with an investigation into the sensitivity of TSB stresses and Relative Panel Displacement (RPD) to the following thirteen design parameters described in Table 6.1: bridge span, TSB spacing, bridge width, panel width, number of lanes, panel material properties, panel thickness, panel-TSB connections, TSB MOE, TSB geometry (aspect ratio), TSB size, and loading position. This allowed the identification of critical loadings and associated design parameters that maximize TSB stresses and relative panel displacements. The adequacy of the current AASHTO design criteria for longitudinal glulam decks was evaluated and changes were proposed. Forty-three bridges were modeled and over 50 load cases were considered in 149 FEA analyses.

6.2.2 Rationale

In determining the range of parameters considered in this study, the effect of the parameter on TSB behavior was the principal concern. This section describes the rationale behind the bridge design parameters selected and the range of values analyzed for each parameter.

Two critical bridge spans that result in maximum TSB spacing were considered: a 20-ft. span bridge and a 35-ft. span bridge. AASHTO criteria require TSB spacing of less than or equal to 10 feet and TSB to be placed at midspan (AASHTO 1996). Thus, a bridge with a 20-foot span and a single TSB at midspan gives the maximum TSB spacing. The longer spans have greater transverse load distribution between panels,

Table 6.1 Parametric study (partial factorial)

Parameter	Parameter Range
Bridge Span (L) Number of TSB	20 ft. (1 TSB at maximum AASHTO spacing) 35 ft. (3 TSB at approximately 8.75-ft. spacing)
Bridge Width (W) Panel Width (w) Number of Lanes	42-in. wide panels: 14-ft. wide bridge – 4 panels (1 lane) 21-ft. wide bridge – 6 panels (1 or 2 lanes) 48-in. wide panels: 16-ft. wide bridge – 4 panels (1 lane) 20-ft. wide bridge – 5 panels (1 or 2 lanes) 24-ft. wide bridge – 6 panels (1 or 2 lanes) 32-ft. wide bridge – 8 panels (2 lanes) 54-in. wide panels: 13.5-ft. wide bridge – 3 panels (1 lane) 22.5-ft. wide bridge – 5 panels (1 or 2 lanes)
Material Properties	Glulam Layup SP Combination #47 (AFPA, AWC 1997)
Panel Thickness	8.5 in. 10.5 in. 12.25 in. 14.25 in. 16.25 in.
Panel Modulus of Elasticity (AFPA, AWC 1997)	875,000 psi (75% of published value with wet-service factor applied) 1,166,000 psi (100%) 1,458,000 psi (125%) 1,749,000 psi (150%)
Panel-to-TSB Connections	Aluminum bracket 5/8-in. diameter through bolt 3/4-in diameter through bolt Seated-beam
TSB Modulus of Elasticity (AFPA, AWC 1997)	1,050,000 psi (75% of published value) 1,400,000 psi (100%) 1,750,000 psi (125%) 2,100,000 psi (150%)
TSB Geometry and Stiffness	See Figure 6.1 and Appendix E, Table E.1.
Live Loading (AASHTO 1996)	HS20-44 Truck (HS20) for 38 load cases (Figure 6.3) HS25-44 Truck (HS25) for 5 load cases Alternate military loading (ML24) for 7 load cases (See Appendix E, Table F.2 for a complete list load cases.)

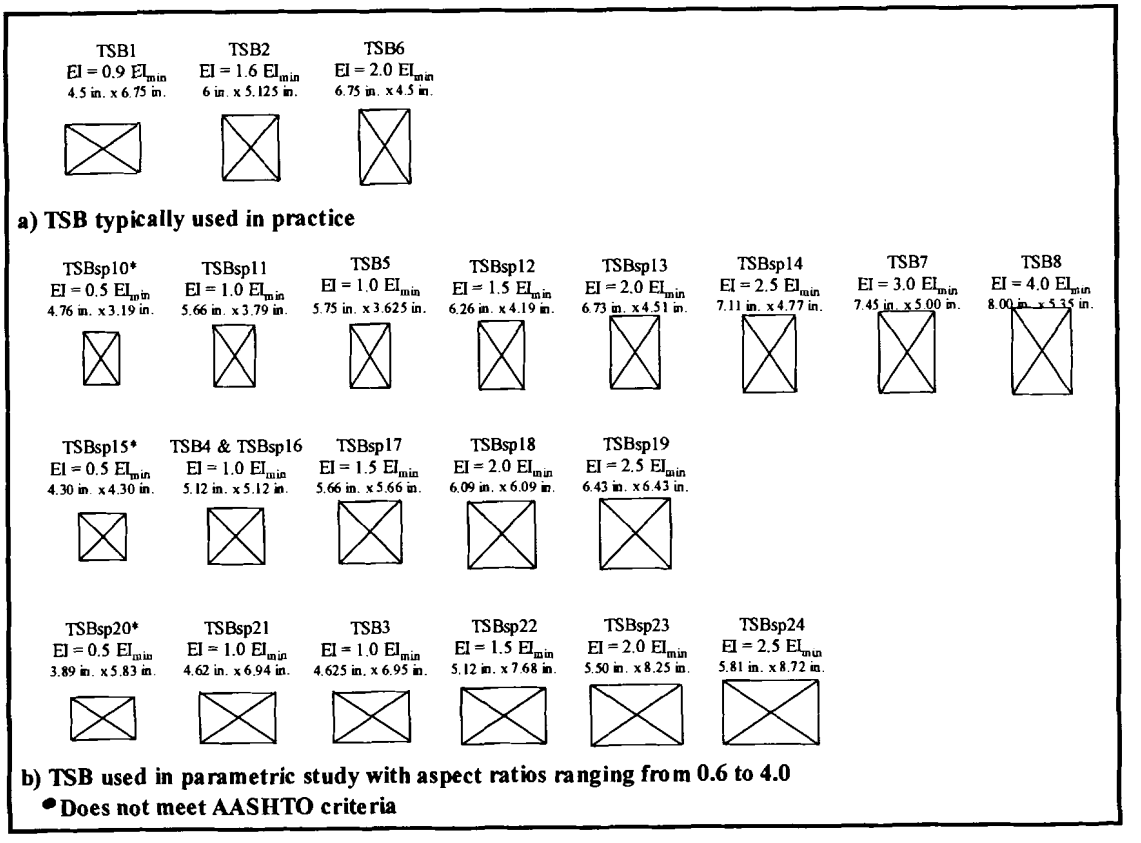

Figure 6.1 TSB configurations and properties used in parametric study (See Appendix E, Table E.1 for details.)

making the 35-foot span potentially critical as well. Following AASHTO requirements, TSB spacing for the 35-foot span bridge is approximately 8.75 feet. Due to the necessity that the placement of the TSB coincide with nodal locations in the FE model, three TSB on the 35-ft. bridge: Two were symmetrically placed nine feet from the ends of the bridge, and the third one was placed at midspan.

The number of panels and panel width depend on bridge width or number of lanes of traffic. Three panel widths were selected for analysis: 42 inches, 48 inches, and 54 inches. These are, respectively, the minimum, typical, and maximum widths used in practice. Initially, 42-inch panels were believed to maximize TSB stresses, since they transfer a greater portion of the live load to the TSB. However, the 48-inch panels can be critical since the AASHTO truck's wheel spacing can cause edge loading on two panels, an occurrence not possible with 42-inch or 54-inch panels. On a bridge constructed of 42-in. wide panels or 54-in. wide panels, when one tire of the AASHTO HS20 truck is placed at the edge of a panel, the other tire is either on a panel joint or close to the center of the panel (Figure 6.2(a) and (c)). This second tire's placement will result in two panels loaded by the tire (tire at panel joint) or less of the panel load being transferred to adjacent panels due to the central placement of the tire on the panel. The six-foot, center-to-center spacing of the AASHTO truck tires, however, will cause edge loading of two 48-in. wide panels whenever one wheel is placed at a panel edge (Figure 6.2(b)). One and two lane bridge configurations were analyzed for each panel width (see Table 6.1). Lane configurations followed AASHTO 3.6 (1996).

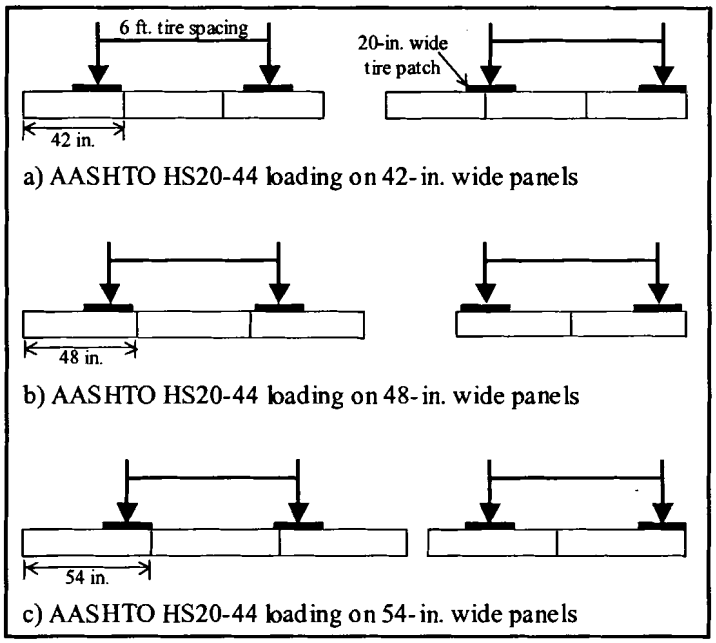

Figure 6.2 Placement of AASHTO HS20-44 tire footprints on various width panels when loading panel edges

The parametric study used material properties of the southern pine glulam layup combination #47 (SP47) allowable stresses (AFPA, AWC 1997) almost exclusively. Tables 6.2 and 6.3 list the allowable stresses and material properties used. For the material properties, typical ratios for the southern pine species were averaged. The ratios are the various material properties divided by the longitudinal modulus of elasticity (E_x). Because the panels are glulam, transverse isotropy was assumed and the radial and tangential properties were averaged. This gave a $E_{z,y}/E_x$ ratio of 0.078, a $G_{xy,xz}/E_x$ ratio of 0.067, a G_{yz}/E_x ratio of 0.012, a ν_{xy} of 0.38, and a $\nu_{yz,xz}$ of 0.38 (FPL 1999). For the panels, the allowable stress and material properties are reduced for exterior exposure by the wet service factor (C_M). The TSB, protected by a watertight deck has a wet-service factor of 1.0 (AASHTO 1996, AFPA, AWC 1997). Panel laminations are loaded parallel to the wide faces of laminations, but TSB are typically oriented more as a beam with laminations loaded perpendicular to the wide faces of laminations. Thus, although the

same layup is commonly used for the panels and TSB, they may have different allowable stresses due to loading and lamination orientation. MOE values were varied as indicated in Table 6.1.

Table 6.2 Allowable stress used for parametric study

Description	Panel F_b (psi)	TSB F_b (psi)	TSB F_v (psi)
SP47	~	1400	270
SP47 with C_M	1410	~	~

(AFPA, AWC 1997; APA 2002)

Table 6.3 Material properties used for parametric study

	E_X	E_Y, E_Z	ν_{XY}	ν_{XZ}, ν_{YZ}	G_{XY}	G_{XZ}	G_{YZ}
SP47	1400	109	0.36	0.38	94	94	16
SP47 with C_M	1166	91	0.36	0.38	78	78	14

(AFPA, AWC 1997; FPL 1999)

Panel thickness was determined using current AASHTO design methodology (AASHTO 1996). Since deflection criteria are not specified (AASHTO 3.25.3.3), panel bending controlled design. The study used discrete panel depths published in the NDS (AFPA, AWC 1997), which are a function of glulam species (Ritter 1990).

Originally, TSB geometry was selected to match sizes typically used in practice (See TSB1, TSB2, and TSB6 in Figure 6.1(a). Iowa State University (ISU) studies used TSB with the same geometry as TSB1. TSB2's geometry is used by Western Wood Structures, Inc. (Gilham 2002). TSB6 was used in this study. All TSB in the parametric study, unless otherwise noted, used SP47 layup glulam with loading perpendicular to the

wide faces of the laminations. However, when other layups are used, TSB stiffness will change. ISU and Western Wood Structures use douglas fir glulam layups.

Additional stiffener beams of different aspect ratios (width/height) but equivalent EI (TSB3, TSB4, and TSB5) and stiffener beams of equivalent aspect ratio (0.67) but different stiffness factors (EI = MOE * moment of inertia) (TSB5, TSB6, TSB7, and TSB8) were then selected to determine the effect of stiffness and aspect ratio on the TSB shear and bending moment. TSB width and height were rounded to typical manufactured dimensions.

However, the FEA results using this variety of TSB (TSB1 through TSB8) did not establish trends of the effect of TSB stiffness and aspect ratio on TSB maximum shear and bending moment. Therefore, a larger matrix of TSB geometries was investigated. Unlike previous TSB investigated, these dimensions were not rounded to typical manufactured dimensions. Three aspect ratios were considered: 0.67, 1.00, and 1.50. For each aspect ratio, TSB dimensions were determined so that stiffness factors (EI) of a SP47 layup would approximately equal 40,000 kip-in^2 (50% of the AASHTO minimum stiffness factor of 80,000 kip-in^2 (AASHTO 1996) (0.5 EI_{min})), 80,000 kip-in^2 (1.0 EI_{min}), 120,000 kip-in^2 (1.5 EI_{min}), 160,000 kip-in^2 (2.0 EI_{min}), and 200,000 kip-in^2 (2.5 EI_{min}).

Live loads used include AASHTO HS20-44 (HS20) (Figure 6.3) and HS25 (HS25) trucks (AASHTO 1996). HS25 is a truck of similar configuration but having tire loads 25% greater than the HS20 truck. For interstate bridges, an alternative military loading of two 24,000 lb. axles spaced four feet apart (ML24) must also be considered (AASHTO 3.7.4).

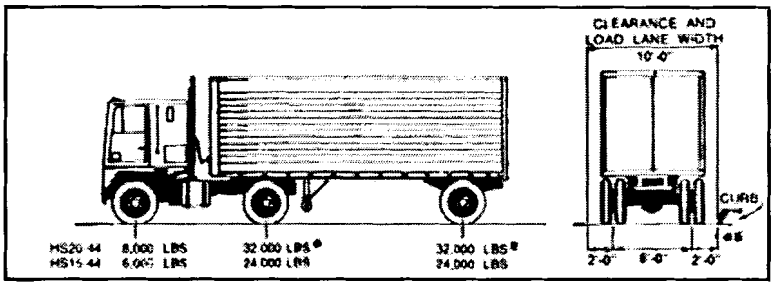

Figure 6.3 HS20-44 live load truck (Courtesy of AASHTO 1996, Figure 3.7.7A)

6.3 Results of Parametric Study

The parametric FE study showed that the TSB may be considerably overstressed under certain conditions, when designed according to current AASHTO criteria (AASHTO 1996). Only the TSB shear forces, shear stresses, bending moments and bending stresses, along with relative movement at longitudinal panel joints, are reported here. Other results obtained from the FE analysis include panel stresses, deflections, forces in connections, and panel-to-TSB bearing forces. These and other FEA results and are given in Appendix E. Loading used to maximize RPD typically placed the truck wheels far from the TSB and thus did not cause it to be critically stressed.

6.3.1 Sensitivity of Transverse Stiffener Beam (TSB) Response and Relative Panel Displacement (RPD) to Bridge Parameters

6.3.1.1 Sensitivity to Panel-to-TSB Connections

The TSB stresses and RPD are sensitive to the panel-to-TSB connection type. However, due to the nonlinear nature of these connections in tension, trends are sometimes difficult to explain intuitively. Chapter 5 provides information on the panel-to-TSB connection models used and Figure 5.7 provides the load-slip curves used to model the nonlinear behavior of the connection in tension. The slip in the connection is

explained in Chapter 5. All connection models have nominal capacity in compression. Connection stiffness significantly changes the amount of load transferred to the TSB and can significantly change the panel-TSB interaction. Analyses #1-4 show the effect of connection type on maximum TSB shear and bending moment, and, by doing so, demonstrate the effect of a change in panel-TSB interaction can have on maximum TSB shear and bending moment.

Analyses #1-4 represent four separate FEA runs of the parametric study. (A full listing of all runs conducted in the parametric study and the corresponding results can be found in Appendix E.) Analyses #1-4 all used the same bridge and loading but different panel-TSB connections. The bridge was a 20-ft long and a 14-ft wide (four 42-in. wide, 10.5-in. thick SP47 panels) with a single 5.75-in. high, 3.625-in. wide SP47 TSB (aspect ratio of 0.63 and stiffness factor of 1.01 EI_{min}) at midspan (Figure 6.4). The bridge was loaded at midspan with a single axle of the HS20 truck as shown in Figure 6.4. Analysis #1 used aluminum brackets for the connections, and Analyses #2, 3, and 4 used 5/8-in. through-bolt, 3/4-in. through-bolt, and seated-beam panel-TSB connections, respectively. Since all parameters other than connections ar held constant, Analyses #1-4 provide a direct means to evaluate the effects of connection stiffness on TSB stresses and RPD.

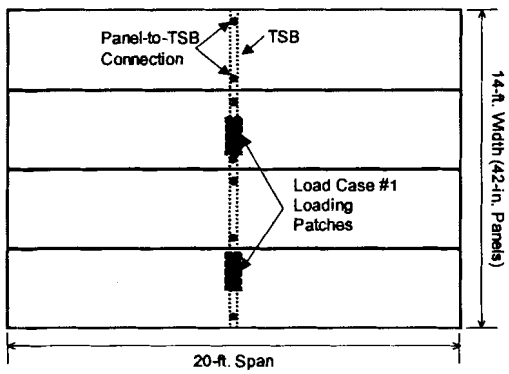

Figure 6.4 Bridge configuration and loading for Analyses #1-4

The results of Analyses #1-4 are presented in the next several figures. Figure 6.5 shows the deflection of the panels at midspan and the deflection of TSB across the width of the bridge. All four analyses are presented in the figure to show the effect of connection type on the panel-TSB interaction. The seated beam's stiffness allows relatively little slip in the connection and, as a result, the TSB bears on the center of the some panels (second and fourth panels from the left) as well as the edges of others (first and third panels and the right edge of the fourth panel). With other connection systems, the bearing of the TSB on the center of a panel does not occur, giving different TSB-deck interaction. The panels' deflections are more uniform with the stiffer connections, showing that the stiffer connection system distributes more of the load to adjacent panels. Graphs of panel and TSB deflection assist in understanding TSB performance by showing panel-TSB interaction. (Appendix E contains maximum panel and TSB deflections for each analysis performed.)

The increased load distribution with the stiffer connection can be seen in plots of connection and bearing forces between the panels and the TSB. In Figure 6.6, the tensile (positive) axial force in each panel-to-TSB connection is plotted using discrete points, and the compressive (negative) force transmitted by panel-TSB bearing is plotted using a continuous line. Since the bearing connections are six inches apart, the deck-TSB bearing forces in Figure 6.6 are essentially given in kips/6 in. In the model the bearing elements are discrete springs that carry only compressive loads; they are further described in Chapter 5. Figure 6.6 shows the differences in forces transferred between the panels and the TSB fore Analyses #1-4. The lower stiffness of the aluminum bracket results in a lower maximum connection load. The maximum load in a seated-beam connection is

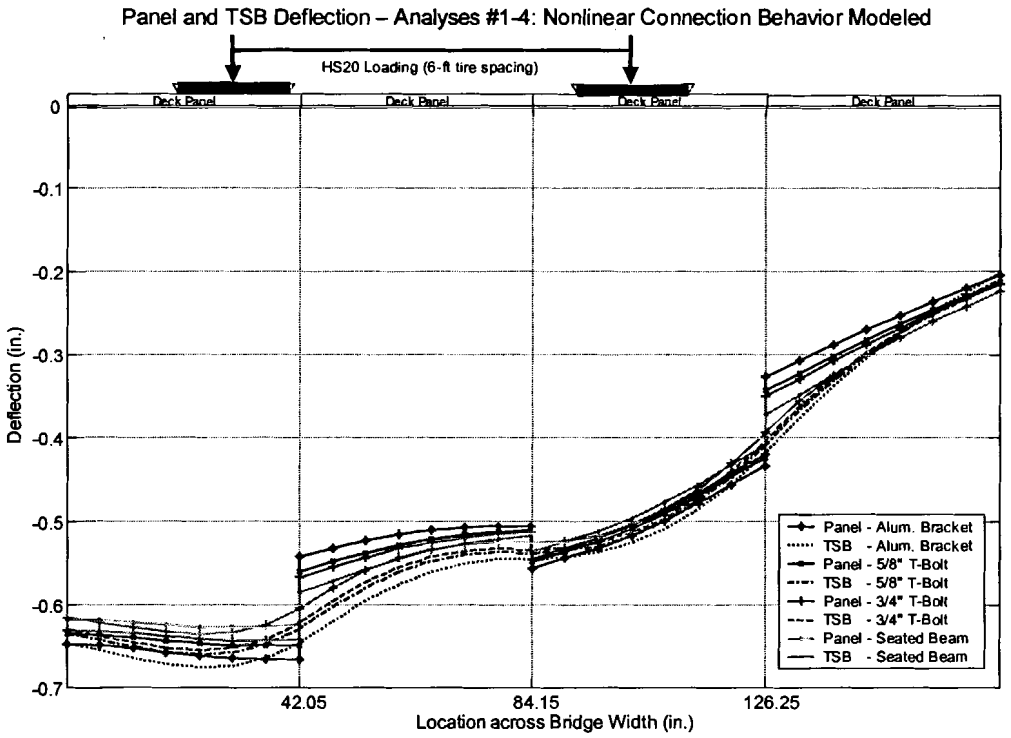

Figure 6.5 Panel and TSB deflections for Analyses #1-4 showing sensitivity to connection type

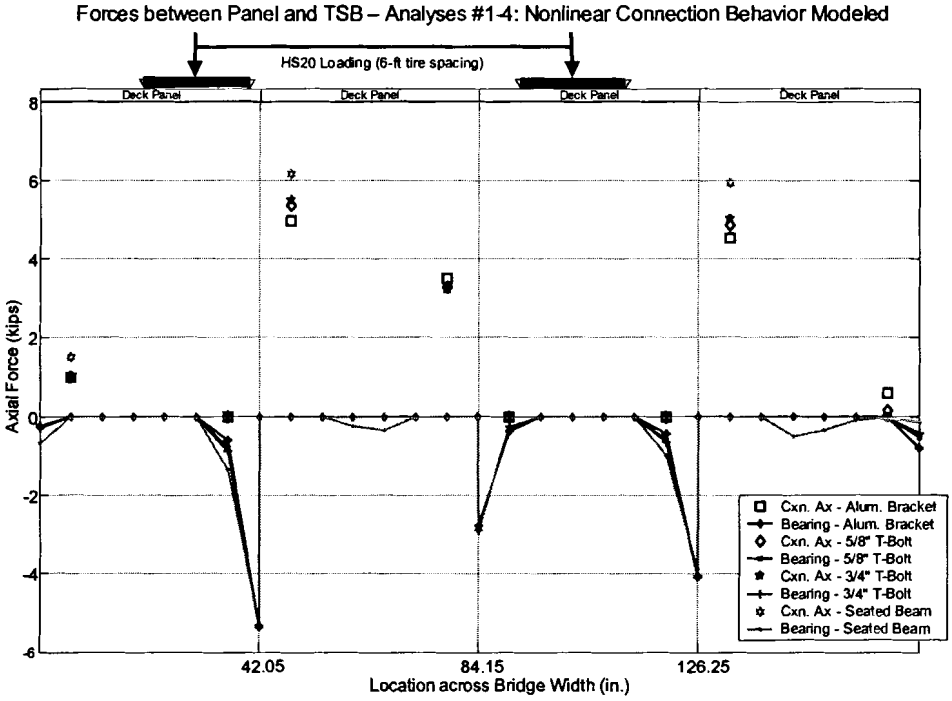

Figure 6.6 Connection and bearing forces between the panels and TSB for Analyses #1-4 showing sensitivity to connection type

24% greater than the maximum in the aluminum bracket connection for this bridge and loading.

A change in panel-TSB connection and bearing forces can affect the TSB shear. Figure 6.7 shows the shear diagram of the TSB for each different connection type in Analyses #1-4. The stiffest connection, the seated beam (Analysis #4), causes the TSB the greatest maximum shear. The lowest maximum shear in the TSB for the same bridge configuration and loading is Analysis #1, which uses aluminum brackets. The seated beam connection results in 11% greater maximum TSB shear than the aluminum bracket connectors.

Figure 6.8 shows the TSB bending moment diagrams for Analyses #1-4. These diagrams show that the bridge with aluminum bracket connections has the greatest maximum bending moment (22.6 kip-in), even though the positive bending moment is largest with the seated-beam connection. A possible explanation for this is related to connection nonlinearity, as discussed in the next paragraph. However, the differences among the maximum bending moments for all connection types are not significant.

It may be thought that the stiffer connection system would cause the greater bending moment in the TSB. However, the nonlinear behavior of the aluminum bracket connection (Figure 6.8) seems to cause the opposite result. Figure 6.8 shows the TSB moment diagram of the aluminum bracket bridge, along with TSB moments for the three other types of connections. At the right edge of the first panel from the left, the moment is still increasing beyond the connection when the aluminum bracket is used, but not for the other three types of connections. The difference can be seen again in the TSB under

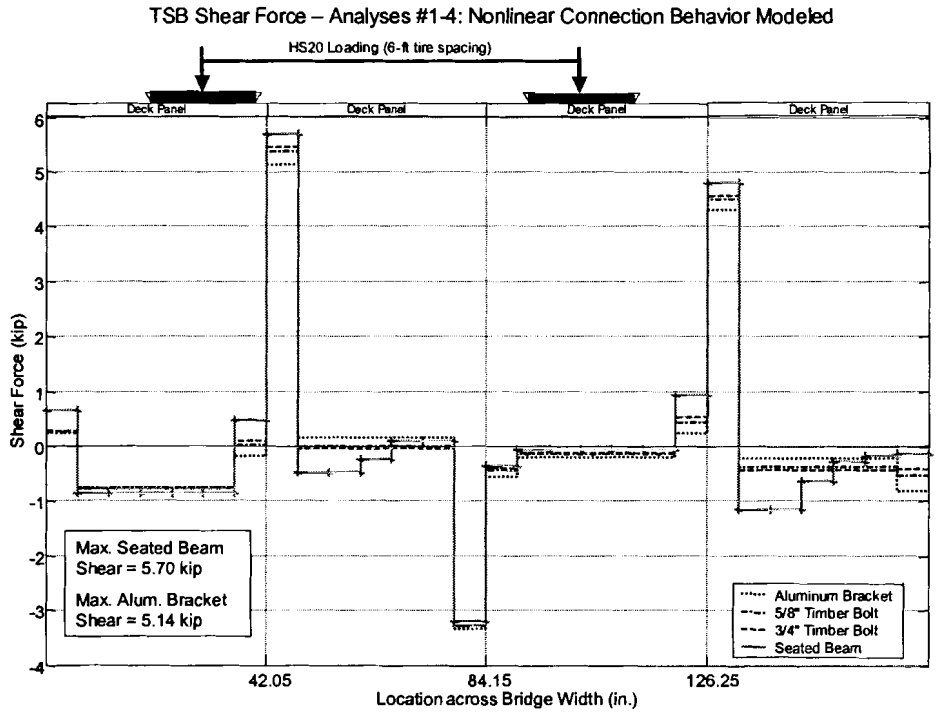

Figure 6.7 TSB shear diagrams for Analyses #1-4 showing sensitivity to panel-to-TSB connection type

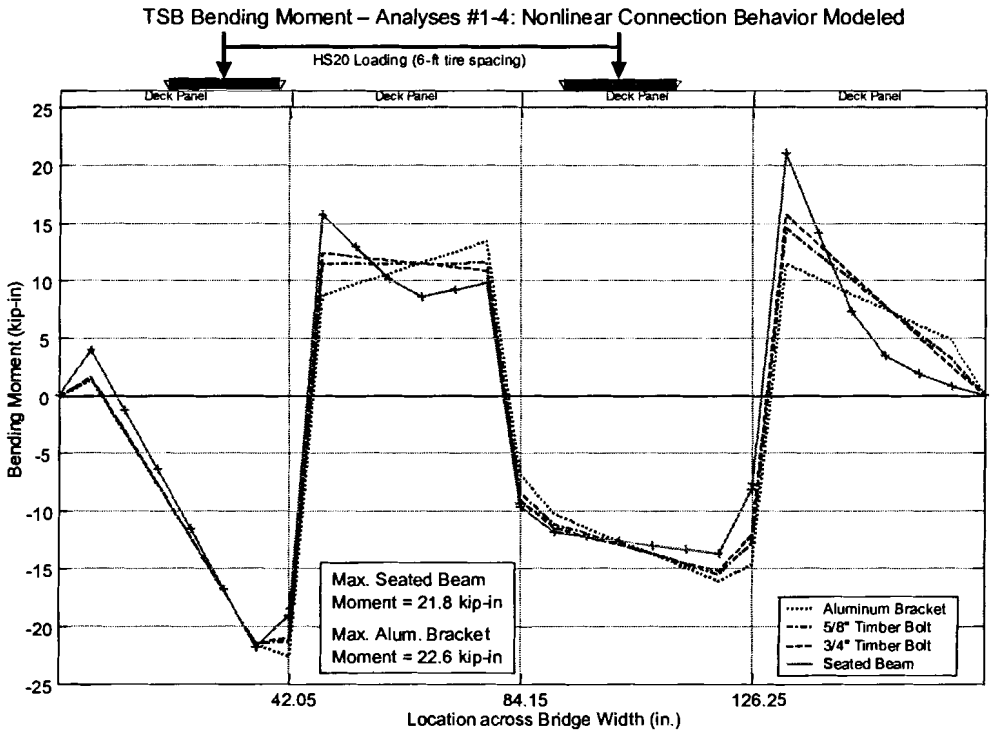

Figure 6.8 TSB bending moments diagrams for Analyses #1-4 showing sensitivity to connection type

the second panel from the left. The bending moment in the TSB connected with aluminum brackets alone increases between connections.

To further investigate the effect the nonlinearity of the connection on the TSB shear and bending moment, Analyses #1-4 were rerun with TSB-deck connections modeled as linear in tension. These reruns are designated as Analyses #1b, 2b, 3b, and 4b. For each connection's axial load-deformation curve, a best-fit line was determined through the initial semi-elastic range. This gave the aluminum bracket, 5/8-in. through bolt, 3/4-in. through bolt, and seated beam stiffness of 89 kips/in, 120 kips/in, 148 kips/in, and 750 kips/in, respectively. Figure 6.9 shows the axial load-deformation curves used in the finite element analysis for the nonlinear and linear models of the deck-to-TSB connections. Included on this figure are the maximum connection forces for each analysis. It can be seen that the aluminum bracket exhibits plastic-like behavior in analysis #1. This plastic behavior changes the TSB-panel interaction and results in higher bending moment than any other connection system (Figure 6.8). Figure 6.10 shows the TSB bending moment diagrams for Analyses #1b-4b. With the linear connection model, the TSB bending moment for the aluminum bracket bridge (Analyses #1b) follows the same trends as the Analyses for other linear connections, increasing where they increase and decreasing where they decrease. When the connections are modeled linearly, the stiffest connection, the seated beam, now gives the TSB the highest maximum bending moment, and the least stiff connection, the aluminum bracket, causes the lowest maximum TSB bending moment. Table 6.4 lists the maximum TSB bending moment, TSB shear force, and connection force for Analyses #1-4 and #1b-4b. With the linear Analyses, the trends toward higher bending moments and shear for higher

connection stiffness can be seen, however, the nonlinear connection behavior affects deck-TSB interaction so that the greatest TSB bending moments from Analyses #1-4 were from the aluminum bracket connection system. For this bridge configuration and loading, the differences are minor, but the analyses explained apparent inconsistencies in TSB bending stresses that the connections' nonlinear behavior caused.

Other trends can be seen in the analyses of this bridge configuration and loading. Comparing the maximum dissipated energy in the connection by the area under the axial load-deformation curves from initial to maximum load in the connection for Analyses #1-4b (Figure 6.9), the maximum force transmitted through the connection increases as the energy dissipated in the connection decreases. Comparing the axial deformation at maximum connection load for Analyses #1-4b (Figure 6.9), the maximum TSB shear increases as axial deformation at maximum connection force increases.

The nonlinear model more accurately represents the behavior of the connection as measured in experiments (Hale 1978) and was thus used on all other analyses (Analyses #5 to #145). Although using the linear connection models instead of the nonlinear connection models would have underestimated the absolute maximum TSB bending moment (all connections considered) by only 3.5%, not a significant amount, for this bridge configuration and loading, it is important to note that the nonlinear behavior of the connection may not always be inconsequential and should be considered in finite element analyses of longitudinal glulam deck bridges.

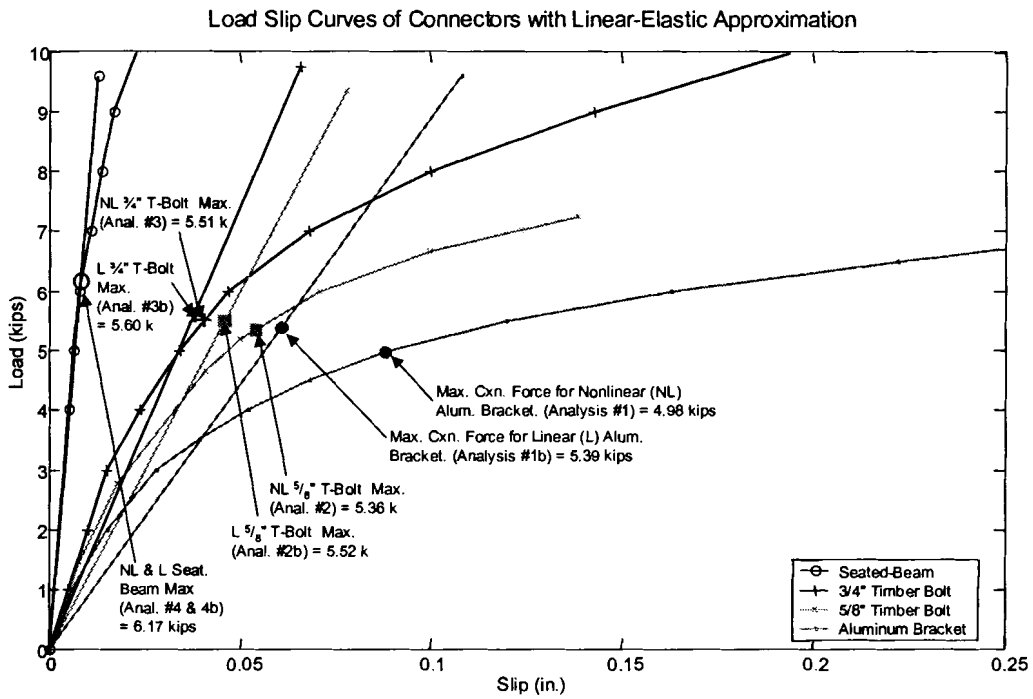

Figure 6.9 Load-slip curves for nonlinear (Hale 1978) and linear panel-to-TSB connection models

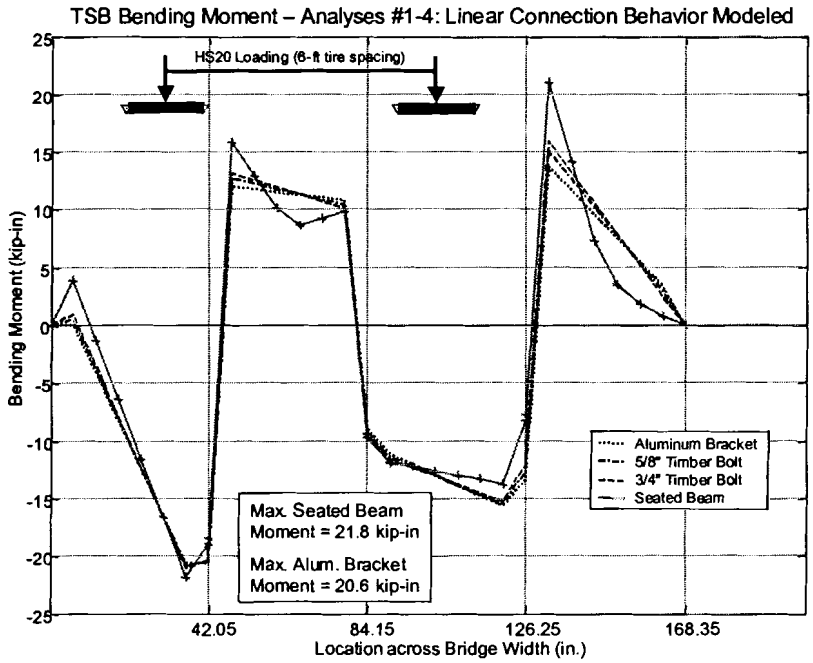

Figure 6.10 TSB bending moments diagrams for Analyses #1b-4b showing sensitivity to connection type (linear connection models)

Table 6.4 Maximum TSB shear forces, TSB bending moments, and connection forces for nonlinear and linear connection behavior (Analyses #1-4b)

Connection Type	Nonlinear Connection Behavior Modeled (Analyses #1-4)			Linear Connection Behavior Modeled (Analyses #1b-4b)		
	Max. Cxn. Force (kips)	TSB Shear (kips)	TSB Moment (kip-in)	Max. Cxn. Force (kips)	TSB Shear (kips)	TSB Moment (kip-in)
Alum. Bracket (Anal. #1 & 1b)	4.98	5.14	**22.6**	5.39	5.35	20.6
$^5/_8$" Through Bolt (Anal. #2 & 2b)	5.36	5.37	21.4	5.52	5.44	20.9
¾" Through Bolt (Anal. #3 & 3b)	5.51	5.46	21.5	5.60	5.49	21.1
Seated Beam (Anal. #4 & 4b)	**6.17**	**5.70**	21.8	**6.17**	**5.70**	**21.8**
Maximums	**6.17**	**5.70**	**22.6**	**6.17**	**5.70**	**21.8**

As can be seen from Figure 6.11, connection type significantly affects RPD. RPD is graphed as the maximum relative displacement of all longitudinal panel edges along the length of the bridge. Changing the connections from seated-beam connections to aluminum brackets caused a 155% increase in relative panel displacement for the bridge configuration and loading in Analyses #1 and 4. Aluminum brackets, being less stiff, allow greater relative panel displacement. In Analysis #1, the aluminum brackets allowed 1.25 in. of RPD, 25% greater than the 0.1 in. serviceability criteria for asphalt wearing surfaces (Ritter 1990). When reported in results tables, RPD will be listed as the ratio of maximum RPD to the 0.1 in. serviceability criteria. This form quickly allows the critical bridge configurations and loadings to be determined. As one would expect, the seated beams allowed the least relative panel displacement (0.049 in.) given equivalent bridge configurations and loading.

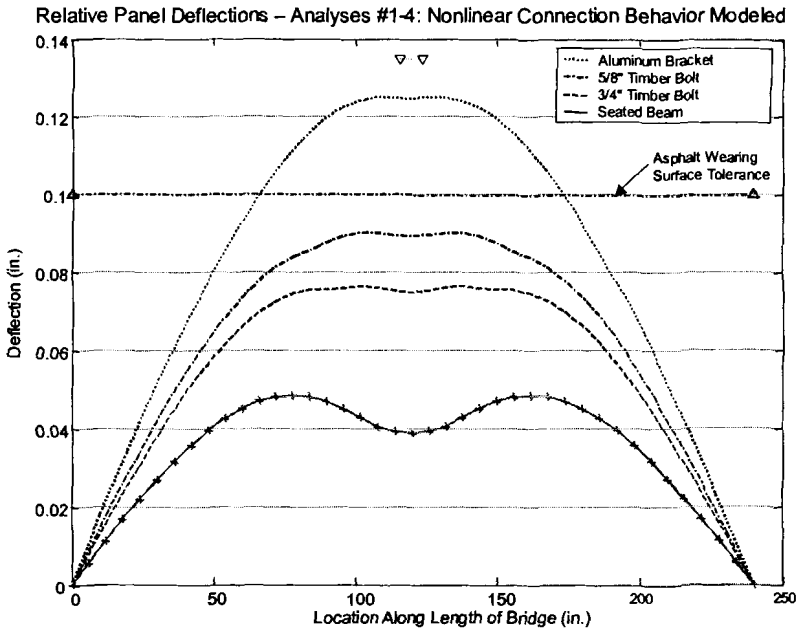

Figure 6.11 Relative panel displacement sensitivity to connection type (nonlinear connection models)

Table 6.5 compares TSB stresses and RPD for different connection types. All analyses in this table and throughout the rest of the thesis model the deck-to-TSB connections with tension behavior as nonlinear. For each set of comparable analyses (i.e. analyses with identical bridge geometries and loadings but different connections), the analyses are listed in order of connection stiffness. The groups of directly comparable analyses are separated by double lines. For these analyses, the bridges with aluminum bracket connections consistently have greater maximum TSB bending moments than the same loading and bridge configurations with seated beam connections. Comparing Analyses #76 to #75, the aluminum bracket caused 25% greater TSB bending moment than the seated beam. The analyses in Table 6.5 also show higher maximum shear for the stiffer seated-beam connection given a bridge configuration and loading. Comparing Analyses #73 to #74, the seated-beam connection caused 20% greater maximum TSB shear than the aluminum bracket connection. The table also includes TSB stress

utilization ratios (f/F`). These stress utilization ratios are the TSB stress obtained from finite element analysis divided by the allowable stress. A stress utilization ratio greater than one indicates that the TSB is overstressed. For these analyses listed, which consist of bridges and loading meeting AASHTO design criteria, in a little less than half the TSB is overstressed in bending and in two thirds the TSB is overstressed in shear. The TSB in Analysis #72 has 49% more bending stress than allowable, and the TSB in Analysis #71 has 68% more shear stress than allowable. (Load cases listed in the table are shown in Figure 6.12.) Only a few of the results have been pointed out here, but the trends noted are supported throughout Table 6.5.

Considering RPD utilization, the analyses in Table 6.5 indicate that RPD for bridges with seated-beam connections are less for bridges with aluminum-bracket connections. Comparing Analyses #102 to #103, the aluminum-bracket connection has a 25% greater RPD utilization ratio than the seated-beam connection. (In Table 6.5, TSB stresses are not listed for Analyses #102, 103, and in other similar cases where loading maximizes RPD but does not critically stress the TSB.) It is also noteworthy that the movement of panels relative to one another is less sensitive to connection systems as the loading moves away from the connection. This is clearly shown in Table 6.5, by comparing analyses using Load Case #19 (Figure 6.12) to analyses using Load Case #49. Analyses of midpan loading resulted in 209% increase in RPD when aluminum brackets are used over seated beams (Analyses #71 and 72). Loading at quarter span causes only a 16% increase in RPD when aluminum brackets replace seated beam connections (Analyses #96 and 97).

Table 6.5 also shows the effect of panel width. With the 42-inch panels, the connections' effects on TSB bending were not as significant as with the 48-in. wide panels. With similar loading cases (Figure 6.12), the 42-in. wide panels showed only 4% bending stress difference between aluminum brackets and seated-beam connections (c.f. Analyses #1 and 4), whereas the 48-in. wide panels showed a 17% difference (c.f. Analyses #71 and 72). Similarly, the 48-in. panel bridge had an increased TSB shear stress of 20% with seated-beam connections rather than aluminum brackets (c.f. Analyses #71 and 72); however, the similar 42-in. panel bridge had an increased TSB shear stress of only 11% with seated-beam connections rather than aluminum brackets (c.f. Analyses #1 and 4).

Table 6.5 Sensitivity of TSB response and RPD to connection type (nonlinear connection models only)

Anal. #	Bridge			Panels				TSB		Panel-to-TSB Cxn.	Load Case #	Relative Panel Deflection Δ/0.10 in.	FEA TSB Bending Moment (kip-in)	TSB fb / Fb	FEA TSB Shear (kips)	TSB fv / Fv
	Span (ft.)	Bridge Width (ft.)	# of Lanes	# of Panels	Panel Width (in)	Panel Thick-ness (in.)	Panel MOE (ksi)	Aspect Ratio	TSB EI/EI_{min}							
1	20	14	1	4	42	10.5	1166	0.83	1.01	AB	1	1.25	22.80	1.01	5.14	1.37
2				4	42	10.5	1166			TB58		0.90	21.40	0.96	5.37	1.43
3				4	42	10.5	1166			TB34		0.76	21.50	0.96	5.46	1.46
4				4	42	10.5	1166			SB		0.49	21.80	0.97	5.70	1.52
72	20	16	1	4	48	10.5	1166	0.67	1.00	AB	19	1.64	33.60	1.49	5.66	1.47
71				4	48	10.5	1166			SB		0.53	28.20	1.24	6.47	1.68
76	20	16	1	4	48	10.5	1166	1.50	2.00	AB	19	1.37	45.20	0.97	5.85	0.72
75				4	48	10.5	1166			SB		0.35	36.20	0.78	6.62	0.61
74	20	16	1	4	48	12.25	1166	0.87	1.00	AB	19	1.43	28.30	1.25	5.23	1.35
73				4	48	12.25	1166			SB		0.50	24.60	1.09	8.26	1.62
76	20	16	1	4	48	12.25	1166	1.50	2.00	AB	19	1.23	38.10	0.82	5.45	0.87
77				4	48	12.25	1166			SB		0.34	31.80	0.66	8.46	0.79
96	20	16	1	4	48	10.5	1166	0.67	1.00	AB	49	1.79	-	-	-	-
97				4	48	10.5	1166			SB		1.54	-	-	-	-
98	20	16	1	4	48	10.5	1166	1.50	2.00	AB	49	1.71	-	-	-	-
99				4	48	10.5	1166			SB		1.45	-	-	-	-
100	20	18	1	4	48	12.25	1166	0.67	1.00	AB	49	1.27	-	-	-	-
101				4	48	12.25	1166			SB		1.04	-	-	-	-
102	20	16	1	4	48	12.25	1166	1.50	2.00	AB	49	1.20	-	-	-	-
103				4	48	12.25	1166			SB		0.96	-	-	-	-

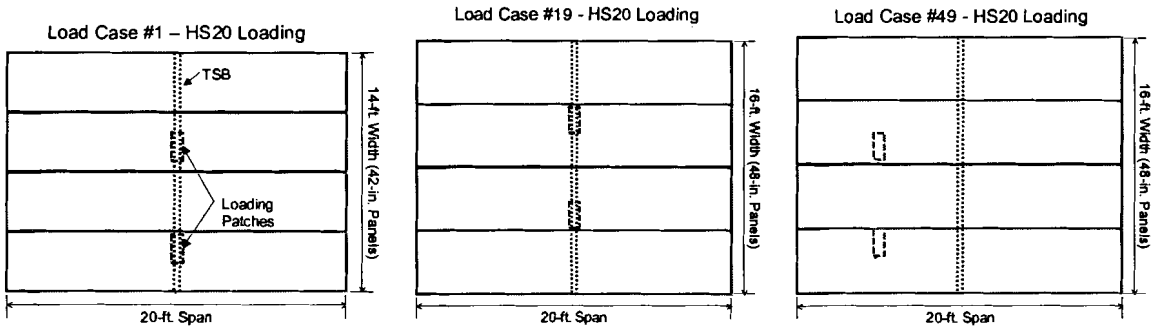

Figure 6.12 Plan view of Load Cases #1, #19, and #49

6.3.1.2 Sensitivity to Panel Thickness and Modulus of Elasticity

As the panel thickness or panel MOE increases, the panels are stiffer and will transfer less load to the TSB. This will typically result in lower TSB shear and bending stresses as panel stiffness increases providing that rest of the bridge design parameters and loading remain constant. Table 6.6 shows that, in the cases analyzed, increasing the panel thickness will reduce TSB shear stress, TSB bending stress, and RPD if the rest of the bridge configuration and the loading are held constant. Comparing Analyses #35 and 47, the utilization ratio for TSB bending stress decreases 28%, from 1.36 to 0.98 as the panel thickness increases 36% from 10.5 in. to 14.25 in. Comparing TSB shear stress utilization ratios for the same analyses, the utilization ratio decreases only 12% (from 1.64 to 1.44), not a very significant amount, as the panel thickness increases. RPD for the same analyses shows a 23% utilization reduction (from 0.93 to 0.81). Table 6.7 shows a similar trend of stress and deflection reduction as panel MOE increases. Comparing Analyses #35 and 50, the utilization ratios decrease as follows for a 50% increase in panel MOE from 1166 ksi to 1749 ksi: TSB bending stress utilization decreases a minor 10%, dropping from 1.36 to 1.23; TSB shear stress utilization

decreases an insignificant 4%, dropping from 1.64 to 1.58; and RPD utilization decreases a minor 9%, dropping from 0.93 to 0.85.

6.3.1.3 Sensitivity to TSB Modulus of Elasticity

TSB bending moment and RPD are sensitive to TSB MOE; however, TSB shear does not appear to be sensitive to TSB MOE. Changing the TSB MOE through an appropriate range of values (1050 ksi – 2100 ksi) shows that the TSB stiffness slightly affects the amount of load transferred between the panels and TSB through connections and bearing. There is no significant change in maximum connection force or in maximum bearing force when the TSB MOE was changed from 150% of the published SP47 value to 75% of it (Analyses #51 and 53) (see also Appendix E). Although the maximum shear force in the TSB is not significantly affected, bending moment is significantly affected (Figure 6.13 and Table 6.8). TSB shear stress utilization ratios increased a mere 2%, rising from 1.63 to 1.67, as TSB MOE increased 100%. For analyses shown in Figure 6.13, maximum TSB bending moment increased by 25.5% as TSB MOE increased from 75% to 150% of SP47 MOE. As would be expected, TSB MOE has a significant effect on relative panel deflection, the TSB with an MOE of 1050 ksi allowing 24% more RPD than a TSB with an MOE of 2100 ksi (Analyses #51 and 53) (Table 6.8).

6.3.1.4 Sensitivity to TSB Geometry

TSB stresses are very sensitive to TSB geometry (aspect ratio and moment of inertia), although due to the nature of the structural system, it is also complicated. If the aspect ratio is maintained, increasing the stiffness by increasing moment of inertia can

Table 6.6 Sensitivity of TSB response and RPD to panel thickness

Anal. #	Bridge			Panels				TSB		Panel-to-TSB Cxn.	Load Case #	Relative Panel Deflection Δ/0.10 in.	FEA TSB Bending Moment (kip-in)	TSB fb / Fb	FEA TSB Shear (kips)	TSB fv / Fv
	Span (ft.)	Bridge Width (ft.)	# of Lanes	# of Panels	Panel Width (in)	Panel Thick-ness (in.)	Panel MOE (ksi)	Aspect Ratio	TSB EI/EI_{min}							
45*	20	16	1	4	48	8.5	1166	0.63	1.01	TB34	19	0.96	38.10	1.70	6.48	1.73
35				4	48	10.5	1166					0.93	30.50	1.36	6.17	1.64
46				4	48	12.25	1166					0.87	25.90	1.16	5.84	1.56
47				4	48	14.25	1166					0.81	21.90	0.98	5.41	1.44
71	20	16	1	4	48	10.5	1166	0.67	1.00	SB	19	0.53	28.20	1.24	6.47	1.68
73				4	48	12.25	1166					0.50	24.60	1.09	6.26	1.62
72	20	16	1	4	48	10.5	1166	0.67	1.00	AB	19	1.64	33.80	1.49	5.66	1.47
74				4	48	12.25	1166					1.43	28.30	1.25	5.23	1.35
75	20	16	1	4	48	10.5	1166	1.50	2.00	SB	19	0.35	36.20	0.78	6.62	0.81
77				4	48	12.25	1166					0.34	31.60	0.68	6.46	0.79
76	20	16	1	4	48	10.5	1166	1.50	2.00	AB	19	1.37	45.20	0.97	5.85	0.72
78				4	48	12.25	1166					1.23	38.10	0.82	5.45	0.67

● Bridge configuration does not meet AASHTO criteria.

Table 6.7 Sensitivity of TSB response and RPD to panel MOE

Anal. #	Bridge			Panels				TSB		Panel-to-TSB Cxn.	Load Case #	Relative Panel Deflection Δ/0.10 in.	FEA TSB Bending Moment (kip-in)	TSB fb / Fb	FEA TSB Shear (kips)	TSB fv / Fv
	Span (ft.)	Bridge Width (ft.)	# of Lanes	# of Panels	Panel Width (in)	Panel Thick-ness (in.)	Panel MOE (ksi)	Aspect Ratio	TSB EI/EI_{min}							
48	20	16	1	4	48	10.5	875	0.63	1.01	TB34	19	0.99	32.80	1.47	6.31	1.68
35				4	48	10.5	1166					0.93	30.50	1.36	6.17	1.64
49				4	48	10.5	1458					0.88	28.90	1.29	6.05	1.61
50				4	48	10.5	1749					0.85	27.50	1.23	5.92	1.56

Table 6.8 Sensitivity of TSB response and RPD to TSB MOE

Anal. #	Bridge			Panels				TSB		Panel-to-TSB Cxn.	Load Case #	Relative Panel Deflection Δ/0.10 in.	FEA TSB Bending Moment (kip-in)	TSB fb / Fb	FEA TSB Shear (kips)	TSB fv / Fv
	Span (ft.)	Bridge Width (ft.)	# of Lanes	# of Panels	Panel Width (in)	Panel Thick-ness (in.)	Panel MOE (ksi)	Aspect Ratio	TSB EI/EI_{min}							
51*	20	16	1	4	48	10.5	875	0.63	0.75	TB34	19	1.02	27.8	1.24	6.10	1.63
35							1166		1.01			0.93	30.5	1.36	6.17	1.64
52							1458		1.26			0.87	32.8	1.47	6.21	1.68
53							1749		1.51			0.82	34.9	1.56	6.25	1.67

● Bridge configuration does not meet AASHTO criteria.

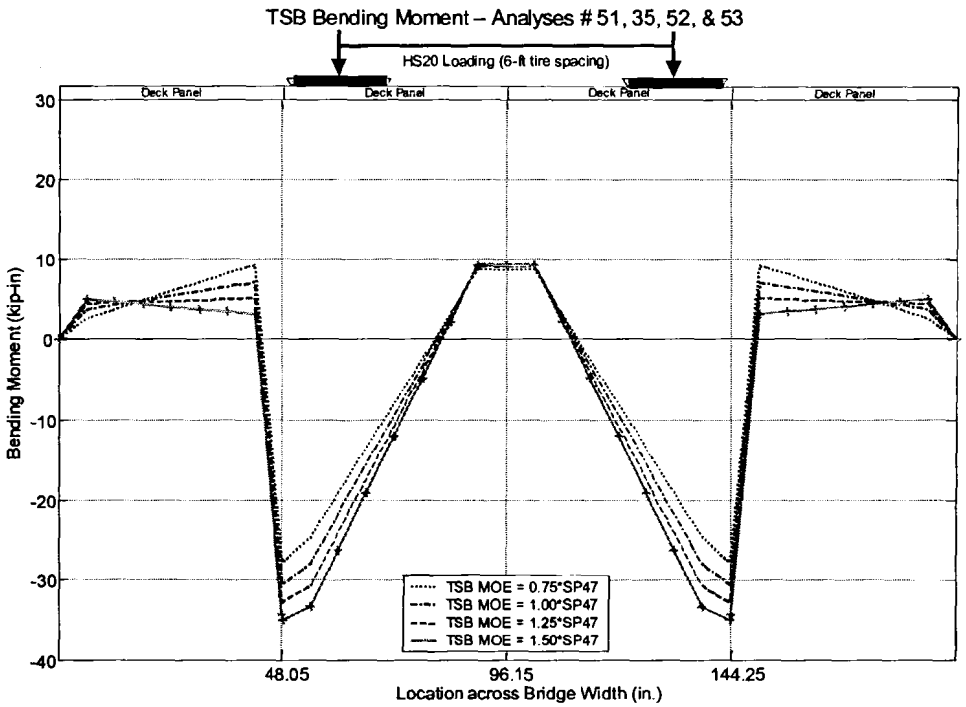

Figure 6.13 TSB bending moments diagrams for Analyses #35 and 51-53 showing sensitivity to TSB MOE

affect results as was seen earlier by increasing the TSB MOE. Changes in TSB geometry affect the FE model's assumed TSB-deck bearing stiffness (see Section 5.2.5 for details), which can affect TSB bending moment. The geometry changes affect the stress calculations as well, therefore in this section, TSB bending moments and shear will be compared more than stress utilization ratios.

Table 6.9 gives the results of analyses grouped by TSB stiffness factor ratio (TSB EI / AASHTO minimum EI) to show the effect of aspect ratio (TSB width/TSB height) on the TSB response and RPD. For the analyses listed in the table, EI is changing due to TSB dimensional changes, not due to TSB MOE changes. In the analyses shown, for a given TSB moment of Inertia (I), bridge configuration, and loading, as the TSB aspect ratio increases (TSB area increases), TSB maximum bending moment is slightly affected and TSB maximum shear increases insignificantly. Comparing Analyses #17 and 13

where TSB aspect ratio increases from 0.63 to 1.50 as TSB stiffness remains at 1.0 EI_{min} shows a 3% increase (from 3.23 kips to 3.32 kips) in shear force. Since the shear force is relatively unchanged, the shear stress utilization ratio decreases at the rate of TSB area increase.

TSB maximum bending moment is slightly affected by the TSB aspect ratio, but the effect is also dependent on the TSB I. Considering Analyses #56-70 (for this bridge configuration and loading), it can be seen that with the TSB EI/EI_{min} of 0.5 and 1.0 the greater aspect ratios (shallower, wider beams) cause greater maximum TSB bending moment, but with the TSB of EI/EI_{min} of 2.0 and 2.5, the smaller aspect ratios (taller, narrower beams) cause the maximum TSB bending moments. Analysis #60 (TSB aspect ratio of 0.67, EI/EI_{min} of 2.5) has a maximum bending moment 9% greater than Analysis #70 (TSB aspect ratio of 1.50, EI/EI_{min} of 2.5). For the same bridge configuration (other than TSB) and loading but with TSB EI/EI_{min} of 1.5, the maximum TSB bending moment is caused by the TSB with a 1.0 aspect ratio.

RPD is affected by aspect ratio and RPD utilization decreases as TSB aspect ratio increases. For these analyses, this effect is not as great if the loading is placed further from the TSB and is placed to maximize RPD. The RPD utilization with a TSB having a 0.67 aspect ratio was typically 17-20% greater than the utilization ratio of TSB with a 1.50 aspect ratio when the loading was placed directly above the TSB (Analyses #56-70). However, the utilization ratios for 0.67 aspect ratios were typically only 1-3% greater than those for 1.50 aspect ratios when the loading was far from the TSB (Analyses #111-125). Thus it appears that the TSB aspect ratio does not significantly affect RPD when the loads are far from the TSB.

Table 6.10 gives the results of analyses grouped by aspect ratio to show the effect of changing TSB I as the aspect ratio is held constant. In the analyses shown, for a given TSB aspect ratio, bridge configuration, and loading, as TSB EI increases, TSB maximum bending moment significantly increases and TSB maximum shear increases slightly, but not significantly, increases. Again, the shear stress utilization reduction is proportional to the increase in TSB area. The maximum TSB bending moment increases as TSB I increases. However, as the aspect ratio increases, the effect of TSB I change is not as significant. For an aspect ratio of 0.67 and a given bridge and loading (Analyses #57-60), TSB maximum bending moment increases 56% as EI/EI_{min} increases from 1.00 to 2.50. For the same bridge and loading but with TSB of a 1.5 aspect ratio (Analyses #67-70), TSB maximum bending moment only increases 33% as EI/EI_{min} increases from 1.00 to 2.50. For RPD utilization, the affect of TSB stiffness was significant when loading was at the TSB, but the effect was not significant when the loading was placed midway between the TSB and the support. The TSB that is critical for this parametric study is the one which causes the greatest overstress while still meeting current AASHTO criteria. Consistently, the worst case for TSB shear stress, TSB bending stress, and RPD is when the TSB has a low aspect ratio (0.63 or 0.67) (narrow and deep beam) and the minimum stiffness (1.0 EI_{min}).

6.3.1.5 Sensitivity to Bridge Configuration and Loading

As previously noted (Section 6.2.2), the sensitivity of bridge response to loading is dependent on panel width. Panel width is dependent on bridge width, and the number of lanes of loading is dependent on bridge width. Loading is dependent on span as well. Typically, a single axle will be seen when loading a 20-ft. span bridge, but a 35-ft. span

Table 6.9 Analysis results of TSB response and RPD showing sensitivity to TSB aspect ratio

Anal. #	Bridge			Panels				TSB		Panel-to-TSB Cxn.	Load Case #	Relative Panel Deflection Δ/0.10 in.	FEA TSB Bending Moment (kip-in)	TSB fb / Fb	FEA TSB Shear (kips)	TSB fv / Fv
	Span (ft.)	Bridge Width (ft.)	# of Lanes	# of Panels	Panel Width (in)	Panel Thick-ness (in.)	Panel MOE (ksi)	Aspect Ratio	TSB EI/EI_{min}							
16	35	14	1	4	42	14.25	1166	0.63	1.01	TB34	5	0.59	18.50	0.83	4.50	1.20
14								1.00				0.56	19.50	0.78	4.54	0.98
12								1.50				0.54	20.20	0.73	4.57	0.79
17	35	14	1	4	42	14.25	1166	0.63	1.01	TB34	6	0.27	23.50	1.05	3.23	0.86
15								1.00				0.24	24.20	0.97	3.29	0.70
13								1.50				0.23	24.80	0.89	3.32	0.57
56*	20	16	1	4	48	10.50	1166	0.67	0.50	TB34	19	0.67	22.90	1.70	6.36	2.33
61*								1.00				0.61	24.50	1.65	6.40	1.92
66*								1.50				0.56	26.10	1.58	6.45	1.58
57								0.67	1.00			0.53	28.20	1.24	6.47	1.68
62								1.00				0.48	29.00	1.16	6.51	1.38
67								1.50				0.44	30.40	1.10	6.54	1.13
58								0.67	1.50			0.46	34.70	1.13	6.53	1.38
63								1.00				0.42	32.70	0.97	6.56	1.14
68								1.50				0.39	33.40	0.89	6.59	0.93
59								0.67	2.00			0.41	39.70	1.04	6.57	1.20
64								1.00				0.38	38.00	0.90	6.59	0.99
69								1.50				0.35	36.20	0.78	6.62	0.81
60								0.67	2.50			0.39	43.90	0.98	6.59	1.08
65								1.00				0.36	42.10	0.85	6.62	0.89
70								1.50				0.33	40.20	0.73	6.64	0.73
126*	20	16	1	4	48	10.5	1166	0.67	0.50	AB	49	1.86	-	-	-	-
131*								1.00				1.84	-	-	-	-
136*								1.50				1.81	-	-	-	-
127								0.67	1.00			1.79	-	-	-	-
132								1.00				1.77	-	-	-	-
137								1.50				1.75	-	-	-	-
128								0.67	1.50			1.75	-	-	-	-
133								1.00				1.74	-	-	-	-
138								1.50				1.72	-	-	-	-
129								0.67	2.00			1.73	-	-	-	-
134								1.00				1.72	-	-	-	-
139								1.50				1.71	-	-	-	-
130								0.67	2.50			1.72	-	-	-	-
135								1.00				1.71	-	-	-	-
140								1.50				1.70	-	-	-	-

- Bridge configuration does not meet AASHTO criteria.

Table 6.10 Analysis results of TSB response and RPD showing sensitivity to TSB stiffness

Anal. #	Bridge			Panels				TSB		Panel-to-TSB Cxn.	Load Case #	Relative Panel Deflection Δ/0.10 in.	FEA TSB Bending Moment (kip-in)	TSB fb / Fb	FEA TSB Shear (kips)	TSB fv / Fv
	Span (ft.)	Bridge Width (ft.)	# of Lanes	# of Panels	Panel Width (in)	Panel Thick-ness (in.)	Panel MOE (ksi)	Aspect Ratio	TSB EI/EI_{min}							
3	20	14	1	4	42	10.50	1166	0.63 - 0.67	1.01	TB34	1	0.76	21.5	0.96	5.46	1.46
9									2.02			0.65	28.3	0.74	5.54	1.01
10									3.02			0.60	32.8	0.63	5.57	0.83
11									3.99			0.58	36.1	0.56	5.58	0.72
56 *	20	16	1	4	48	10.50	1166	0.67	0.50	TB34	19	0.67	22.9	1.70	6.36	2.33
57									1.00			0.53	26.2	1.24	6.47	1.68
58									1.50			0.46	34.7	1.13	6.53	1.38
59									2.00			0.41	39.7	1.04	6.57	1.20
60									2.50			0.39	43.9	0.98	6.59	1.08
61 *								1.00	0.50			0.61	24.5	1.65	6.40	1.92
62									1.00			0.46	29.0	1.16	6.51	1.38
63									1.50			0.42	32.7	0.97	6.56	1.14
64									2.01			0.38	38.0	0.90	6.59	0.99
65									2.49			0.38	42.1	0.85	6.62	0.89
66 *								1.50	0.50			0.56	26.1	1.58	6.45	1.58
67									1.00			0.44	30.4	1.10	6.54	1.13
68									1.50			0.39	33.4	0.89	6.59	0.93
69									2.00			0.35	36.2	0.78	6.62	0.81
70									2.49			0.33	40.2	0.73	6.64	0.73
111 *	20	16	1	4	48	10.5	1166	0.67	0.50	SB	49	1.60	-	-	-	-
112									1.00			1.54	-	-	-	-
113									1.50			1.50	-	-	-	-
114									2.00			1.48	-	-	-	-
115									2.50			1.48	-	-	-	-
116 *								1.00	0.50			1.57	-	-	-	-
117									1.00			1.52	-	-	-	-
118									1.50			1.48	-	-	-	-
119									2.01			1.46	-	-	-	-
120									2.49			1.45	-	-	-	-
121 *								1.50	0.50			1.55	-	-	-	-
122									1.00			1.50	-	-	-	-
123									1.50			1.47	-	-	-	-
124									2.00			1.45	-	-	-	-
125									2.49			1.44	-	-	-	-

- Bridge configuration does not meet AASHTO criteria.

will typically have all three HS20 axles on it when loading for maximum stresses. Because of the high level of interdependence of these parameters, this section considers the sensitivity of TSB shear and bending stresses and RPD to panel width, bridge width, span, and loading. The sensitivity of maximum TSB shear and bending stresses is presented first, followed by sensitivity of maximum RPD to the parameters. Results are grouped by panel width.

To quickly compare analyses and load cases for 42-inch wide panels, Figure 6.14 lists an analysis' results each in a separate cell. Each cell shows a sketch of the bridge and loading locations. (All loading in this part is HS20 loading) Each cell of the figure also contains the maximum TSB shear stress and bending stress utilization ratios. To emphasize the configurations and loading which overstress the TSB, the utilization ratios greater than one are in a bold font. If the utilization ratio is the maximum for the 42-inch wide panels for the analyses considered, then the label and utilization ratio are in bold and underlined font. The analyses are organized first by bridge span and then by analyses number. Further details of the analyses and loading can be found in Table 6.11 and in the load case and parametric study results sections of Appendix E. Table 6.11 presents the results in a fashion similar to the previous results tables. Results for the other panel widths are presented through similar figures and tables.

As is intuitively obvious, the TSB shear and bending stresses and RPD are significantly affected by panel width, bridge width, and loading. Sensitivity to bridge span is not as significant since the TSB shear and bending stresses and RPD are most significantly affected by proximity of the load truck axle to the TSB. Therefore, aware of

these sensitivities, the study sought to determine the bridge configuration and loading that would critically affect TSB shear and bending stresses and RPD.

For the 42-inch wide panels, maximum TSB shear stress was found when the panels were loaded with a tire at the panel edge as in Load Case #1 (Analysis #3 in Figure 6.14 and Table 6.11). Increasing the number of lanes on a bridge may not increase the TSB stress, as can be seen by comparing the shear stress results of Analysis #3 where the bridge has single lane of traffic for the 14-foot width to the results of Analysis #21 where the bridge has two lanes of traffic on the 21-foot wide superstructure. Taking the same bridge used in Analysis #21 and reducing it to a single lane of traffic (Analysis #22), maximized TSB bending stress utilization ratio for the 42-inch panels. Bridges of 35-foot spans with various loading configurations did not cause greater stress utilization ratios than the TSB maximum shear stress utilization ratio (1.46) found in Analysis #3 and the TSB maximum bending stress utilization ratio (1.60) found in Analysis #22. TSB maximum bending stress utilization ratio (1.59) in Analysis #32 is equal to that for Analysis #22 for practical purposes (Figure 6.14 and Table 6.11).

For the 48-inch wide panels, the maximum TSB shear stress utilization (1.64) and bending stress utilization (1.36) occurred in Analysis #35 (Figure 6.15 and Table 6.12). Again the greater TSB spacing of the 20-foot span bridge, maximized TSB shear and bending stresses.

For the 54-inch wide panels, it was determined with just a few loading and bridge configurations that the wider panels transferred less load to the TSB, and thus would not control the TSB shear and bending stress utilization. Analysis #41 had the maximum

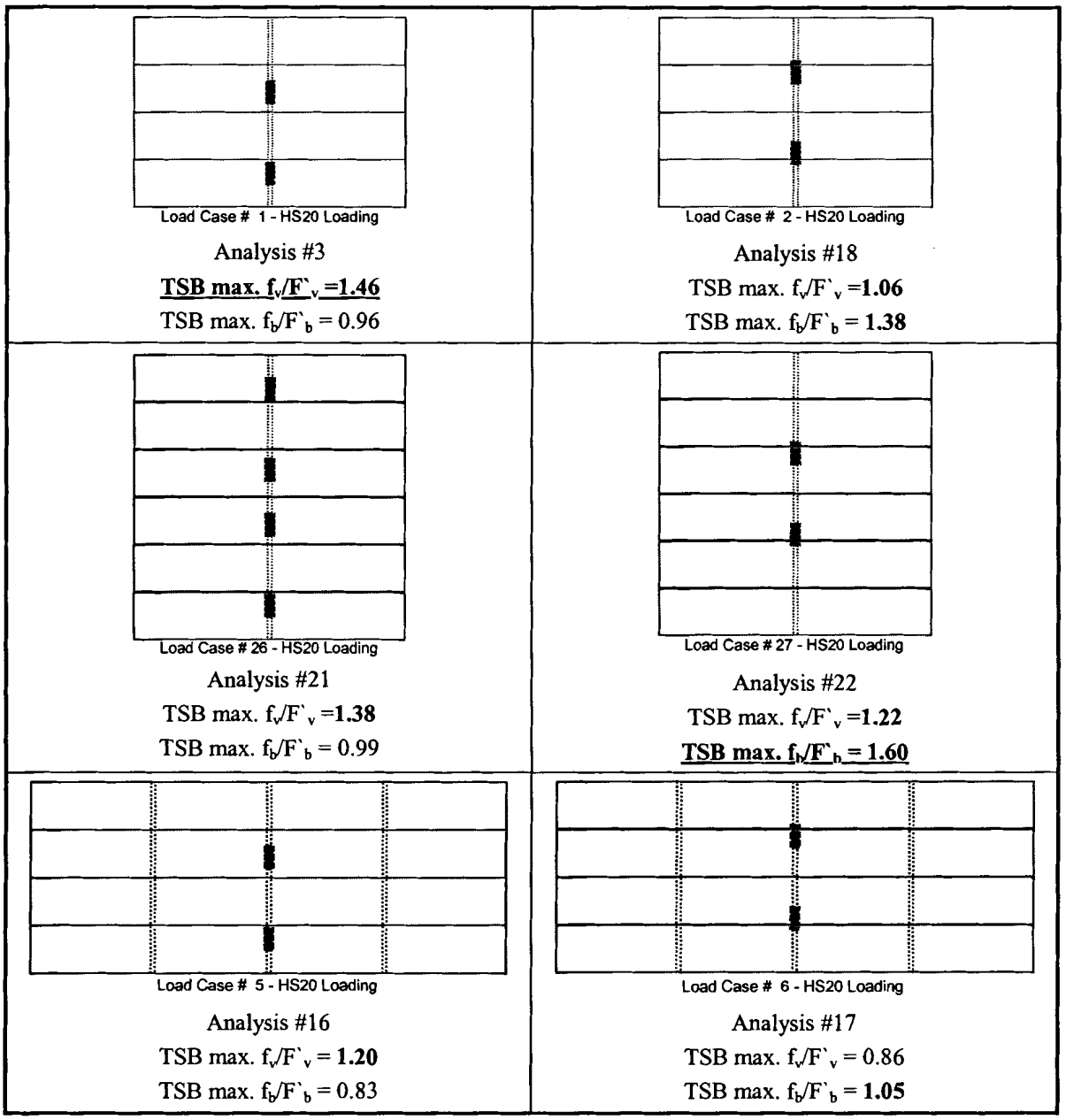

Figure 6.14 Critical load cases and TSB shear and bending utilization ratios for 42-inch wide panels (See Table 6.11 and Appendix E for analysis details.)

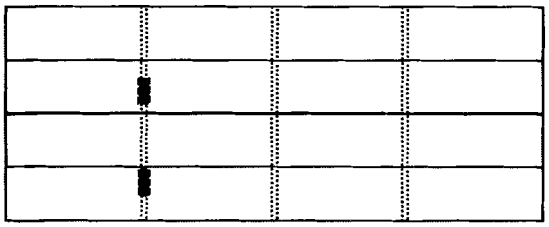

Load Case # 7 - HS20 Loading

Analysis #23

TSB max. f_v/F'_v = **1.21**

TSB max. f_b/F'_b = 0.76

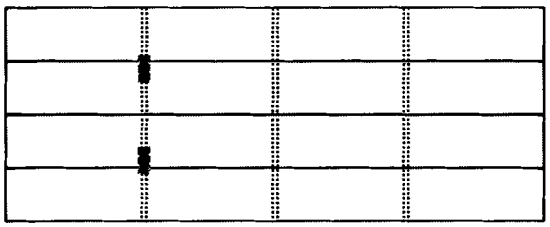

Load Case # 8 - HS20 Loading

Analysis #24

TSB max. f_v/F'_v = 0.87

TSB max. f_b/F'_b = 0.93

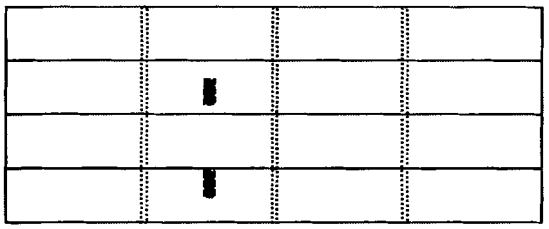

Load Case # 9 - HS20 Loading

Analysis #25

TSB max. f_v/F'_v = 0.91

TSB max. f_b/F'_b = 0.93

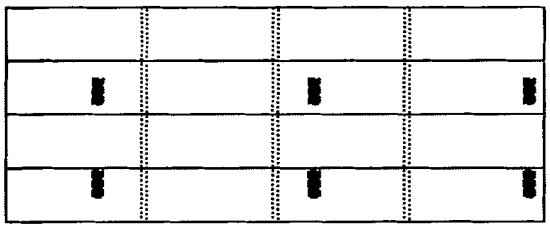

Load Case # 10 - HS20 Loading

Analysis #26

TSB max. f_v/F'_v = **1.23**

TSB max. f_b/F'_b = 0.91

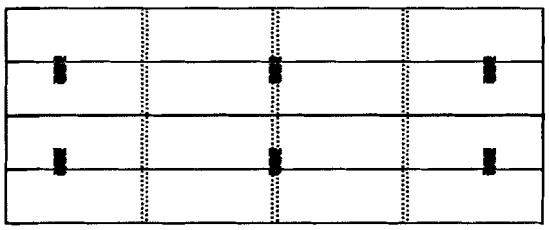

Load Case # 11 - HS20 Loading

Analysis #28

TSB max. f_v/F'_v = 0.91

TSB max. f_b/F'_b = **1.22**

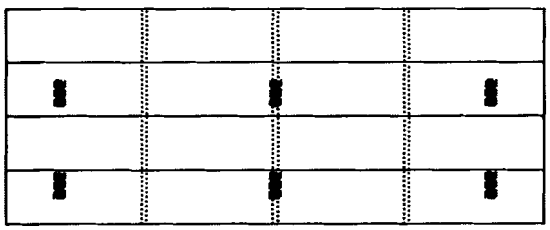

Load Case # 12 - HS20 Loading

Analysis #27

TSB max. f_v/F'_v = **1.27**

TSB max. f_b/F'_b = 0.93

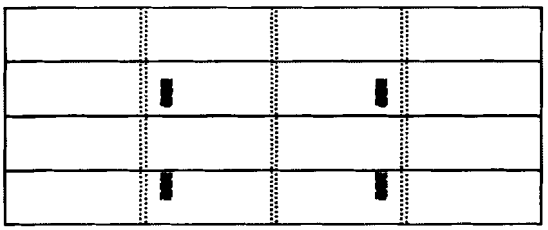

Load Case # 13 - HS20 Loading

Analysis #29

TSB max. f_v/F'_v = **1.21**

TSB max. f_b/F'_b = 0.85

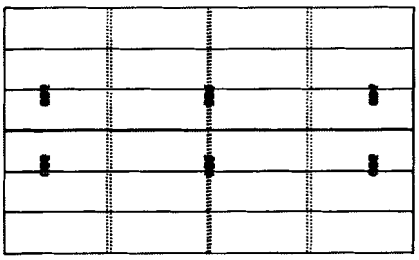

Load Case # 29 - HS20 Loading

Analysis #32

TSB max. f_v/F'_v = **1.18**

TSB max. f_b/F'_b = **1.59**

Figure 6.14 (Continued) Critical load cases and TSB shear and bending utilization ratios for 42-inch wide panels

Table 6.11 TSB stresses and RPD for TSB-critical 42-inch-wide panel bridges

Anal. #	Bridge			Panels				TSB		Panel-to-TSB Cxn.	Load Case #	Relative Panel Deflection Δ/0.10 in.	FEA TSB Bending Moment (kip-in)	TSB fb / Fb	FEA TSB Shear (kips)	TSB fv / Fv
	Span (ft.)	Bridge Width (ft.)	# of Lanes	# of Panels	Panel Width (in)	Panel Thick-ness (in.)	Panel MOE (ksi)	Aspect Ratio	TSB EI/EI_{min}							
3	20	14	1	4	42	10.5	1166	0.63	1.01	TB34	1	0.76	21.50	0.96	5.46	1.46
18											2	0.38	30.90	1.38	3.97	1.06
21	20	21	2	6	42	10.5	1166	0.63	1.01	TB34	28	0.68	22.10	0.99	5.18	1.38
22			1								27	0.46	35.70	1.60	4.57	1.22
16	35	14	1	4	42	14.25	1166	0.63	1.01	TB34	5	0.59	18.50	0.83	4.50	1.20
17											6	0.27	23.50	1.05	3.23	0.86
23											7	0.61	17.10	0.76	4.53	1.21
24											8	0.32	20.70	0.93	3.28	0.87
25											9	0.76	14.00	0.63	3.41	0.91
26											10	0.76	20.30	0.91	4.62	1.23
27											12	0.72	20.80	0.93	4.78	1.27
28											11	0.38	27.40	1.22	3.41	0.91
29											13	0.76	19.00	0.85	4.53	1.21
28	35	14	1	4	42	14.25	1166	0.63	1.01	TB34	11	0.38	27.40	1.22	3.41	0.91
32		21		6							29	0.55	35.60	1.59	4.41	1.18

Table 6.12 TSB stresses and RPD for TSB-critical 48-inch-wide panel bridges

Anal. #	Bridge			Panels				TSB		Panel-to-TSB Cxn.	Load Case #	Relative Panel Deflection Δ/0.10 in.	FEA TSB Bending Moment (kip-in)	TSB fb / Fb	FEA TSB Shear (kips)	TSB fv / Fv
	Span (ft.)	Bridge Width (ft.)	# of Lanes	# of Panels	Panel Width (in)	Panel Thick-ness (in.)	Panel MOE (ksi)	Aspect Ratio	TSB EI/EI_{min}							
33	20	16	1	4	48	10.5	1166	0.63	1.01	TB34	17	0.64	28.10	1.17	4.33	1.15
34											18	0.70	21.60	0.97	5.20	1.39
35											19	0.93	30.50	1.36	6.17	1.64
36											21	0.71	24.00	1.07	5.43	1.45
35	20	16	1	4	48	10.5	1166	0.63	1.01	TB34	19	0.93	30.50	1.36	6.17	1.64
36		20		5							25	0.65	23.10	1.03	4.45	1.19
37			2								24	0.49	25.50	1.14	2.89	0.77
39		24		6							28	0.65	20.10	0.90	5.07	1.35
35	20	16	1	4	48	10.5	1166	0.63	1.01	TB34	19	0.93	30.50	1.36	6.17	1.64
40	35					14.25					30	0.73	27.20	1.22	5.26	1.41
40	35	16	1	4	48	14.25	1166	0.63	1.01	TB34	30	0.73	27.20	1.22	5.26	1.41
81											33	0.81	25.10	1.12	4.97	1.32
80											34	0.63	28.90	1.20	5.16	1.38
82											35	0.67	24.20	1.08	4.97	1.32

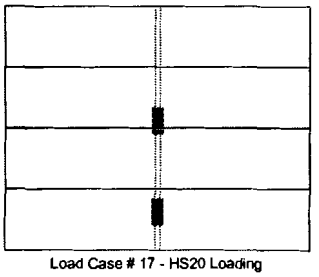

Load Case # 17 - HS20 Loading

Analysis #33

TSB max. f_v/F'_v = **1.15**

TSB max. f_b/F'_b = **1.17**

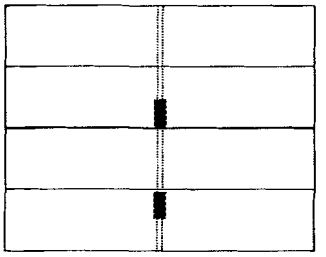

Load Case # 18 - HS20 Loading

Analysis #34

TSB max. f_v/F'_v = **1.39**

TSB max. f_b/F'_b = 0.97

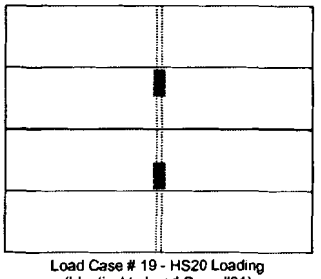

Load Case # 19 - HS20 Loading
(Identical to Load Case #31)

Analysis #35

TSB max. f_v/F'_v = 1.64

TSB max. f_b/F'_b = 1.36

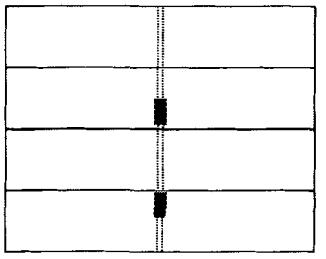

Load Case # 21 - HS20 Loading

Analysis #36

TSB max. f_v/F'_v = **1.45**

TSB max. f_b/F'_b = **1.07**

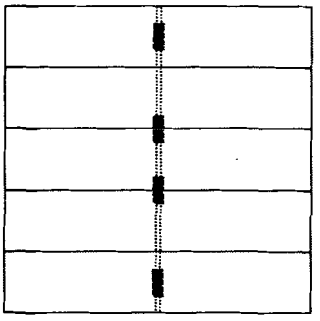

Load Case # 24 - HS20 Loading

Analysis #37

TSB max. f_v/F'_v = 0.77

TSB max. f_b/F'_b = **1.14**

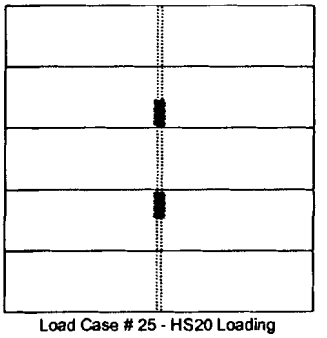

Load Case # 25 - HS20 Loading

Analysis #38

TSB max. f_v/F'_v = **1.19**

TSB max. f_b/F'_b = **1.03**

Figure 6.15 Critical load cases and TSB shear and bending utilization ratios for 48-inch wide panels (See Table 6.12 and Appendix E for analysis details.)

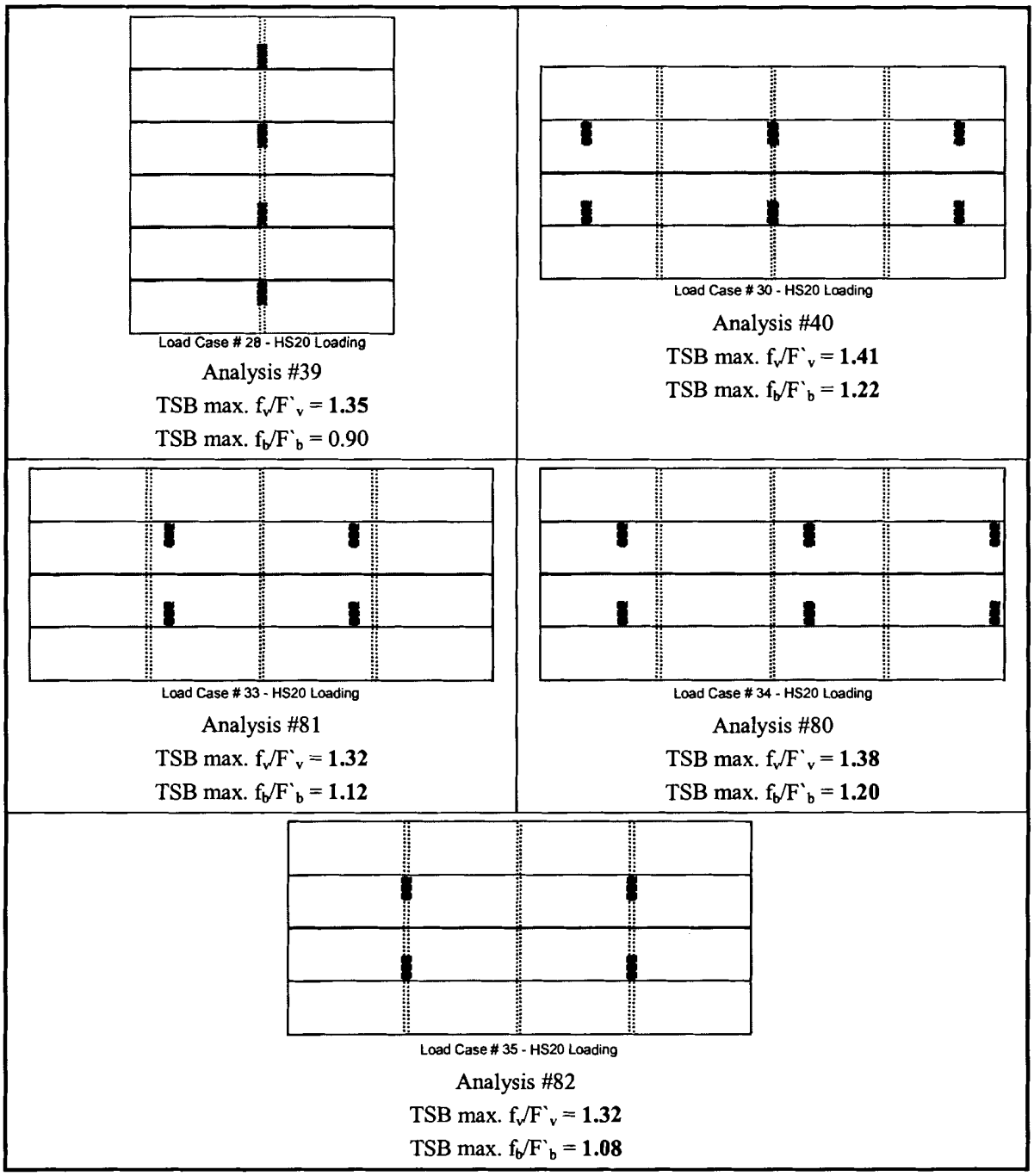

Figure 6.15 (Continued) Critical load cases and TSB shear and bending utilization ratios for 48-inch wide panels

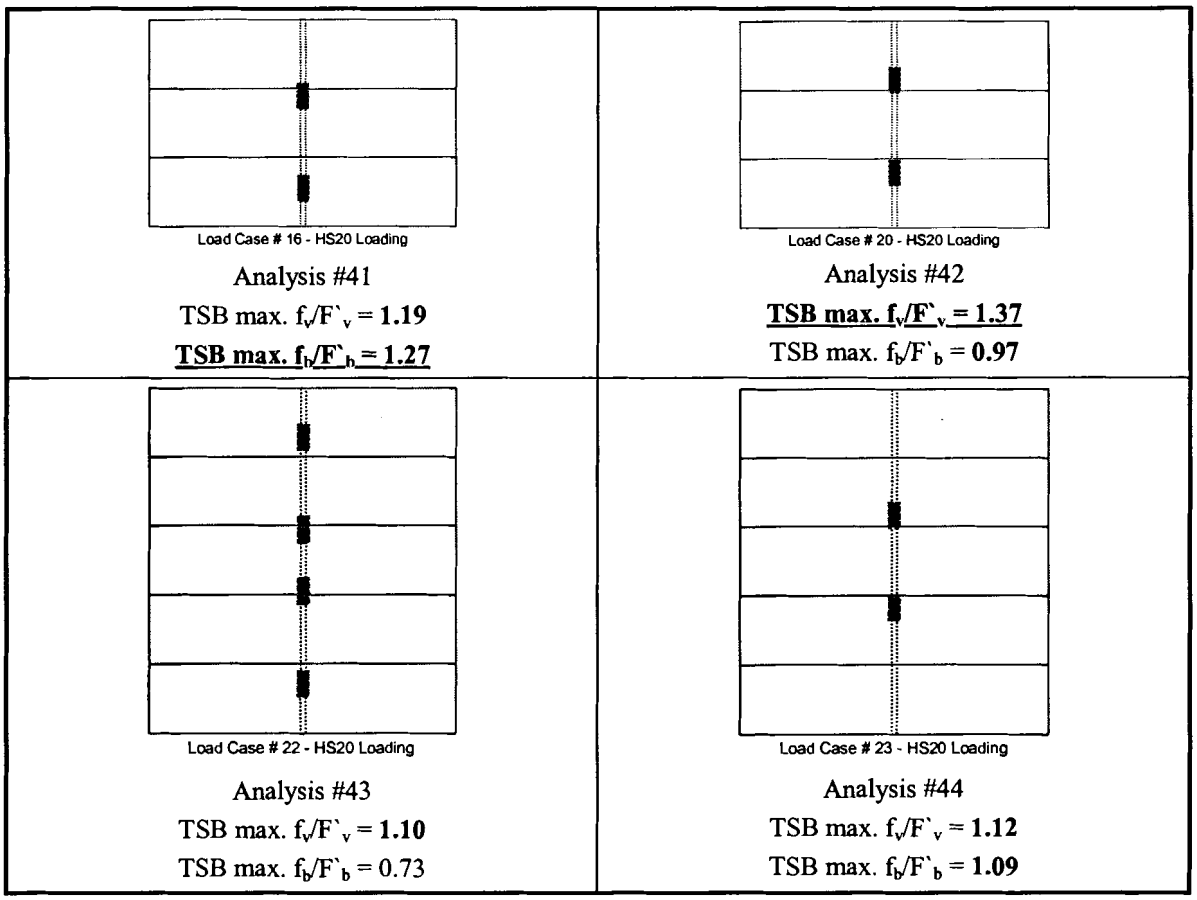

Figure 6.16 Critical load cases and TSB shear and bending utilization ratios for 54-inch wide panels (See Table 6.13 and Appendix E for analysis details.)

Table 6.13 TSB stresses and RPD for TSB-critical 54-inch-wide panel bridges

Anal. #	Bridge			Panels				TSB		Panel-to-TSB Cxn.	Load Case #	Relative Panel Deflection Δ/0.10 in.	FEA TSB Bending Moment (kip-in)	TSB fb / Fb	FEA TSB Shear (kips)	TSB fv / Fv
	Span (ft.)	Bridge Width (ft.)	# of Lanes	# of Panels	Panel Width (in)	Panel Thick-ness (in.)	Panel MOE (ksi)	Aspect Ratio	TSB EI/EI_{min}							
41	20	13.5	1	3	54	10.5	1166	0.63	1.01	TB34	16	0.49	28.40	1.27	4.46	1.19
42											20	0.66	21.80	0.97	5.15	1.37
44		22.5		5							23	0.56	24.40	1.09	4.21	1.12
43			2								22	0.54	16.30	0.73	4.11	1.10

TSB shear stress utilization (1.27), and Analysis #42 had the maximum bending stress utilization (1.37) (Figure 6.16 and Table 6.13).

Analyses showed (Appendix E) that there is only one axle location for each bridge that will maximize RPD, midway between TSB or midway between a TSB and the support. Several load cases on the 35-ft. span bridges were checked to verify that the 20-ft. span controlled RPD due to the greater TSB spacing. Both the 42-in. wide and 48-in. wide panels were checked and the maximum RPD values were essentially equivalent (1.62 RPD utilization ratio for the 42-in. and 1.64 utilization ratio for the 48-in. panels). The load cases and analysis results are given in Figure 6.17 and Table 6.14.

6.3.2 Critical TSB Shear and Bending Stresses and RPD

Once the sensitivity of TSB shear and bending stresses and RPD to the parameters was known, the critical, HS20-loaded bridge was analyzed. Panel MOE and TSB MOE, although found to have an effect on the results being considered, were not changed from their published values.

6.3.2.1 MaximumTSB Shear Stress

For TSB shear stress, the critical bridge was analyzed in Analysis #71. The critical bridge configuration is a 20-ft. span, 16-ft. wide bridge consisting of four 48-in. wide, 10.5-in. thick panels. The TSB has an aspect ratio of 0.67 and the minimum required AASHTO EI. The TSB is connected to the panels with the stiffest connection system, the seated-beam. HS20 loading to maximize utilization was Load Case #19.

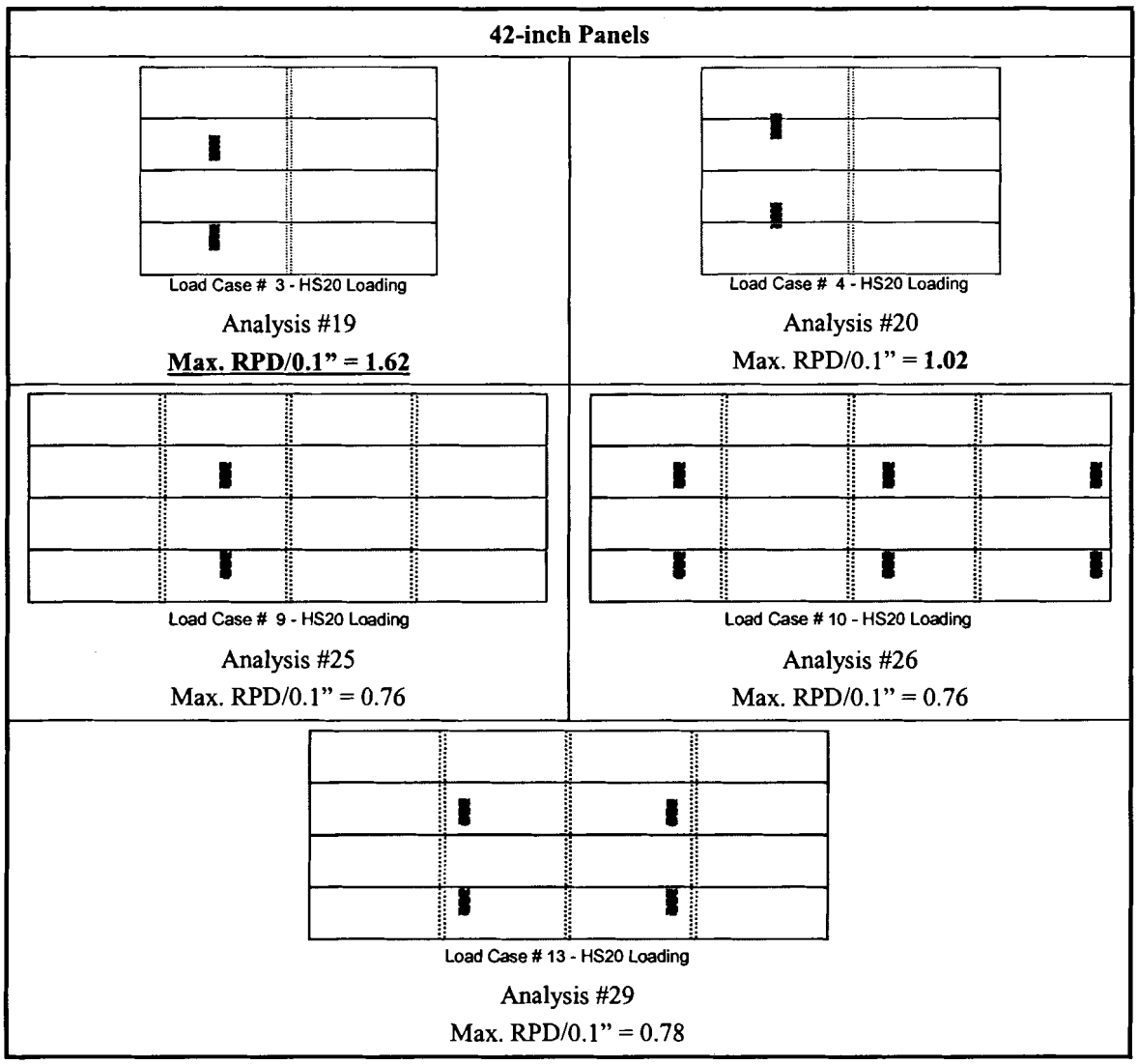

Figure 6.17 Critical load cases and RPD utilization ratios for bridge configurations and loading locations (See Table 6.14 and Appendix E for analysis details.)

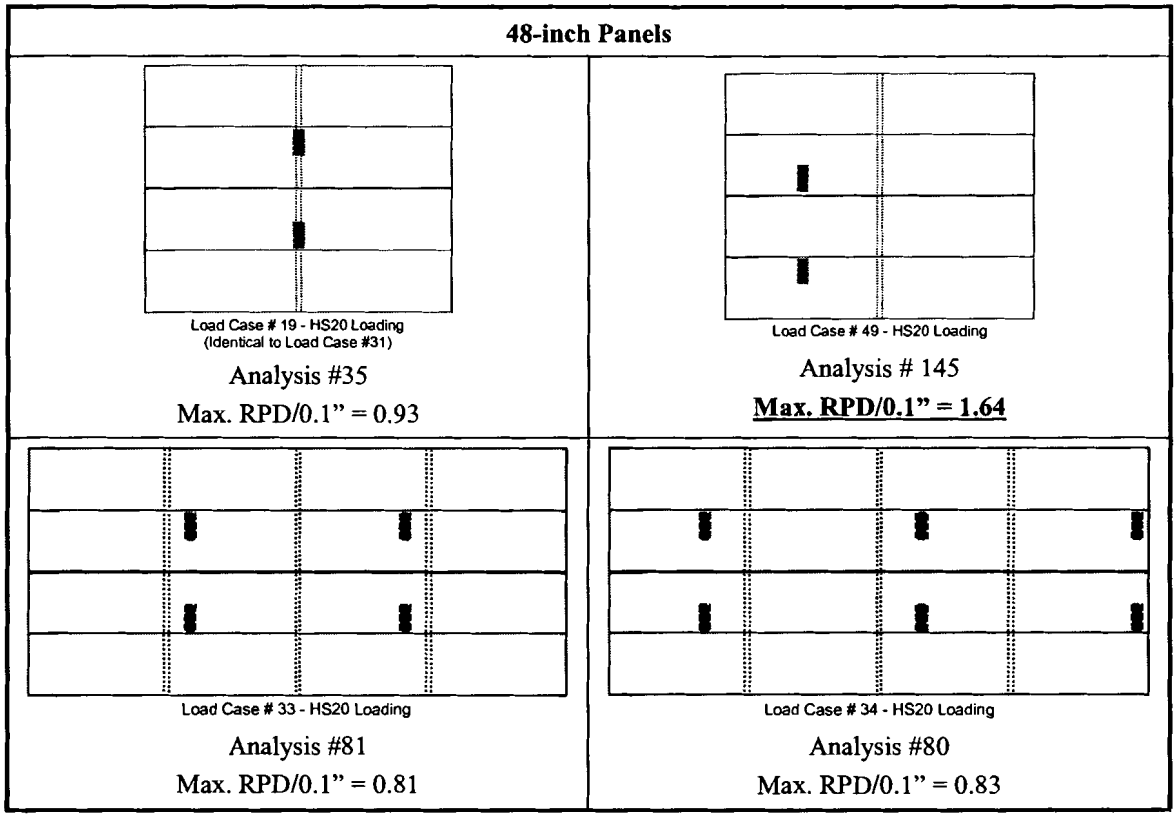

Figure 6.17 (Continued) Critical load cases and RPD utilization ratios for bridge configurations and loading locations

Table 6.14 RPD and TSB stresses for RPD-critical bridges

Anal. #	Bridge			Panels				TSB		Panel-to-TSB Cxn.	Load Case #	Relative Panel Deflection Δ/0.10 in.	FEA TSB Bending Moment (kip-in)	TSB fb / Fb	FEA TSB Shear (kips)	TSB fv / Fv
	Span (ft.)	Bridge Width (ft.)	# of Lanes	# of Panels	Panel Width (in)	Panel Thick-ness (in.)	Panel MOE (ksi)	Aspect Ratio	TSB EI/EI_{min}							
19	20	14	1	4	42	10.5	1166	0.63	1.01	TB34	3	1.62	13.50	0.60	3.73	0.99
20											4	1.02	19.10	0.85	2.69	0.72
25	35					14.25					9	0.76	14.00	0.63	3.41	0.91
26											10	0.76	20.30	0.91	4.62	1.23
29											13	0.78	19.00	0.85	4.53	1.21
35	20	18	1	4	48	10.5	1166	0.63	1.01	TB34	19	0.93	30.50	1.36	6.17	1.64
145											49	1.64	-	-	-	-
80						14.25					34	0.83	26.90	1.20	5.16	1.38
81											33	0.81	25.10	1.12	4.97	1.32

Maximum TSB shear stress utilization ratio for HS20 was 1.68. This high utilization ratio shows the need for a improved design methodology for TSB shear.

6.3.2.2 Maximum TSB Bending Stress

For TSB bending stress, the critical bridge was analyzed in Analysis #90. The critical bridge configuration is a 20-ft. span, 21-ft. wide bridge consisting of six 42-in. wide, 10.5-in. thick panels. The TSB has an aspect ratio of 0.67 and the minimum AASHTO EI required. The TSB is connected to the panels with the least stiff connection system, the aluminum bracket. HS20 loading used to maximize utilization was Load Case #45. Maximum TSB bending stress utilization ratio for HS20 was 1.61. This high utilization ratio shows the need for a improved design methodology for TSB bending.

6.3.2.3 Maximum Relative Panel Movement

For RPD, the critical bridge was analyzed in Analysis #127. The critical bridge configuration is a 20-ft. span, 16-ft. wide bridge consisting of four 48-in. wide, 10.5-in. thick panels. The TSB has an aspect ratio of 0.67 and the minimum AASHTO EI required. The TSB is connected to the panels with the least stiff connection system, the aluminum bracket. HS20 loading to maximize utilization was Load Case #49. Maximum RPD utilization ratio for HS20 loading was 1.79. This analysis shows the potential inadequacy of the current AASHTO TSB spacing to meet the 0.1-in. asphalt serviceability criteria.

6.4 TSB Design

Before making recommendations for changes to the current AASHTO TSB design criteria, other live load trucks were considered for analysis. The HS25 truck,

which has wheel loads 25% greater than the HS20 truck, was used, as was the alternate military loading of two 24-kip axles spaced four feet apart. The alternate military loading is designated ML24 in this thesis. The standard ML24 loading was also increased 25% in a manner similar to the HS25 truck, and this has been designated as ML30. When the ML24 truck is considered, the TSB shear stress utilization ratio can be 1.81 (Table 6.15), the TSB bending stress utilization ratio can be 2.29 (Table 6.16), and the RPD utilization ratio can be 2.39 (Table 6.17).

In recommending TSB design criteria, simplicity was desired. In considering TSB design shear, the maximum shear forces obtained from analyses were divided by the load truck wheel load (Appendix E). For the ML24 truck where the axles are only four feet apart, a factor of 1.75 was applied to obtain an effective wheel load. The maximum ratio of wheel load recommended for TSB shear design was 0.45.

For TSB design bending moment, the maximum bending moments obtained from analyses were divided by the load truck wheel load (Appendix E) to give a moment arm. The ML24 wheel loads were in the same manner as they had been for TSB design shear. The maximum wheel load moment arm recommended for TSB bending moment design was 3.5 inches.

6.5 Conclusions and Recommendations

The parametric study has shown that the current AASHTO design criteria for the TSB of longitudinal glulam deck bridges can be inadequate. HS20 loading can cause the TSB to be overstressed in shear by 68% and in bending by 61%. With HS20 loading the RPD may be 79% greater than the limit set by the serviceability criteria for asphalt

Table 6.15 Critical TSB shear stress utilization ratios

Anal. #	Bridge			Panels				TSB		Panel-to-TSB Cxn.	Load Case #	Load Case Description	Relative Panel Deflection Δ/0.10 in.	FEA TSB Bending Moment (kip-in)	TSB fb / Fb	FEA TSB Shear (kips)	TSB fv / Fv
	Span (ft.)	Bridge Width (ft.)	# of Lanes	# of Panels	Panel Width (in)	Panel Thick-ness (in.)	Panel MOE (ksi)	Aspect Ratio	TSB EI/EI_{min}								
71	20	16	1	4	48	10.5	1166	0.67	1.00	SB	19	HS20	0.53	28.20	1.24	6.47	1.68
83	35	16	1	4	48	14.25	1166	0.63	1.01	TB34	36	ML24	1.01	33.40	1.49	6.48	1.73
84	35	16	1	4	48	14.25	1166	0.63	1.01	TB34	37	ML30	1.12	32.10	1.43	6.27	1.67
87	35	32	2	8	48	16.25	1166	0.67	1.00	SB	40	2 HS25 Trucks	0.56	26.40	1.16	6.78	1.76
88	35	32	2	8	48	16.25	1166	0.67	1.00	SB	42	2 ML24 Trucks	0.59	26.50	1.17	7.00	1.81
89	35	32	2	8	48	16.25	1166	0.67	1.00	SB	41	2 ML30 Trucks	0.77	33.10	1.46	8.61	2.23

Table 6.16 Critical TSB bending stress utilization ratios

Anal. #	Bridge			Panels				TSB		Panel-to-TSB Cxn.	Load Case #	Load Case Description	Relative Panel Deflection Δ/0.10 in.	FEA TSB Bending Moment (kip-in)	TSB fb / Fb	FEA TSB Shear (kips)	TSB fv / Fv
	Span (ft.)	Bridge Width (ft.)	# of Lanes	# of Panels	Panel Width (in)	Panel Thick-ness (in.)	Panel MOE (ksi)	Aspect Ratio	TSB EI/EI_{min}								
90	20	21	1	6	42	10.5	1166	0.67	1.00	AB	45	HS20	0.71	36.50	1.61	4.37	1.13
91	20	21	1	6	42	10.5	1166	0.67	1.00	AB	44	HS25	1.02	46.40	2.05	5.35	1.39
92	20	21	1	6	42	10.5	1166	0.67	1.00	AB	43	ML24	1.37	52.00	2.29	5.94	1.54

Table 6.17 Critical RPD utilization ratios

Anal. #	Bridge			Panels				TSB		Panel-to-TSB Cxn.	Load Case #	Load Case Description	Relative Panel Deflection Δ/0.10 in.	FEA TSB Bending Moment (kip-in)	TSB fb / Fb	FEA TSB Shear (kips)	TSB fv / Fv
	Span (ft.)	Bridge Width (ft.)	# of Lanes	# of Panels	Panel Width (in)	Panel Thick-ness (in.)	Panel MOE (ksi)	Aspect Ratio	TSB EI/EI_{min}								
127	20	16	1	4	48	10.5	1166	0.67	1.00	AB	49	HS20	1.79	-	-	-	-
141	20	16	1	4	48	10.5	1166	0.67	1.00	AB	48	HS25	2.32	-	-	-	-
142	20	16	1	4	48	10.5	1166	0.67	1.00	AB	47	ML24	2.39	-	-	-	-

(Ritter 1990). Other AASHTO live load trucks cause even greater overstress and RPD. Clearly, the current AASHTO design criteria for the TSB are not adequate.

Based on the parametric study performed, the following design criteria are recommended to replace the current AASHTO TSB design criteria.

In lieu of a more accurate analysis, the transverse stiffener beam shall be designed for the following bending moment and shear.

1. Shear = 0.45*wheel load
2. Bending Moment = 3.5 arm*wheel load

   Where wheel load is the maximum wheel load for HS & H vehicles and 1.75*maximum wheel load for alternate military loading

To give an example of the potential effect these recommendations would have, a design example is included. For a 20-ft. span, 16-ft. wide bridge designed for a single, HS20-rated lane and built using ¾-in. through bolts for panel-to-TSB connections, the current AASHTO design criteria (AASHTO 1996) are used. The 48-in. wide, SP47 glulam panels would be 10.5 inches thick. A SP47 TSB at midspan and with a height of 6.75 in. and a width of 4.5 in. would easily meet the ASSHTO TSB spacing and minimum EI criteria, but, as the analyses in this chapter has shown, the TSB may be critically overstressed. With the recommended 0.45 wheel load shear design fraction and the recommended 3.5 in. wheel load moment arm, the TSB would have to meet the current AASHTO 80,000 kip-in^2 minimum stiffness factor and now be designed for a shear of 7.2 kips and a bending moment of 56 in-kips. A SP47 TSB placed at midspan and with a height of 6 in. and a width of 6.67 in. meets current and recommended

AASHTO TSB design criteria. Thus, the recommended changes should not significantly affect the cost of longitudinal glulam bridges while providing adequate safety.

Chapter 7

CONCLUSIONS AND RECOMMENDATIONS

7.1 Conclusions

The conclusions from this study are divided into three areas: the longitudinal FRP-reinforced glulam deck panels, the finite element model for longitudinal glulam deck bridges, and the parametric study of the Transverse Stiffener Beam (TSB) in longitudinal glulam deck bridges.

7.1.1 Longitudinal FRP-Reinforced Glulam Deck Panels

Specific conclusions with regard to longitudinal FRP-reinforced glulam deck bridges are restricted to the particular design details, materials, and field conditions this project.

1. FRP-glulam panels can be handled, on the construction site, in a manner and with equipment similar to that used for conventional glulam panels and prestressed concrete planks.
2. The weight of the FRP-glulam panels used in this project was only one third the weight of equivalent prestressed concrete planks. This weight reduction allows for cost savings in construction.
3. One percent (by area) FRP tension reinforcing of glulam panels with wet-layup E-glass/phenol resorcinol formaldehyde composite in the middle two-thirds of the span increased bending stiffness by an average of six percent.

4. The durability of the FRP is crucial for proper performance of the FRP-glulam deck panels. Although laboratory testing indicates durability concerns with a PRF matrix (Battles 2000), the FRP used on the Milbridge Pier has so far performed well in the marine environment. Visual inspection has shown no apparent degradation after the first year of service.

5. At an FOB cost of $\$36.37/ft^2$, the FRP-glulam deck used on the Milbridge Pier was cost competitive with the prestressed concrete deck.

6. The wearing surface criteria for the Milbridge pier required resistance to gasoline and oil spills, which pre-empted the use of an economically competitive asphalt surface with an underlying waterproof membrane. A more expensive oil-spill resistant wearing surface, consisting of two different products (CIM1000 and Transpo T45) was developed and used. This increased the square foot cost, so that the cost of the structure with the special wearing surface on the FRP-glulam was no longer competitive with prestressed concrete on a first-cost basis.

7.1.2 Finite Element Model for Longitudinal Glulam Deck Bridges

1. The finite element model of longitudinal deck bridges developed in this study was compared with full-scale laboratory test data of longitudinal deck bridges conducted as part of this study at The University of Maine as well as test data published by Iowa State University. The UMaine test data included panel deflections and strain in the seated-beam connection.

Iowa State University's test data included midspan panel deflections, midspan panel bending strain, and TSB bending strain. This showed that the FEA model developed in this study accurately analyses longitudinal glulam deck bridges.

2. The nonlinear tension connection model used in this study more closely represents the actual connection behavior than the linear models in the published literature. However, the connection nonlinearity only slightly influences the longitudinal glulam deck bridge's response.

3. The addition of connection elements that can be pretensioned allows incorporation of the effect of initial tightening of the connections. The element may also allow modeling of loose connections.

4. TSB-deck bearing elements should be included in a finite element model, since the TSB bending moment is sensitive to the stiffness of the bearing elements (see Section 5.2.5)

7.1.3 Parametric Study of Longitudinal Glulam Deck Bridges

1. The finite element model developed as part of this study and described-in this thesis was used to perform a parametric study of longitudinal glulam deck bridges. Forty-three bridges were designed according to AASHTO and were then analyzed under 50 loading conditions. Parameters varied included two spans (20 ft. and 35 ft.), three AASHTO live loadings (HS20, HS25, and alternate military loading), three panel widths (42 in., 48 in., and 54 in.), eight bridge widths (13.5 ft., 14 ft., 16 ft., 20 ft., 21 ft.,

22.5 ft., 24 ft., and 32 ft.), five panel thickness (8.5 in., 10.5 in., 12.25 in., 14.25 in., and 16.25 in.), 23 TSB sizes (from 4.75 in. by 3.19 in. to 8.00 in. by 5.35 in.), four connection systems (aluminum brackets, 5/8-in. through bolts, ¾-in. through bolts, and seated beam), and four panel and TSB MOE (75%, 100%, 125%, and 150% of published MOE (AFPA, AWC 1997)). Response values examined included maximum bending and shears stresses in the TSB as well as differential deflection between adjacent panels.

2. The current AASHTO design criteria for TSB (AASHTO 1996, Section 3.25.3.4) may result in overstressing the TSB under AASHTO HS20 loading as follows:

   a. The TSB may be 68% overstressed in shear. The critical bridge configuration that causes this condition is a 16-ft. wide, 20-ft. span bridge constructed of four 48-in. wide, 10.5-in. thick, southern pine glulam axial combination #47 (SP47) panels joined through seated-beam connections to a 5.66-in. high, 3.79-in. wide, SP47 TSB (EI equals 80,000 ksi, the AASHTO minimum) placed at midspan. The critical AASHTO HS20 loading that causes this condition is a 32-kip axle placed symmetrically on the bridge at midspan.

   b. The TSB may be 61% overstressed in bending. The critical bridge configuration that causes this condition is a 21-ft. wide, 20-ft. span bridge constructed of six 42-in. wide, 10.5-in. thick, SP47 panels joined through aluminum-bracket connections to a 5.66-in. high, 3.79-

in. wide, SP47 TSB (EI equals 80,000 ksi, the AASHTO minimum) placed at midspan. The critical AASHTO HS20 loading that causes this condition is a 32-kip axle placed symmetrically on the bridge at midspan.

c. The bridge may experience relative deflection between adjacent panels 79% greater than the often-cited 0.1-inch serviceability criteria for asphalt (Ritter 1990). The critical bridge configuration that causes this condition is a 16-ft. wide, 20-ft. span bridge constructed of four 48-in. wide, 10.5-in. thick, SP47 panels joined through aluminum-bracket connections to a 5.66-in. high, 3.79-in. wide, SP47 TSB (EI equals 80,000 ksi, the AASHTO minimum) placed at midspan. The critical AASHTO HS20 loading that causes this condition is a 32-kip axle placed at quarter span and such that one tire is placed at the inside edge of an outer bridge panel.

3. Other bridge configurations designed under the current AASHTO design criteria can also result in overstressing of the TSB under AASHTO HS20 loading (see Chapter 6).

4. Under AASHTO HS25 or alternate military loading, the maximum TSB overstress and relative panel deflection are greater than the values described in (2) above.

5. Using the results of the parametric study, the following TSB design criteria are proposed, in addition to the current AASHTO requirements (AASHTO 1996, Section 3.25.3.4)

In lieu of a more accurate analysis, the transverse stiffener beam shall be designed for the following bending moment and shear, in addition to maintaining EI> 80,000 ksi:

Shear = 0.45*wheel load

Bending Moment = (3.6 inches) * wheel load

In which the wheel load is the maximum wheel load for HS & H vehicles and 1.75*maximum wheel load for alternate military loading

7.2 Recommendations for Future Work

Recommendations listed here for future work would broaden the research scope and would increase the utilization of the work reported in this thesis.

1. An alternative, more durable FRP should be investigated for reinforcing glulam panels. Options that may be researched include the E-glass/vinyl ester composite researched by Xu (2001) and preconsolidated E-glass composite.
2. An alternative membrane/wearing surface system should be researched that meets the flexibility, water-impermeability, impact resistance, petroleum-product spill durability, and adhesion criteria for marine piers.
3. Kurain has shown that the curbs' effect on TSB bending stress can be significant (Kurain 2001). The bridge configurations and loading that produce maximum TSB moments, TSB shears, and relative panel deflections should be analyzed with "typical" glulam curbs. Analyses of

two models, one with non-composite curbs and one with composite curbs, would provide bounds for the curbs' effect on the TSB-stress critical bridge configurations and loadings. Upon analysis, the changes recommended in this thesis to AASHTO design criteria should be evaluated and adjusted as necessary.

4. Although major changes are not expected from analyses with other wood species, it is recommended that other wood species/glulam layups commonly used for longitudinal glulam deck bridges be analyzed. The change in panel MOE and shear modulus may change the system's behavior and thus may warrant a slight change in the recommended shear wheel load fraction or the bending moment wheel load arm. One recommended layup would be the commonly used douglas fir axial combination #2 glulam layup. Upon analysis, the recommended changes to AASHTO design criteria should be evaluated and adjusted as necessary.

REFERENCES

AASHTO. (1996). *Standard Specifications for Highway Bridges.* Washington, DC: American Association of State Highway and Transportation Officials.

AFPA, AWC. (1997). *Design Values for Wood Construction. A Supplement to the National Design Specification for Wood Construction.* Washington, DC: American Wood Council - American Forest and Paper Association.

Agarwal, B.D., Broutman, L. J. (1990). *Analysis and Performance of Fiber Composites.* New York: John Wiley and Sons, Inc.

AITC. (1994). *Timber Construction Manual.* 4th ed. New York: John Wiley and Sons, Inc.

AITC. (2001). Design Standard Specification For Structural Glued Laminated Timber Of Softwood Species. *AITC 117-2001-Design.* Englewood, CO: American Institute Of Timber Construction.

ANSYS. (2000a). *ANSYS 5.7 University High Option.* [CD-ROM] Canonsburg, PA: SAS IP, Inc. Available: SAS IP, Inc.

ANSYS. (2000b). *ANSYS Online Help.* [Online] Canonsburg, PA: SAS IP, Inc. Available: http://www1.ansys.com/customer/content/documentation/57/ansystoc.html.

APA. (2001). "Engineering Bulletin Number 98-3: Allowable Horizontal Shear Stresses for Glulam." Tacoma, WA: APA – the Engineered Wood Association Headquarters.

ASTM. (2000a). *ASTM A153/A153M-01a Standard Specification for Zinc Coating (Hot-Dip) on Iron and Steel Hardware.* West Conshohocken, PA: American Society for Testing and Materials.

ASTM. (2000b). *ASTM D198-99 Standard Test Methods of Static Tests of Lumber in Structural Sizes.* West Conshohocken, PA: American Society for Testing and Materials.

Battles, E.P. (2000). "Environmental Durability of FRP Reinforcement for Timber Bridges." Summary Report. Orono, ME: Advanced Engineered Wood Composites Center, University of Maine.

Bhide, S. (2001). *Material Usage on Condition of Existing Bridges in the U.S.* Skokie, IL: Portland Cement Association.

Busel, J. (2000). "Environmental Durability of Composites." *FRP Composite Products for Bridge Applications – Product Selection Guide.* Harrison, NY: Market Development Alliance.

CERF. (2001). *Gap Analysis for Durability of Fiber Reinforced Polymer Composites in Civil Infrastructure.* Reston, VA: American Society of Civil Engineers.

Dagher, H.J., Kimball, T., Abdel-Magid B., and Shaler, S.M. (1996). "Effect of FRP Reinforcement on Low-Grade Eastern Hemlock Glulams." *National Conference on Wood Transportation Structures*, Madison, WI.

Dagher, H.J., Poulin, J., Abdel-Magid, B., Shaler, S.M., Tjoelker, W., and Yeh, B. (1998a). "FRP Reinforcement of Douglas Fir and Western Hemlock Glulam Beams." *International Composites Expo '98*, Nashville, TN.

Dagher, H.J., Bragdon, M.M. (2001). "Advanced FRP-Wood Composites in Bridge Applications" *Structural Engineering Institute 2001 Structures Congress*, Washington, DC.

Dagher, H.J., Abdel-Magid, B., Lindyberg, R.F., Poulin, J., Shaler, S.M. (1998b). *Static Bending Test Results of Douglas Fir and Western Hemlock FRP-Reinforced Glulam Beams: 21 foot Span Series.* AEWC Report 98-4. Orono, ME: Advanced Engineered Wood Composites Center, University of Maine.

Foster, B.W. (1998). *Flexural repair and strengthening of timer beams using fiber reinforced polymers.* MS Thesis. Orono, ME: University of Maine.

FPL. (1974). *Wood Handbook – Wood as an Engineering Material.* Agriculture Handbook No. 72 Washington, DC: U.S. Department of Agriculture, Forest Service, Forest Products Laboratory.

FPL. (1999). *Wood Handbook – Wood as an Engineering Material.* Gen. Tech. Rep. FPL-GTR-113. Madison, WI: U.S. Department of Agriculture, Forest Service, Forest Products Laboratory.

Funke, R.W. (1986). *Behavior of Longitudinal Glued Laminated Timber Deck Bridges.* MS Thesis. Ames, IA: Iowa State University.

Gilham, P. (2002) Personal Phone Conversation on September 10.

Hajdu, T. (1994). *Dynamic Behavior of Longitudinal Glued Laminated Timber Bridges.* MS Thesis. Ames, IA: Iowa State University.

Hale, C.Y. (1978). "Stiffened Longitudinal Decked Bridge – Evaluation of Stiffener Hardware." [Unpublished Report] Report No. 045-1609-3. Tacoma, WA: Weyerhaeuser Company.

Iqbal, M.A. (2000). *Fatigue Life of Pultruded and Hand Lay-Up GFRP Exposed to Different Environmental Conditions*. MS Thesis. Orono, ME: University of Maine.

Kurain, A.V. (2001). *Finite Element Analysis of Longitudinal Glulam Timber Deck and Glulam Timber Girder Bridges*. MS Thesis. Ames, IA: Iowa State University.

Lacross, V.D. (1997). *Fatigue of Interconnected Deck Connections in Hardwood Glued-Laminated Bridge Decks*. MS Thesis. University Park, PA: Penn State.

Mathcad. (2000). *Mathcad 2000 Professional*. [CD-ROM]. Eden Prairie, MN: Mathsoft Engineering & Education, Inc. Available: Mathsoft Engineering & Education, Inc.

Matlab. (2000). *Matlab 6.0.0.42a Release 12 Student Version*. [CD-ROM]. Natick, MA: The Mathworks, Inc. Available: The Mathworks, Inc.

Novotoney, M.E. (2001). "Wearing Surfaces for FRP-Glulam Composite Ocean Pier Decks." [Unpublished Report]. Orono, ME: Advanced Engineered Wood Composites Center, University of Maine.

Pottle, P., Dagher, H.J. (2000). Phone Conversation.

Ritter, M.A. (1990). *Timber Bridges: Design, Construction, Inspection, and Maintenance*. Washington, DC: U.S. Department of Agriculture, Forest Service, Forest Products Laboratory.

Sanders, W.W., Jr., Klaiber, F.W., Wipf, T.J. (1985). "Load Distribution in Glued Laminated Longitudinal Timber Deck Highway Bridges." Report No. ERI-85441. Ames, IA: Iowa State University – Engineering Research Institute.

Tomforde, D.G. (1996). *Lag Screw and Deck Clip Performance Evaluation in Hardwood Glulam Timber Bridge Decking Connections*. MS Thesis. University Park, PA: Penn State.

Waldron, P., Byars, E.A., Dejke, V. (2001). "Durability of FRP in Concrete – A State of the Art." In *Proceedings of The International Workshop of Composites in Construction: A Reality*, July 20-21, 2001, Capri, Italy.

Witmer, R.W. (1996). *Load Distribution Characteristics of Hardwood Glued-Laminated Timber Bridges and Bridge Components*. MS Thesis. University Park, PA: Penn State.

Wood, K.S. (2000). *Environmental exposure characterization of fiber reinforced polymer materials used in bridge deck systems*. MS Thesis. Orono, ME: University of Maine.

Xu, H. (2001). *Development of FRP-Glulam Panel for Bridge Deck Replacement.* MS Thesis. Orono, ME: University of Maine.

APPENDICES

Appendix A

LONGITUDINAL GLULAM DECK BRIDGE DESIGN METHODOLOGY

A.1 Milbridge Pier Design Calculations

Milbridge Pier Design

References:
AASHTO. 1996. *Standard Specifications for Highway Bridges.*
AITC. 1994. *Timber Construction Manual*. New York: John Wiley & Sons, Inc. pp. 6-397 - 6-400.
Ritter, Michael A. 1990. *Timber Bridges: Design, Construction, Inspection, and Maintenance* . Washington, D.C.: United States Department of Agriculture, Forest Service.

Notes:

- This method is based on the design requirements of 1996 AASHTO Standard Specifications for Highway Bridges.
- Longitudinal decks are designed for design vehicles with wheel loads assumed to act as point loads and no reduction of wheel loads of H20-44 or HS20-44 as allowed by AASHTO special provisions.
- Per AASHTO: Panels are designed under wet-use conditions and the transverse stiffener design is assumed to have dry conditions since a watertight glulam deck is provided. AITC allows the assumption of dry-use conditions if there is a watertight glulam deck and if transverse stiffener is treated with oil-borne preservatives.

Input:

$L := 21.5ft$ — Simple Span Length (14-35 ft)
Measured ctr to ctr on bearings

$W := 16ft$ — Bridge Width
Roadway width + curb/railing requirements

$n_{lane} := 1$ — Number of Lanes (1 or 2)

Loading := "HS20" — AASHTO Live Loading
(HS20 or HS25)

species := "SP" Gspec := "other" — Wood Species & Glulam Spec.
species: SP, DF, or other
Gspec: SP Combo #47 (SP47), DF Combo #2 (DF2), or other

$F_{by\_other} := 2000psi$ $E_{other} := 1700ksi$ $F_{vy\_other} := 90psi$ $F_{cperp\_other} := 560psi$

$t := 10.5in$ — Panel Thickness Estimate
Ritter, Table 8-1, pg 8-6

SP: 5, 6.75, 8.5, 10.5, 12.25, 14.25
W: 5.125, 6.75, 8.75, 10.75, 12.25, 14.25
12.25 & 14.25 require multiple piece lams. which must be edge glued to use horiz. shear design values, otherwise, reduce all. shear 50%.

$w_p := 48in$ — Panel Width

$b_s := 4.5in$ — Stiffener Width

$d_s := 6.75in$ — Stiffener Depth

Design Live Load Moment & Deflection

$M_{other} := 1031.44kip \cdot in$ $yEI_{other} := 5743240kip \cdot in^3$

$M_{max} := if\left[Loading = "HS20", if\left[L = 20ft, 960, if\left[L = 35ft, 2167, \frac{M_{other}}{(kip \cdot in)}\right]\right], if\left[Loading = "HS25", if\left[L = 20ft, 1200, if\left[L = 35ft, 2709, \frac{M_{other}}{(kip \cdot in)}\right]\right], \frac{M_{other}}{(kip \cdot in)}\right]\right] kip \cdot in$

$yEI_{max} := if\left[Loading = "HS20", if\left[L = 20ft, 4608000, if\left[L = 35ft, 39118500, \frac{yEI_{other}}{(kip \cdot in^3)}\right]\right], if\left[Loading = "HS25", if\left[L = 20ft, 5760000, if\left[L = 35ft, 48898100, \frac{yEI_{other}}{(kip \cdot in^3)}\right]\right], \frac{yEI_{other}}{(kip \cdot in^3)}\right]\right] kip \cdot in^3$

$M_{max} = 85.95kip \cdot ft$ $yEI_{max} = 5.74 \times 10^6 kip \cdot in^3$

1. Define Deck Geometric Requirements and Design Loads

$L = 21.5ft$ — Simple Span Length (14-35 ft)
Measured ctr to ctr on bearings

$W = 16ft$ — Bridge Width
Roadway width + curb/railing requirements

$n_{lane} = 1$ — Number of Lanes (1 or 2)

$Loading = "HS20"$ — AASHTO Live Loading

$Palt_a := 0kip$ $Palt_b := 0kip$

Design Live Load (AASHTO HS 20-44 shown)

Only one wheel line considered per panel

Front Axle: $P20_a := \frac{8kip}{2}$

Second Axle: $P20_b := \frac{32kip}{2}$

Rear Axle: $P20_c := P20_b$

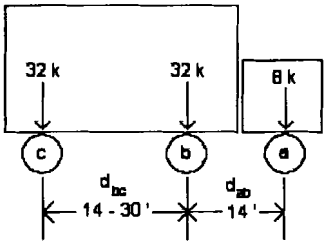

$d_{ab} := 14ft$

For simply supported decks: $d_{bc} := 14ft$

$P_a := if(Loading = "HS20", P20_a, if(Loading = "HS25", P20_a \cdot 1.25, Palt_a))$

$P_b := if(Loading = "HS20", P20_b, if(Loading = "HS25", P20_b \cdot 1.25, Palt_b))$

$P_c := P_b$

2. Estimate Panel Thickness and Width and Compute Section Properties

$t = 10.5in$ — Panel Thickness Estimate
Ritter, Table 8-1, pg 8-6

$t_{lam} := if(species = "SP", 1.375in, if(species = "DF", 1.5in, 0in))$

$t_{lam} = 1.38in$ — Thickness of laminations

$n_{lamW} := round\left(\frac{W}{t_{lam}}\right)$ $n_{lamW} = 140$ — Laminations per Span Width

$w_{p\_typ} := 48in$ — Panel Width (typ. 4 ft)

$n_p := \frac{W}{w_{p\_typ}}$ $n_p = 4$ — Number of Panels

$n_{lamP} := round\left(\frac{n_{lamW}}{round(n_p)}\right)$ $n_{lamP} = 35$ — Laminations per Panel

$w_{p\_rec} := round(n_{lamP} \cdot t_{lam}, 1)$ $w_{p\_rec} = 48in$

$w_p = 48in$ — Panel Width

$A := w_p \cdot t$ $A = 504in^2$ Panel Area

$S_y := \frac{w_p \cdot t^2}{6}$ $S_y = 882in^3$ Panel Section Modulus

$I_y := \frac{w_p \cdot t^3}{12}$ $I_y = 4.63 \times 10^3 in^4$ Panel Moment of Inertia

3. Compute Panel Dead Load

$w_{DLp} := 50pcf \cdot A$ $w_{DLp} = 175plf$ Panel Dead Load
AASHTO 3.3.6

$w_{DLws} := 150pcf \cdot 3in \cdot w_p$ $w_{DLws} = 150plf$ Asphalt Wearing Surface DL
AASHTO 3.3.6

$w_{DLs} := 5plf$ Est. Transverse Stiffener DL

$w_{DLr} := 50plf$ Est. Curb/Railings DL
On outer panel AASHTO 3.3.6 in Tonias (1995) pg 93.

$w_{DL} := w_{DLp} + w_{DLws} + w_{DLs} + w_{DLr}$ $w_{DL} = 380plf$ TOTAL DEAD LOAD

4. Determine Wheel Load Fraction for Live Load Distribution

No longitudinal distribution of wheel loads is assumed; wheel loads act as point loads.

$$WLF := if\left(n_{lane} = 1, \max\left(\frac{w_p}{4.25ft + \frac{L}{28}}, \frac{w_p}{5.50ft}\right), \max\left(\frac{w_p}{3.75ft + \frac{L}{28}}, \frac{w_p}{5.00ft}\right)\right) \qquad WLF = 0.797$$

5. Determine Dead Load and Live Load Moment

$M_{DL} := \frac{1}{8} \cdot w_{DL} \cdot L^2$ $M_{DL} = 21.96kip \cdot ft$

$M_{WL} := M_{max}$ $M_{WL} = 85.95kip \cdot ft$

$M_{LL} := M_{WL} \cdot WLF$ $M_{LL} = 68.52kip \cdot ft$

6. Compute Bending Stress and Select a Deck Combination Symbol

Design Stresses (based on standard glulam choices or manually input)

Species values from the 1999 ASD Structural Glued Laminated Timber Supplement
Combination Symbol 2 for Western Species and 47 for Southern Pine

Bending

$F_{by} := if(Gspec = "SP47", 1750psi, if(Gspec = "DF2", 1800psi, F_{by\_other}))$ Table 3.2

$F_{by} = 2 \times 10^3 psi$

$C_{fu} := if(t < 6in, 1.10, if(t < 8in, 1.07, if(t < 10in, 1.04, 1.01)))$ Table 4.6

$C_{fu} = 1.01$

$C_M := 0.80$ Table 3.2

$C_D := 1.0$ $C_t := 1.0$ $C_L := 1.0$ $C_v := 1.0$

$F'_{by} := F_{by} \cdot C_D \cdot C_M \cdot C_t \cdot C_L \cdot C_v \cdot C_{fu}$ $F'_{by} = 1.616 \times 10^3 psi$ Allowable Bending Stress

MOE

$E := if(Gspec = "SP47", 1.4 \cdot 10^6 psi, if(Gspec = "DF2", 1.7 \cdot 10^6 psi, E_{other}))$ Table 3.2 AITC 117-2001 Design gives 1.6Msi for combination 2

$E = 1.7 \times 10^6 psi$

$C_M := 0.833$ Table 3.2

$C_t := 1.0$

$E' := E \cdot C_M \cdot C_t$ $E' = 1.42 \times 10^6 psi$ Allowable MOE

Shear Parallel to Grain

$F_{vy} := if(Gspec = "SP47", 270psi, if(Gspec = "DF2", 240psi, F_{vy\_other}))$ Table 3.2 APA Engineering Bulletin Number 98-3

$F_{vy} = 90psi$

$F_{vy} := if\left(t \geq 12.25in, \frac{F_{vy}}{2}, F_{vy}\right)$ $F_{vy} = 90psi$ Reduction for non-edge gluing of multiple-piece laminations

$C_M := 0.875$ Table 3.2

$C_D := 1.0$ $C_t := 1.0$

$F'_{vy} := F_{vy} \cdot C_D \cdot C_M \cdot C_t$ $F'_{vy} = 78.75psi$ Allowable Shear Stress

Compression Perpendicular to Grain

$F_{cperp} := if(Gspec = "SP47", 650psi, if(Gspec = "DF2", 560psi, F_{cperp\_other}))$ Table 3.1

$F_{cperp} = 560psi$

$C_M := 0.53$ Table 3.1

$C_t := 1.0$ $C_b := 1.0$

$F'_{cperp} := F_{cperp} \cdot C_M \cdot C_t \cdot C_b$ $F'_{cperp} = 296.8psi$ Allowable Compressive Stress

Bending Stress

$$f_b := \frac{(M_{DL} + M_{LL})\frac{t}{2}}{I_y}$$

$f_b = 1.231\times 10^3$ psi $F'_{by} = 1.616\times 10^3$ psi

$Check_b$ = "Okay in bending"

7. Check Live Load Deflection

FRP_factor := 1.06 Increase in Stiffness due to FRP
UM exp. testing

$E'_{FRPglulam} := E'\cdot FRP\_factor$ $E' := E'_{FRPglulam}$ $E'_{FRPglulam} = 1.5\times 10^3$ ksi Stiffness of FRP-glulam

$E' = 1.5\times 10^3$ ksi

$$\Delta_{DL} := \frac{5\cdot w_{DL}\cdot L^4}{384\cdot E'\cdot I_y}$$

$\Delta_{DL} = 0.26$in

$$\Delta_{WL} := \frac{yEI_{max}}{E'\cdot I_y}$$

$\Delta_{WL} = 0.83$in

$\Delta_{LL} := \Delta_{WL}\cdot WLF$ $\Delta_{LL} = 0.66$in AASHTO 3.25.3.3

$$\Delta_{LLall} := \frac{L}{500}$$

$\Delta_{LLall} = 0.52$in Allowable Deflection - not specified
AASHTO Sect. 13.4.3 - recommends L/500
In Ritter, allowable is L/360 based on ISU studies which indicated relative panel displacement will not exceed approx. 0.10" with this allowable.
AITC uses a L/300 allowable.

$Check_{\Delta LL}$ = "Fails L/500, but meets L/360 criteria"

8. Check Horizontal Shear

$d := \min(3\cdot t, 0.25L)$ $d = 2.62$ft Location at which to place axle
AASHTO 13.6.5.2

$$WLF_R := \min\left(\frac{w_p}{4ft}, 1.0\right)$$

$WLF_R = 1$ Wheel Load Fraction for Reaction
Ritter uses the other WLF, but AASHTO 3.25.3.2 and AITC use this due to the proximity to the support

$$V_{DL} := w_{DL}\cdot\left(\frac{L}{2} - t\right)$$

$V_{DL} = 3.75$kip

$d2 := d + d_{bc}$ $d3 := d + d_{bc} + d_{ab}$

$$V_{LU} := \text{if}\left[L < d2, \frac{P_c\cdot(L-d)}{L}, \text{if}\left[L < d3, \frac{P_b\cdot(L-d2) + P_c\cdot(L-d)}{L}, \frac{P_a\cdot(L-d3) + P_b\cdot(L-d2) + P_c\cdot(L-d)}{L}\right]\right]$$

$V_{LU} = 17.67$kip

$V_{LD} := V_{LU}\cdot WLF_R$ $V_{LD} = 17.67$kip

$V_{LL} := V_{LD}$ $V_{LL} = 17.67$kip

$V := V_{DL} + V_{LL}$ $V = 21.43\text{kip}$

$f_v := \frac{3 \cdot V}{2A}$ $f_v = 63.77\text{psi}$ $F'_{vy} = 78.75\text{psi}$

$\text{Check}_v = \text{"Okay in shear"}$

9. Determine Stiffener Spacing and Configuration

$s_{min} := 10\text{ft}$ $num_s := \left(\text{round}\left(\frac{L}{s_{min}}\right)\right) - 1$ $num_s = 1$

Number of Stiffeners
AASHTO 3.25.3.4
AASHTO requires 1@ midspan & s <= 10ft.
Ritter recommends using AITC's s <= 8ft

$num_s := \text{if}\left[\frac{num_s}{2} = \text{round}\left(\frac{num_s}{2}\right), (num_s + 1), num_s\right]$ $num_s = 1$

$s := \frac{L}{num_s + 1}$ $s = 10.75\text{ft}$ Stiffener Spacing

$\text{Check}_s = \text{"Stiffener spacing exceeds criteria"}$

$E'_s := E$ $E'_s = 1.7 \times 10^6\text{psi}$ Stiffener Allowable MOE
Assumed same E as deck
Watertight glulam deck => dry-use cond.

$EI_{min} := 80000\text{kip} \cdot \text{in}^2$ Minimum Stiffness Factor Allowed
AASHTO 3.25.3.4 - Based on ISU's research

$EI_{max} := 2 \cdot EI_{min}$ Maximum Stiffness Recommended
Based on ISU's research; in Ritter, but not in AASHTO or AITC.

$ratio := 0.67$ Stiffener Depth to Width Ratio for Initial Estimate - try d=1.5b

$b_s := \left[\frac{12 \cdot EI_{min}}{E'_s \cdot (ratio)^3}\right]^{\frac{1}{4}}$ $b_s = 4.5\text{in}$ Stiffener Width

$d_s := ratio \cdot b_s$ $d_s = 6.75\text{in}$ Stiffener Depth

$I_s := \frac{b_s \cdot d_s^3}{12}$ $I_s = 115.33\text{in}^4$

$EI_s := E'_s \cdot I_s$ $EI_s = 1.96 \times 10^5\text{kip} \cdot \text{in}^2$ Actual Stiffness Factor

$\text{Check}_{EIs} = \text{"Stiffener may be too stiff"}$

10. Determine Bearing Configuration and Check Bearing Stress

$l_b := 12in$ Length of Bearing

Ritter recommends 10-12" for stability & deck attachment, pg 8-13, if less than 6" Cb /= 1

$d4 := d_{bc} + d_{ab}$

$$R_{WL} := if\left[L < d4, \frac{P_b \cdot (L - d_{bc}) + P_c \cdot L}{L}, \frac{P_a \cdot (L - d4) + P_b \cdot (L - d_{bc}) + P_c \cdot L}{L}\right] \qquad R_{WL} = 21.58kip$$

$R_{LL} := R_{WL} \cdot WLF_R$ $R_{LL} = 21.58kip$ Live Load Reaction to Panel

$R_{DL} := w_{DL} \cdot \frac{L}{2}$ $R_{DL} = 4.08kip$ Dead Load Reaction

$f_{cperp} := \frac{R_{DL} + R_{LL}}{w_p \cdot l_b}$ $f_{cperp} = 44.56psi$ $F'_{cperp} = 296.8psi$

$Check_{cperp} = "Okay\ in\ bearing"$

Longitudinal Glulam Deck Design Summary - Milbridge Pier

General Information

$L = 21.5ft$	$W = 16ft$	$n_{lane} = 1$	Bridge Span, Width, & # of Lanes
Loading = "HS20"			AASHTO Loading
	$M_{max} = 85.95kip \cdot ft$	$yEI_{max} = 5.74 \times 10^6 kip \cdot in^3$	Maximum Moment & Deflection
species = "SP"			Material Species
$w_p = 48in$	$t = 10.5in$		Panel Width
$b_s = 4.5in$	$d_s = 6.75in$		Stiffener Width, Depth, Spacing, & Number
	$s = 10.75ft$	$num_s = 1$	

Design

Panels

$f_b = 1.23 \times 10^3 psi$	$\frac{f_b}{F'_{by}} = 0.76$	$WLF = 0.8$	Longitudinal Bending
$f_v = 63.77psi$	$\frac{f_v}{F'_{vy}} = 0.81$		Horizontal Shear
$f_{cperp} = 44.56psi$	$\frac{f_{cperp}}{F'_{cperp}} = 0.15$		Bearing
$\Delta_{LL} = 0.66in$	$\frac{\Delta_{LL}}{\Delta_{LLall}} = 1.28$		Live Load Deflection
	$Check_{\Delta LL}$ = "Fails L/500, but meets L/360 criteria"		$\frac{L}{\Delta_{LL}} = 391.7$

Transverse Stiffener Beams

$EI_s = 1.96 \times 10^5 kip \cdot in^2$	$\frac{EI_s}{EI_{min}} = 2.45$	TSB Stiffness Factor
	$Check_{EIs}$ = "Stiffener may be too stiff"	
$s = 10.75ft$	$\frac{s}{s_{min}} = 1.07$	
	$Check_s$ = "Stiffener spacing exceeds criteria"	

Appendix B

MILBRIDGE PIER LOAD TEST RESULTS

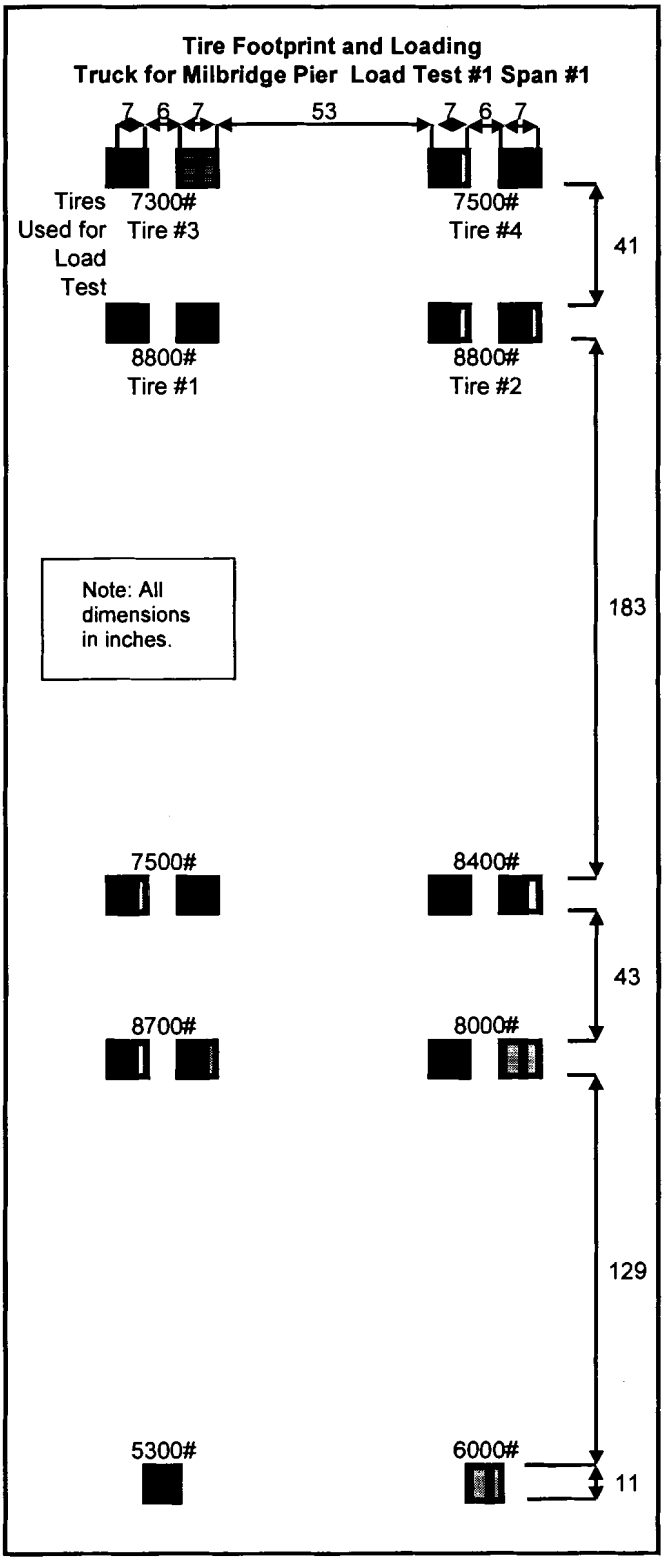

Figure B.1 Truck footprint and wheel loads for pier load test

Table B.1 Deflections measured during the Milbridge Pier Load Test

Milbridge Pier Load Test
Deflection Readings

Ruler #	X (transverse to deck)	Y (longitudinal to deck)
1	11 2/8	52 5/8
2	35 3/8	52 5/8
3	60	52 5/8
4	83 1/8	52 5/8
5	107 4/8	52 5/8
6	132 2/8	52 5/8
7	156 3/8	52 5/8
8	181	52 5/8
9	12 7/8	100 4/8
10	36	100 5/8
11	59 1/8	100 6/8
12	82 5/8	100 7/8
13	107 6/8	101 1/8
14	132	101 2/8
15	156	101 3/8
16	181 4/8	101 4/8
17	12 7/8	105
18	36	105 2/8
19	59 1/8	105 3/8
20	82 5/8	105 5/8
21	107 6/8	105 7/8
22	132	106 1/8
23	156	106 2/8
24	181 4/8	106 4/8

Load Case # 1

Ruler #	Initial Reading	Loaded Reading	Deflect. (in.)
1	7.12	7.15	-0.03
2	1.11	1.23	-0.12
3	7.11	7.23	-0.11
4	7.02	7.10	-0.08
5	0.93	1.08	-0.15
6	7.09	7.24	-0.15
7	1.04	1.15	-0.11
8	7.22	7.28	-0.06
9	1.23	1.25	-0.02
10	7.14	7.27	-0.13
11	1.09	1.26	-0.17
12	6.95	7.07	-0.12
13	6.95	7.14	-0.19
14	7.20	7.40	-0.20
15	6.67	6.79	-0.12
16	7.11	7.23	-0.12
17	10.11	10.16	-0.05
18	4.03	4.16	-0.13
19	9.95	10.17	-0.22
20	9.90	10.08	-0.18
21	3.90	4.12	-0.22
22	9.95	10.15	-0.20
23	3.88	4.05	-0.18
24	10.04	10.17	-0.13

Load Case # 2

Ruler #	Initial Reading	Loaded Reading	Deflect. (in.)
1	7.12	7.24	-0.12
2	1.14	1.30	-0.16
3	7.12	7.25	-0.13
4	7.02	7.12	-0.10
5	0.94	1.05	-0.11
6	7.08	7.15	-0.07
7	1.04	1.08	-0.04
8	7.22	7.23	-0.01
9	1.20	1.40	-0.20
10	7.15	7.35	-0.20
11	1.09	1.29	-0.20
12	6.97	7.10	-0.13
13	6.95	7.12	-0.17
14	7.19	7.29	-0.10
15	6.63	6.67	-0.04
16	7.11	7.13	-0.02
17	10.11	10.30	-0.19
18	4.04	4.24	-0.20
19	9.96	10.16	-0.20
20	9.95	10.09	-0.14
21	3.93	4.11	-0.18
22	9.95	10.06	-0.11
23	3.88	3.93	-0.05
24	10.05	10.06	-0.01

Load Case # 3

Ruler #	Initial Reading	Loaded Reading	Deflect. (in.)
1	7.11	7.13	-0.02
2	1.16	1.20	-0.04
3	7.13	7.20	-0.07
4	7.02	7.09	-0.07
5	0.94	1.08	-0.14
6	7.09	7.23	-0.14
7	1.03	1.20	-0.17
8	7.21	7.39	-0.18
9	1.20	1.23	-0.03
10	7.15	7.20	-0.05
11	1.10	1.20	-0.10
12	6.91	7.06	-0.15
13	6.95	7.17	-0.22
14	7.20	7.41	-0.21
15	6.63	6.87	-0.24
16	7.10	7.35	-0.25
17	10.11	10.11	0.00
18	4.04	4.09	-0.05
19	9.97	10.09	-0.12
20	9.89	10.04	-0.15
21	3.93	4.15	-0.22
22	9.96	10.18	-0.22
23	3.87	4.11	-0.24
24	10.03	10.27	-0.24

Load Case # 4

Ruler #	Initial Reading	Loaded Reading	Deflect. (in.)
1	7.10	7.13	-0.03
2	1.14	1.20	-0.06
3	7.10	7.19	-0.09
4	7.02	7.13	-0.11
5	0.93	1.07	-0.14
6	7.08	7.22	-0.14
7	1.03	1.19	-0.16
8	7.22	7.36	-0.14
9	1.22	1.22	0.00
10	7.14	7.22	-0.08
11	1.07	1.20	-0.13
12	6.93	7.12	-0.19
13	6.94	7.15	-0.21
14	7.20	7.40	-0.20
15	6.65	6.89	-0.24
16	7.10	7.31	-0.21
17	10.10	10.11	-0.01
18	4.02	4.11	-0.09
19	9.95	10.05	-0.10
20	9.91	10.08	-0.17
21	3.89	4.10	-0.21
22	9.97	10.18	-0.21
23	3.90	4.09	-0.19
24	10.05	10.23	-0.18

Load Case # 5

Ruler #	Initial Reading	Loaded Reading	Deflect. (in.)
1	7.11	7.20	-0.09
2	1.17	1.29	-0.12
3	7.12	7.24	-0.12
4	7.03	7.12	-0.09
5	0.94	1.07	-0.13
6	7.09	7.17	-0.08
7	1.04	1.09	-0.05
8	7.20	7.25	-0.05
9	1.20	1.35	-0.15
10	7.14	7.34	-0.20
11	1.10	1.28	-0.18
12	6.97	7.09	-0.12
13	6.95	7.13	-0.18
14	7.20	7.32	-0.12
15	6.62	6.70	-0.08
16	7.11	7.15	-0.04
17	10.11	10.25	-0.14
18	4.03	4.23	-0.20
19	9.96	10.16	-0.20
20	9.95	10.09	-0.14
21	3.94	4.10	-0.16
22	9.96	10.10	-0.14
23	3.89	3.96	-0.07
24	10.05	10.10	-0.05

Load Case # 6

Ruler #	Initial Reading	Loaded Reading	Deflect. (in.)
1	7.11	7.20	-0.09
2	1.15	1.21	-0.06
3	7.11	7.20	-0.09
4	6.99	7.09	-0.10
5	0.94	1.04	-0.10
6	7.10	7.15	-0.05
7	1.04	1.07	-0.03
8	7.25	7.25	0.00
9	1.22	1.30	-0.08
10	7.14	7.26	-0.12
11	1.10	1.22	-0.12
12	6.91	7.03	-0.12
13	6.94	7.07	-0.13
14	7.20	7.28	-0.08
15	6.64	6.69	-0.05
16	7.14	7.15	-0.01
17	10.17	10.24	-0.07
18	4.03	4.16	-0.13
19	9.96	10.09	-0.13
20	9.90	10.03	-0.13
21	3.93	4.04	-0.11
22	9.97	10.04	-0.07
23	3.87	3.94	-0.07
24	10.08	10.10	-0.02

Load Case # 7

Ruler #	Initial Reading	Loaded Reading	Deflect. (in.)
1	7.12	7.13	-0.01
2	1.15	1.20	-0.05
3	7.11	7.19	-0.08
4	6.99	7.10	-0.11
5	0.93	1.05	-0.12
6	7.09	7.21	-0.12
7	1.04	1.17	-0.13
8	7.23	7.33	-0.10
9	1.22	1.22	0.00
10	7.15	7.20	-0.05
11	1.09	1.18	-0.09
12	6.91	7.03	-0.12
13	6.94	7.09	-0.15
14	7.20	7.34	-0.14
15	6.63	6.79	-0.16
16	7.12	7.25	-0.13
17	10.15	10.15	0.00
18	4.03	4.09	-0.06
19	9.95	10.05	-0.10
20	9.90	10.02	-0.12
21	3.93	4.08	-0.15
22	9.96	10.11	-0.15
23	3.85	4.03	-0.18
24	10.06	10.20	-0.14

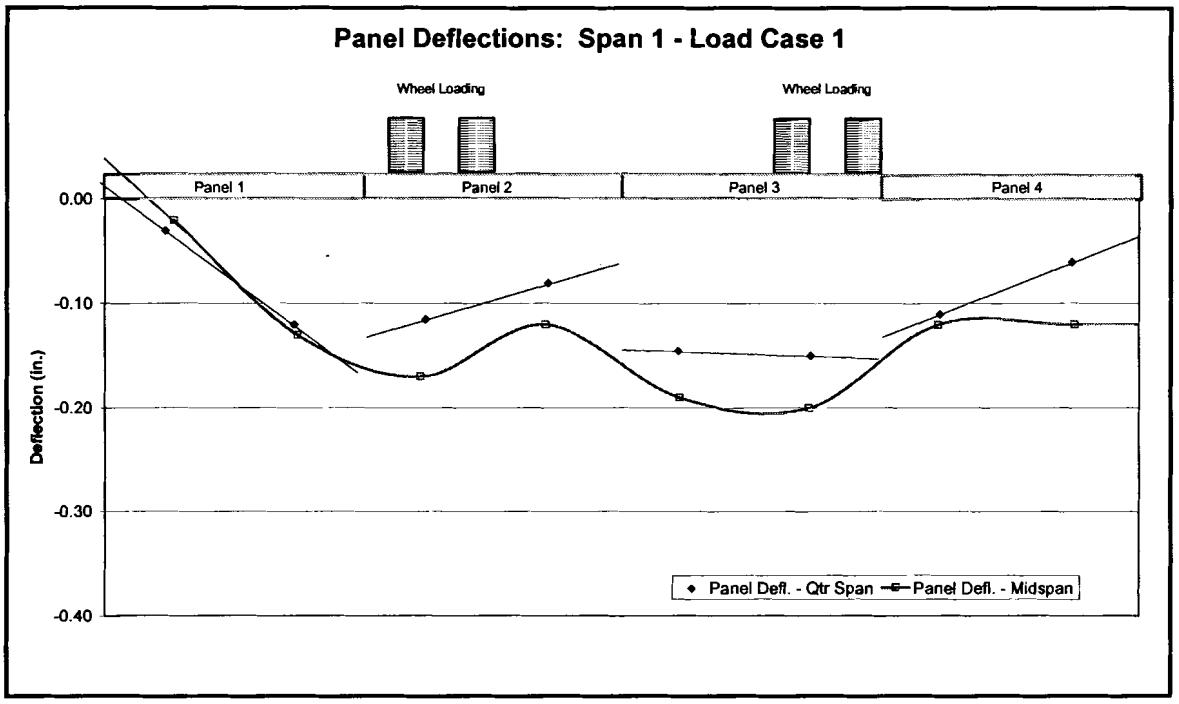

Figure B.2 Panel deflections during load test: Load Case 1

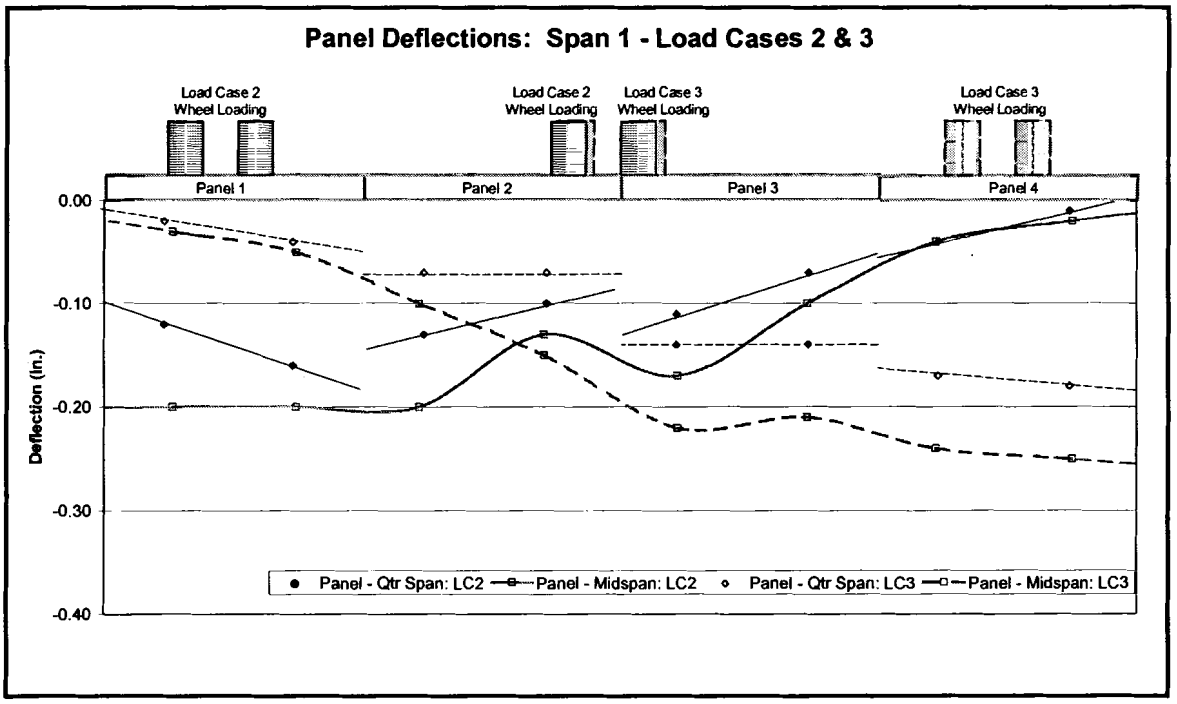

Figure B.3 Panel deflections during load test: Load Cases 2 & 3

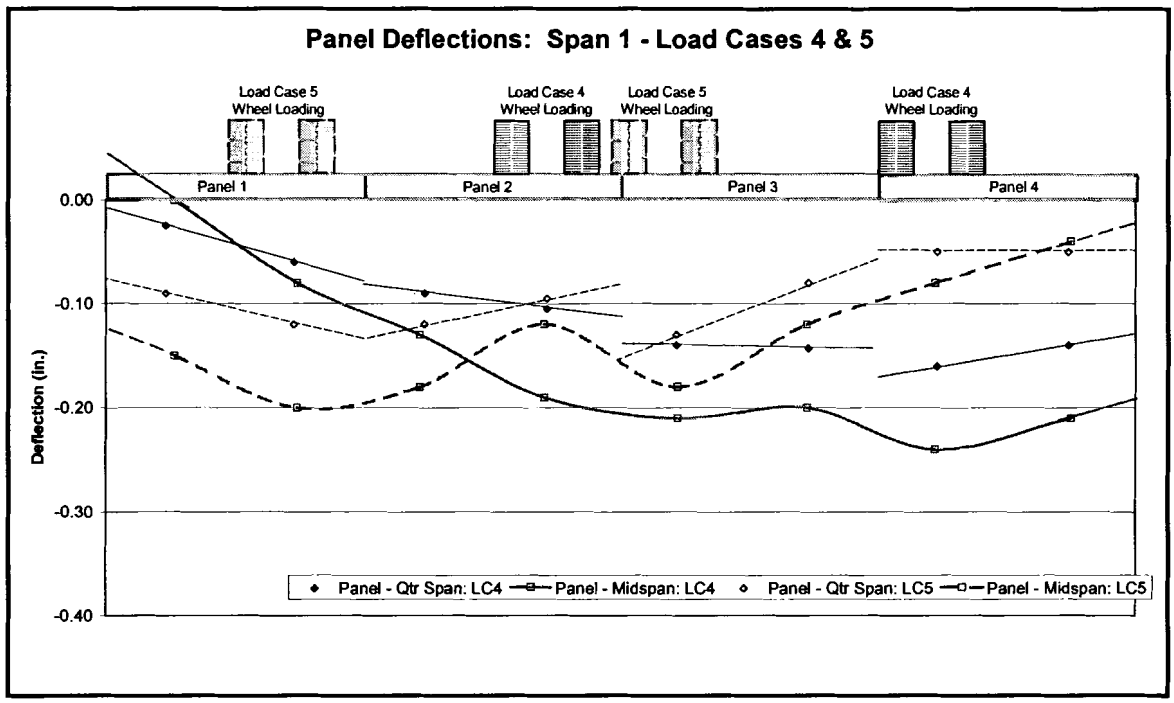

Figure B.4 Panel deflections during load test: Load Cases 4 & 5

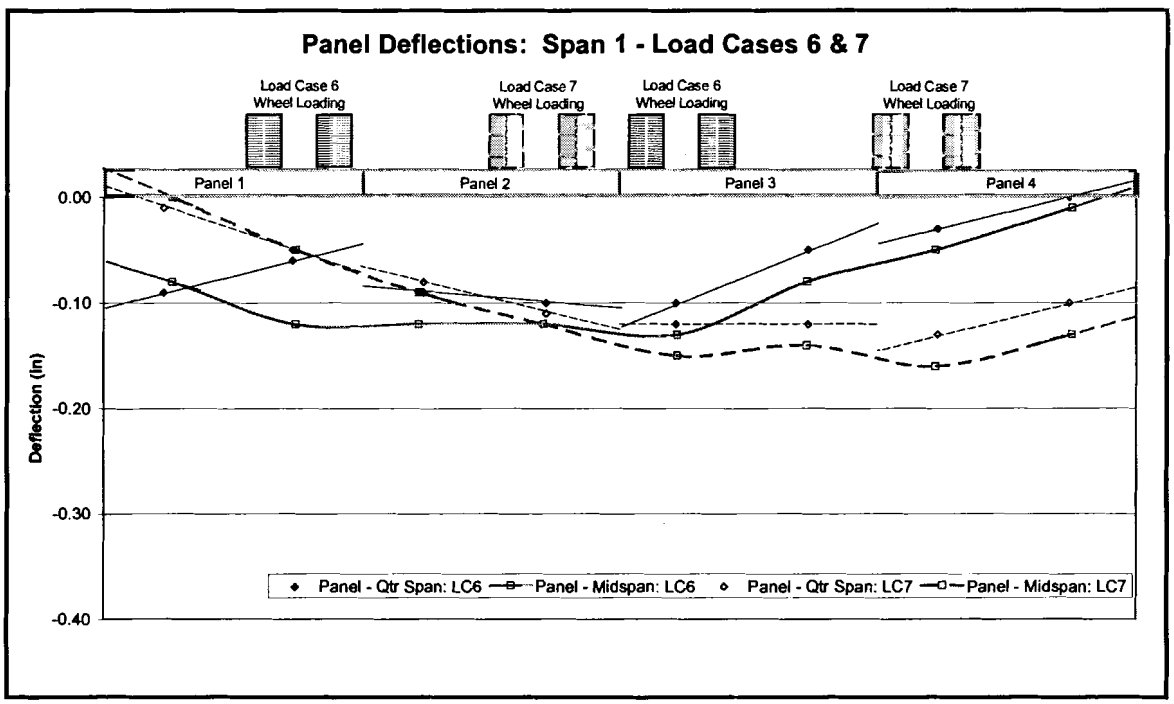

Figure B.5 Panel deflections during load test: Load Cases 6 & 7

Appendix C

LABORATORY TEST RESULTS

The laboratory test results presented in this appendix are discussed and the testing described in Chapter 4 of this thesis. Tables C.1 to C.3 present the DCDT deflection readings at maximum loads. The figures show the deflections at several loadings as the panels were loaded.

Table C.1 Deflection readings from laboratory testing, Load Case #1

Load Case #1			DCDT Locations Across Bridge Width (in.)					
			27.75	51.00	77.25	113.88	137.56	165.25
TSB#	*Connection*	*Load Cell Reading*	*DCDT Measured Deflection (in.)*					
1	Through Bolt - Tight	-32	-0.23	-0.42	-0.45	-0.41	-0.43	-0.19
	Seated Beam - Tight	~	~	~	~	~	~	~
	Through Bolt - Loose	~	~	~	~	~	~	~
	Seated Beam - Loose	~	~	~	~	~	~	~
2	Through Bolt - Tight	-32	-0.18	-0.47	-0.49	-0.44	-0.43	-0.18
	Seated Beam - Tight	-32	-0.26	-0.40	-0.43	-0.40	-0.38	-0.21
	Through Bolt - Loose	~	~	~	~	~	~	~
	Seated Beam - Loose	-32	-0.23	-0.43	-0.46	-0.42	-0.44	-0.18
3	Through Bolt - Tight	-32	-0.26	-0.42	-0.43	-0.38	-0.39	-0.23
	Seated Beam - Tight	-32	-0.26	-0.40	-0.42	-0.37	-0.37	-0.24
	Through Bolt - Loose	~	~	~	~	~	~	~
	Seated Beam - Loose	-32	-0.23	-0.44	-0.47	-0.44	-0.48	-0.14

Table C.2 Deflection readings from laboratory testing, Load Case #2

Load Case #2			DCDT Locations Across Bridge Width (in.)					
			24.00	72.10	102.20	138.20	150.30	186.30
TSB#	Connection	Load Cell Reading	DCDT Measured Deflection (in.)					
1	Through Bolt - Tight	~	~	~	~	~	~	~
	Seated Beam - Tight	~	~	~	~	~	~	~
	Through Bolt - Loose	~	~	~	~	~	~	~
	Seated Beam - Loose	~	~	~	~	~	~	~
2	*Through Bolt - Tight (Actual Reading)*	*-24*	*-0.01*	*-0.16*	*-0.34*	*-0.35*	*-0.41*	*-0.52*
	Through Bolt - Tight (Data Extrapolated)	-32	-0.02	-0.21	-0.46	-0.46	-0.54	-0.70
	Seated Beam - Tight (Actual Readings)	*-24*	*-0.01*	*-0.16*	*-0.34*	*-0.34*	*-0.42*	*-0.53*
	Seated Beam - Tight (Data Extrapolated)	-32	-0.02	-0.21	-0.45	-0.45	-0.56	-0.70
	Through Bolt - Loose	~	~	~	~	~	~	~
	Seated Beam - Loose	~	~	~	~	~	~	~
3	Through Bolt - Tight	-32	0.00	-0.18	-0.46	-0.46	-0.56	-0.68
	Seated Beam - Tight	-32	-0.01	-0.19	-0.45	-0.44	-0.56	-0.71
	Through Bolt - Loose	~	~	~	~	~	~	~
	Seated Beam - Loose	~	~	~	~	~	~	~

Table C.3 Deflection readings from laboratory testing, Load Case #3

Load Case #3			DCDT Locations Across Bridge Width (in.)					
			-0.02	-0.21	-0.45	-0.46	-0.54	-0.69
TSB#	Connection	Load Cell Reading	DCDT Measured Deflection (in.)					
1	Through Bolt - Tight	-16	-0.02	-0.08	-0.11	-0.16	-0.37	-0.30
	Seated Beam - Tight (Actual Readings)	*-14*	*-0.03*	*-0.06*	*-0.10*	*-0.13*	*-0.31*	*-0.26*
	Seated Beam - Tight (Data Extrapolated)	-16	-0.03	-0.07	-0.12	-0.15	-0.36	-0.30
	Through Bolt - Loose (Actual Reading)	*-15*	*0.00*	*-0.09*	*-0.10*	*-0.13*	*-0.36*	*-0.30*
	Through Bolt - Loose (Data Extrapolated)	-16	0.00	-0.09	-0.10	-0.13	-0.38	-0.31
	Seated Beam - Loose (Actual Readings)	*-15*	*0.00*	*-0.09*	*-0.08*	*-0.12*	*-0.34*	*-0.28*
	Seated Beam - Loose (Data Extrapolated)	-16	0.00	-0.09	-0.09	-0.13	-0.37	-0.31
2	Through Bolt - Tight	-16	-0.01	-0.10	-0.12	-0.15	-0.36	-0.32
	Seated Beam - Tight	-16	-0.02	-0.09	-0.11	-0.17	-0.35	-0.30
	Through Bolt - Loose	-16	0.00	-0.09	-0.14	-0.16	-0.38	-0.32
	Seated Beam - Loose	-16	0.00	-0.10	-0.12	-0.15	-0.38	-0.32
3	Through Bolt - Tight	-16	-0.01	-0.09	-0.13	-0.17	-0.37	-0.33
	Seated Beam - Tight	-16	0.00	-0.09	-0.12	-0.18	-0.33	-0.30
	Through Bolt - Loose	-16	0.01	-0.10	-0.10	-0.13	-0.41	-0.35
	Seated Beam - Loose	-16	0.00	-0.09	-0.10	-0.14	-0.40	-0.34

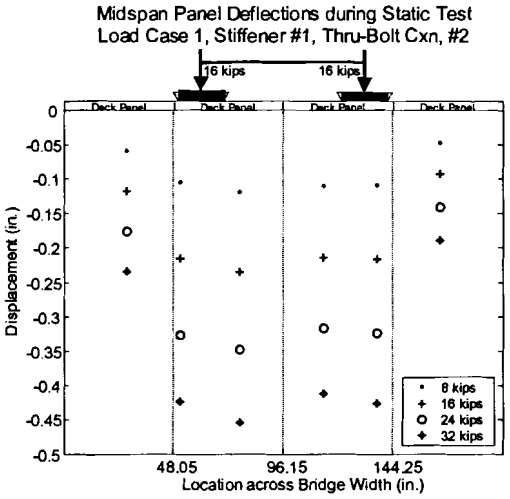

Figure C.1 Measured midspan panel deflections, Load Case #1, TSB#1

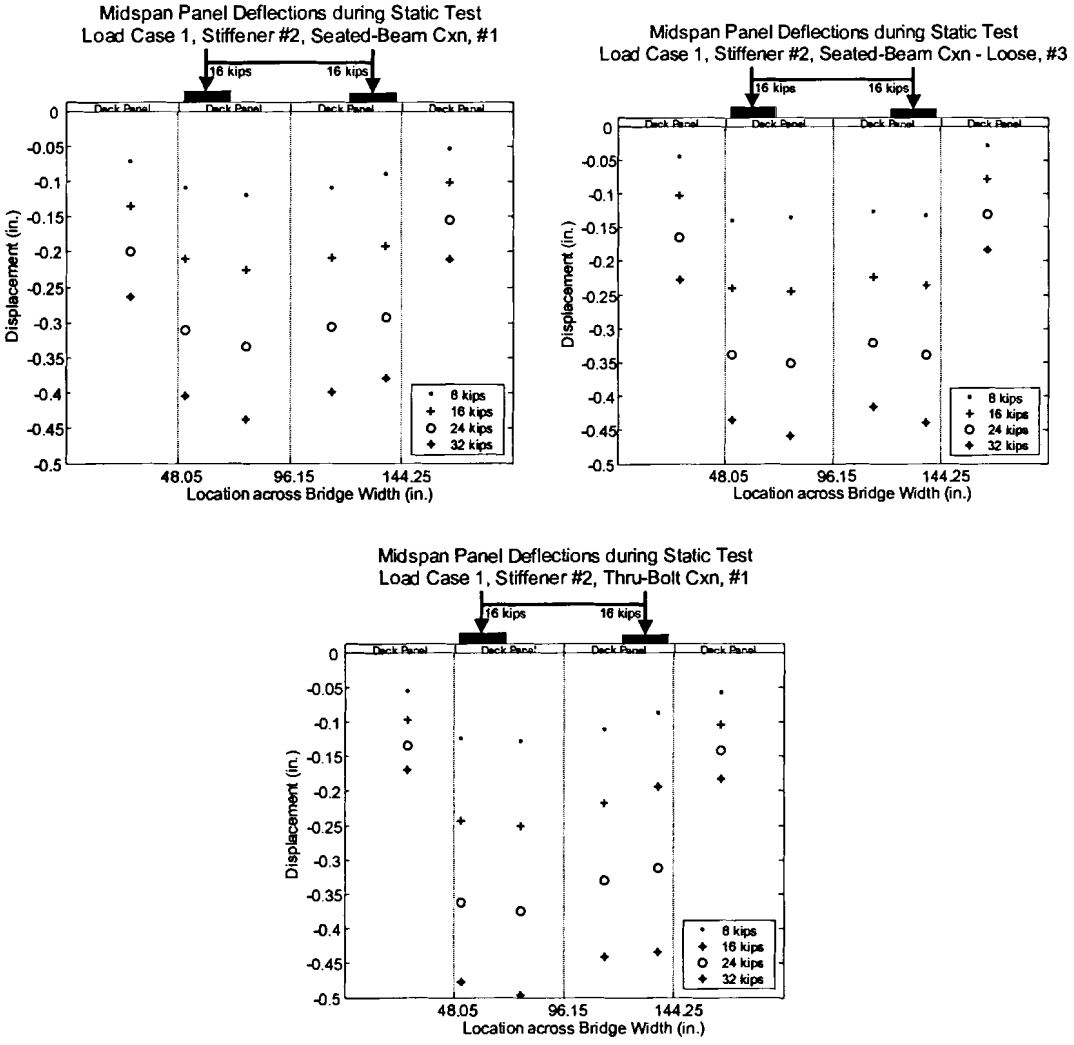

Figure C.2 Measured midspan panel deflections, Load Case #1, TSB#2

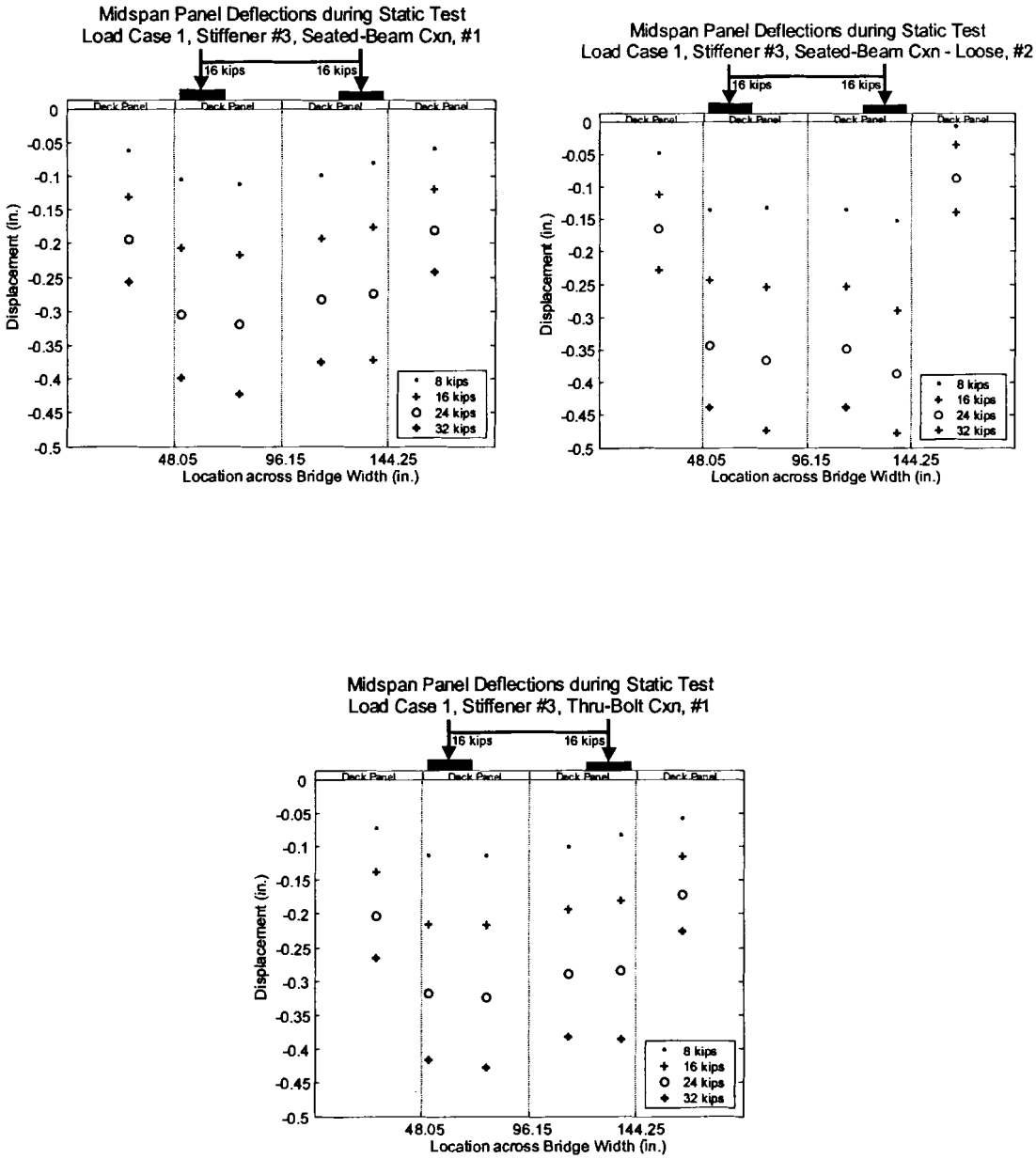

Figure C.3 Measured midspan panel deflections, Load Case #1, TSB#3

Load Case #1

Panel A1 | Panel A01 | Panel A02 | Panel A3

TSB#	Connection	Strain State	Connection Strain (microstrain)							
1	Seated Beam - Tight	Initial Strain	542	1287	274	60	211	115	~	261
		Strain at Load	525	1557	-52	230	315	13	~	235
		Change in Strain	-17	271	-326	170	104	-102	~	-26
	Seated Beam - Loose	Initial Strain	~	~	~	~	~	~	~	~
		Strain at Load	~	~	~	~	~	~	~	~
		Change in Strain	~	~	~	~	~	~	~	~
2	Seated Beam - Tight	Initial Strain	553	272	113	328	256	585	~	337
		Strain at Load	607	935	-1	416	311	466	~	323
		Change in Strain	54	663	-114	88	56	-119	~	-14
	Seated Beam - Loose	Initial Strain	-5	104	-3	18	-19	46	~	10
		Strain at Load	-3	720	37	83	91	8	~	10
		Change in Strain	2	616	39	65	109	-38	~	1
3	Seated Beam - Tight	Initial Strain	928	358	709	148	644	483	~	485
		Strain at Load	956	950	399	299	834	249	~	506
		Change in Strain	28	592	-310	151	190	-234	~	21
	Seated Beam - Loose	Initial Strain	101	31	21	81	11	5	~	-3
		Strain at Load	92	244	15	222	-47	3	~	20
		Change in Strain	-9	213	-6	141	-58	-2	~	23

Figure C.4 Measured strain in seated-beam connections, Load Case #1

Load Case #2

Panel A1 | Panel A01 | Panel A02 | Panel A3

TSB#	Connection	Strain State	Connection Strain (microstrain)							
1	Seated Beam - Tight	Initial Strain	~	~	~	~	~	~	~	~
		Strain at Load	~	~	~	~	~	~	~	~
		Change in Strain	~	~	~	~	~	~	~	~
	Seated Beam - Loose	Initial Strain	~	~	~	~	~	~	~	~
		Strain at Load	~	~	~	~	~	~	~	~
		Change in Strain	~	~	~	~	~	~	~	~
2	*Seated Beam - Tight (Actual Readings)*	Initial Strain	*325*	*225*	*52*	*63*	*456*	*35*	~	*1050*
		Strain at Load	*281*	*228*	*25*	*484*	*219*	*240*	~	*1062*
		Change in Strain	*-44*	*3*	*-27*	*421*	*-238*	*206*	~	*12*
	Seated Beam - Tight (Data Extrapolated)	Initial Strain	325	225	52	63	456	35	~	1050
		Strain at Load	375	303	33	645	292	320	~	1415
		Change in Strain	-44	3	-27	421	-238	206	~	12
	Seated Beam - Loose	Initial Strain	~	~	~	~	~	~	~	~
		Strain at Load	~	~	~	~	~	~	~	~
		Change in Strain	~	~	~	~	~	~	~	~
3	Seated Beam - Tight	Initial Strain	154	221	508	686	79	89	30	1692
		Strain at Load	129	193	456	1019	5	235	23	1746
		Change in Strain	-25	-28	-52	333	-75	146	-7	54
	Seated Beam - Loose	Initial Strain	~	~	~	~	~	~	~	~
		Strain at Load	~	~	~	~	~	~	~	~
		Change in Strain	~	~	~	~	~	~	~	~

Figure C.5 Measured strain in seated-beam connections, Load Case #2

Load Case #3

TSB#	Connection	Strain State	Connection Strain (microstrain)							
1	Seated Beam - Tight	Initial Strain	1079	486	761	537	446	64	201	351
		Strain at Load	1057	515	746	130	430	809	99	494
		Change in Strain	-22	29	-15	-407	-16	746	-102	143
	Seated Beam - Loose	Initial Strain	5	9	-10	3	8	3	-4	-20
		Strain at Load	10	2	-87	1	5	544	0	299
		Change in Strain	5	-7	-77	-2	-3	541	4	319
2	Seated Beam - Tight	Initial Strain	745	158	409	582	731	5	475	1179
		Strain at Load	723	168	366	557	687	669	239	1315
		Change in Strain	-22	10	-43	-25	-45	664	-236	136
	Seated Beam - Loose	Initial Strain	9	10	26	18	-807	-452	-7	97
		Strain at Load	2	41	-4	13	-722	425	-4	614
		Change in Strain	-7	31	-30	-5	85	877	3	517
3	Seated Beam - Tight	Initial Strain	-113	-10	66	56	506	548	497	1747
		Strain at Load	-89	-2	67	72	445	895	282	1859
		Change in Strain	24	8	1	16	-61	347	-215	112
	Seated Beam - Loose	Initial Strain	7	16	55	-8	4	30	13	79
		Strain at Load	-2	11	59	-9	-1	673	2	139
		Change in Strain	-9	-5	4	-1	-5	643	-11	60

Figure C.6 Measured strain in seated-beam connections, Load Case #3

Appendix D

EXPERIMENTAL & FINITE ELEMENT ANALYSIS CORRELATIONS

D.1 Correlation of Panel Deflections

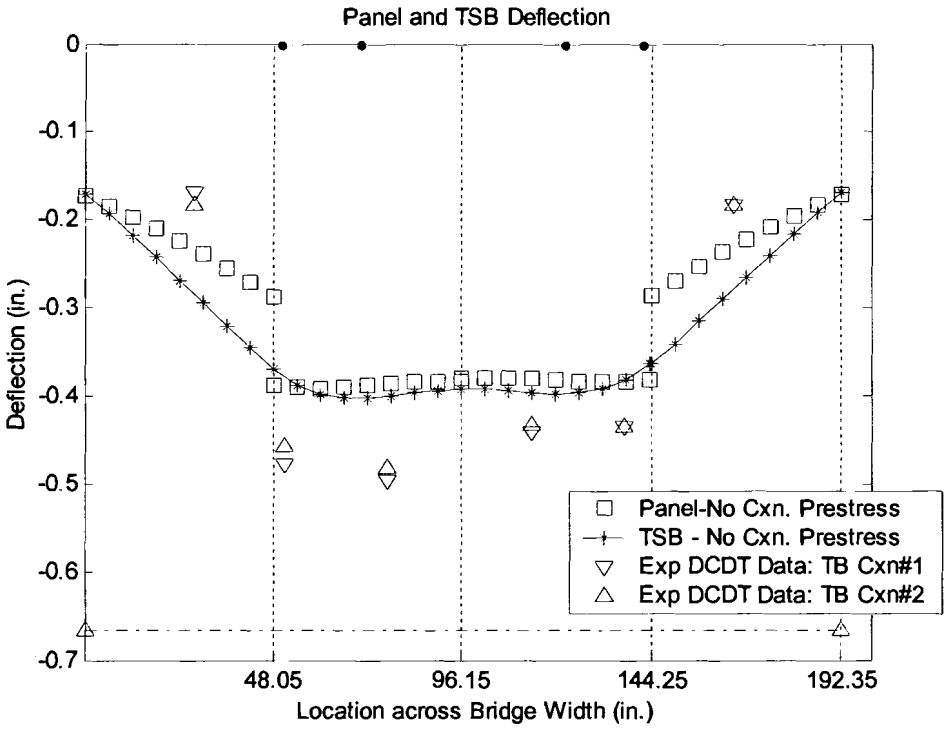

Figure D.1 Deflection correlation, Load Case #1, TSB #2, Thru-Bolt Conn.

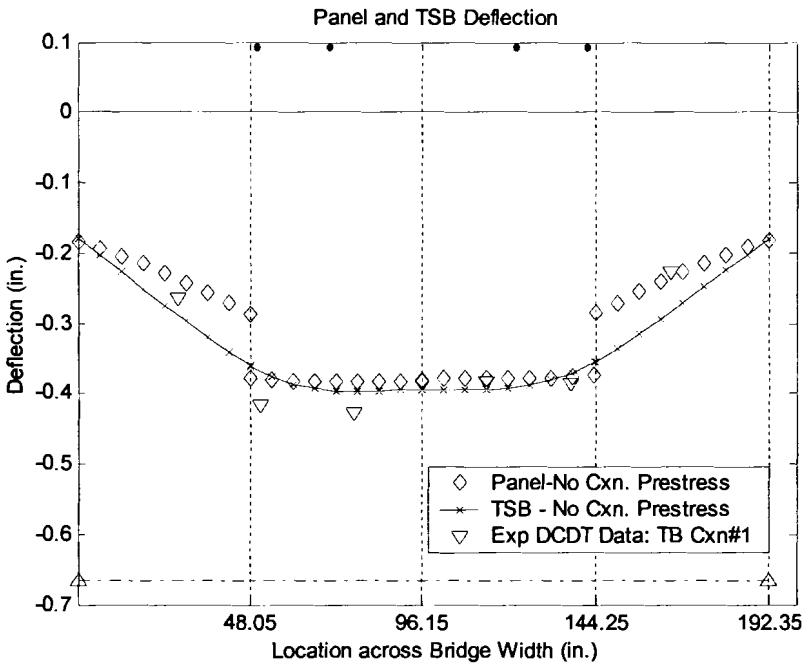

Figure D.2 Deflection correlation, Load Case #1, TSB #3, Thru-Bolt Conn.

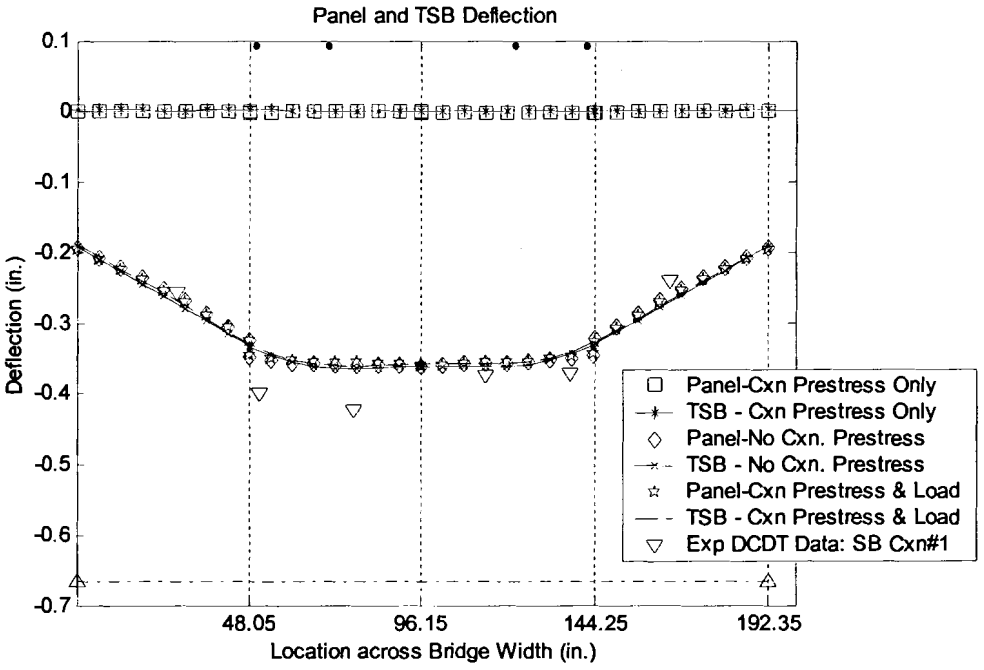

Figure D.3 Deflection correlation, Load Case #1, TSB #3, Seated-Beam Conn.

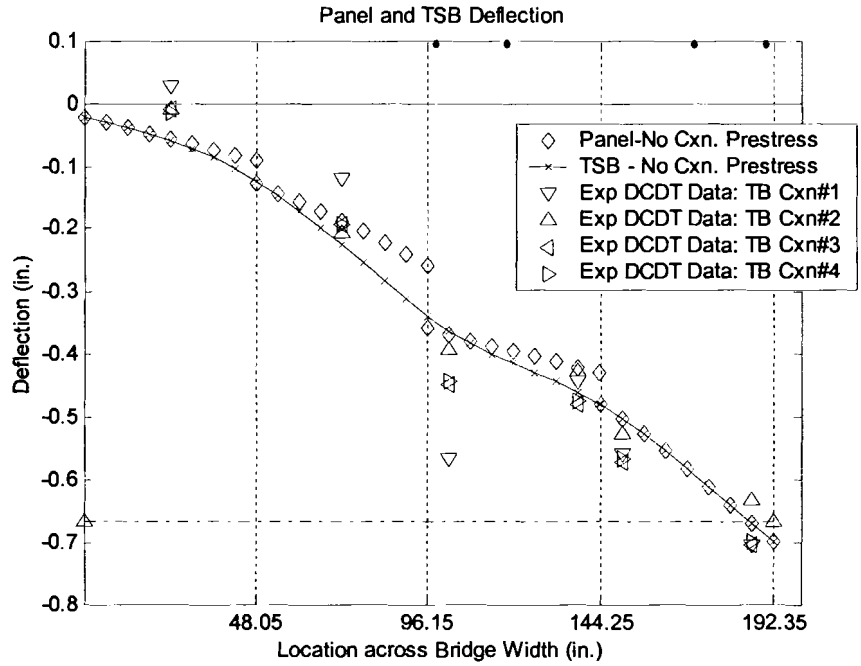

Figure D.4 Deflection correlation, Load Case #2, TSB #3, Thru-Bolt Conn.

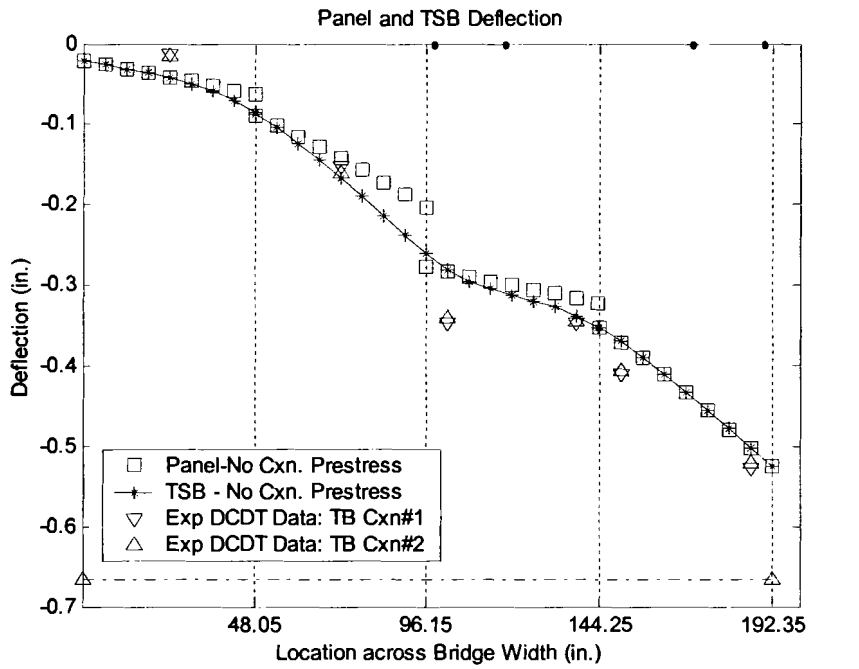

Figure D.5 Deflection correlation, Load Case #2b, TSB #2, Thru-Bolt Conn.

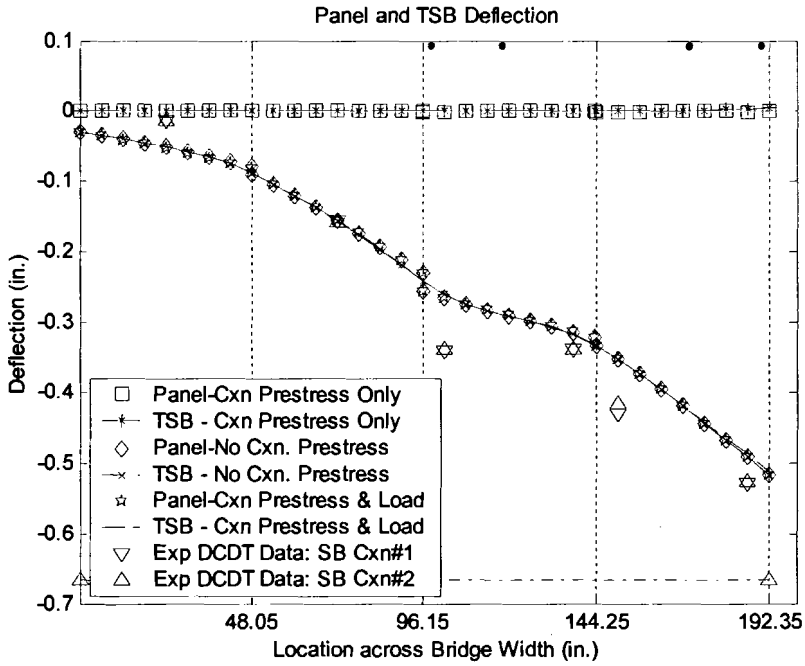

Figure D.6 Deflection correlation, Load Case #2b, TSB #2, Seated-Beam Conn.

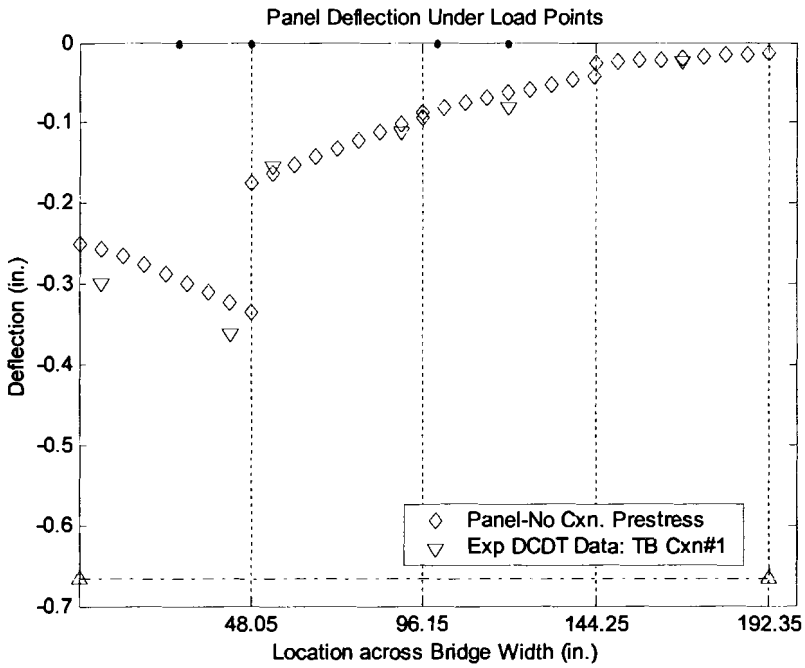

Figure D.7 Deflection correlation, Load Case #3a, TSB #1, Thru-Bolt Conn.

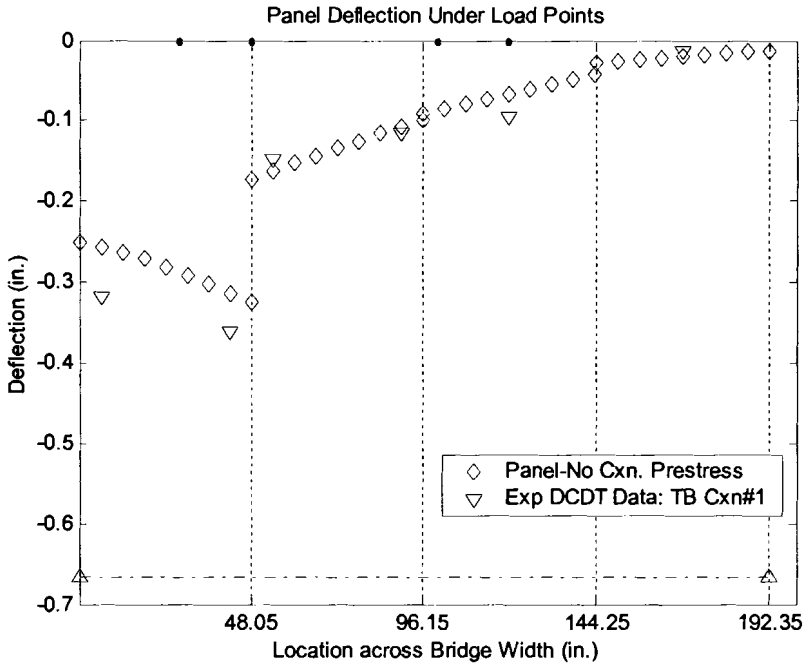

Figure D.8 Deflection correlation, Load Case #3a, TSB #2, Thru-Bolt Conn.

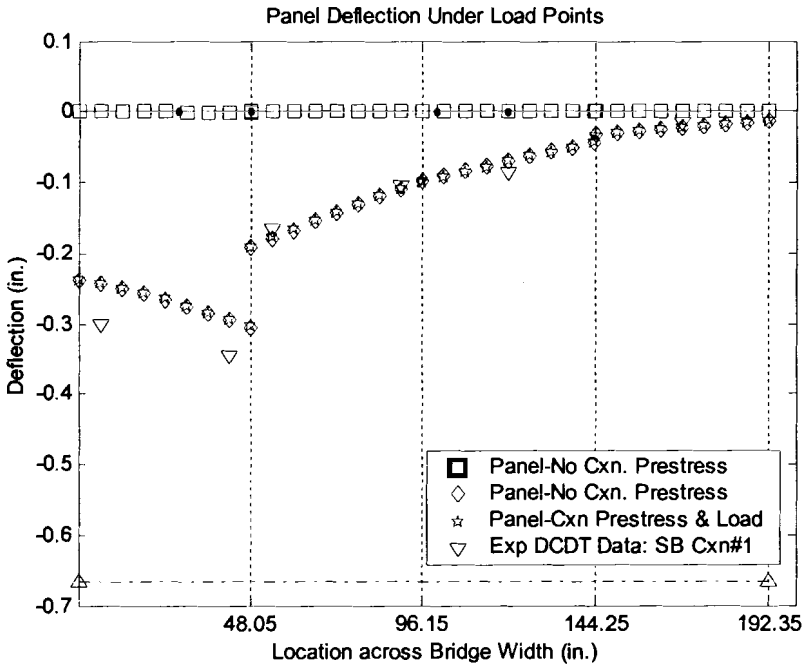

Figure D.9 Deflection correlation, Load Case #3a, TSB #2, Seated-Beam Conn.

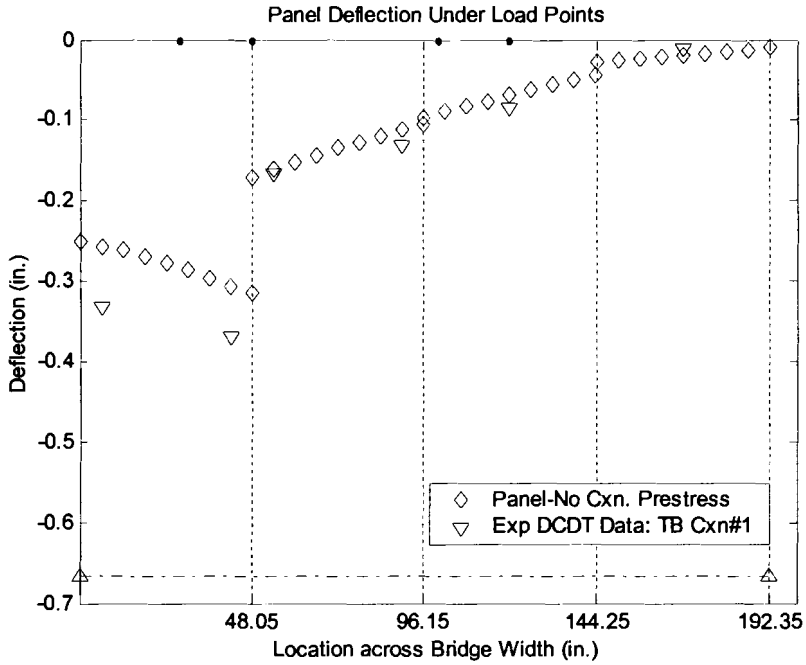

Figure D.10 Deflection correlation, Load Case #3a, TSB #3, Thru-Bolt Conn.

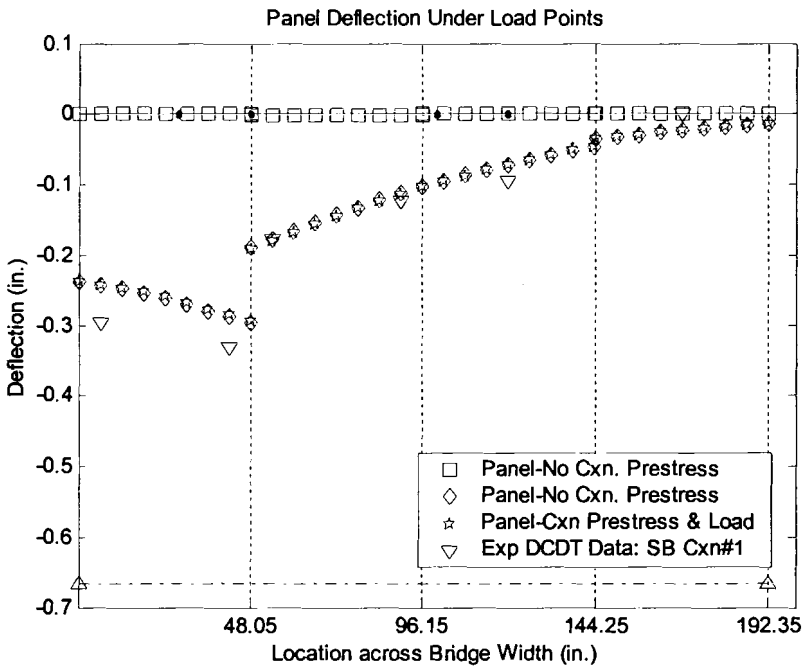

Figure D.11 Deflection correlation, Load Case #3a, TSB #3, Seated-Beam Conn.

D.2 Correlation of Conn. Forces

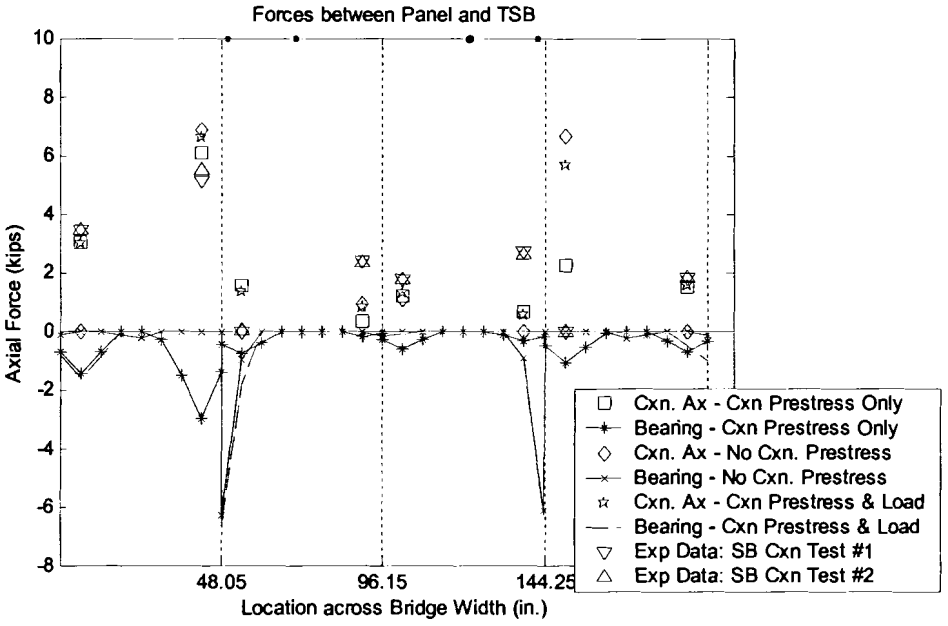

Figure D.12 Axial forces correlation, Load Case #1, TSB #1, Seated-Beam Conn.

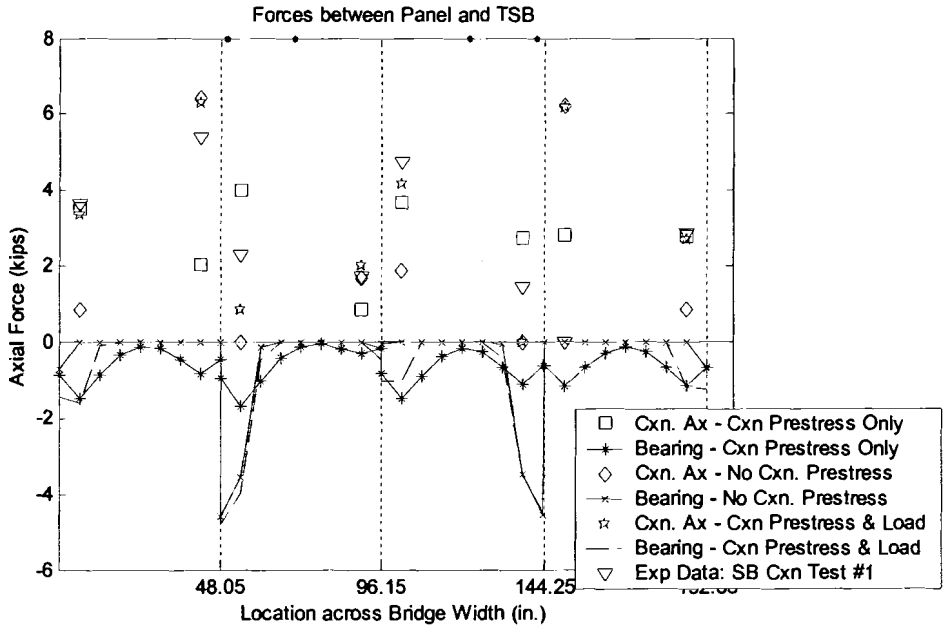

Figure D.13 Axial forces correlation, Load Case #1, TSB #3, Seated-Beam Conn.

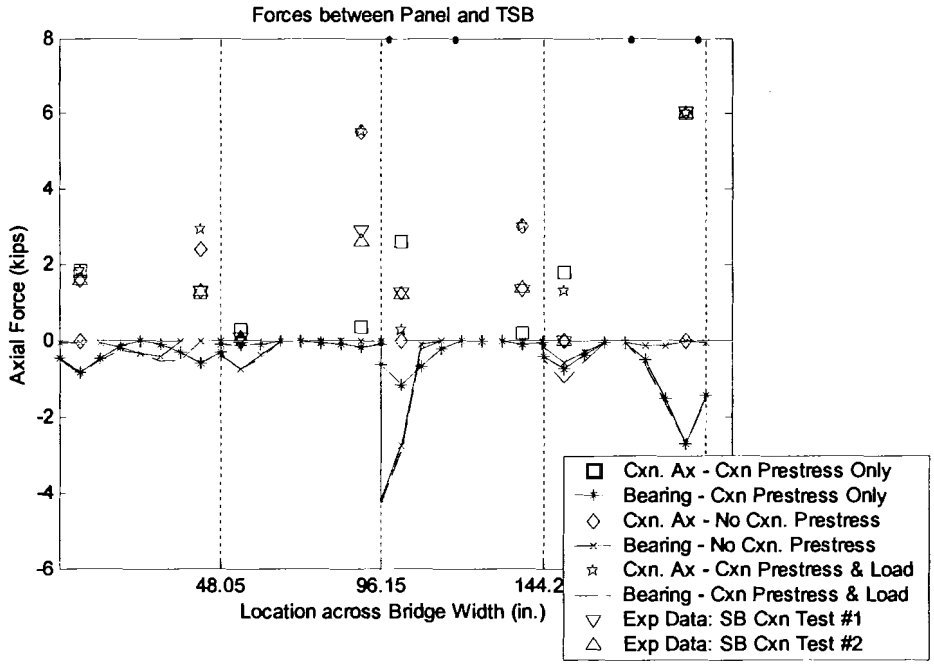

Figure D.14 Axial forces correlation, Load Case #2b, TSB #2, Seated-Beam Conn.

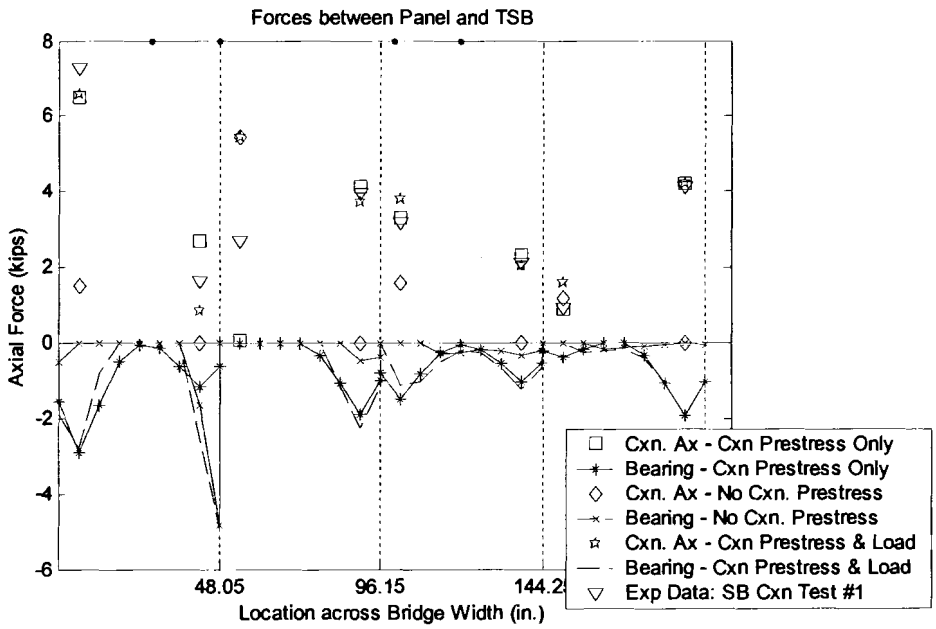

Figure D.15 Axial forces correlation, Load Case #3a, TSB #2, Seated-Beam Conn.

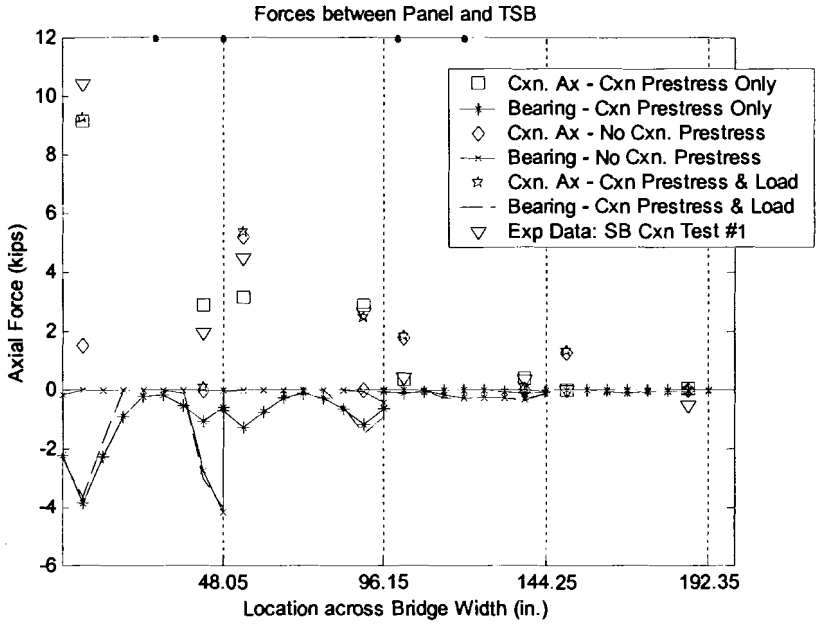

Figure D.16 Axial forces correlation, Load Case #3a, TSB #3, Seated-Beam Conn.

Appendix E

PARAMETRIC STUDY TABLES AND CHARTS

Table E.1 Geometry of TSB used the parametric study

TSB Designation	Height (in.)	Width (in.)	width/ height	Area (in^2)	I (in^4)	EI/EI min
TSB1	4.5	6.75	1.50	30.38	51.26	0.90
TSB2	6	5.125	0.85	30.75	92.25	1.61
TSB3	4.625	6.95	1.50	32.14	57.30	1.00
TSB4	5.12	5.12	1.00	26.21	57.27	1.00
TSB5	5.75	3.625	0.63	20.84	57.43	1.01
TSB6	6.75	4.5	0.67	30.38	115.33	2.02
TSB7	7.45	5	0.67	37.25	172.29	3.02
TSB8	8	5.35	0.67	42.80	228.27	3.99
TSBsp10	4.76	3.19	0.67	15.18	28.67	0.50
TSBsp11	5.66	3.79	0.67	21.45	57.27	1.00
TSBsp12	6.26	4.19	0.67	26.23	85.66	1.50
TSBsp13	6.73	4.51	0.67	30.35	114.56	2.00
TSBsp14	7.11	4.77	0.67	33.91	142.87	2.50
TSBsp15	4.30	4.30	1.00	18.49	28.49	0.50
TSBsp16	5.12	5.12	1.00	26.21	57.27	1.00
TSBsp17	5.66	5.66	1.00	32.04	85.52	1.50
TSBsp18	6.09	6.09	1.00	37.09	114.63	2.01
TSBsp19	6.43	6.43	1.00	41.34	142.45	2.49
TSBsp20	3.89	5.83	1.50	22.68	28.60	0.50
TSBsp21	4.62	6.94	1.50	32.06	57.03	1.00
TSBsp22	5.12	7.68	1.50	39.32	85.90	1.50
TSBsp23	5.50	8.25	1.50	45.38	114.38	2.00
TSBsp24	5.81	8.72	1.50	50.66	142.52	2.49

Notes: 1. All use SP 47 glulam properties.
2. See Figure 6.1 for sketches of each TSB.

E.1 Load Cases Used in the Parametric Study

This section contains information on the load cases used in the Parametric Study reported in Chapter 6 of this thesis. Figure E.1 is a detailed figure of a general load case showing how tire locations specified in Table E.2 in which complete descriptions of each load case may be found. Load Cases #1 to 13 were applied using the simple distribution of the tire point load to point loads at nodes under the tire patch as described in Chapter 5. Load Case #14 applied the entire tire load to a single node. All Load Cases numbered 15 and greater used a uniform surface load applied to the deck elements as described in Chapter 5. Load Cases #12, 14, and 15 have identical loading, but different methods of applying the loads in the finite element program. Figures E.2, E.3, and E.4 show plan views of each load case used in this study. The plan views of the load cases are grouped according to panel width of the bridges to which they are applied.

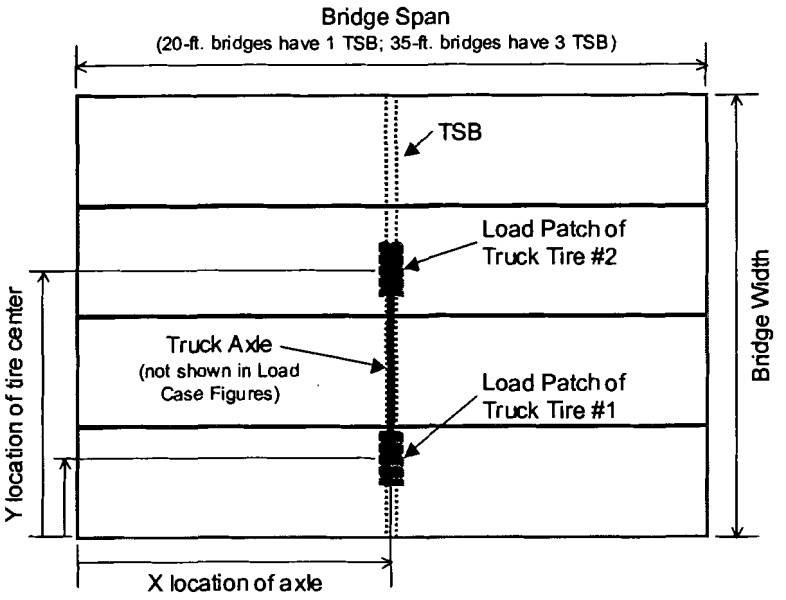

Figure E.1 Key to figures of Load Cases

Table E.2 Load cases used the parametric study

#	Bridge Span (ft.)	Bridge Width (ft.)	Panel Width (in.)	# of Lanes	Loading	Truck #	Tire Load (kips)	Axle (Front, Middle, or Rear)	X-location (longit.) of axle (in.)	Y-location (trans.) of tire #1 center (in.)	Y-location (trans.) of tire #2 center (in.)
1	20	14	42	1	HS20	1	16	R	120	30	102.2
2	20	14	42	1	HS20	1	16	R	120	48.1	120.2
3	20	14	42	1	HS20	1	16	R	60	30	102.2
4	20	14	42	1	HS20	1	16	R	60	48.1	120.2
5	35	14	42	1	HS20	1	16	R	210	30	102.2
6	35	14	42	1	HS20	1	16	R	210	48.1	120.2
7	35	14	42	1	HS20	1	16	R	108	30	102.2
8	35	14	42	1	HS20	1	16	R	108	48.1	120.2
9	35	14	42	1	HS20	1	16	R	159	30	102.2
10	35	14	42	1	HS20	1	16	R	72	30	102.2
							16	M	240	30	102.2
							4	F	408	30	102.2
11	35	14	42	1	HS20	1	16	R	42	48.1	120.2
							16	M	210	48.1	120.2
							4	F	378	48.1	120.2
12	35	14	42	1	HS20	1	16	R	42	30	102.2
							16	M	210	30	102.2
							4	F	378	30	102.2
13	35	14	42	1	HS20	1	16	R	126	30	102.2
							16	M	294	30	102.2
14	35	14	42	1	HS20	1	16	R	42	30	102.2
							16	M	210	30	102.2
							4	F	378	30	102.2
15	35	14	42	1	HS20	1	16	R	42	30	102.2
							16	M	210	30	102.2
							4	F	378	30	102.2
16	20	13.5	54	1	HS20	1	16	R	120	30	102.2
17	20	16	48	1	HS20	1	16	R	120	30	102.2
18	20	16	48	1	HS20	1	16	R	120	36	108.2
19	20	16	48	1	HS20	1	16	R	120	60.1	132.2
20	20	13.5	54	1	HS20	1	16	R	120	44	116.2
21	20	16	48	1	HS20	1	16	R	120	38	110.2
22	20	22.5	54	2	HS20	1	16	R	120	39	111.2
						2	16	R	120	159.2	231.4
23	20	22.5	54	1	HS20	1	16	R	120	99.1	171.3
24	20	20	48	2	HS20	1	16	R	120	24	96.2
						2	16	R	120	144.2	216.4
25	20	20	48	1	HS20	1	16	R	120	84.1	156.3
26	20	21	42	2	HS20	2	16	R	120	30	102.2
							16	R	120	150.3	222.5
27	20	21	42	1	HS20	1	16	R	120	90.2	162.3
28	20	24	48	2	HS20	2	16	R	120	36	108.2
							16	R	120	180.3	252.5

Table E.2 (Continued) Load cases used the parametric study

#	Bridge Span (ft.)	Bridge Width (ft.)	Panel Width (in.)	# of Lanes	Loading	Truck #	Tire Load (kips)	Axle (Front, Middle, or Rear)	X-location (longit.) of axle (in.)	Y-location (trans.) of tire #1 center (in.)	Y-location (trans.) of tire #2 center (in.)
29	35	21	42	1	HS20	1	16	R	42	90.2	162.3
							16	M	210	90.2	162.3
							4	F	378	90.2	162.3
30	35	16	48	1	HS20	1	16	R	42	60.1	132.2
							16	M	210	60.1	132.2
							4	F	378	60.1	132.2
31	20	16	48	1	HS20	1	16	R	120	60.1	132.2
32	20	16	48	1	HS25	1	20	R	120	60.1	132.2
33	35	16	48	1	HS20	1	16	R	126	60.1	132.2
							16	M	294	60.1	132.2
34	35	16	48	1	HS20	1	16	R	75	60.1	132.2
							16	M	243	60.1	132.2
							4	F	411	60.1	132.2
35	35	16	48	1	HS20	1	16	R	108	60.1	132.2
							16	M	312	60.1	132.2
36	35	16	48	1	ML24	1	12	R	186	60.1	132.2
							12	F	234	60.1	132.2
37	35	16	48	1	ML30	1	15	R	162	60.1	132.2
							15	F	210	60.1	132.2
38	35	16	48	1	LL26	1	Line Load of 26 kips	LINE LOAD	210	–	–
							Uniform Load	UNIFORM LOAD OVER CENTER PANELS			
39	35	32	48	2	HS20	1	16	R	42	60.1	132.2
							16	M	210	60.1	132.2
							4	F	378	60.1	132.2
						2	16	R	42	252.5	324.6
							16	M	210	252.5	324.6
							4	F	378	252.5	324.6
40	35	32	48	2	HS25	1	20	R	42	60.1	132.2
							20	M	210	60.1	132.2
							5	F	378	60.1	132.2
						2	20	R	42	252.5	324.6
							20	M	210	252.5	324.6
							5	F	378	252.5	324.6
41	35	32	48	2	ML30	1	15	R	186	60.1	132.2
							15	F	234	60.1	132.2
						2	15	R	186	252.5	324.6
							15	F	234	252.5	324.6
42	35	32	48	2	ML24	1	12	R	186	60.1	132.2
							12	F	234	60.1	132.2
						2	12	R	186	252.5	324.6
							12	F	234	252.5	324.6
43	20	21	42	1	ML24	1	12	R	96	90.2	162.3
							12	F	144	90.2	162.3

Table E.2 (Continued) Load cases used the parametric study

#	Bridge Span (ft.)	Bridge Width (ft.)	Panel Width (in.)	# of Lanes	Loading	Truck #	Tire Load (kips)	Axle (Front, Middle, or Rear)	X-location (longit.) of axle (in.)	Y-location (trans.) of tire #1 center (in.)	Y-location (trans.) of tire #2 center (in.)
44	20	21	42	1	HS25	1	20	R	120	90.2	162.3
45	20	21	42	1	HS20	1	16	R	120	90.2	162.3
46	20	16	48	1	ML24	1	12	R	60	38	110.2
							12	F	108	38	110.2
47	20	16	48	1	ML24	1	12	R	36	38	110.2
							12	F	84	38	110.2
48	20	16	48	1	HS25	1	20	R	60	38	110.2
49	20	16	48	1	HS20	1	16	R	60	38	110.2
50	20	21	42	1	ML24	1	12	R	60	32	104.2
							12	F	108	32	104.2
51	20	21	42	1	ML24	1	12	R	36	32	104.2
							12	F	84	32	104.2
52	20	21	42	1	HS25	1	20	R	60	32	104.2
53	20	21	42	1	HS20	1	16	R	60	32	104.2

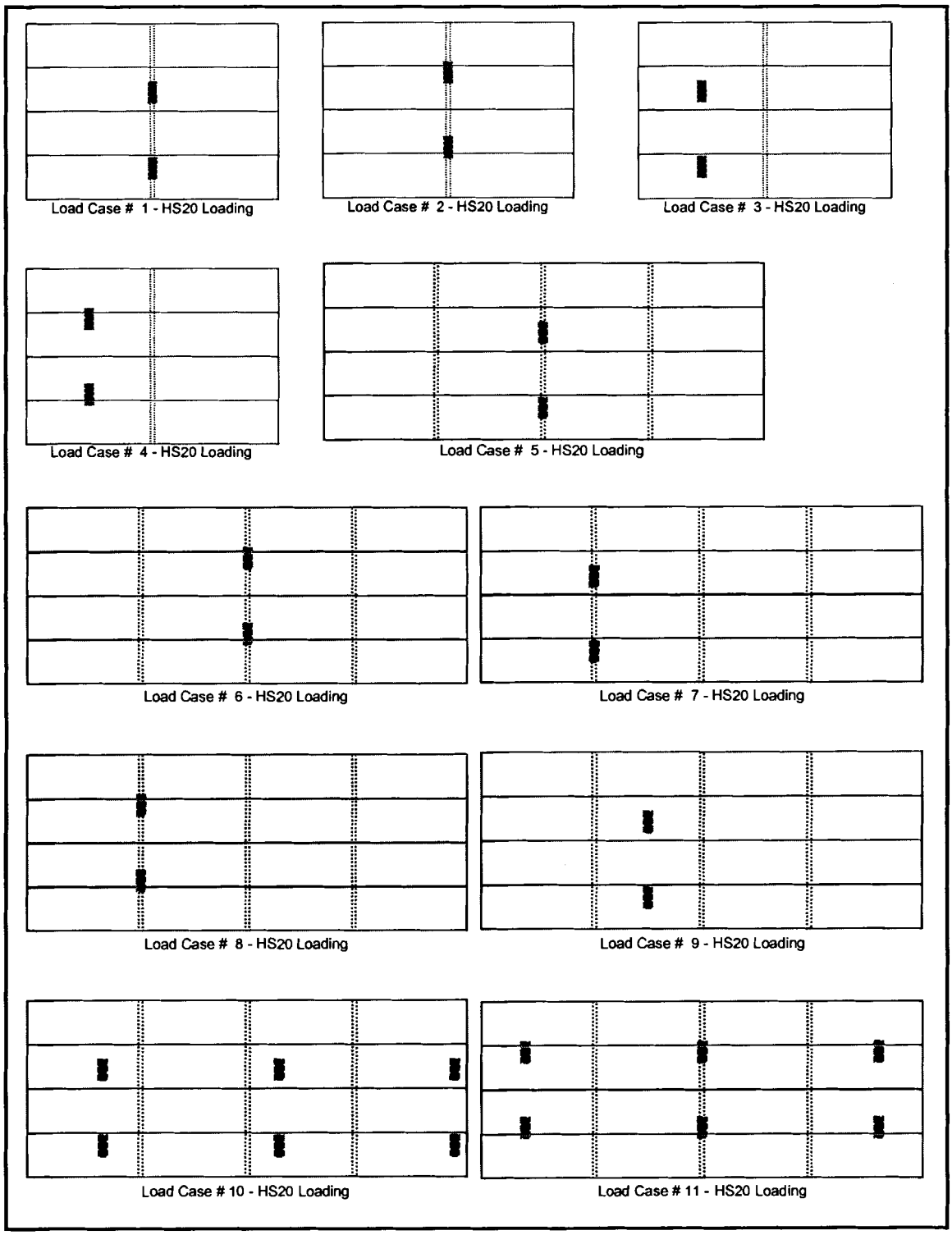

Figure E.2 Load cases for 42-inch panel bridges

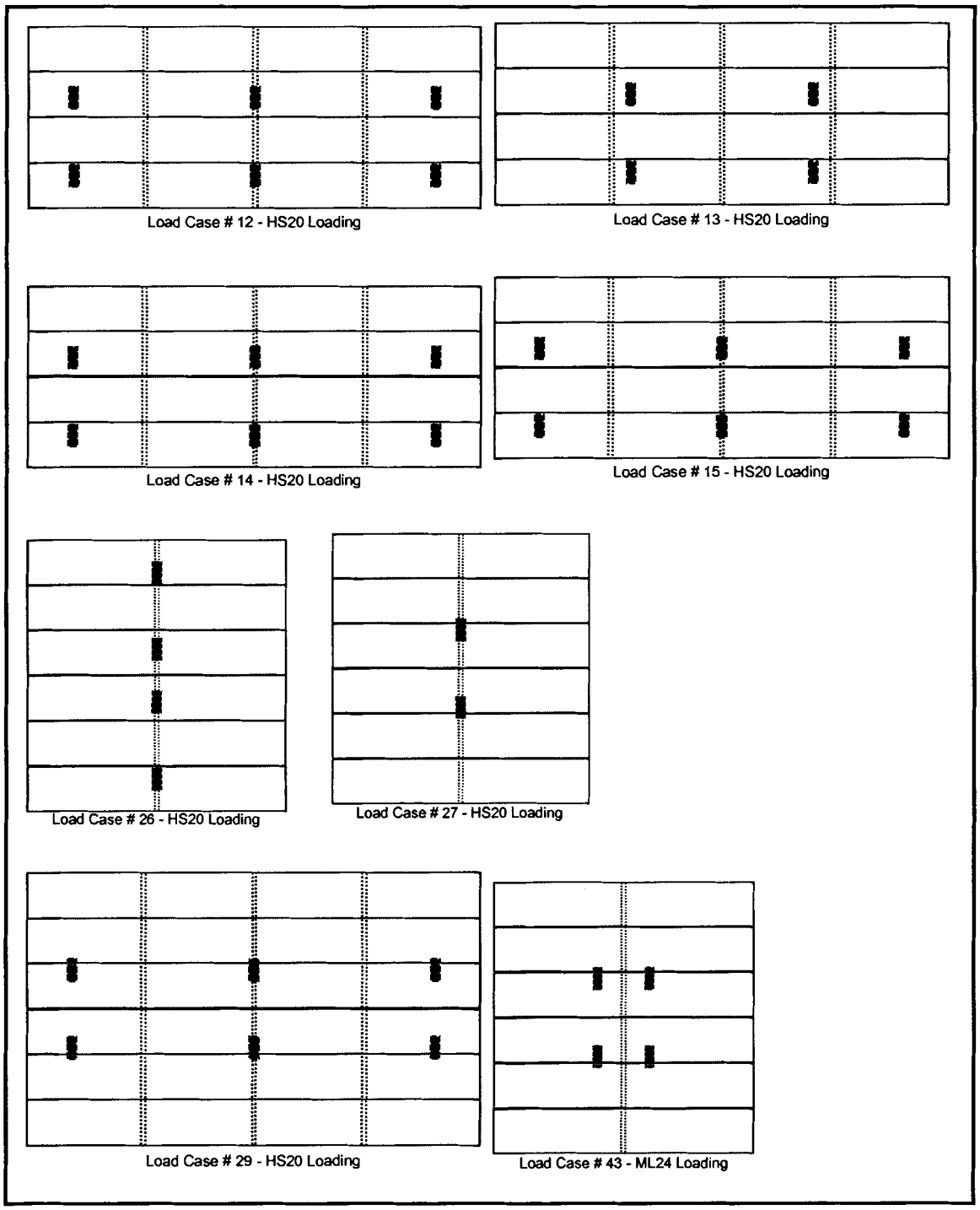

Figure E.2 (Continued) Load cases for 42-inch bridges

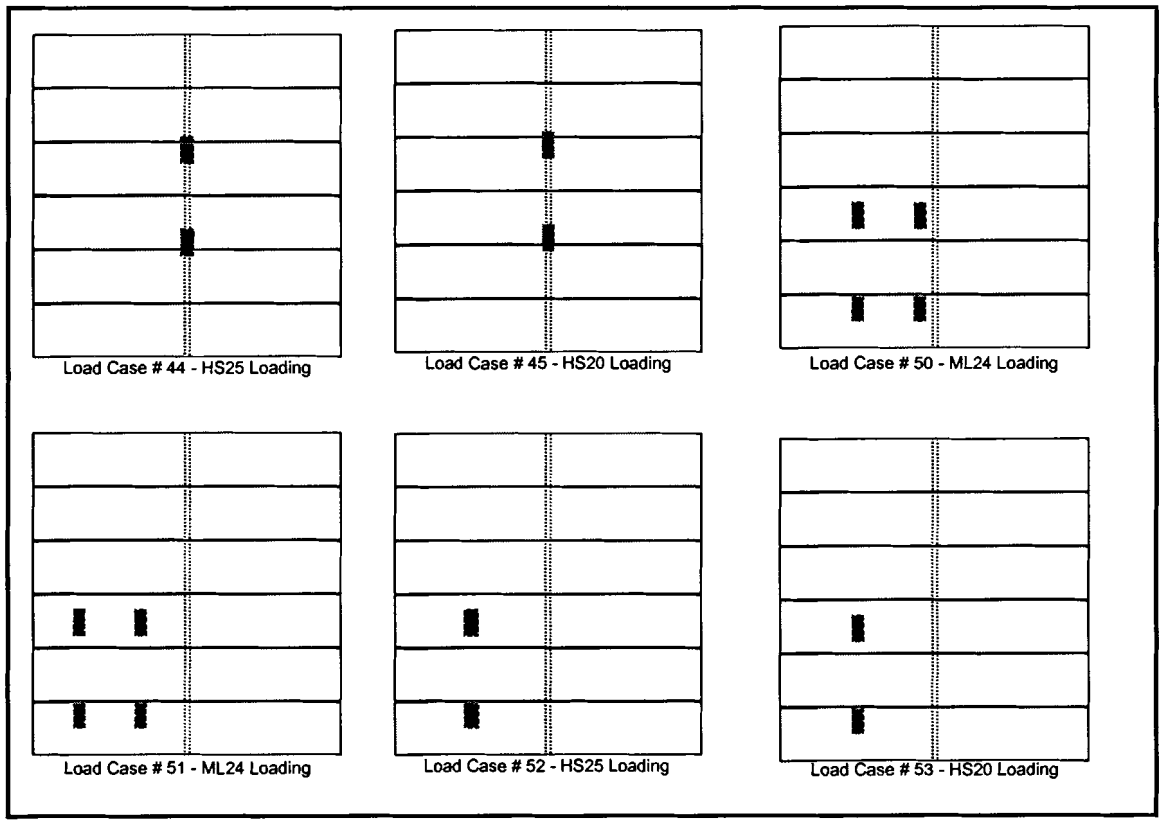

Figure E.2 (Continued) Load cases for 42-inch bridges

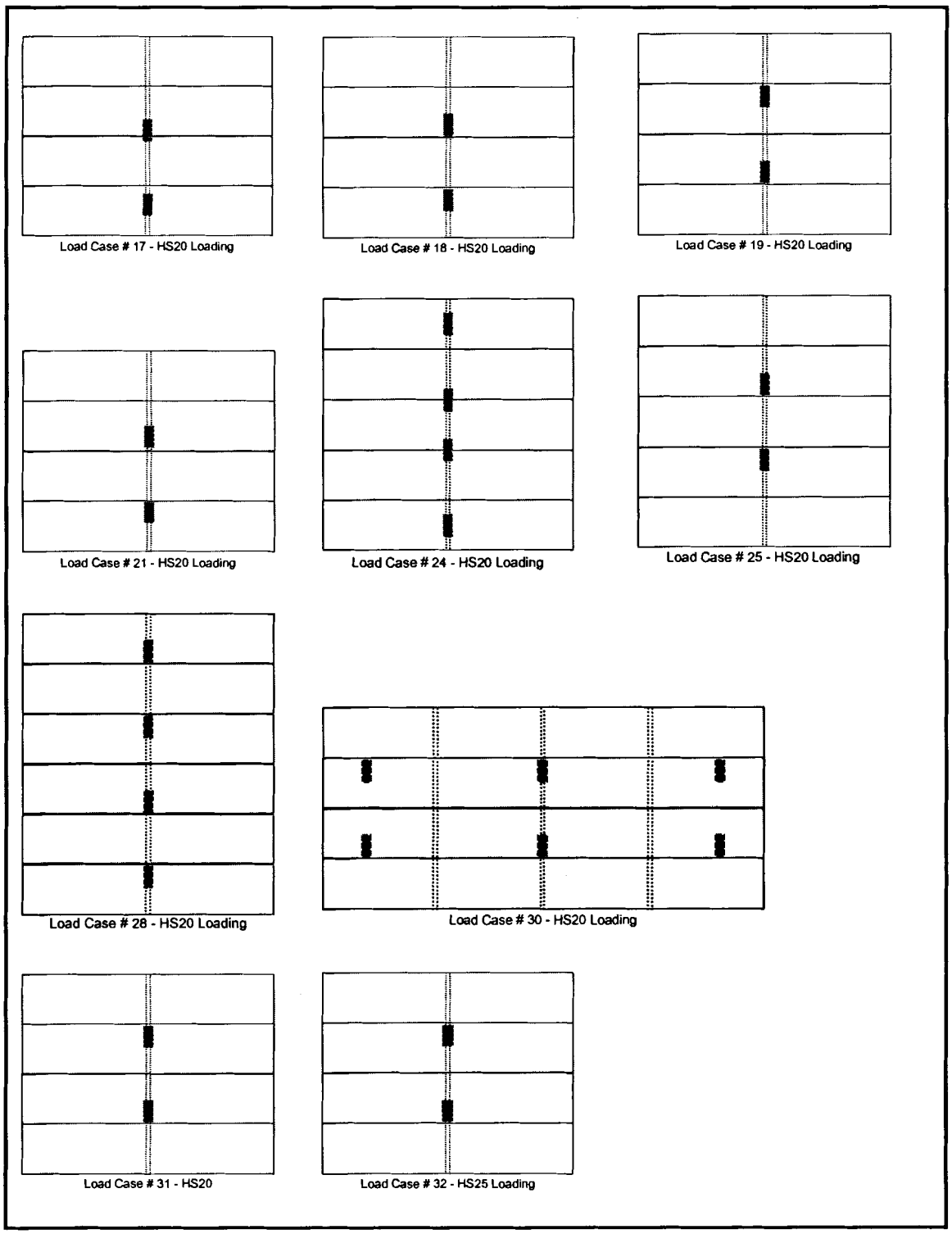

Figure E.3 Load cases for 48-inch bridges

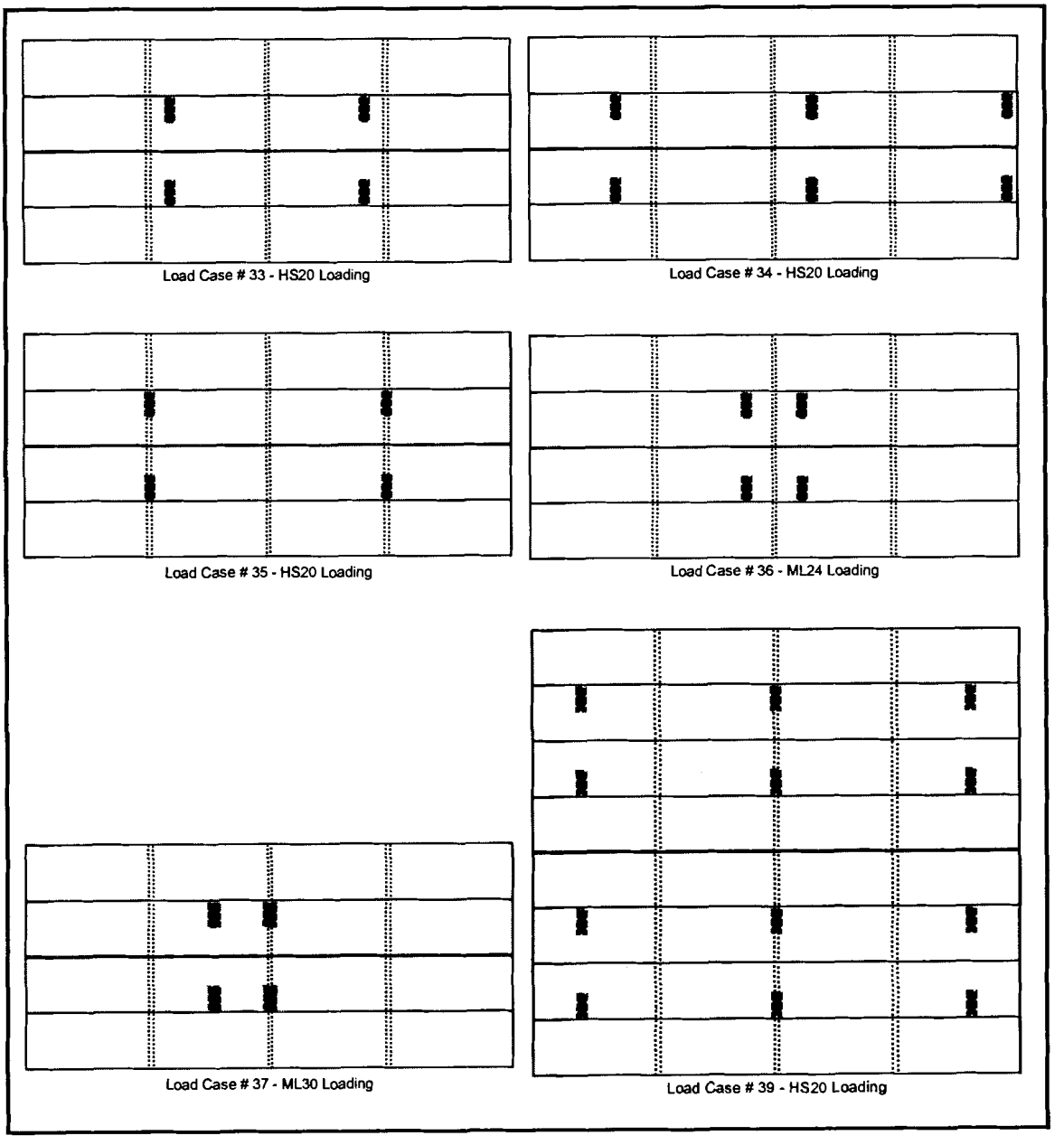

Figure E.3 (Continued) Load cases for 48-inch bridges

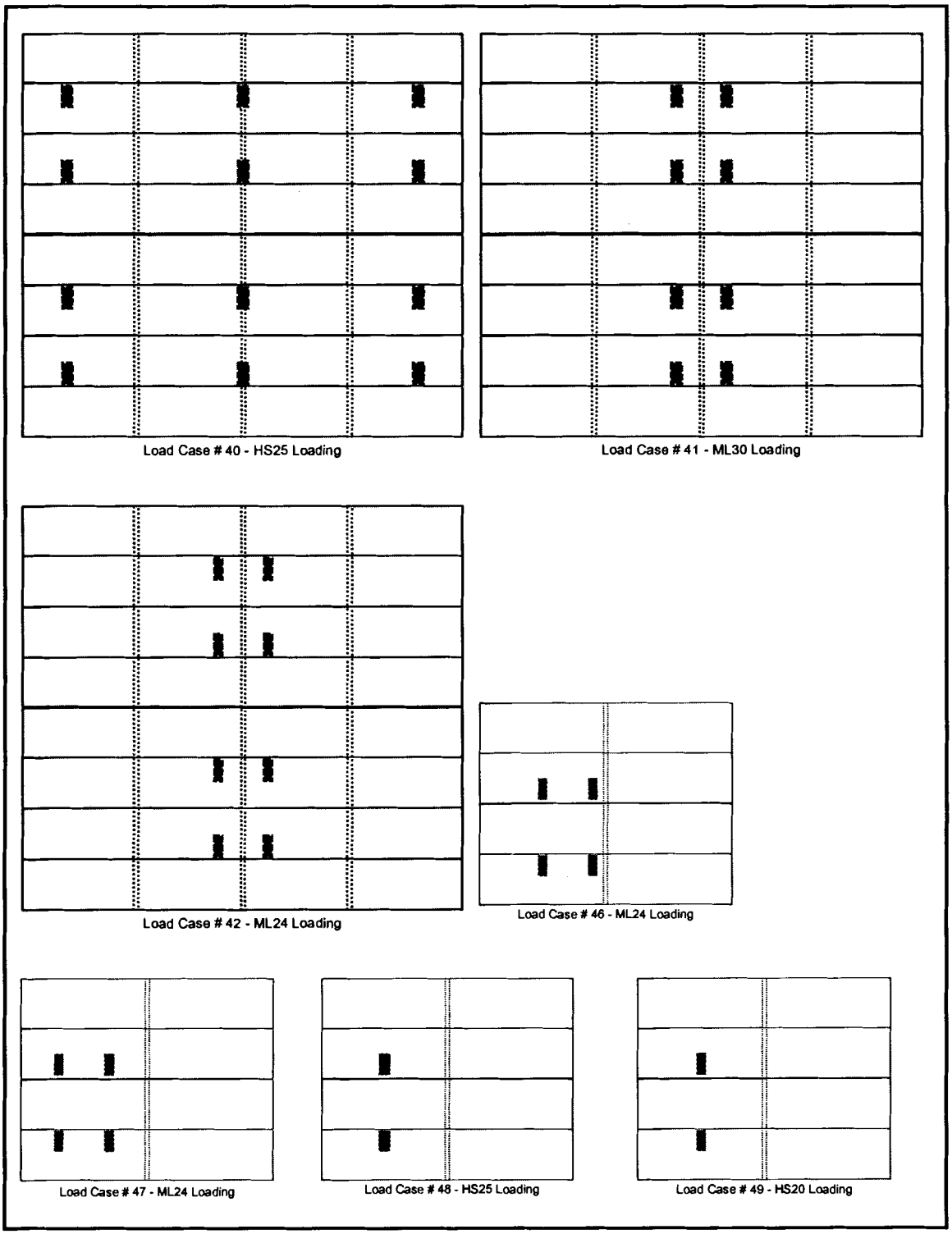

Figure E.3 (Continued) Load cases for 48-inch bridges

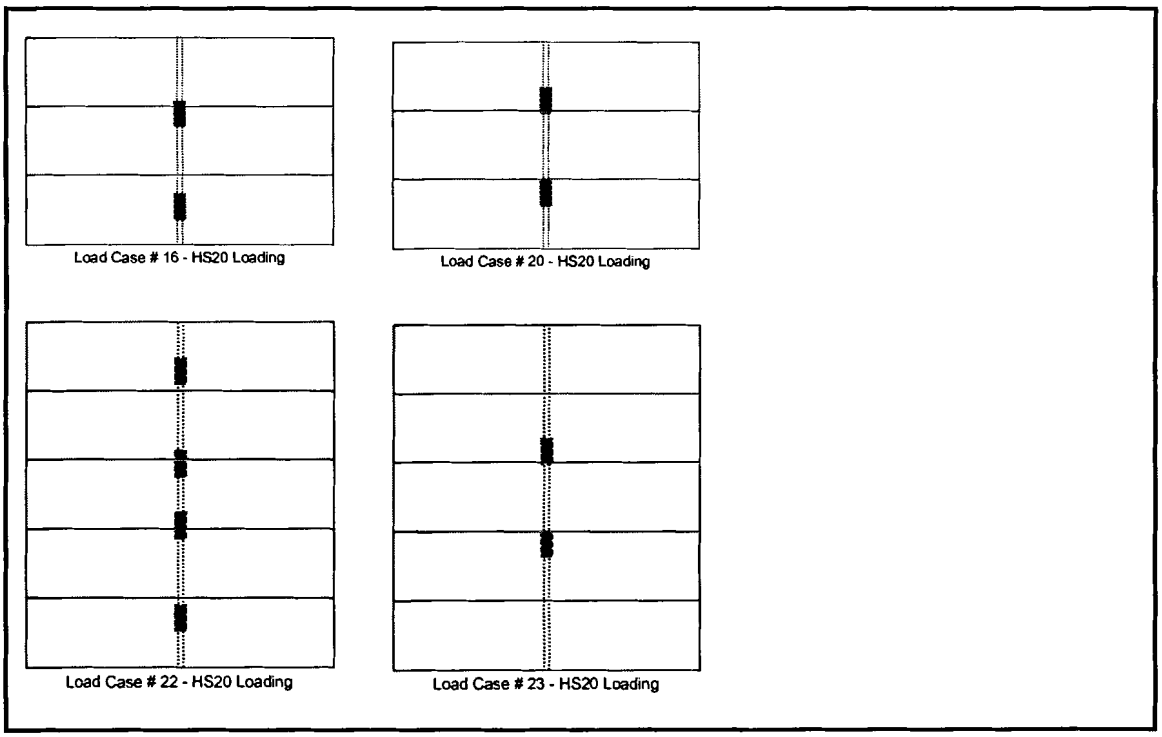

Figure E.4 Load cases for 54-inch bridges

Table E.3 Analyses run in parametric study

Test #	Span (ft)	Bridge Width (ft)	Panel Width (in)	Deck Thick-ness (in)	Material	Connec-tion Type	Curbs	No. of Lanes	AASHTO Loading	Load Case #
1	20	14	42	10.5	SP47	AB	No	1	HS20	1
2	20	14	42	10.5	SP47	TB58	No	1	HS20	1
3	20	14	42	10.5	SP47	TB34	No	1	HS20	1
4	20	14	42	10.5	SP47	SB	No	1	HS20	1
1b	20	14	42	10.5	SP47	AB linear	No	1	HS20	1
2b	20	14	42	10.5	SP47	TB58 linear	No	1	HS20	1
3b	20	14	42	10.5	SP47	TB34 linear	No	1	HS20	1
4b	20	14	42	10.5	SP47	SB linear	No	1	HS20	1
5	20	14	42	10.5	SP47	TB34	No	1	HS20	1
6	20	14	42	10.5	SP47	TB34	No	1	HS20	1
7	20	14	42	10.5	SP47	TB34	No	1	HS20	1
8	20	14	42	10.5	SP47	TB34	No	1	HS20	1
3	20	14	42	10.5	SP47	TB34	No	1	HS20	1
9	20	14	42	10.5	SP47	TB34	No	1	HS20	1
10	20	14	42	10.5	SP47	TB34	No	1	HS20	1
11	20	14	42	10.5	SP47	TB34	No	1	HS20	1
12	35	14	42	14.25	SP47	TB34	No	1	HS20	5
13	35	14	42	14.25	SP47	TB34	No	1	HS20	6
14	35	14	42	14.25	SP47	TB34	No	1	HS20	5
15	35	14	42	14.25	SP47	TB34	No	1	HS20	6
16	35	14	42	14.25	SP47	TB34	No	1	HS20	5
17	35	14	42	14.25	SP47	TB34	No	1	HS20	6
3	20	14	42	10.5	SP47	TB34	No	1	HS20	1
18	20	14	42	10.5	SP47	TB34	No	1	HS20	2
19	20	14	42	10.5	SP47	TB34	No	1	HS20	3
20	20	14	42	10.5	SP47	TB34	No	1	HS20	4

Table E.3 (Continued) Analyses run for parametric study

Test #	# of TSB (AASHTO Spec.)	TSB #	TSB Spacing (ft)	TSB E (kip/in^2)	TSB Depth (in)	TSB Width (in)	TSB I (in^4)	TSB EI ($kip\text{-}in^2$)
1	1	TSB5	10	1400	5.75	3.625	57.43	80400
2	1	TSB5	10	1400	5.75	3.625	57.43	80400
3	1	TSB5	10	1400	5.75	3.625	57.43	80400
4	1	TSB5	10	1400	5.75	3.625	57.43	80400
1b	1	TSB5	10	1400	5.75	3.625	57.43	80400
2b	1	TSB5	10	1400	5.75	3.625	57.43	80400
3b	1	TSB5	10	1400	5.75	3.625	57.43	80400
4b	1	TSB5	10	1400	5.75	3.625	57.43	80400
5	1	TSB1	10	1400	4.5	6.75	51.26	71761
6	1	TSB2	10	1400	6	5.125	92.25	129150
7	1	TSB3	10	1400	4.625	6.95	57.30	80217
8	1	TSB4	10	1400	5.12	5.12	57.27	80173
3	1	TSB5	10	1400	5.75	3.625	57.43	80400
9	1	TSB6	10	1400	6.75	4.5	115.33	161462
10	1	TSB7	10	1400	7.45	5	172.29	241205
11	1	TSB8	10	1400	8	5.35	228.27	319573
12	3	TSB3	8.75	1400	4.625	6.95	57.30	80217
13	3	TSB3	8.75	1400	4.625	6.95	57.30	80217
14	3	TSB4	8.75	1400	5.12	5.12	57.27	80173
15	3	TSB4	8.75	1400	5.12	5.12	57.27	80173
16	3	TSB5	8.75	1400	5.75	3.625	57.43	80400
17	3	TSB5	8.75	1400	5.75	3.625	57.43	80400
3	1	TSB5	10	1400	5.75	3.625	57.43	80400
18	1	TSB5	10	1400	5.75	3.625	57.43	80400
19	1	TSB5	10	1400	5.75	3.625	57.43	80400
20	1	TSB5	10	1400	5.75	3.625	57.43	80400

Table E.3 (Continued) Analyses run for parametric study

Test #	Span (ft)	Bridge Width (ft)	Panel Width (in)	Deck Thick-ness (in)	Material	Connec-tion Type	Curbs	No. of Lanes	AASHTO Loading	Load Case #
21	20	21	42	10.5	SP47	TB34	No	2	HS20	26
22	20	21	42	10.5	SP47	TB34	No	1	HS20	27
16	35	14	42	14.25	SP47	TB34	No	1	HS20	5
17	35	14	42	14.25	SP47	TB34	No	1	HS20	6
23	35	14	42	14.25	SP47	TB34	No	1	HS20	7
24	35	14	42	14.25	SP47	TB34	No	1	HS20	8
25	35	14	42	14.25	SP47	TB34	No	1	HS20	9
26	35	14	42	14.25	SP47	TB34	No	1	HS20	10
27	35	14	42	14.25	SP47	TB34	No	1	HS20	12
28	35	14	42	14.25	SP47	TB34	No	1	HS20	11
29	35	14	42	14.25	SP47	TB34	No	1	HS20	13
27	35	14	42	14.25	SP47	TB34	No	1	HS20	12
30	35	14	42	14.25	SP47	TB34	No	1	HS20	14
31	35	14	42	14.25	SP47	TB34	No	1	HS20	15
32	35	21	42	14.25	SP47	TB34	No	1	HS20	29
33	20	16	48	10.5	SP47	TB34	No	1	HS20	17
34	20	16	48	10.5	SP47	TB34	No	1	HS20	18
35	20	16	48	10.5	SP47	TB34	No	1	HS20	19
36	20	16	48	10.5	SP47	TB34	No	1	HS20	21
37	20	20	48	10.5	SP47	TB34	No	2	HS20	24
38	20	20	48	10.5	SP47	TB34	No	1	HS20	25
39	20	24	48	10.5	SP47	TB34	No	2	HS20	28
40	35	16	48	14.25	SP47	TB34	No	1	HS20	30
41	20	13.5	54	10.5	SP47	TB34	No	1	HS20	16
42	20	13.5	54	10.5	SP47	TB34	No	1	HS20	20
43	20	22.5	54	10.5	SP47	TB34	No	2	HS20	22
44	20	22.5	54	10.5	SP47	TB34	No	1	HS20	23

Table E.3 (Continued) Analyses run for parametric study

Test #	# of TSB (AASHTO Spec.)	TSB #	TSB Spacing (ft)	TSB E (kip/in2)	TSB Depth (in)	TSB Width (in)	TSB I (in4)	TSB EI (kip-in2)
21	1	TSB5	10	1400	5.75	3.625	57.43	80400
22	1	TSB5	10	1400	5.75	3.625	57.43	80400
16	3	TSB5	8.75	1400	5.75	3.625	57.43	80400
17	3	TSB5	8.75	1400	5.75	3.625	57.43	80400
23	3	TSB5	8.75	1400	5.75	3.625	57.43	80400
24	3	TSB5	8.75	1400	5.75	3.625	57.43	80400
25	3	TSB5	8.75	1400	5.75	3.625	57.43	80400
26	3	TSB5	8.75	1400	5.75	3.625	57.43	80400
27	3	TSB5	8.75	1400	5.75	3.625	57.43	80400
28	3	TSB5	8.75	1400	5.75	3.625	57.43	80400
29	3	TSB5	8.75	1400	5.75	3.625	57.43	80400
27	3	TSB5	8.75	1400	5.75	3.625	57.43	80400
30	3	TSB5	8.75	1400	5.75	3.625	57.43	80400
31	3	TSB5	8.75	1400	5.75	3.625	57.43	80400
32	3	TSB5	8.75	1400	5.75	3.625	57.43	80400
33	1	TSB5	10	1400	5.75	3.625	57.43	80400
34	1	TSB5	10	1400	5.75	3.625	57.43	80400
35	1	TSB5	10	1400	5.75	3.625	57.43	80400
36	1	TSB5	10	1400	5.75	3.625	57.43	80400
37	1	TSB5	10	1400	5.75	3.625	57.43	80400
38	1	TSB5	10	1400	5.75	3.625	57.43	80400
39	1	TSB5	10	1400	5.75	3.625	57.43	80400
40	3	TSB5	8.75	1400	5.75	3.625	57.43	80400
41	1	TSB5	10	1400	5.75	3.625	57.43	80400
42	1	TSB5	10	1400	5.75	3.625	57.43	80400
43	1	TSB5	10	1400	5.75	3.625	57.43	80400
44	1	TSB5	10	1400	5.75	3.625	57.43	80400

Table E.3 (Continued) Analyses run for parametric study

Test #	Span (ft)	Bridge Width (ft)	Panel Width (in)	Deck Thick-ness (in)	Material	Connec-tion Type	Curbs	No. of Lanes	AASHTO Loading	Load Case #
45	20	16	48	8.5	SP47	TB34	No	1	HS20	19
35	20	16	48	10.5	SP47	TB34	No	1	HS20	19
46	20	16	48	12.25	SP47	TB34	No	1	HS20	19
47	20	16	48	14.25	SP47	TB34	No	1	HS20	19
48	20	16	48	10.5	Panel SP47 MOE * 0.75 -- TSB SP47	TB34	No	1	HS20	19
35	20	16	48	10.5	SP47	TB34	No	1	HS20	19
49	20	16	48	10.5	Panel SP47 MOE * 1.25 -- TSB SP47	TB34	No	1	HS20	19
50	20	16	48	10.5	Panel SP47 MOE * 1.50 -- TSB SP47	TB34	No	1	HS20	19
51	20	16	48	10.5	TSB SP47 MOE * 0.75 -- Panel SP47	TB34	No	1	HS20	19
35	20	16	48	10.5	SP47	TB34	No	1	HS20	19
52	20	16	48	10.5	TSB SP47 MOE * 1.25 -- Panel SP47	TB34	No	1	HS20	19
53	20	16	48	10.5	TSB SP47 MOE * 1.50 -- Panel SP47	TB34	No	1	HS20	19
56	20	16	48	10.5	SP47	TB34	No	1	HS20	19
57	20	16	48	10.5	SP47	TB34	No	1	HS20	19
58	20	16	48	10.5	SP47	TB34	No	1	HS20	19
59	20	16	48	10.5	SP47	TB34	No	1	HS20	19
60	20	16	48	10.5	SP47	TB34	No	1	HS20	19
61	20	16	48	10.5	SP47	TB34	No	1	HS20	19
62	20	16	48	10.5	SP47	TB34	No	1	HS20	19
63	20	16	48	10.5	SP47	TB34	No	1	HS20	19
64	20	16	48	10.5	SP47	TB34	No	1	HS20	19
65	20	16	48	10.5	SP47	TB34	No	1	HS20	19
66	20	16	48	10.5	SP47	TB34	No	1	HS20	19
67	20	16	48	10.5	SP47	TB34	No	1	HS20	19

Table E.3 (Continued) Analyses run for parametric study

Test #	# of TSB (AASHTO Spec.)	TSB #	TSB Spacing (ft)	TSB E (kip/in2)	TSB Depth (in)	TSB Width (in)	TSB I (in4)	TSB EI (kip-in2)
45	1	TSB5	10	1400	5.75	3.625	57.43	80400
35	1	TSB5	10	1400	5.75	3.625	57.43	80400
46	1	TSB5	10	1400	5.75	3.625	57.43	80400
47	1	TSB5	10	1400	5.75	3.625	57.43	80400
48	1	TSB5	10	1400	5.75	3.625	57.43	80400
35	1	TSB5	10	1400	5.75	3.625	57.43	80400
49	1	TSB5	10	1400	5.75	3.625	57.43	80400
50	1	TSB5	10	1400	5.75	3.625	57.43	80400
51	1	TSB5	10	1050	5.75	3.625	57.43	60300
35	1	TSB5	10	1400	5.75	3.625	57.43	80400
52	1	TSB5	10	1750	5.75	3.625	57.43	100501
53	1	TSB5	10	2100	5.75	3.625	57.43	120601
56	1	TSB#sp10	10	1400	4.76	3.19	28.67	40138
57	1	TSB#sp11	10	1400	5.66	3.79	57.27	80174
58	1	TSB#sp12	10	1400	6.26	4.19	85.66	119918
59	1	TSB#sp13	10	1400	6.73	4.51	114.56	160387
60	1	TSB#sp14	10	1400	7.11	4.77	142.87	200020
61	1	TSB#sp15	10	1400	4.30	4.30	28.49	39886
62	1	TSB#sp16	10	1400	5.12	5.12	57.27	80173
63	1	TSB#sp17	10	1400	5.66	5.66	85.52	119733
64	1	TSB#sp18	10	1400	6.09	6.09	114.63	160478
65	1	TSB#sp19	10	1400	6.43	6.43	142.45	199430
66	1	TSB#sp20	10	1400	3.89	5.83	28.60	40037
67	1	TSB#sp21	10	1400	4.62	6.94	57.03	79842

Table E.3 (Continued) Analyses run for parametric study

Test #	Span (ft)	Bridge Width (ft)	Panel Width (in)	Deck Thick-ness (in)	Material	Connec-tion Type	Curbs	No. of Lanes	AASHTO Loading	Load Case #
68	20	16	48	10.5	SP47	TB34	No	1	HS20	19
69	20	16	48	10.5	SP47	TB34	No	1	HS20	19
70	20	16	48	10.5	SP47	TB34	No	1	HS20	19
71	20	16	48	10.5	SP47	SB	No	1	HS20	19
72	20	16	48	10.5	SP47	AB	No	1	HS20	19
73	20	16	48	12.25	SP47	SB	No	1	HS20	19
74	20	16	48	12.25	SP47	AB	No	1	HS20	19
75	20	16	48	10.5	SP47	SB	No	1	HS20	19
76	20	16	48	10.5	SP47	AB	No	1	HS20	19
77	20	16	48	12.25	SP47	SB	No	1	HS20	19
78	20	16	48	12.25	SP47	AB	No	1	HS20	19
40	35	16	48	14.25	SP47	TB34	No	1	HS20	30
80	35	16	48	14.25	SP47	TB34	No	1	HS20	34
81	35	16	48	14.25	SP47	TB34	No	1	HS20	33
82	35	16	48	14.25	SP47	TB34	No	1	HS20	35
83	35	16	48	14.25	SP47	TB34	No	1	ML24	36
84	35	16	48	14.25	SP47	TB34	No	1	ML24	37
85	35	16	48	14.25	SP47	TB34	No	1	LL26	38
86	35	32	48	16.25	SP47	SB	No	2	HS20	39
87	35	32	48	16.25	SP47	SB	No	2	HS25	40
88	35	32	48	16.25	SP47	SB	No	2	ML24	42
89	35	32	48	16.25	SP47	SB	No	2	ML30	41
90	20	21	42	10.5	SP47	AB	No	1	HS20	45
91	20	21	42	10.5	SP47	AB	No	1	HS25	44
92	20	21	42	10.5	SP47	AB	No	1	ML24	43
93	20	21	42	10.5	SP47	SB	No	1	HS20	45
94	20	21	42	10.5	SP47	SB	No	1	HS25	44

Table E.3 (Continued) Analyses run for parametric study

Test #	# of TSB (AASHTO Spec.)	TSB #	TSB Spacing (ft)	TSB E (kip/in2)	TSB Depth (in)	TSB Width (in)	TSB I (in4)	TSB EI (kip-in2)
68	1	TSB#sp22	10	1400	5.12	7.68	85.90	120259
69	1	TSB#sp23	10	1400	5.50	8.25	114.38	160136
70	1	TSB#sp24	10	1400	5.81	8.72	142.52	199522
71	1	TSB#sp11	10	1400	5.66	3.79	57.27	80174
72	1	TSB#sp11	10	1400	5.66	3.79	57.27	80174
73	1	TSB#sp11	10	1400	5.66	3.79	57.27	80174
74	1	TSB#sp11	10	1400	5.66	3.79	57.27	80174
75	1	TSB#sp23	10	1400	5.50	8.25	114.38	160136
76	1	TSB#sp23	10	1400	5.50	8.25	114.38	160136
77	1	TSB#sp23	10	1400	5.50	8.25	114.38	160136
78	1	TSB#sp23	10	1400	5.50	8.25	114.38	160136
40	3	TSB5	8.75	1400	5.75	3.625	57.43	80400
80	3	TSB5	8.75	1400	5.75	3.625	57.43	80400
81	3	TSB5	8.75	1400	5.75	3.625	57.43	80400
82	3	TSB5	8.75	1400	5.75	3.625	57.43	80400
83	3	TSB5	8.75	1400	5.75	3.625	57.43	80400
84	3	TSB5	8.75	1400	5.75	3.625	57.43	80400
85	3	TSB5	8.75	1400	5.75	3.625	57.43	80400
86	3	TSB#sp11	8.75	1400	5.66	3.79	57.27	80174
87	3	TSB#sp11	8.75	1400	5.66	3.79	57.27	80174
88	3	TSB#sp11	8.75	1400	5.66	3.79	57.27	80174
89	3	TSB#sp11	8.75	1400	5.66	3.79	57.27	80174
90	1	TSB#sp11	10	1400	5.66	3.79	57.27	80174
91	1	TSB#sp11	10	1400	5.66	3.79	57.27	80174
92	1	TSB#sp11	10	1400	5.66	3.79	57.27	80174
93	1	TSB#sp23	10	1400	5.50	8.25	114.38	160136
94	1	TSB#sp23	10	1400	5.50	8.25	114.38	160136

Table E.3 (Continued) Analyses run for parametric study

Test #	Span (ft)	Bridge Width (ft)	Panel Width (in)	Deck Thick-ness (in)	Material	Connec-tion Type	Curbs	No. of Lanes	AASHTO Loading	Load Case #
95	20	21	42	10.5	SP47	SB	No	1	ML24	43
96	20	16	48	10.5	SP47	AB	No	1	HS20	49
97	20	16	48	10.5	SP47	SB	No	1	HS20	49
98	20	16	48	10.5	SP47	AB	No	1	HS20	49
99	20	16	48	10.5	SP47	SB	No	1	HS20	49
100	20	16	48	12.25	SP47	AB	No	1	HS20	49
101	20	16	48	12.25	SP47	SB	No	1	HS20	49
102	20	16	48	12.25	SP47	AB	No	1	HS20	49
103	20	16	48	12.25	SP47	SB	No	1	HS20	49
104	20	16	48	10.5	SP47	SB	No	1	HS20	49
105	20	16	48	10.5	SP47	SB	No	1	HS25	48
106	20	16	48	10.5	SP47	SB	No	1	ML24	47
107	20	16	48	10.5	SP47	SB	No	1	ML24	46
108	20	16	48	10.5	SP47	SB	No	1	HS20	49
109	20	16	48	10.5	SP47	SB	No	1	HS25	48
110	20	16	48	10.5	SP47	SB	No	1	ML24	47
111	20	16	48	10.5	SP47	SB	No	1	HS20	49
112	20	16	48	10.5	SP47	SB	No	1	HS20	49
113	20	16	48	10.5	SP47	SB	No	1	HS20	49
114	20	16	48	10.5	SP47	SB	No	1	HS20	49
115	20	16	48	10.5	SP47	SB	No	1	HS20	49
116	20	16	48	10.5	SP47	SB	No	1	HS20	49
117	20	16	48	10.5	SP47	SB	No	1	HS20	49
118	20	16	48	10.5	SP47	SB	No	1	HS20	49
119	20	16	48	10.5	SP47	SB	No	1	HS20	49
120	20	16	48	10.5	SP47	SB	No	1	HS20	49
121	20	16	48	10.5	SP47	SB	No	1	HS20	49

Table E.3 (Continued) Analyses run for parametric study

Test #	# of TSB (AASHTO Spec.)	TSB #	TSB Spacing (ft)	TSB E (kip/in2)	TSB Depth (in)	TSB Width (in)	TSB I (in4)	TSB EI (kip-in2)
95	1	TSB#sp23	10	1400	5.50	8.25	114.38	160136
96	1	TSB#sp11	10	1400	5.66	3.79	57.27	80174
97	1	TSB#sp11	10	1400	5.66	3.79	57.27	80174
98	1	TSB#sp23	10	1400	5.50	8.25	114.38	160136
99	1	TSB#sp23	10	1400	5.50	8.25	114.38	160136
100	1	TSB#sp11	10	1400	5.66	3.79	57.27	80174
101	1	TSB#sp11	10	1400	5.66	3.79	57.27	80174
102	1	TSB#sp23	10	1400	5.50	8.25	114.38	160136
103	1	TSB#sp23	10	1400	5.50	8.25	114.38	160136
104	1	TSB#sp11	10	1400	5.66	3.79	57.27	80174
105	1	TSB#sp11	10	1400	5.66	3.79	57.27	80174
106	1	TSB#sp11	10	1400	5.66	3.79	57.27	80174
107	1	TSB#sp11	10	1400	5.66	3.79	57.27	80174
108	1	TSB#sp23	10	1400	5.50	8.25	114.38	160136
109	1	TSB#sp23	10	1400	5.50	8.25	114.38	160136
110	1	TSB#sp23	10	1400	5.50	8.25	114.38	160136
111	1	TSB#sp10	10	1400	4.76	3.19	28.67	40138
112	1	TSB#sp11	10	1400	5.66	3.79	57.27	80174
113	1	TSB#sp12	10	1400	6.26	4.19	85.66	119918
114	1	TSB#sp13	10	1400	6.73	4.51	114.56	160387
115	1	TSB#sp14	10	1400	7.11	4.77	142.87	200020
116	1	TSB#sp15	10	1400	4.30	4.30	28.49	39886
117	1	TSB#sp16	10	1400	5.12	5.12	57.27	80173
118	1	TSB#sp17	10	1400	5.66	5.66	85.52	119733
119	1	TSB#sp18	10	1400	6.09	6.09	114.63	160478
120	1	TSB#sp19	10	1400	6.43	6.43	142.45	199430
121	1	TSB#sp20	10	1400	3.89	5.83	28.60	40037

Table E.3 (Continued) Analyses run for parametric study

Test #	Span (ft)	Bridge Width (ft)	Panel Width (in)	Deck Thick-ness (in)	Material	Connec-tion Type	Curbs	No. of Lanes	AASHTO Loading	Load Case #
122	20	16	48	10.5	SP47	SB	No	1	HS20	49
123	20	16	48	10.5	SP47	SB	No	1	HS20	49
124	20	16	48	10.5	SP47	SB	No	1	HS20	49
125	20	16	48	10.5	SP47	SB	No	1	HS20	49
126	20	16	48	10.5	SP47	AB	No	1	HS20	49
127	20	16	48	10.5	SP47	AB	No	1	HS20	49
128	20	16	48	10.5	SP47	AB	No	1	HS20	49
129	20	16	48	10.5	SP47	AB	No	1	HS20	49
130	20	16	48	10.5	SP47	AB	No	1	HS20	49
131	20	16	48	10.5	SP47	AB	No	1	HS20	49
132	20	16	48	10.5	SP47	AB	No	1	HS20	49
133	20	16	48	10.5	SP47	AB	No	1	HS20	49
134	20	16	48	10.5	SP47	AB	No	1	HS20	49
135	20	16	48	10.5	SP47	AB	No	1	HS20	49
136	20	16	48	10.5	SP47	AB	No	1	HS20	49
137	20	16	48	10.5	SP47	AB	No	1	HS20	49
138	20	16	48	10.5	SP47	AB	No	1	HS20	49
139	20	16	48	10.5	SP47	AB	No	1	HS20	49
140	20	16	48	10.5	SP47	AB	No	1	HS20	49
127	20	16	48	10.5	SP47	AB	No	1	HS20	49
141	20	16	48	10.5	SP47	AB	No	1	HS25	48
142	20	16	48	10.5	SP47	AB	No	1	ML24	47
139	20	16	48	10.5	SP47	AB	No	1	HS20	49
143	20	16	48	10.5	SP47	AB	No	1	HS25	48
144	20	16	48	10.5	SP47	AB	No	1	ML24	47
145	20	16	48	10.5	SP47	TB34	No	1	HS20	49

Table E.3 (Continued) Analyses run for parametric study

Test #	# of TSB (AASHTO Spec.)	TSB #	TSB Spacing (ft)	TSB E (kip/in2)	TSB Depth (in)	TSB Width (in)	TSB I (in4)	TSB EI (kip-in2)
122	1	TSB#sp21	10	1400	4.62	6.94	57.03	79842
123	1	TSB#sp22	10	1400	5.12	7.68	85.90	120259
124	1	TSB#sp23	10	1400	5.50	8.25	114.38	160136
125	1	TSB#sp24	10	1400	5.81	8.72	142.52	199522
126	1	TSB#sp10	10	1400	4.76	3.19	28.67	40138
127	1	TSB#sp11	10	1400	5.66	3.79	57.27	80174
128	1	TSB#sp12	10	1400	6.26	4.19	85.66	119918
129	1	TSB#sp13	10	1400	6.73	4.51	114.56	160387
130	1	TSB#sp14	10	1400	7.11	4.77	142.87	200020
131	1	TSB#sp15	10	1400	4.30	4.30	28.49	39886
132	1	TSB#sp16	10	1400	5.12	5.12	57.27	80173
133	1	TSB#sp17	10	1400	5.66	5.66	85.52	119733
134	1	TSB#sp18	10	1400	6.09	6.09	114.63	160478
135	1	TSB#sp19	10	1400	6.43	6.43	142.45	199430
136	1	TSB#sp20	10	1400	3.89	5.83	28.60	40037
137	1	TSB#sp21	10	1400	4.62	6.94	57.03	79842
138	1	TSB#sp22	10	1400	5.12	7.68	85.90	120259
139	1	TSB#sp23	10	1400	5.50	8.25	114.38	160136
140	1	TSB#sp24	10	1400	5.81	8.72	142.52	199522
127	1	TSB#sp11	10	1400	5.66	3.79	57.27	80174
141	1	TSB#sp11	10	1400	5.66	3.79	57.27	80174
142	1	TSB#sp11	10	1400	5.66	3.79	57.27	80174
139	1	TSB#sp23	10	1400	5.50	8.25	114.38	160136
143	1	TSB#sp23	10	1400	5.50	8.25	114.38	160136
144	1	TSB#sp23	10	1400	5.50	8.25	114.38	160136
145	1	TSB5	10	1400	5.75	3.625	57.43	80400

Table E.4 Results of parametric study analyses

Test #	PANELS								Max Cxn Force (kips) (FEA)
	Max Panel Longit. Bending (ksi) (FEA)	F_b (ksi)	ANSYS f_b / F_b	Max Panel Deflec- tion (in) (FEA)	Δ_{all}	FEA Δ / Δ_{all}	Max Relative Panel Displ. (in) (FEA)	Rel Disp / 0.10 in	
1	0.909	1.410	0.65	0.68	0.67	**1.01**	0.125	**1.25**	4.98
2	0.891	1.410	0.63	0.66	0.67	0.99	0.090	0.90	5.36
3	0.883	1.410	0.63	0.65	0.67	0.98	0.076	0.76	5.51
4	0.863	1.410	0.61	0.64	0.67	0.95	0.049	0.49	6.17
5	0.886	1.410	0.63	0.65	0.67	0.98	0.073	0.73	5.52
6	0.875	1.410	0.62	0.65	0.67	0.97	0.067	0.67	5.53
7	0.884	1.410	0.63	0.65	0.67	0.98	0.071	0.71	5.53
8	0.884	1.410	0.63	0.65	0.67	0.98	0.073	0.73	5.52
3	0.883	1.410	0.63	0.65	0.67	0.98	0.076	0.76	5.51
9	0.872	1.410	0.62	0.64	0.67	0.97	0.065	0.65	5.52
10	0.866	1.410	0.61	0.64	0.67	0.96	0.060	0.60	5.51
11	0.863	1.410	0.61	0.64	0.67	0.96	0.058	0.58	5.50
12	0.774	1.410	0.55	1.24	1.17	**1.06**	0.054	0.54	4.65
13	0.688	1.410	0.49	1.10	1.17	0.94	0.023	0.23	3.08
14	0.774	1.410	0.55	1.24	1.17	**1.06**	0.056	0.56	4.63
15	0.689	1.410	0.49	1.10	1.17	0.94	0.024	0.24	3.03
16	0.775	1.410	0.55	1.24	1.17	**1.07**	0.059	0.59	4.61
17	0.690	1.410	0.49	1.10	1.17	0.94	0.027	0.27	3.02
3	0.883	1.410	0.63	0.65	0.67	0.98	0.076	0.76	5.51
18	0.774	1.410	0.55	0.57	0.67	0.85	0.036	0.36	3.63

Table E.4 (Continued) Results of parametric study analyses

Test #	TSB									
	Max TSB Bending Moment (kip-in) (FEA)	Max TSB Bending Stress (ksi) (FEA)	TSB F_b (ksi)	FEA TSB fb / Fb	Max TSB Shear (kips) (FEA)	Max TSB Shear Stress (ksi) (FEA)	TSB F_v (ksi)	FEA TSB fv / Fv	b/d Ratio	Ratio of TSB EI to Min. EI
1	22.6	1.131	1.120	**1.01**	5.14	0.370	0.270	**1.37**	0.63	1.01
2	21.4	1.071	1.120	0.96	5.37	0.386	0.270	**1.43**	0.63	1.01
3	21.5	1.076	1.120	0.96	5.46	0.393	0.270	**1.46**	0.63	1.01
4	21.8	1.091	1.120	0.97	5.70	0.410	0.270	**1.52**	0.63	1.01
5	22.4	0.983	1.120	0.88	5.48	0.271	0.270	**1.00**	1.50	0.90
6	25.2	0.820	1.120	0.73	5.53	0.270	0.270	1.00	0.85	1.61
7	22.7	0.916	1.120	0.82	5.49	0.256	0.270	0.95	1.50	1.00
8	21.8	0.977	1.120	0.87	5.48	0.314	0.270	**1.16**	1.00	1.00
3	21.5	1.076	1.120	0.96	5.46	0.393	0.270	**1.46**	0.63	1.01
9	28.3	0.828	1.120	0.74	5.54	0.274	0.270	**1.01**	0.67	2.02
10	32.8	0.709	1.120	0.63	5.57	0.224	0.270	0.83	0.67	3.02
11	36.1	0.633	1.120	0.56	5.58	0.196	0.270	0.72	0.67	3.99
12	20.2	0.815	1.120	0.73	4.57	0.213	0.270	0.79	1.50	1.00
13	24.8	1.001	1.120	0.89	3.32	0.155	0.270	0.57	1.50	1.00
14	19.5	0.872	1.120	0.78	4.54	0.260	0.270	0.96	1.00	1.00
15	24.2	1.082	1.120	0.97	3.29	0.188	0.270	0.70	1.00	1.00
16	18.5	0.926	1.120	0.83	4.50	0.324	0.270	**1.20**	0.63	1.01
17	23.5	1.176	1.120	**1.05**	3.23	0.232	0.270	0.86	0.63	1.01
3	21.5	1.076	1.120	0.96	5.46	0.393	0.270	1.46	0.63	1.01
18	30.9	1.547	1.120	**1.38**	3.97	0.286	0.270	**1.06**	0.63	1.01

Table E.4 (Continued) Results of parametric study analyses

Test #	WLF	Live Load Information			TSB Information		Calc. TSB Shear WLF {TSB shear/Wheel Load}	Calc. TSB Moment Arm (in) {TSB moment/Wheel Load}
		AASHTO Loading	Tire Load (kips) (ML adj. bc wheels are so close)	Loading #	Max TSB Shear (kips) (FEA)	Max TSB Bending Moment (kip-in) (FEA)		
1	0.705	HS20	16	1	5.14	22.6	0.32	1.4
2	0.705	HS20	16	1	5.37	21.4	0.34	1.3
3	0.705	HS20	16	1	5.46	21.5	0.34	1.3
4	0.705	HS20	16	1	5.70	21.8	0.36	1.4
5	0.705	HS20	16	1	5.48	22.401	0.34	1.4
6	0.705	HS20	16	1	5.53	25.2	0.35	1.6
7	0.705	HS20	16	1	5.49	22.7	0.34	1.4
8	0.705	HS20	16	1	5.48	21.847	0.34	1.4
3	0.705	HS20	16	1	5.46	21.5	0.34	1.3
9	0.705	HS20	16	1	5.54	28.3	0.35	1.8
10	0.705	HS20	16	1	5.57	32.8	0.35	2.1
11	0.705	HS20	16	1	5.58	36.1	0.35	2.3
12	0.636	HS20	16	5	4.57	20.2	0.29	1.3
13	0.636	HS20	16	6	3.32	24.8	0.21	1.6
14	0.636	HS20	16	5	4.54	19.5	0.28	1.2
15	0.636	HS20	16	6	3.29	24.2	0.21	1.5
16	0.636	HS20	16	5	4.50	18.5	0.28	1.2
17	0.636	HS20	16	6	3.23	23.5	0.20	1.5
3	0.705	HS20	16	1	5.46	21.5	0.34	1.3
18	0.705	HS20	16	2	3.97	30.9	0.25	1.9

Table E.4 (Continued) Results of parametric study analyses

Test #	PANELS								Max Cxn Force (kips) (FEA)
	Max Panel Longit. Bending (ksi) (FEA)	F`b (ksi)	ANSYS fb / Fb	Max Panel Deflec- tion (in) (FEA)	$\Delta\alpha\lambda\lambda$	FEA D / Dall	Max Relative Panel Displ. (in) (FEA)	Rel Disp / 0.10 In	
19	0.518	1.410	0.37	0.48	0.67	0.71	0.162	**1.62**	3.83
20	0.407	1.410	0.29	0.42	0.67	0.63	0.102	**1.02**	2.54
21	0.935	1.410	0.66	0.73	0.67	**1.09**	0.068	0.68	4.91
22	0.695	1.410	0.49	0.52	0.67	0.78	0.048	0.48	4.14
16	0.775	1.410	0.55	1.24	1.17	1.07	0.059	0.59	4.61
17	0.690	1.410	0.49	1.11	1.17	0.95	0.027	0.27	3.02
23	0.382	1.410	0.27	0.89	1.17	0.76	0.061	0.61	4.60
24	0.323	1.410	0.23	0.78	1.17	0.67	0.032	0.32	3.18
25	0.556	1.410	0.39	1.15	1.17	0.98	0.076	0.76	3.55
26	0.867	1.410	0.61	1.84	1.17	**1.58**	0.076	0.76	4.86
27	0.930	1.410	0.66	1.70	1.17	**1.46**	0.072	0.72	4.97
28	0.827	1.410	0.59	1.51	1.17	**1.29**	0.036	0.36	3.05
29	0.892	1.410	0.63	1.97	1.17	**1.69**	0.078	0.78	4.73
27	0.930	1.410	0.66	1.70	1.17	**1.46**	0.072	0.72	4.97
30	0.960	1.410	0.68	1.70	1.17	**1.46**	0.072	0.72	4.96
31	0.914	1.410	0.65	1.70	1.17	**1.46**	0.072	0.72	4.97
32	0.662	1.410	0.47	1.21	1.17	**1.04**	0.055	0.55	3.98
33	0.844	1.410	0.60	0.63	0.67	0.94	0.064	0.64	5.06
34	0.797	1.410	0.57	0.60	0.67	0.91	0.070	0.70	5.39
35	0.717	1.410	0.51	0.54	0.67	0.81	0.093	0.93	6.26
36	0.788	1.410	0.56	0.61	0.67	0.91	0.071	0.71	5.51
37	0.972	1.410	0.69	0.75	0.67	**1.12**	0.049	0.49	3.76
38	0.694	1.410	0.49	0.53	0.67	0.80	0.065	0.65	4.45
39	0.807	1.410	0.57	0.61	0.67	0.92	0.065	0.65	5.05

Table E.4 (Continued) Results of parametric study analyses

Test #	TSB									
	Max TSB Bending Moment (klp-in) (FEA)	Max TSB Bending Stress (ksi) (FEA)	TSB Fb (ksl)	FEA TSB fb / Fb	Max TSB Shear (kips) (FEA)	Max TSB Shear Stress (ksi) (FEA)	TSB Fv (ksi)	FEA TSB fv / Fv	b/d Ratio	Ratio of TSB EI to Min. EI
19	13.5	0.676	1.120	0.60	3.73	0.268	0.270	0.99	0.63	1.01
20	19.1	0.956	1.120	0.85	2.69	0.194	0.270	0.72	0.63	1.01
21	22.1	1.106	1.120	0.99	5.18	0.373	0.270	**1.38**	0.63	1.01
22	35.7	1.787	1.120	**1.60**	4.57	0.329	0.270	**1.22**	0.63	1.01
16	18.5	0.926	1.120	0.83	4.50	0.324	0.270	1.20	0.63	1.01
17	23.5	1.176	1.120	1.05	3.23	0.232	0.270	0.86	0.63	1.01
23	17.1	0.856	1.120	0.76	4.53	0.326	0.270	**1.21**	0.63	1.01
24	20.7	1.036	1.120	0.93	3.28	0.236	0.270	0.87	0.63	1.01
25	14	0.701	1.120	0.63	3.41	0.245	0.270	0.91	0.63	1.01
26	20.3	1.016	1.120	0.91	4.62	0.332	0.270	**1.23**	0.63	1.01
27	20.8	1.041	1.120	0.93	4.78	0.344	0.270	**1.27**	0.63	1.01
28	27.4	1.372	1.120	**1.22**	3.41	0.245	0.270	0.91	0.63	1.01
29	19	0.951	1.120	0.85	4.53	0.326	0.270	**1.21**	0.63	1.01
27	20.8	1.041	1.120	0.93	4.78	0.344	0.270	**1.27**	0.63	1.01
30	20.5	1.026	1.120	0.92	4.76	0.343	0.270	**1.27**	0.63	1.01
31	20.8	1.041	1.120	0.93	4.78	0.344	0.270	**1.27**	0.63	1.01
32	35.6	1.782	1.120	**1.59**	4.41	0.317	0.270	**1.18**	0.63	1.01
33	26.1	1.307	1.120	**1.17**	4.33	0.312	0.270	**1.15**	0.63	1.01
34	21.6	1.081	1.120	0.97	5.20	0.374	0.270	1.39	0.63	1.01
35	30.5	1.527	1.120	**1.36**	6.17	0.444	0.270	**1.64**	0.63	1.01
36	24	1.201	1.120	**1.07**	5.43	0.391	0.270	**1.45**	0.63	1.01
37	25.5	1.277	1.120	**1.14**	2.89	0.208	0.270	0.77	0.63	1.01
38	23.1	1.156	1.120	**1.03**	4.45	0.320	0.270	**1.19**	0.63	1.01
39	20.1	1.006	1.120	0.90	5.07	0.365	0.270	**1.35**	0.63	1.01

Table E.4 (Continued) Results of parametric study analyses

Test #	WLF	Live Load Information			TSB Information		Calc. TSB Shear WLF {TSB shear/Wheel Load}	Calc. TSB Moment Arm (in) {TSB moment/Wheel Load}
		AASHTO Loading	Tire Load (kips) (ML adj. bc wheels are so close)	Loading #	Max TSB Shear (kips) (FEA)	Max TSB Bending Moment (kip-in) (FEA)		
19	0.705	HS20	16	3	3.73	13.5	0.23	0.8
20	0.705	HS20	16	4	2.69	19.1	0.17	1.2
21	0.784	HS20	16	26	5.18	22.1	0.32	1.4
22	0.705	HS20	16	27	4.57	35.7	0.29	2.2
16	0.636	HS20	16	5	4.50	18.5	0.28	1.2
17	0.636	HS20	16	6	3.23	23.5	0.20	1.5
23	0.636	HS20	16	7	4.53	17.1	0.28	1.1
24	0.636	HS20	16	8	3.28	20.7	0.21	1.3
25	0.636	HS20	16	9	3.41	14	0.21	0.9
26	0.636	HS20	16	10	4.62	20.3	0.29	1.3
27	0.636	HS20	16	12	4.78	20.8	0.30	1.3
28	0.636	HS20	16	11	3.41	27.4	0.21	1.7
29	0.636	HS20	16	13	4.53	19	0.28	1.2
27	0.636	HS20	16	12	4.78	20.8	0.30	1.3
30	0.636	HS20	16	14	4.76	20.5	0.30	1.3
31	0.636	HS20	16	15	4.78	20.8	0.30	1.3
32	0.636	HS20	16	29	4.41	35.6	0.28	2.2
33	0.806	HS20	16	17	4.33	26.1	0.27	1.6
34	0.806	HS20	16	18	5.20	21.6	0.33	1.4
35	0.806	HS20	16	19	6.17	30.5	0.39	1.9
36	0.806	HS20	16	21	5.43	24	0.34	1.5
37	0.896	HS20	16	24	2.89	25.5	0.18	1.6
38	0.806	HS20	16	25	4.45	23.1	0.28	1.4
39	0.896	HS20	16	28	5.07	20.1	0.32	1.3

Table E.4 (Continued) Results of parametric study analyses

Test #	PANELS								Max Cxn Force (kips) (FEA)
	Max Panel Longit. Bending (ksi) (FEA)	F`b (ksi)	ANSYS fb / Fb	Max Panel Deflec- tion (in) (FEA)	Δallow	FEA D / Dall	Max Relative Panel Displ. (in) (FEA)	Rel Disp / 0.10 in	
40	0.756	1.410	0.54	1.37	1.17	**1.17**	0.073	0.73	5.34
41	0.847	1.410	0.60	0.63	0.67	0.94	0.049	0.49	4.35
42	0.768	1.410	0.55	0.59	0.67	0.88	0.066	0.66	5.30
43	0.955	1.410	0.68	0.74	0.67	**1.11**	0.054	0.54	4.44
44	0.696	1.410	0.49	0.53	0.67	0.79	0.056	0.56	4.19
45	1.057	1.410	0.75	0.97	0.67	**1.46**	0.098	0.98	6.36
35	0.717	1.410	0.51	0.54	0.67	0.81	0.093	0.93	6.26
46	0.546	1.410	0.39	0.36	0.67	0.54	0.087	0.87	6.03
47	0.422	1.410	0.30	0.24	0.67	0.36	0.081	0.81	5.66
48	0.704	1.410	0.50	0.70	0.67	**1.06**	0.099	0.99	6.35
35	0.717	1.410	0.51	0.54	0.67	0.81	0.093	0.93	6.26
49	0.729	1.410	0.52	0.44	0.67	0.66	0.088	0.88	6.17
50	0.739	1.410	0.52	0.37	0.67	0.56	0.085	0.85	6.08
51	0.725	1.410	0.51	0.55	0.67	0.82	0.102	**1.02**	6.28
35	0.717	1.410	0.51	0.54	0.67	0.81	0.093	0.93	6.26
52	0.712	1.410	0.51	0.53	0.67	0.80	0.087	0.87	6.23
53	0.708	1.410	0.50	0.53	0.67	0.80	0.082	0.82	6.20
56	0.712	1.410	0.50	0.53	0.67	0.80	0.067	0.67	7.30
57	0.694	1.410	0.49	0.52	0.67	0.78	0.053	0.53	6.82
58	0.685	1.410	0.49	0.51	0.67	0.77	0.046	0.46	6.72
59	0.678	1.410	0.48	0.51	0.67	0.77	0.041	0.41	6.66
60	0.674	1.410	0.48	0.51	0.67	0.76	0.039	0.39	6.60
61	0.712	1.410	0.50	0.53	0.67	0.79	0.061	0.61	7.24
62	0.695	1.410	0.49	0.52	0.67	0.78	0.048	0.48	6.78

Table E.4 (Continued) Results of parametric study analyses

Test #	TSB									
	Max TSB Bending Moment (kip-in) (FEA)	Max TSB Bending Stress (ksi) (FEA)	TSB Fb (ksi)	FEA TSB fb / Fb	Max TSB Shear (kips) (FEA)	Max TSB Shear Stress (ksi) (FEA)	TSB Fv (ksi)	FEA TSB fv / Fv	b/d Ratio	Ratio of TSB EI to Min. EI
40	27.2	1.362	1.120	**1.22**	5.28	0.380	0.270	**1.41**	0.63	1.01
41	28.4	1.422	1.120	**1.27**	4.46	0.321	0.270	**1.19**	0.63	1.01
42	21.8	1.091	1.120	0.97	5.15	0.371	0.270	**1.37**	0.63	1.01
43	16.3	0.816	1.120	0.73	4.11	0.296	0.270	**1.10**	0.63	1.01
44	24.4	1.222	1.120	**1.09**	4.21	0.303	0.270	**1.12**	0.63	1.01
45	38.1	1.907	1.120	**1.70**	6.48	0.466	0.270	**1.73**	0.63	1.01
35	30.5	1.527	1.120	**1.36**	6.17	0.444	0.270	**1.64**	0.63	1.01
46	25.9	1.297	1.120	**1.16**	5.84	0.420	0.270	**1.56**	0.63	1.01
47	21.9	1.096	1.120	0.98	5.41	0.389	0.270	**1.44**	0.63	1.01
48	32.8	1.642	1.120	**1.47**	6.31	0.454	0.270	**1.68**	0.63	1.01
35	30.5	1.527	1.120	**1.36**	6.17	0.444	0.270	**1.64**	0.63	1.01
49	28.9	1.447	1.120	**1.29**	6.05	0.435	0.270	**1.61**	0.63	1.01
50	27.5	1.377	1.120	**1.23**	5.92	0.426	0.270	**1.58**	0.63	1.01
51	27.8	1.392	1.120	**1.24**	6.10	0.439	0.270	**1.63**	0.63	0.75
35	30.5	1.527	1.120	**1.36**	6.17	0.444	0.270	**1.64**	0.63	1.01
52	32.8	1.642	1.120	**1.47**	6.21	0.447	0.270	**1.66**	0.63	1.26
53	34.9	1.747	1.120	1.56	6.25	0.450	0.270	1.67	0.63	1.51
56	22.9	1.901	1.120	**1.70**	6.36	0.628	0.270	**2.33**	0.67	0.50
57	28.2	1.394	1.120	**1.24**	6.47	0.452	0.270	**1.68**	0.67	1.00
58	34.7	1.268	1.120	**1.13**	6.53	0.373	0.270	**1.38**	0.67	1.50
59	39.7	1.166	1.120	**1.04**	6.57	0.325	0.270	**1.20**	0.67	2.00
60	43.9	1.092	1.120	0.98	6.59	0.291	0.270	**1.08**	0.67	2.50
61	24.5	1.849	1.120	**1.65**	6.40	0.519	0.270	**1.92**	1.00	0.50
62	29	1.296	1.120	**1.16**	6.51	0.373	0.270	**1.38**	1.00	1.00

Table E.4 (Continued) Results of parametric study analyses

Test #	WLF	Live Load Information			TSB Information		Calc. TSB Shear WLF {TSB shear/Wheel Load}	Calc. TSB Moment Arm (in) {TSB moment/Wheel Load}
		AASHTO Loading	Tire Load (kips) (ML adj. bc wheels are so close)	Loading #	Max TSB Shear (kips) (FEA)	Max TSB Bending Moment (kip-in) (FEA)		
40	0.727	HS20	16	30	5.28	27.2	0.33	1.7
41	0.906	HS20	16	16	4.46	28.4	0.28	1.8
42	0.906	HS20	16	20	5.15	21.8	0.32	1.4
43	1.008	HS20	16	22	4.11	16.3	0.26	1.0
44	0.906	HS20	16	23	4.21	24.4	0.26	1.5
45	0.806	HS20	16	19	6.48	38.1	0.41	2.4
35	0.806	HS20	16	19	6.17	30.5	0.39	1.9
46	0.806	HS20	16	19	5.84	25.9	0.37	1.6
47	0.806	HS20	16	19	5.41	21.9	0.34	1.4
48	0.806	HS20	16	19	6.31	32.8	0.39	2.1
35	0.806	HS20	16	19	6.17	30.5	0.39	1.9
49	0.806	HS20	16	19	6.05	28.9	0.38	1.8
50	0.806	HS20	16	19	5.92	27.5	0.37	1.7
51	0.806	HS20	16	19	6.10	27.8	0.38	1.7
35	0.806	HS20	16	19	6.17	30.5	0.39	1.9
52	0.806	HS20	16	19	6.21	32.8	0.39	2.1
53	0.806	HS20	16	19	6.25	34.9	0.39	2.2
56	0.806	HS20	16	19	6.36	22.9	0.40	1.4
57	0.806	HS20	16	19	6.47	28.2	0.40	1.8
58	0.806	HS20	16	19	6.53	34.7	0.41	2.2
59	0.806	HS20	16	19	6.57	39.7	0.41	2.5
60	0.806	HS20	16	19	6.59	43.9	0.41	2.7
61	0.806	HS20	16	19	6.40	24.5	0.40	1.5
62	0.806	HS20	16	19	6.51	29	0.41	1.8

Table E.4 (Continued) Results of parametric study analyses

Test #	PANELS								Max Cxn Force (kips) (FEA)
	Max Panel Longit. Bending (ksi) (FEA)	F`b (ksi)	ANSYS fb / Fb	Max Panel Deflec- tion (in) (FEA)	Δαλλ	FEA D / Dall	Max Relative Panel Displ. (in) (FEA)	Rel Disp / 0.10 in	
63	0.685	1.410	0.49	0.51	0.67	0.77	0.042	0.42	6.71
64	0.679	1.410	0.48	0.51	0.67	0.76	0.038	0.38	6.64
65	0.674	1.410	0.48	0.51	0.67	0.76	0.036	0.36	6.58
66	0.711	1.410	0.50	0.52	0.67	0.79	0.056	0.56	7.18
67	0.696	1.410	0.49	0.51	0.67	0.77	0.044	0.44	6.76
68	0.686	1.410	0.49	0.51	0.67	0.76	0.039	0.39	6.69
69	0.680	1.410	0.48	0.51	0.67	0.76	0.035	0.35	6.62
70	0.676	1.410	0.48	0.50	0.67	0.76	0.033	0.33	6.55
71	0.694	1.410	0.49	0.52	0.67	0.78	0.053	0.53	6.82
72	0.753	1.410	0.53	0.57	0.67	0.85	0.164	**1.64**	5.49
73	0.522	1.410	0.37	0.34	0.67	0.51	0.050	0.50	6.95
74	0.578	1.410	0.41	0.38	0.67	0.57	0.143	1.43	5.18
75	0.680	1.410	0.48	0.51	0.67	0.76	0.035	0.35	6.62
76	0.736	1.410	0.52	0.55	0.67	0.83	0.137	**1.37**	5.36
77	0.508	1.410	0.36	0.33	0.67	0.49	0.034	0.34	6.67
78	0.563	1.410	0.40	0.37	0.67	0.55	0.123	**1.23**	5.12
40	0.756	1.410	0.54	1.37	1.17	**1.17**	0.073	0.73	5.34
80	0.700	1.410	0.50	1.49	1.17	**1.28**	0.083	0.83	5.20
81	0.719	1.410	0.51	1.58	1.17	**1.36**	0.081	0.81	5.04
82	0.616	1.410	0.44	1.40	1.17	**1.20**	0.067	0.67	5.06
83	0.785	1.410	0.56	1.48	1.17	**1.27**	0.101	**1.01**	6.54
84	0.788	1.410	0.56	1.46	1.17	**1.25**	0.112	**1.12**	6.33
85	0.723	1.410	0.51	1.31	1.17	**1.12**	0.075	0.75	5.07
86	0.576	1.410	0.41	0.92	1.17	0.79	0.044	0.44	6.21

Table E.4 (Continued) Results of parametric study analyses

Test #	TSB									
	Max TSB Bending Moment (kip-in) (FEA)	Max TSB Bending Stress (ksi) (FEA)	TSB Fb (ksi)	FEA TSB fb / Fb	Max TSB Shear (kips) (FEA)	Max TSB Shear Stress (ksi) (FEA)	TSB Fv (ksi)	FEA TSB fv / Fv	b/d Ratio	Ratio of TSB EI to Min. EI
63	32.7	1.082	1.120	0.97	6.56	0.307	0.270	**1.14**	1.00	1.50
64	38	1.009	1.120	0.90	6.59	0.267	0.270	0.99	1.00	2.01
65	42.1	0.950	1.120	0.85	6.62	0.240	0.270	0.89	1.00	2.49
66	26.1	1.775	1.120	**1.58**	6.45	0.427	0.270	**1.58**	1.50	0.50
67	30.4	1.231	1.120	**1.10**	6.54	0.306	0.270	**1.13**	1.50	1.00
68	33.4	0.995	1.120	0.89	6.59	0.251	0.270	0.93	1.50	1.50
69	36.2	0.870	1.120	0.78	6.62	0.219	0.270	0.81	1.50	2.00
70	40.2	0.819	1.120	0.73	6.64	0.197	0.270	0.73	1.50	2.49
71	28.2	1.394	1.120	**1.24**	6.47	0.452	0.270	**1.68**	0.67	1.00
72	33.8	1.670	1.120	**1.49**	5.66	0.396	0.270	**1.47**	0.67	1.00
73	24.6	1.216	1.120	**1.09**	6.26	0.438	0.270	**1.62**	0.67	1.00
74	28.3	1.399	1.120	1.25	5.23	0.366	0.270	1.35	0.67	1.00
75	36.2	0.870	1.120	0.78	6.62	0.219	0.270	0.81	1.50	2.00
76	45.2	1.087	1.120	0.97	5.85	0.193	0.270	0.72	1.50	2.00
77	31.6	0.760	1.120	0.68	6.46	0.214	0.270	0.79	1.50	2.00
78	38.1	0.916	1.120	0.82	5.45	0.180	0.270	0.67	1.50	2.00
40	27.2	1.362	1.120	**1.22**	5.28	0.380	0.270	**1.41**	0.63	1.01
80	26.9	1.347	1.120	**1.20**	5.16	0.371	0.270	**1.38**	0.63	1.01
81	25.1	1.257	1.120	**1.12**	4.97	0.358	0.270	**1.32**	0.63	1.01
82	24.2	1.212	1.120	**1.08**	4.97	0.358	0.270	**1.32**	0.63	1.01
83	33.4	1.672	1.120	**1.49**	6.48	0.466	0.270	**1.73**	0.63	1.01
84	32.1	1.607	1.120	**1.43**	6.27	0.451	0.270	**1.67**	0.63	1.01
85	25.2	1.262	1.120	**1.13**	4.73	0.340	0.270	**1.26**	0.63	1.01
86	21.1	1.043	1.120	0.93	5.49	0.384	0.270	**1.42**	0.67	1.00

Table E.4 (Continued) Results of parametric study analyses

Test #	WLF	Live Load Information			TSB Information		Calc. TSB Shear WLF (TSB shear/Wheel Load)	Calc. TSB Moment Arm (in) (TSB moment/Wheel Load)
		AASHTO Loading	Tire Load (kips) (ML adj. bc wheels are so close)	Loading #	Max TSB Shear (kips) (FEA)	Max TSB Bending Moment (kip-in) (FEA)		
63	0.806	HS20	16	19	6.56	32.7	0.41	2.0
64	0.806	HS20	16	19	6.59	38	0.41	2.4
65	0.806	HS20	16	19	6.62	42.1	0.41	2.6
66	0.806	HS20	16	19	6.45	26.1	0.40	1.6
67	0.806	HS20	16	19	6.54	30.4	0.41	1.9
68	0.806	HS20	16	19	6.59	33.4	0.41	2.1
69	0.806	HS20	16	19	6.62	36.2	0.41	2.3
70	0.806	HS20	16	19	6.64	40.2	0.42	2.5
71	0.806	HS20	16	19	6.47	28.2	0.40	1.8
72	0.806	HS20	16	19	5.66	33.8	0.35	2.1
73	0.806	HS20	16	19	6.26	24.6	0.39	1.5
74	0.806	HS20	16	19	5.23	28.3	0.33	1.8
75	0.806	HS20	16	19	6.62	36.2	0.41	2.3
76	0.806	HS20	16	19	5.85	45.2	0.37	2.8
77	0.806	HS20	16	19	6.46	31.6	0.40	2.0
78	0.806	HS20	16	19	5.45	38.1	0.34	2.4
40	0.727	HS20	16	30	5.28	27.2	0.33	1.7
80	0.727	HS20	16	34	5.16	26.9	0.32	1.7
81	0.727	HS20	16	33	4.97	25.1	0.31	1.6
82	0.727	HS20	16	35	4.97	24.2	0.31	1.5
83	0.727	ML24	21	36	6.48	33.4	0.31	1.6
84	0.727	ML24	21	37	6.27	32.1	0.30	1.5
85	0.727	LL26	13	38	4.73	25.2	0.36	1.9
86	0.800	HS20	16	39	5.49	21.1	0.34	1.3

Table E.4 (Continued) Results of parametric study analyses

Test #	PANELS								Max Cxn Force (kips) (FEA)
	Max Panel Longit. Bending (ksi) (FEA)	F`b (ksi)	ANSYS fb / Fb	Max Panel Deflec- tion (in) (FEA)	Δαλλ	FEA D / Dall	Max Relative Panel Displ. (in) (FEA)	Rel Disp / 0.10 in	
87	0.722	1.410	0.51	1.15	1.17	0.99	0.056	0.56	7.53
88	0.596	1.410	0.42	1.00	1.17	0.85	0.059	0.59	7.87
89	0.747	1.410	0.53	1.25	1.17	**1.07**	0.077	0.77	9.51
90	0.686	1.410	0.49	0.53	0.67	0.80	0.071	0.71	3.82
91	0.867	1.410	0.61	0.67	0.67	**1.01**	0.102	**1.02**	4.59
92	0.828	1.410	0.59	0.77	0.67	**1.15**	0.137	**1.37**	5.05
93	0.675	1.410	0.48	0.49	0.67	0.74	0.030	0.30	4.78
94	0.843	1.410	0.60	0.61	0.67	0.92	0.037	0.37	6.03
95	0.821	1.410	0.58	0.69	0.67	1.04	0.048	0.48	6.42
96	-	-	-	-	-	-	0.179	**1.79**	-
97	-	-	-	-	-	-	0.154	**1.54**	-
98	-	-	-	-	-	-	0.171	**1.71**	-
99	-	-	-	-	-	-	0.145	**1.45**	-
100	-	-	-	-	-	-	0.127	**1.27**	-
101	-	-	-	-	-	-	0.104	**1.04**	-
102	-	-	-	-	-	-	0.120	**1.20**	-
103	-	-	-	-	-	-	0.096	0.96	-
104	-	-	-	-	-	-	0.154	**1.54**	-
105	-	-	-	-	-	-	0.193	**1.93**	-
106	-	-	-	-	-	-	0.183	**1.83**	-
107	-	-	-	-	-	-	0.163	**1.63**	-
108	-	-	-	-	-	-	0.145	**1.45**	-
109	-	-	-	-	-	-	0.145	**1.45**	-
110	-	-	-	-	-	-	0.145	1.45	-

Table E.4 (Continued) Results of parametric study analyses

Test #	TSB									
	Max TSB Bending Moment (kip-in) (FEA)	Max TSB Bending Stress (ksi) (FEA)	TSB Fb (ksi)	FEA TSB fb / Fb	Max TSB Shear (kips) (FEA)	Max TSB Shear Stress (ksi) (FEA)	TSB Fv (ksi)	FEA TSB fv / Fv	b/d Ratio	Ratio of TSB EI to Min. EI
87	26.4	1.305	1.120	**1.16**	6.78	0.474	0.270	**1.76**	0.67	1.00
88	26.5	1.310	1.120	**1.17**	7.00	0.489	0.270	**1.81**	0.67	1.00
89	33.1	1.636	1.120	**1.46**	8.61	0.602	0.270	**2.23**	0.67	1.00
90	36.5	1.804	1.120	**1.61**	4.37	0.306	0.270	**1.13**	0.67	1.00
91	46.4	2.293	1.120	**2.05**	5.35	0.374	0.270	**1.39**	0.67	1.00
92	52	2.570	1.120	**2.29**	5.94	0.415	0.270	**1.54**	0.67	1.00
93	50.4	1.212	1.120	**1.08**	5.64	0.186	0.270	0.69	1.50	2.00
94	63.1	1.517	1.120	**1.35**	7.08	0.234	0.270	0.87	1.50	2.00
95	68.7	1.652	1.120	1.47	7.60	0.251	0.270	0.93	1.50	2.00
96	-	-	-	-	-	-	-	-	0.67	1.00
97	-	-	-	-	-	-	-	-	0.67	1.00
98	-	-	-	-	-	-	-	-	1.50	2.00
99	-	-	-	-	-	-	-	-	1.50	2.00
100	-	-	-	-	-	-	-	-	0.67	1.00
101	-	-	-	-	-	-	-	-	0.67	1.00
102	-	-	-	-	-	-	-	-	1.50	2.00
103	-	-	-	-	-	-	-	-	1.50	2.00
104	-	-	-	-	-	-	-	-	0.67	1.00
105	-	-	-	-	-	-	-	-	0.67	1.00
106	-	-	-	-	-	-	-	-	0.67	1.00
107	-	-	-	-	-	-	-	-	0.67	1.00
108	-	-	-	-	-	-	-	-	1.50	2.00
109	-	-	-	-	-	-	-	-	1.50	2.00
110	-	-	-	-	-	-	-	-	1.50	2.00

Table E.4 (Continued) Results of parametric study analyses

Test #	WLF	Live Load Information			TSB Information		Calc. TSB Shear WLF {TSB shear/Wheel Load}	Calc. TSB Moment Arm (in) {TSB moment/Wheel Load}
		AASHTO Loading	Tire Load (kips) (ML adj. bc wheels are so close)	Loading #	Max TSB Shear (kips) (FEA)	Max TSB Bending Moment (kip-in) (FEA)		
87	0.800	HS25	20	40	6.78	26.4	0.34	1.3
88	0.800	ML24	21	42	7.00	26.5	0.33	1.3
89	0.800	ML30	26	41	8.61	33.1	0.33	1.3
90	0.705	HS20	16	45	4.37	36.5	0.27	2.3
91	0.705	HS25	20	44	5.35	46.4	0.27	2.3
92	0.705	ML24	21	43	5.94	52	0.28	2.5
93	0.705	HS20	16	45	5.64	50.4	0.35	3.2
94	0.705	HS25	20	44	7.08	63.1	0.35	3.2
95	0.705	ML24	21	43	7.60	68.7	0.36	3.3
96	0.806	HS20	16	49	-	-		
97	0.806	HS20	16	49	-	-		
98	0.806	HS20	16	49	-	-		
99	0.806	HS20	16	49	-	-		
100	0.806	HS20	16	49	-	-		
101	0.806	HS20	16	49	-	-		
102	0.806	HS20	16	49	-	-		
103	0.806	HS20	16	49	-	-		
104	0.806	HS20	16	49	-	-		
105	0.806	HS25	20	48	-	-		
106	0.806	ML24	21	47	-	-		
107	0.806	ML24	21	46	-	-		
108	0.806	HS20	16	49	-	-		
109	0.806	HS25	20	48	-	-		
110	0.806	ML24	21	47	-	-		

Table E.4 (Continued) Results of parametric study analyses

Test #	PANELS								Max Cxn Force (kips) (FEA)
	Max Panel Longit. Bending (ksi) (FEA)	F`b (ksi)	ANSYS fb / Fb	Max Panel Deflec- tion (in) (FEA)	$\Delta\alpha\lambda\lambda$	FEA D / Dall	Max Relative Panel Displ. (in) (FEA)	Rel Disp / 0.10 in	
111	-	-	-	-	-	-	0.160	1.60	-
112	-	-	-	-	-	-	0.154	1.54	-
113	-	-	-	-	-	-	0.150	1.50	-
114	-	-	-	-	-	-	0.148	1.48	-
115	-	-	-	-	-	-	0.146	1.48	-
116	-	-	-	-	-	-	0.157	1.57	-
117	-	-	-	-	-	-	0.152	1.52	-
118	-	-	-	-	-	-	0.148	1.48	-
119	-	-	-	-	-	-	0.146	1.46	-
120	-	-	-	-	-	-	0.145	1.45	-
121	-	-	-	-	-	-	0.155	1.55	-
122	-	-	-	-	-	-	0.150	1.50	-
123	-	-	-	-	-	-	0.147	1.47	-
124	-	-	-	-	-	-	0.145	1.45	-
125	-	-	-	-	-	-	0.144	1.44	-
126	-	-	-	-	-	-	0.186	1.86	-
127	-	-	-	-	-	-	0.179	1.79	-
128	-	-	-	-	-	-	0.175	1.75	-
129	-	-	-	-	-	-	0.173	1.73	-
130	-	-	-	-	-	-	0.172	1.72	-
131	-	-	-	-	-	-	0.184	1.84	-
132	-	-	-	-	-	-	0.177	1.77	-
133	-	-	-	-	-	-	0.174	1.74	-

Table E.4 (Continued) Results of parametric study analyses

Test #	TSB									
	Max TSB Bending Moment (kip-in) (FEA)	Max TSB Bending Stress (ksi) (FEA)	TSB Fb (ksi)	FEA TSB fb / Fb	Max TSB Shear (kips) (FEA)	Max TSB Shear Stress (ksi) (FEA)	TSB Fv (ksi)	FEA TSB fv / Fv	b/d Ratio	Ratio of TSB EI to Min. EI
111	-	-	-	-	-	-	-	-	0.67	0.50
112	-	-	-	-	-	-	-	-	0.67	1.00
113	-	-	-	-	-	-	-	-	0.67	1.50
114	-	-	-	-	-	-	-	-	0.67	2.00
115	-	-	-	-	-	-	-	-	0.67	2.50
116	-	-	-	-	-	-	-	-	1.00	0.50
117	-	-	-	-	-	-	-	-	1.00	1.00
118	-	-	-	-	-	-	-	-	1.00	1.50
119	-	-	-	-	-	-	-	-	1.00	2.01
120	-	-	-	-	-	-	-	-	1.00	2.49
121	-	-	-	-	-	-	-	-	1.50	0.50
122	-	-	-	-	-	-	-	-	1.50	1.00
123	-	-	-	-	-	-	-	-	1.50	1.50
124	-	-	-	-	-	-	-	-	1.50	2.00
125	-	-	-	-	-	-	-	-	1.50	2.49
126	-	-	-	-	-	-	-	-	0.67	0.50
127	-	-	-	-	-	-	-	-	0.67	1.00
128	-	-	-	-	-	-	-	-	0.67	1.50
129	-	-	-	-	-	-	-	-	0.67	2.00
130	-	-	-	-	-	-	-	-	0.67	2.50
131	-	-	-	-	-	-	-	-	1.00	0.50
132	-	-	-	-	-	-	-	-	1.00	1.00
133	-	-	-	-	-	-	-	-	1.00	1.50

Table E.4 (Continued) Results of parametric study analyses

Test #	WLF	Live Load Information			TSB Information		Calc. TSB Shear WLF {TSB shear/Wheel Load}	Calc. TSB Moment Arm (in) {TSB moment/Wheel Load}
		AASHTO Loading	Tire Load (kips) (ML adj. bc wheels are so close)	Loading #	Max TSB Shear (kips) (FEA)	Max TSB Bending Moment (kip-in) (FEA)		
111	0.806	HS20	16	49	-	-		
112	0.806	HS20	16	49	-	-		
113	0.806	HS20	16	49	-	-		
114	0.806	HS20	16	49	-	-		
115	0.806	HS20	16	49	-	-		
116	0.806	HS20	16	49	-	-		
117	0.806	HS20	16	49	-	-		
118	0.806	HS20	16	49	-	-		
119	0.806	HS20	16	49	-	-		
120	0.806	HS20	16	49	-	-		
121	0.806	HS20	16	49	-	-		
122	0.806	HS20	16	49	-	-		
123	0.806	HS20	16	49	-	-		
124	0.806	HS20	16	49	-	-		
125	0.806	HS20	16	49	-	-		
126	0.806	HS20	16	49	-	-		
127	0.806	HS20	16	49	-	-		
128	0.806	HS20	16	49	-	-		
129	0.806	HS20	16	49	-	-		
130	0.806	HS20	16	49	-	-		
131	0.806	HS20	16	49	-	-		
132	0.806	HS20	16	49	-	-		
133	0.806	HS20	16	49	-	-		

Table E.4 (Continued) Results of parametric study analyses

Test #	PANELS								Max Cxn Force (kips) (FEA)
	Max Panel Longit. Bending (ksi) (FEA)	F`b (ksi)	ANSYS fb / Fb	Max Panel Deflec- tion (in) (FEA)	$\Delta\alpha\lambda\lambda$	FEA D / Dall	Max Relative Panel Displ. (in) (FEA)	Rel Disp / 0.10 in	
134	-	-	-	-	-	-	0.172	**1.72**	-
135	-	-	-	-	-	-	0.171	**1.71**	-
136	-	-	-	-	-	-	0.181	**1.81**	-
137	-	-	-	-	-	-	0.175	**1.75**	-
138	-	-	-	-	-	-	0.172	**1.72**	-
139	-	-	-	-	-	-	0.171	**1.71**	-
140	-	-	-	-	-	-	0.170	**1.70**	-
127	-	-	-	-	-	-	0.179	**1.79**	-
141	-	-	-	-	-	-	0.232	**2.32**	-
142	-	-	-	-	-	-	0.239	2.39	-
139	-	-	-	-	-	-	0.171	**1.71**	-
143	-	-	-	-	-	-	0.222	**2.22**	-
144	-	-	-	-	-	-	0.227	**2.27**	-
145	-	-	-	-	-	-	0.164	**1.64**	-

Table E.4 (Continued) Results of parametric study analyses

Test #	TSB									
	Max TSB Bending Moment (kip-in) (FEA)	Max TSB Bending Stress (ksi) (FEA)	TSB Fb (ksi)	FEA TSB fb / Fb	Max TSB Shear (kips) (FEA)	Max TSB Shear Stress (ksi) (FEA)	TSB Fv (ksi)	FEA TSB fv / Fv	b/d Ratio	Ratio of TSB EI to Min. EI
134	-	-	-	-	-	-	-	-	1.00	2.01
135	-	-	-	-	-	-	-	-	1.00	2.49
136	-	-	-	-	-	-	-	-	1.50	0.50
137	-	-	-	-	-	-	-	-	1.50	1.00
138	-	-	-	-	-	-	-	-	1.50	1.50
139	-	-	-	-	-	-	-	-	1.50	2.00
140	-	-	-	-	-	-	-	-	1.50	2.49
127	-	-	-	-	-	-	-	-	0.67	1.00
141	-	-	-	-	-	-	-	-	0.67	1.00
142	-	-	-	-	-	-	-	-	0.67	1.00
139	-	-	-	-	-	-	-	-	1.50	2.00
143	-	-	-	-	-	-	-	-	1.50	2.00
144	-	-	-	-	-	-	-	-	1.50	2.00
145	-	-	-	-	-	-	-	-	0.63	1.01

Table E.4 (Continued) Results of parametric study analyses

Test #	WLF	Live Load Information			TSB Information		Calc. TSB Shear WLF {TSB shear/Wheel Load}	Calc. TSB Moment Arm (in) {TSB moment/Wheel Load}
		AASHTO Loading	Tire Load (kips) (ML adj. bc wheels are so close)	Loading #	Max TSB Shear (kips) (FEA)	Max TSB Bending Moment (kip-in) (FEA)		
134	0.806	HS20	16	49	-	-		
135	0.806	HS20	16	49	-	-		
136	0.806	HS20	16	49	-	-		
137	0.806	HS20	16	49	-	-		
138	0.806	HS20	16	49	-	-		
139	0.806	HS20	16	49	-	-		
140	0.806	HS20	16	49	-	-		
127	0.806	HS20	16	49	-	-		
141	0.806	HS25	20	48	-	-		
142	0.806	ML24	21	47	-	-		
139	0.806	HS20	16	49	-	-		
143	0.806	HS25	20	48	-	-		
144	0.806	ML24	21	47	-	-		
145	0.806	HS20	16	49	-	-		

BIOGRAPHY OF THE AUTHOR

Melanie Bragdon was born in Bangor, Maine, on June 17, 1973. She was raised in Bangor and graduated from Bangor Christian High School in 1991. She attended the University of Maine and graduated in 1995 with a Bachelor's degree in Civil Engineering. She entered the Civil Engineering graduate program at the University of Maine in the summer of 2000.

After receiving her degree, Melanie will be joining Florida Power and Light and beginning her career in structural engineering. Melanie is a candidate for the Master of Science degree in Civil Engineering from The University of Maine in December, 2002.